INVESTIGATIONS INTO PROTIEN-SURFACE INTERACTIONS VIA ATOMIC FORCE MICROSCOPY AND SURFACE PLASMON RESONANCE

By

Jenifer K. Settle

Submitted to the graduate degree program in the Department of Chemistry and the Graduate Faculty of the University of Kansas in partial fulfillment of the requirements for the degree of Doctor of Philosophy.

_____

Chairperson, Dr. Cindy L. Berrie

_____

Dr. Heather Desaire

_____

Dr. Robert C. Dunn

_____

Dr. Craig E. Lunte

_____

Dr. Susan M. Williams

Date Defended: July 19, 2012

The Dissertation Committee for Jenifer Kaye Settle

certifies that this is the approved version of the following dissertation:

INVESTIGATIONS INTO PROTIEN-SURFACE INTERACTIONS VIA ATOMIC FORCE MICROSCOPY AND SURFACE PLASMON RESONANCE

_____

Chairperson Dr. Cindy L. Berrie

Date approved: July 27, 2012

Abstract

Jenifer K. Settle, Ph.D.
Department of Chemistry
University of Kansas

Protein surface interactions are important in many diverse applications. In this dissertation nonspecific and specific interactions of two proteins (fibrinogen and F_1-ATP synthase) with a variety of surfaces have been investigated via atomic force microscopy and surface plasmon resonance. Chapter one provides background information on protein surfaces interactions. Chapter 2 summarizes the techniques and surfaces utilized in the investigations in the following chapters. Chapter 3 provides background and investigations on nonspecific fibrinogen to surfaces. Fibrinogen is an important plasma protein involved in the blood clotting cascade. To improve design of materials for biodevices and implants, more knowledge about the interactions controlling fibrinogen adsorption is essential. Nonspecific adsorption of fibrinogen was investigated on model surfaces of graphite and mica as well as on self-assembled monolayer (SAM) via atomic force microscopy (AFM) to determine conformation. Complementary studies were performed via surface plasmon resonance (SPR) to investigate the dynamics of this adsorption process on gold, and an amine-, carboxyl-, methyl- and hydroxyl-terminated SAM films. Chapter 4 provides background and investigation into F_1-Adenosine triphosphate synthase (ATPase) adsorption to surfaces. ATPase is a tiny molecular motor which synthesizes ATP. This motor is of interest in the fabrication of hybrid nanobiodevices. Incorporation of this protein into devices requires precise control over immobilization properties such as location, concentration, orientation, and function. Orientation of ATPase adsorbed nonspecifically on a mica surface was observed via AFM. Control over placement within the device was investigated via nanopatterning of a 1-dodecene SAM surface. Control over orientation was performed via engineering a landing pad within a resist matrix with AFM. This involved patterning a dithiol into a methyl resist matrix and addition of maleimide-NTA with coordination to nickel ions and histidine tags in the protein. The chemistry of this process was validated with SPR and fluorescence microscopy. Information on the kinetic of ATPase-his binding to the NTA surface was obtained. Hopefully information learned from these investigations enables the development of enhanced biocompatible materials design and control over the fabrication of functional hybrid nanobiodevices.

Acknowledgments

I would like to thank my advisor, Dr. Cindy Berrie, for her guidance and insight throughout my time at KU. I would also like to thank my committee members, Dr. Heather Desaire, Dr. Robert Dunn, Dr. Craig Lunte, and Dr. Susan Williams.

I am grateful to the members of the Berrie group, both past and present, who have enriched my scientific endeavors. I am especially grateful to both Jills for the initial lab assistance and to Brad for the much needed support and comic relief. To Dave, Tyler, Ryan, Greg, Tina, and Rodi, thanks for making the Berrie group what it is today.

To Dave Arnett—I appreciate your encouragement to not "settle." The basement and sixth floor physical chemists (you know who you are) all of you have greatly enhanced my experience here at KU (despite your punniness). To Matt and Natasha—friendship is hard to come by, but ours turned into something great; our writing parties and your revisions enabled this dissertation to mold into shape. Cassie and Jenna—thanks for all your formatting assistance and chats. More importantly, I cherish the many laughs along the way—this truly kept me balanced. To Dan and Sara, without you I could not have made it through, and I will always value our friendship.

I would like to thank Dr. Ward Thompson for cultivating school spirit (in my defense, I often wore KU attire, somehow just not when I ran into you). To the people who attended/watched KU games and to the trivia team—I had a blast!

Cheers to the chemistry softball team, both for providing comradery and for supplying a pseudo-physical activity—hopefully my ninja skills will not soon be forgotten. Thank you to my fellow runners who taught me perseverance and endurance when faced with challenges. Last but not least, thanks to my Kansas City friends, the law crew, and my sand volleyball team.

To my cowboy lawyer, Jesse Tucker, who would have thought that crashing the Law Ball would change my life and that I would end up with the "nicest guy you will ever meet"? To the Tucker family, you've provided endless encouragement and support—including "all the answers" to my endless farm questions. And especially to Leonard—your enthusiasm and spirit are greatly missed.

I would like to thank my family, "adoptive St. Louis family", and "surrogate KC family", for their continual love and support. Without it, I would not be the person I am today.

I would like to express gratitude to our collaborators, Mark Richter for the ATP synthase protein samples and Judy Wu for helpful ideas for electrical detection of rotation. For financial support, I would like to thank the University of Kansas, the Ralph Adams Institute of Bioanalytical Chemistry, United States Army Research Office, Department of Defense (Grant #FED51570), and KU COBRE Center in Protein Structure and Function, specifically NIH grant RR-017708 for use of SPR.

And finally, I know that I will look back and think of something else someone did along the way to encourage me or had a positive impact upon my experience here at KU, so if you are not explicitly listed, please know that I still appreciate you.

Table of Contents

List of Figures

List of Tables

CHAPTER ONE:

Introduction to Protein Adsorption

1. Overview

Protein adsorption to surfaces plays a role in materials design,[1] biocompatibility,[2,3] physiological responses,[4] device engineering,[5] device functionality,[6] disease diagnostics,[7] drug discovery,[8] protein arrays,[9-11] sensors,[3,12] purifications,[13] and separations.[14,15] The concentration, affinity, orientation, conformation, and dynamics of protein adsorption all may influence the success of these applications. Successful incorporation of proteins within devices is often a determining factor of subsequent functionality.[14,16] Adsorption of proteins to a variety of surfaces is therefore a key step in a number of these applications. Maintaining proper protein orientation and conformation after immobilization may be imperative in terms of maintaining functionality.[17] Discrimination of the spatial location of proteins upon a surface may also be a critical aspect in device design. Additionally, minimizing (nonspecific) protein adsorption is also important in a number of systems ranging from contact lenses, to implants, to sensors. Protein immobilization is also involved in complex systems for analyte detection. Thus, fundamental knowledge about factors influencing protein immobilization at interfaces may provide insight into control of this process, or at least allow one to narrow down possible strategies to viable options, reducing the trial and error approach. While trial and error is useful in determining what works and what does not, it is a laborious, time consuming process. Additionally, simple *in vitro* studies do not always match up with much more complicated *in vivo* studies. Additional information on proteins and their impacts will be discussed.

1.1. Background and Relevance of Protein Adsorption

Protein adsorption to surfaces is a complex process that typically involves multiple steps. Adsorption may be nonspecific via hydrophobic interaction, van der Waals forces, hydrogen bonding or ionic forces. Alternatively, adsorption may be specific via a myriad of options including but not limited to amine coupling, maleimide-thiol coupling via cysteine groups, or controlled via nickel-NTA coordination with histidine tags, streptavidin-biotin binding or antibody binding.

Before discussing these adsorption modes in more detail, a short segment on basic protein characteristics will be presented. Proteins consist of a chain of amino acids with different functional groups (primary sequence) arranged into three-dimensional structures (secondary and tertiary structures). Some proteins consist of dimers, trimers, or more multiple units (quaternary structure). The primary amino acid sequence dictates the charge, charge distribution, as well as the hydrophilic and hydrophobic components of each protein. The three-dimensional structure dictates which of these groups is exposed on the surface of the protein. Thus, number of contact or adhesion sites of proteins to surfaces may vary depending on the 3D structure of the protein.

Information about general protein structure has been elucidated by techniques such as x-ray crystallography, nuclear magnetic resonance (NMR), and transmission electron microscopy (TEM). Of these, only TEM is amenable to investigations of single molecules on solid supports. Additionally, bulk techniques such as circular dichroism and infrared spectroscopy yield information about the distribution of alpha

helixes and beta sheets, or about the presence of amide I and amide II peaks within the protein, respectively. These techniques provide details about bulk properties and the distribution of structural components, but fail to yield a distinct image of the conformation and orientation of proteins on the surface.

Proteins are large, complex, heterogeneous molecules containing numerous binding sites and, as such, potentially have a wide variety of possible interactions.[18-20] Protein-surface interactions can therefore be inherently complicated as well.[4] To understand and control these interactions, additional information needs to be elucidated. Proteins are dynamic and as such can unfold, change shape, aggregate, lose stability, etc.[19] This can happen in solution, upon, or even after adsorbing onto a surface. This unfolding can be reversible or irreversible. Unfolding can then result in denaturation of the protein, rendering it either inactive or in some cases activating the protein.

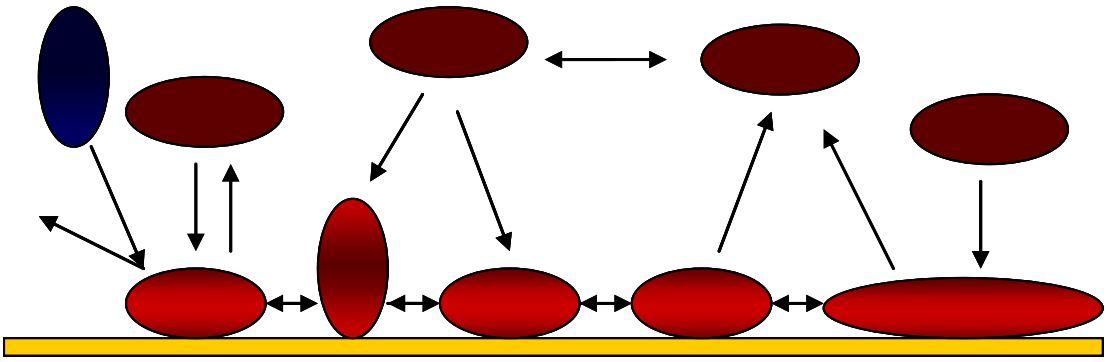

Figure 1.1: Schematic of Potential Protein-Surface Interactions. The gold bar represents the surface, the blue and red ovals are proteins, and the arrows demonstrate potential dynamic aspects.

Figure 1.1 depicts a schematic of some possible interactions proteins can have with surfaces. Proteins can have different affinities for different surfaces. If two

proteins are in solution (as indicated by the blue and red ovals), competitive adsorption may occur in which one may adsorb preferentially over the other to the surface. Alternatively, both proteins may adsorb to the surface or even interact with each other. Proteins may adsorb in a side-on (parallel to the surface) or end-on (perpendicular to the surface) orientation. This orientation may change in solution or after adsorption. Additionally, the protein may move over the surface (migrate or diffuse).[21] Once adsorbed, the molecule might desorb or come off the surface. Once desorbed, the protein may readsorb to either the same or a different spot on the surface. After adsorption, the protein may undergo structural rearrangements[22] such as spreading out and conformational changes. Proteins may denature in such a way as to become irreversibly adsorbed to the surface.[23] Denaturation may lead to a lack of functionality. Additionally, proteins may interact with other proteins or molecules in the solution or on the surface. The length of adsorption time may also influence protein adsorption characteristics. These interactions can be both protein and surface dependent.

Additionally, these protein-surface interactions can be dependent upon solution conditions. Factors such as the isoelectric point of the protein along with the pH and ionic strength of the solution and surface can impact adsorption properties[24] as well as protein aggregation and interactions in solution. Interactions are also reliant upon protein purity, protein concentration, and protein stability in solution.[25] Surface dependent interactions include the chemical moieties on the surface and the relative surface charge. Conformation or orientation of proteins on surfaces is often

influenced by the surface chemistry.[26] Surface topography may also play a role in protein interactions.

Sometimes proteins can be forcibly removed from the surface. This can happen either by disrupting the interaction(s) with the surface by changing solution conditions such as ionic strength or pH that alters charge distribution or alters the charge on the protein both of which can disrupt ionic interactions. Alternatively, the flow through the system can be increased to force the protein off the surface. Or, proteins can selectively remove other adsorbed proteins. A specific case of this with plasma proteins is the Vroman effect.[27-29] In this case, the most abundant plasma proteins adsorb to a surface initially, only to be later replaced by proteins with higher surface affinity. This happens in sequence, with higher molecular weight proteins gradually replacing lower molecular weight proteins. Knowledge of solution or conditions either capable or incapable of removing a protein from the surface (disrupt interactions) is useful in determining the relative strength of binding to the surface. If any minor change in solution parameters enables desorption, then the binding strength was low, and vice versa.

Fundamental aspects of protein surface interactions that can yield important information include, but are not limited to, competitive interactions, affinity, binding strength, conformation, orientation, kinetics, dynamics, concentration, and footprint. Learning about these fundamental properties should help in understanding and controlling protein adsorption on surfaces.

One issue associated with protein adsorption to surfaces is that these interactions are not well understood. Protein-surface interactions rely on the properties of the protein, solution, and surface. This means a universal guideline as to how a protein will interact is complex and as such is not currently feasible. Each protein must be studied independently with different surfaces and conditions to gain information about important interactions involved in surface immobilization. Once this is accomplished, the data can be compiled and analyzed to determine possible trends in adsorption behavior and key characteristic properties involved in such reactions. In order to control what is happening with protein-surface interactions, a greater understanding of these protein-surface interactions is imperative.

In some experiments, there is a desire to minimize protein adsorption, typically nonspecific adsorption. Current strategies to minimize protein adsorption include use of thin films of specific functionality,[30] oligo(phosphorylcholine) self-assembled monolayers (SAMs),[31] alkanethiolate SAMs with a mannitol functional group,[32] and passivation, among others.[33-35] Poly(ethylene glycol) (PEG) and oligo(ethylene glycol) (OEG) are two typical functionalities utilized within thin films to resist protein adsorption.[36, 37] These are initially fairly effective, but their mechanism is not well understood.[36] A few key factors are thought to play a role in this resistance, including its hydrophilicity and steric repulsion capability. The effectiveness of this inertness depends on structure of these coatings on the surface as well as the chain length, spacing, and density.[38] SAMs of oligo(phosphorylcholine) were also found to be effective at resisting protein and cell adsorption and are

potentially more biocompatible as they utilize functional groups found in cell membranes.[31] Alkanethiolate SAMs with a mannitol functional group are inert and resist protein adsorption, however the mechanistic repellant force remains unclear.[32] Passivating the surface with other proteins (albumin) or molecules has also been employed to deter additional protein adsorption by occupying available sites on the surface.

Another method for decreasing undesired interactions involves simply controlling the surface hydrophobicity and/or the surface charge, so that proteins with different or similar characteristics may be repelled, respectively. For example, lysozyme has a net negative charge and would be repelled from a negatively charged surface. However, in complex solutions something else may adsorb to the surface, which can change surface characteristics and modify surfaces as is the case with a double layer effect, which may counteract the original surface resistance. Additionally, in order to employ such a method, one would need to have information as to the adsorption and adhesion properties of these undesirable proteins to engineer the surface. Sometimes, if it is not possible to initially deter protein adsorption, one can disrupt these interactions with salt addition, change in pH, or surfactants.

If undesired nonspecific protein can be minimized, the next step is to immobilize the desired protein in such a conformation that it remains active and in an orientation such that it remains functional. Current ways to control protein orientation include amine coupling,[39] protein G,[40,41] protein A,[42] antibodies,[16] histidine tags,[43] thiols,[17] streptavidin-biotin,[44] and complementary strands of DNA,[45]

among others.[16] Controlling protein orientation with these methods is often a challenge because there can be multiple accessible binding groups and other complications as a results of a specific protein's characteristics. This means that utilizing these methods requires specific forethought into the composition of a specific protein. Additionally, some information must be known upfront about the protein to enable successful modification with a tag (to avoid disrupting protein activity), to utilize these methods. And proteins typically contain lots of lysine groups, resulting in a wide distribution of possible orientations. Addition of a DNA tag (or any tag) may modify the protein and adversely impact its function.

A current way to maintain protein activity after surface adsorption involves incorporation of a linker group (spacer) that separates the protein from the surface while still tethering it to the surface in order to try to alleviate spreading and denaturation effects on activity that can happen upon direct adsorption to the surface.

Sometimes to study or inhibit a protein's activity after immobilization, the protein must be inactivated. By fixing a protein so that it is less mobile, it is easier to image. A current way to inactivate proteins adsorbed on the surface includes adsorption through active groups. Another method of inactivation would be via glutaraldehyde addition, which molds proteins together. Cross-linking or uranyl acetate treatments are also methods of stabilizing the protein film structurally.[42,46] Another method is crystallization of proteins via phospholipase A_2 treatment.[47] These protein modifications are typically performed as a preparation step in certain techniques such as TEM and even scanning force microscopy.[48]

Once a protein is adsorbed to a surface, the structure of the resulting protein film must be investigated to ensure that the immobilization has taken place in the desired fashion. A wide variety of physical and biochemical methods can be employed for such investigations. Current techniques to study protein adsorption to surfaces include, but are not limited to, atomic force microscopy, ellipsometry, sum frequency generation spectroscopy, total internal reflection fluorescence, quartz crystal microbalance, surface plasmon resonance, attenuated total reflection infrared spectroscopy, secondary ion mass spectroscopy, solution depletion, isotopic radiolabeling, and others.

1.1.1. Applications of Protein Adsorption

Protein adsorption is critical in the manufacture and performance of such products as biosensors, implants, micro- and nanofluidic devices, enzyme-linked immunoassays, separations, and others. Biosensors can either incorporate proteins as sensors, can have protein as an analyte, or may need to function in a protein environment. If the protein is part of the sensory device, it needs to be bound to the biosensor surface in such a fashion as it is maintains activity and the analyte target site is still available after immobilization. If the biosensor is to function within an environment which contains proteins (such as plasma in glucose sensors), it must either withstand or resist protein adsorption in order to maintain its functionality. Similarly, with implants, when they are placed within a subject they must either deter protein adsorption or proteins must be adsorbed in such a fashion that rejection or fouling do not occur. Protein adsorption can trigger an immune response that can

result in a cascade of events ultimately causing in a walling off or encapsulation of the implant. Naturally, this is detrimental to the implant.

With both microfluidic and nanofluidic devices, proteins must be active if they are in the detection zone. If the protein is not capable of binding to or detecting the analyte, then false negative results may ensue. Additionally, channels within these devices must not get clogged. The narrow channels must be unobstructed to allow analyte to reach detector. If proteins bind to the device surface or within the channels of these devices, they might block the channels from analyte flow, again decreasing device efficiency.

Immunoassays also rely on protein adsorption for detection. In a typical immunoassay device, antibodies are bound to the surface and detect antigens in solution. One example of an immunoassay is enzyme-linked immunosorbent assay (ELISA), which can be performed via indirect, sandwich or competitive methods. In a typical sandwich enzyme-linked immunoassay, antibodies are first adsorbed to a surface (Figure 1.2a). This is performed either nonspecifically or specifically through amine groups from the lysine amino acids of the antibody. Another immobilization option is to immobilize one half of the antibody dimer via native thiol moiety after cleavage of the disulfide bond in the fc region.[49] After immobilization, typically a blocking step is performed with bovine serum albumin, and then the analyte is introduced into the system. The analyte will bind specifically to the antibody. The reverse is also possible, with analyte being bound to the surface and antibody captured from solution (Figure 1.2b). In the first case, a secondary antibody is

introduced into the system that binds to the analyte. A reporter antibody is then introduced into the system to bind to the secondary antibody or initial antibody in the case of the analyte bound to surface scheme. The reporter antibody typically has a horseradish peroxidase enzyme attached. Upon reaction, this enzyme will activate a reporter colorimetric molecule to create a colored solution. The intensity of this color is related to and indicative of the concentration of analyte bound to the antibody.

a)

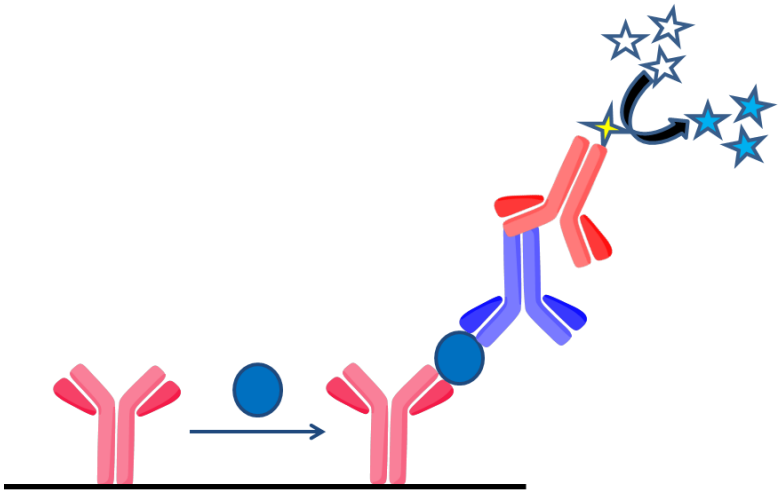

b)

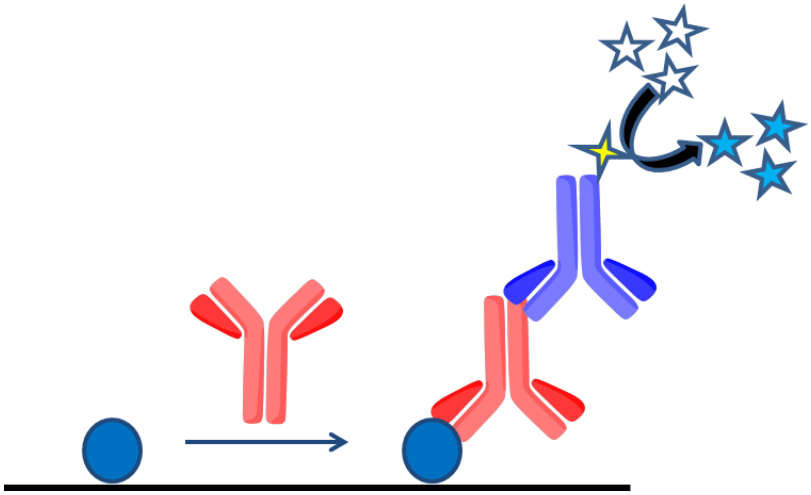

Figure 1.2: General schematic of ELISA assay. a) ELISA with antibody bound to surface, and subsequent attachment of analyte, secondary antibody, and reporter antibody, along with enzymatically catalyzed reaction of colorimetric reagent. b) ELISA with analyte bound to surface, and subsequent attachment of secondary antibody, and reporter antibody, along with enzymatically catalyzed reaction of colorimetric reagent.

Through investigation of a variety of different protein systems under a wide range of conditions, trends in adsorption characteristics may be determined which would make it possible to establish a database that aims to predict and to control protein surface interactions. Outstanding problems involving such interactions need to be solved to improve such devices and applications as protein assays, biosensors, implants, micro and nanofluidic devices, etc.

1.1.2. Current Problems and Limitations

Systems commonly susceptible to undesirable fouling issues are biosensors, implants, and micro- or nano-fluidic devices. Fouling is considered any undesirable adsorption that inhibits the function of the device, typically via nonspecific adsorption routes. For nano- or micro-fluidic devices this may mean proteins have nonspecifically bound to the channels, blocking the flow path of the analyte through the system and inhibiting its path to the detector. In addition to fouling, implants can also nonspecifically adsorb fibrinogen, a blood clotting protein. After adsorption, fibrinogen can be cleaved by thrombin to form fibrils that polymerize to form a blood clot which can cause rejection of the device or implant.

Sometimes, the intended function of the device or sensor is adversely influenced by the method of protein immobilization. For example, with ELISA only a small fraction of the bound antibodies remain active after adsorption to the surface.[50] Antibodies consist of two fab regions which have antigen binding sites and one fc region (Figure 1.3). The two sides (left and right) of the antibody are connected via a disulfide bond.

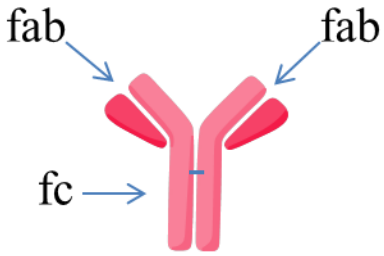

Figure 1.3: General antibody structure with fc and fabs identified.

When adsorbed to the surface in a manner that fails to control orientation, a random orientation of the protein ensues (Figure 1.4). The antibody may be upright, upside-down, on one side or on the other side, or tilted at some angle (not shown in diagram).

Figure 1.4: Random orientations of antibodies on a surface.

If the antibody is oriented upside-down, then the antibody active site, which is only one side of molecule (the fab portion), is bound to the surface and inaccessible. If this happens, the binding site is not available, and the analyte will not be detected. Fortunately, for some bound antibodies, the active site may be available. If there is a large concentration of analyte within the sample or sufficient signal amplification, this may not be a problem. However, if either of those were not feasible, the device activity needs improvement to yield conclusive results. Typically, the amount of functional antibodies after adsorption to the surface is low relative to the solution activity.[50] Part of this low functionality is thought to arise from small number of antibodies that are adsorbed in the correct orientation for analyte binding. Part of

why this is not such an issue in typical assays is that after analyte binding, a second antibody is attached which has an enzyme which will react with a colorimetric reagent to form a colored solution, thus amplifying the signal. This is acceptable if testing on a large scale and plenty of analyte is available, but if miniaturization of the system (since there are only a very small number of antibodies present) or decrease the limits of detection are desired, a greater amount of functional molecules is required.

Besides random orientation of proteins upon adsorption to surfaces, sometimes nonspecific protein adsorption itself can be detrimental or undesired. A common technique to inhibit or repel proteins from adsorbing to surfaces is coating the surface with a PEG or OEG. However, some compelling evidence reports that the protein resistance capability of these PEG or OEG components may change or degrade over time. Implications have been made that over time or under certain conditions PEG breaks down.[51] An article investigating potential future medicine utilizing PEGylated nanoparticles implied that PEG coating is not enough to completely eliminate protein adsorption.[52] Rouxhet, *et al.* studied grafted oligoethylene glycol (OEG) silanes on silicon oxide wafers via X-ray photoelectron spectroscopy (XPS).[51] These layers were still functional to resist protein adsorption after incubation at room temperature in phosphate buffered saline (PBS). However, 37ºC for 24 hour incubation in PBS, pseudo-physiological conditions, they determined that hydrolysis within the silicon oxide layer caused these silanes to detach from the silicon surface. Thus, these films were no longer capable of resisting

protein adsorption after incubation at body temperatures.[51] Additionally, solution conditions affect PEG packing which changes its protein resistant capabilities. And things that work in the lab (resist fouling) do not work once they are transferred to real implant situations, as they foul. So while in theory the solution to creating a protein resistant surface by simply applying a coating of PEGs or OEGs seems to work, the practical application of this system seems to fail.

Another approach would be to block surface sites with a relatively inert protein matrix, such as albumin, which is used because it adheres to a wide variety of surfaces. However, passivation with albumin may not be an ideal solution to minimize nonspecific adsorption to surfaces because other proteins can bind to albumin, which still results in an undesired response.

1.2. Nonspecific Protein Adsorption Studies

Nonspecific adsorption of proteins occurs under a wide variety of conditions, some intended and some unintended. Nonspecific immobilization of proteins to surfaces often involves intermolecular forces via noncovalent interactions and physical adsorption. Problems where nonspecific adsorption is important include ELISA, microfluidics, implants, contact lenses, sensors, and others.

Passivation utilizes nonspecific adsorption to block available surface sites from other proteins nonspecifically binding. Studies of nonspecific adsorption can reveal binding properties such as affinity and strength of binding. They can also reveal kinetic or dynamic information about the protein surface system. Additionally, nonspecific adsorptions studies help determine which surfaces are nonfouling.

1.2.1. Interactions Involved in Nonspecific Protein Adsorption

Factors controlling nonspecific adsorption include van der Waals forces, ionic attraction or repulsion, hydrophobic interactions, and hydrophilic interactions.[25] The strengths of each of these are relatively weak. Nonspecific adsorption is mostly physisorption of proteins at interfaces and typically these are noncovalent interactions. Protein, surface, and solution conditions can be altered under different conditions, which lead to large changes in protein adsorption, for the same molecules.

1.2.2. Issues with Nonspecific Protein Adsorption

Although in many cases nonspecific protein adsorption is imperative to experiments, in some cases it is detrimental. Nonspecific adsorption of proteins is often undesirable for implants or sensors. This type of adsorption also may lead to the failure of microfluidic devices due to clogging issues.

Nonspecific adsorption can lead to a variety of orientations and conformation of the protein on the surface. This may hinder the capability of additional binding or sensing applications. These noncovalent interactions are often weak and sometimes easily reversible. Since nonspecific adsorption of protein often induces a response in specific protein adsorption studies, this may complicate determination of kinetic parameters.

1.3. Specific Protein Adsorption Studies

Contrary to just random adsorption to surfaces, specific protein adsorption involves interaction of a unique moiety on the protein with the surface. These interactions are typically covalent interactions. In this manner, specific adsorption

involves targeting a specific group or functionality within the protein as an active surface capture agent. This process may include an intermediate ligand or linker to tether the protein to the surface. One advantage of this specific targeted approach is potential control over orientation.

Sometimes it is feasible to pattern in this moiety, creating landing pads for the protein. This attachment scheme is useful in devices due to the ability to immobilize proteins in a specific desired location and have them do work. Also, proteins may be patterned in an array format for detection of a variety of analytes simultaneously from the same sample.

Specific adsorption has the potential to improve immunoassays by orienting antibodies to increase active immobilized antibodies in ELISAs. This is important in miniaturization of devices as the smaller amount of surface area, the smaller amount of adsorbed antibodies and a greater fraction of them must be functional to detect the smaller amount of analyte.

In general this type of method to study interactions may be beneficial in isolating the protein of interest from a complex solution, determining which interactions are important and for monitoring dynamics. These interactions are often known and thus are often reversible since information is known on what bond needs to be disrupted. Studies with these reactions and building surfaces with specific immobilization schemes are often more reproducible than nonspecific schemes.

1.3.1. Types of Specific Protein Adsorption

Numerous types of specific protein adsorption exist,[45,53,54] only a few of which will be highlighted here including amine coupling,[55] antigen-antibody,[56] streptavidin-biotin,[41] and histidine tags.[25,45] Specific adsorption of proteins is more likely to be through chemisorption.

In amine coupling, a carboxylated surface is activated to succinimide esters by injecting a mixture of 1-ethyl-3-(3-dimethylaminopropyl) carbodiimide hydrochloride and N-hydroxysuccinimide (EDC and NHS) (Figure 1.5).[55,57] These esters are then available to react with any available amine group on the ligand or protein in a suitably acidic buffer solution to form an amide bond. After ligand or protein immobilization, remaining sites are blocked with ethanolamine. If a ligand is attached, then a protein can subsequently be captured by this ligand. One advantage of this type of immobilization is that all proteins have amines so this scheme is ubiquitous for all proteins.

a)

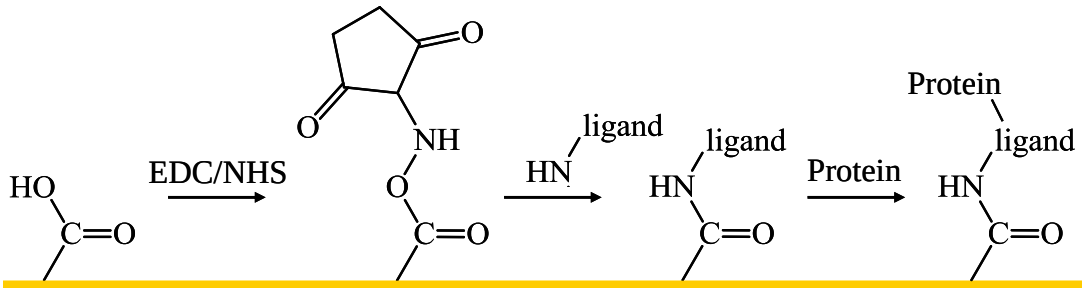

b)

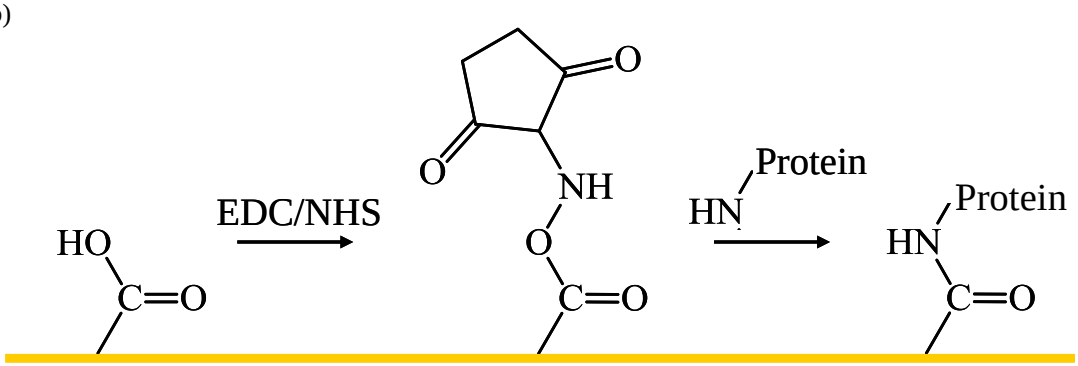

Figure 1.5: Schematic of Amine Coupling Chemistry. a) Carboxyl-terminated surface is activated with EDC/NHS, followed by amine coupling of the ligand, and subsequent protein attachment. b) Carboxyl-terminated surface is activated by EDC/NHS and then an amine on protein links protein to surface.

In antibody-analyte capture (Figure 1.6a), the antibody is immobilized on the surface and the analyte is introduced to the system and subsequently detected. Alternatively, this can also be performed in reverse, with the analyte bound to the surface and antibody subsequently adsorbed and detected (Figure 1.6b). This method is very specific if used with monoclonal antibodies. Also, if done properly, antibody orientation can be controlled and thus binding of analyte enhanced. This can control the orientation of the analyte or antibody and improve further coupling.

a)

b)

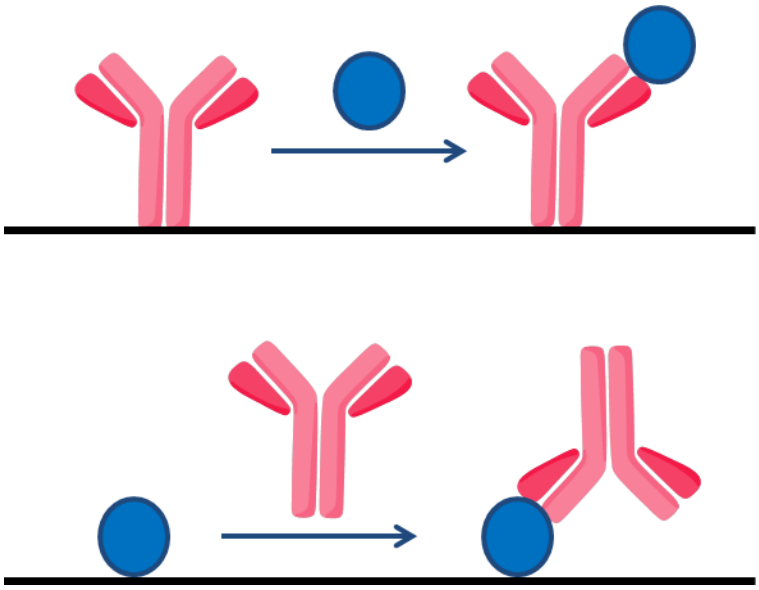

Figure 1.6: Antibody-Analyte interaction schemes. a) Antibody is bound to surface, analyte is introduced into system, and analyte binds to antibody. b) Analyte is bound to surface, antibody is introduced into system, and antibody binds to analyte.

Coupling of proteins to surfaces may also be performed by attaching single-stranded DNA to the surface via a thiol and the complementary strand into the protein sequence (Figure 1.7).[45] This enables protein immobilization via hybridization of the single strands. Alternatively, aptamer capturing (with a DNA loop) may be utilized. These methods provide a spacer between the surface and the protein and specific interaction in an oriented manner. This method results in very tight binding and is very specific, but involved modification of the protein, which may affect activity. This immobilization scheme results in the protein bound to the surface in a particular orientation, depending on the linkage between the protein and the single-stranded DNA.

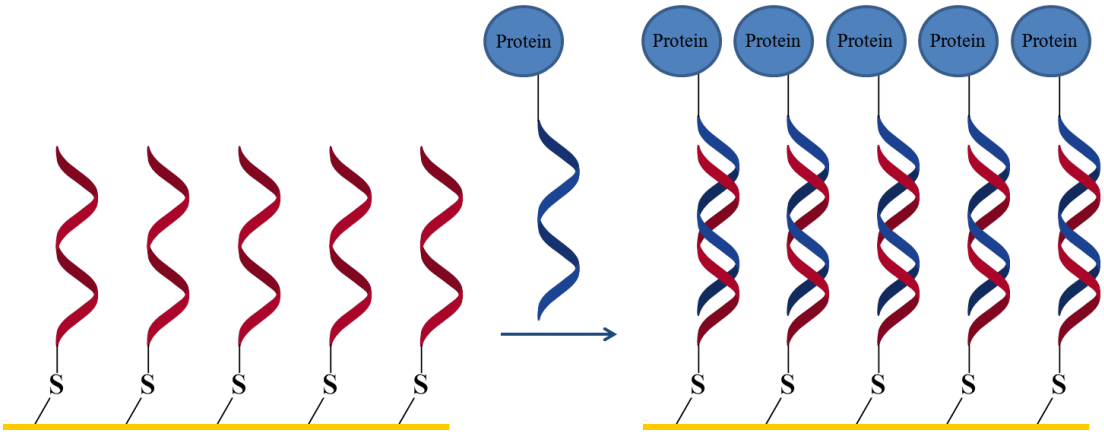

Figure 1.7: DNA capture schematic. Single-stranded DNA is attached to a gold surface via a thiol bond, complementary single-stranded DNA with linker to protein is introduced into the system. DNA hybridization occurs, specifically immobilizing protein to the surface via linker.

Biotin-Streptavidin is where either biotin or streptavidin is immobilized to the surface and a protein tagged with the other is detected (Figure 1.8). An advantage of this immobilization scheme is the strength of this interaction with a measured K_a of 10^{14}-10^{15} M^{-1}, indicative of very strong binding.[58,59] This is partially due to the multiple

binding sites (four binding sites, two on each side). This allows for the ability to link the protein to the surface and then link something else.

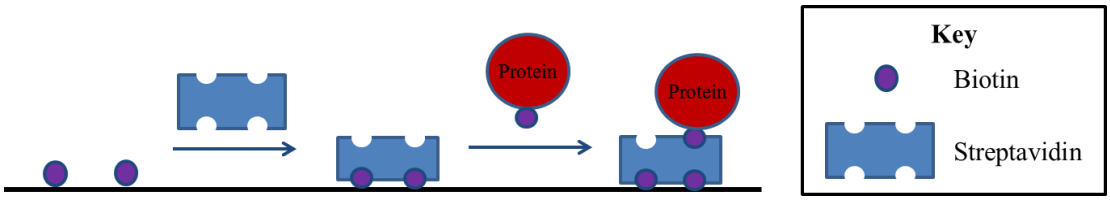

Figure 1.8: Biotin-streptavidin capture schematic.

Histidine tags are used in affinity chromatography to separate and purify proteins.[60] One of the most common uses of this is via nickel ion coordination to nitrilotriacetic acid and histidine tags via noncovalent interaction in ion metal affinity chromatography (IMAC) to purify proteins.[60] Nitrilotriacetic acid has three sets of carboxyl terminal groups. These can coordinate to transition metal ions (Ni^{2+}, Co^{2+}, Zn^{2+}) leaving two free coordination sites in these tetradentate molecules. These ions can then somewhat selectively bind to the imidazole group on histidine tags attached to proteins (Figure 1.9). This is a common protein purification technique and is also used to immobilize ligands to NTA chips for use in further analyte binding via SPR. This immobilization scheme takes advantage of a moiety already incorporated into protein for purification purposes and this interaction can be specifically disrupted, enabling multiple assays on the same surface.

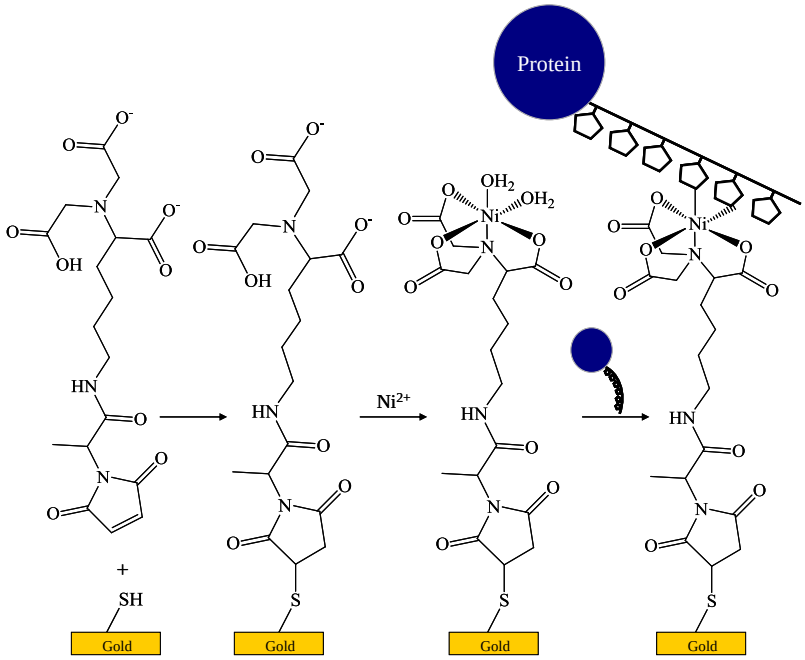

Figure 1.9: General schematic of M-NTA immobilization of nickel ions and hexahistidine tagged protein.

1.3.2. Issues with Specific Protein Adsorption

Although a great number of specific coupling methods exist, all types are not equal, and thus one must choose wisely which type of coupling to use. In order to achieve optimal coupling, you must know something about the protein of interest and what functional groups it might have available.

If amine coupling was chosen, one must realize that this method will couple any amine on the protein. This means that while specific in terms of attachment chemistry, this method is not as controlled, as you may end up reacting with an amine on the wrong (active) side of the protein. This makes the active site unavailable and as such would not improve the availability of the binding site. If there is plenty of surface area, this might not matter as an array (assortment – distribution) of orientations would probably exist. However, to move to smaller surfaces this random assortment of orientation becomes more critical. Additionally, while the reaction might be specific in interaction it may not be specific in terms of area and therefore if spatial control is desired, additional steps must be performed.

Other sensors that rely on analyte-antibody interactions have similar issues as ELISA. If the antibody is not oriented with the antigen binding site available, a false negative result may ensue.

Issue with biotin-streptavidin include that this binding is so strong it is essentially irreversible. Thus to perform further studies, the surface is not easily regenerated and one must start with a fresh surface.

DNA immobilization suffers from a prior knowledge issue. One must know the complementary sequence and label protein appropriately for this scheme to work.

Histidine tag reactions with M-NTA suffer from a noncovalent bond, which means the reaction can be disrupted. Additionally, there is a potential of metal ion leaching. In complex solutions this may lead to heterogeneous protein binding as histidine can be in natural amino acid sequence of other proteins in solution.

Despite these potential drawbacks, many of these specific immobilization methods have been utilized to successfully immobilize proteins in a uniform and desired manner.

1.4. Background Information on Protein Systems of Interest

This dissertation involves two protein systems of interest, specifically, fibrinogen and F_1-Adenosine Triphosphate Synthase (F_1-ATP synthase). Nonspecific adsorption for fibrinogen and both nonspecific and specific adsorption of F_1-ATPase were studied via AFM and SPR in chapters three and four, respectively.

1.4.1. Fibrinogen

Fibrinogen is a key component in the blood clotting cascade and thus of importance when investigating biocompatibility. The goal of fibrinogen experiments was to study fundamental aspects of nonspecific protein adsorption to a variety of surfaces in an effort to gather information that would enable engineers to design improved biocompatible surfaces.

1.4.2. F-ATP Synthase

Once knowledge of the rotary capability became prevalent, development of hybrid nanobiodevices utilizing this enzyme emerged. F_1-ATP synthase was imaged via AFM to determine nonspecific adsorption orientation(s). To improve the number of functional protein motors on surface, specific immobilization was performed via surface nanoengineering to both study and control rotation. The goal of this particular project was to improve the number of functional devices via elucidating important fundamental adsorption properties of the motor in order to immobilize the protein on the surface in the desired location with proper functional orientation.

1.5. Summary

Protein adsorption to surfaces is a dynamic and complicated process. Studying both nonspecific and specific protein-surface interactions will provide an avenue towards learning fundamental aspects of protein adsorption to surfaces as well as in determining ways to control this adsorption. For fibrinogen, control over this adsorption should lead to more biocompatible devices. For ATPase, control over the location and orientation of adsorption should lead to its successful incorporation into functional nanobiodevices.

1.6. References

1. Mrksich, M., Using self-assembled monolayers to understand the biomaterials interface. *Current Opinion in Colloid & Interface Science* **1997,** *2* (1), 83-88.
2. Anderson, J. M.; Rodriguez, A.; Chang, D. T., Foreign body reaction to biomaterials. *Seminars in Immunology* **2008,** *20* (2), 86-100.
3. Hlady, V.; Buijs, J., Protein adsorption on solid surfaces. *Current Opinion in Biotechnology* **1996,** *7* (1), 72-77.
4. Brash John, L.; Horbett Thomas, A., Proteins at Interfaces. In *Proteins at Interfaces II*, American Chemical Society: 1995; Vol. 602, pp 1-23.
5. Wolny, P. M.; Spatz, J. P.; Richter, R. P., On the Adsorption Behavior of Biotin-Binding Proteins on Gold and Silica. *Langmuir* **2009,** *26* (2), 1029-1034.
6. Tan, W.; Huang, Y.; Nan, T.; Xue, C.; Li, Z.; Zhang, Q.; Wang, B., Development of Protein A Functionalized Microcantilever Immunosensors for the Analyses of Small Molecules at Parts per Trillion Levels. *Analytical Chemistry* **2009,** *82* (2), 615-620.
7. McCabe, R. P.; Lamm, D. L.; Haspel, M. V.; Pomato, N.; Smith, K. O.; Thompson, E.; Hanna, M. G., A Diagnostic-Prognostic Test for Bladder Cancer Using a Monoclonal Antibody-based Enzyme-linked Immunoassay for Detection of Urinary Fibrin(ogen) Degradation Products. *Cancer Research* **1984,** *44* (12 Part 1), 5886-5893.
8. Veerapandian, M.; Yun, K., Study of Atomic Force Microscopy in Pharmaceutical and Biopharmaceutical Interactions - A Mini Review. *Current Pharmaceutical Analysis* **2009,** *5* (3), 256-268.
9. Kenseth, J. R.; Harnisch, J. A.; Jones, V. W.; Porter, M. D., Investigation of Approaches for the Fabrication of Protein Patterns by Scanning Probe Lithography. *Langmuir* **2001,** *17* (13), 4105-4112.
10. Zhou; Wang, X.; Birch, L.; Rayment, T.; Abell, C., AFM Study on Protein Immobilization on Charged Surfaces at the Nanoscale: Toward the Fabrication of Three-Dimensional Protein Nanostructures. *Langmuir* **2003,** *19* (25), 10557-10562.
11. MacBeath, G.; Schreiber, S. L., Printing Proteins as Microarrays for High-Throughput Function Determination. *Science* **2000,** *289* (5485), 1760-1763.
12. Mooney, J. F.; Hunt, A. J.; McIntosh, J. R.; Liberko, C. A.; Walba, D. M.; Rogers, C. T., Patterning of functional antibodies and other proteins by photolithography of silane monolayers. *Proceedings of the National Academy of Sciences* **1996,** *93* (22), 12287-12291.
13. Kim, J.-S.; Raines, R. T., Ribonuclease S-peptide as a carrier in fusion proteins. *Protein Science* **1993,** *2* (3), 348-356.
14. Mallik, R.; Wa, C.; Hage, D. S., Development of Sulfhydryl-Reactive Silica for Protein Immobilization in High-Performance Affinity Chromatography. *Analytical Chemistry* **2007,** *79* (4), 1411-1424.
15. Chung, W. K.; Evans, S. T.; Freed, A. S.; Keba, J. J.; Baer, Z. C.; Rege, K.; Cramer, S. M., Utilization of Lysozyme Charge Ladders to Examine the Effects of

Protein Surface Charge Distribution on Binding Affinity in Ion Exchange Systems. *Langmuir* **2009,** *26* (2), 759-768.
16. Turková, J., Oriented immobilization of biologically active proteins as a tool for revealing protein interactions and function. *Journal of Chromatography B: Biomedical Sciences and Applications* **1999,** *722* (1-2), 11-31.
17. Yoshimoto, K.; Nishio, M.; Sugasawa, H.; Nagasaki, Y., Direct Observation of Adsorption-Induced Inactivation of Antibody Fragments Surrounded by Mixed-PEG Layer on a Gold Surface. *Journal of the American Chemical Society* **2010,** *132* (23), 7982-7989.
18. Haynes, C. A.; Norde, W., Globular proteins at solid/liquid interfaces. *Colloids and Surfaces B: Biointerfaces* **1994,** *2* (6), 517-566.
19. Norde, W.; Buijs, J.; Lyklema, H.; Lyklema, J., 3 Adsorption of globular proteins. In *Fundamentals of Interface and Colloid Science*, Academic Press: 2005; Vol. Volume 5, pp 1-59.
20. Chinn, J. A. S., Steven M., *The Biomedical Engineering Handbook - "Biomaterials: Protein-Surface Interactions."*. CRC Press: 2000.
21. Marchin, K. L.; Phung, S.; Berrie, C. L., Evidence for Fibrinogen Mobility on Hydrophobic Surfaces. *e-Journal of Surface Science and Nanotechnology* **2005,** *3*, 173-178.
22. Haynes, C. A.; Norde, W., Structures and Stabilities of Adsorbed Proteins. *Journal of Colloid and Interface Science* **1995,** *169* (2), 313-328.
23. Déjardin, P., *Proteins at Solid-Liquid Interfaces*. Springer: 2006.
24. Tsapikouni, T. S.; Missirlis, Y. F., pH and ionic strength effect on single fibrinogen molecule adsorption on mica studied with AFM. *Colloids and Surfaces B: Biointerfaces* **2007,** *57* (1), 89-96.
25. Wagner, P., Immobilization strategies for biological scanning probe microscopy. *FEBS Letters* **1998,** *430* (1–2), 112-115.
26. Malmström, J.; Shipovskov, S.; Christensen, B.; Sørensen, E.; Kingshott, P.; Sutherland, D., Adsorption and enzymatic cleavage of osteopontin at interfaces with different surface chemistries. *Biointerphases* **2009,** *4* (3), 47-55.
27. Horbett, T. A., Mass action effects on competitive adsorption of fibrinogen from hemoglobin solutions and from plasma. *Thrombosis and haemostasis* **1984,** *51* (2), 174-181.
28. Slack Steven, M.; Horbett Thomas, A., The Vroman Effect. In *Proteins at Interfaces II*, American Chemical Society: 1995; Vol. 602, pp 112-128.
29. Brash, J. L.; ten Hove, P., Effect of plasma dilution on adsorption of fibrinogen to solid surfaces. *Thrombosis and Haemostasis* **1984,** *51* (3), 326-330.
30. Ostuni, E.; Chapman, R. G.; Holmlin, R. E.; Takayama, S.; Whitesides, G. M., A Survey of Structure−Property Relationships of Surfaces that Resist the Adsorption of Protein. *Langmuir* **2001,** *17* (18), 5605-5620.
31. Chen, S.; Liu, L.; Jiang, S., Strong Resistance of Oligo(phosphorylcholine) Self-Assembled Monolayers to Protein Adsorption. *Langmuir* **2006,** *22* (6), 2418-2421.

32. Luk, Y.-Y.; Kato, M.; Mrksich, M., Self-Assembled Monolayers of Alkanethiolates Presenting Mannitol Groups Are Inert to Protein Adsorption and Cell Attachment. *Langmuir* **2000,** *16* (24), 9604-9608.
33. Gunkel, G.; Weinhart, M.; Becherer, T.; Haag, R.; Huck, W. T. S., Effect of Polymer Brush Architecture on Antibiofouling Properties. *Biomacromolecules* **2011,** *12* (11), 4169-4172.
34. Zhang, Z.; Chen, S.; Jiang, S., Dual-Functional Biomimetic Materials: Nonfouling Poly(carboxybetaine) with Active Functional Groups for Protein Immobilization. *Biomacromolecules* **2006,** *7* (12), 3311-3315.
35. Chen, Y.; Thayumanavan, S., Amphiphilicity in Homopolymer Surfaces Reduces Nonspecific Protein Adsorption†. *Langmuir* **2009,** *25* (24), 13795-13799.
36. Li, L.; Chen, S.; Zheng, J.; Ratner, B. D.; Jiang, S., Protein Adsorption on Oligo(ethylene glycol)-Terminated Alkanethiolate Self-Assembled Monolayers: The Molecular Basis for Nonfouling Behavior. *The Journal of Physical Chemistry B* **2005,** *109* (7), 2934-2941.
37. Kankate, L.; Werner, U.; Turchanin, A.; Gölzhäuser, A.; Großmann, H.; Tampé, R., Protein resistant oligo(ethylene glycol) terminated self-assembled monolayers of thiols on gold by vapor deposition in vacuum. *Biointerphases* **2010,** *5* (2), 30-36.
38. Ivanchenko Maria, I.; Kulik Eduard, A.; Ikada, Y., Serum Protein Adsorption and Platelet Adhesion to Polyurethane Grafted with Methoxypoly(ethylene glycol) Methacrylate Polymers. In *Proteins at Interfaces II*, American Chemical Society: 1995; Vol. 602, pp 463-477.
39. O'Shannessy, D. J.; Brigham-Burke, M.; Peck, K., Immobilization chemistries suitable for use in the BIAcore surface plasmon resonance detector. *Analytical Biochemistry* **1992,** *205* (1), 132-136.
40. Jung, Y.; Lee, J. M.; Jung, H.; Chung, B. H., Self-Directed and Self-Oriented Immobilization of Antibody by Protein G−DNA Conjugate. *Analytical Chemistry* **2007,** *79* (17), 6534-6541.
41. Song, H. Y.; Zhou, X.; Hobley, J.; Su, X., Comparative Study of Random and Oriented Antibody Immobilization as Measured by Dual Polarization Interferometry and Surface Plasmon Resonance Spectroscopy. *Langmuir* **2011,** *28* (1), 997-1004.
42. Nakanishi, K.; Muguruma, H.; Karube, I., A Novel Method of Immobilizing Antibodies on a Quartz Crystal Microbalance Using Plasma-Polymerized Films for Immunosensors. *Analytical Chemistry* **1996,** *68* (10), 1695-1700.
43. Sigal, G. B.; Bamdad, C.; Barberis, A.; Strominger, J.; Whitesides, G. M., A Self-Assembled Monolayer for the Binding and Study of Histidine-Tagged Proteins by Surface Plasmon Resonance. *Anal. Chem.* **1996,** *68* (3), 490-497.
44. Lin, P.-C.; Weinrich, D.; Waldmann, H., Protein Biochips: Oriented Surface Immobilization of Proteins. *Macromolecular Chemistry and Physics* **2010,** *211* (2), 136-144.
45. Rusmini, F.; Zhong, Z.; Feijen, J., Protein Immobilization Strategies for Protein Biochips. *Biomacromolecules* **2007,** *8* (6), 1775-1789.

46. Takeyasu, K.; Omote, H.; Nettikadan, S.; Tokumasu, F.; Iwamoto-Kihara, A.; Futai, M., Molecular imaging of Escherichia coli F_0F_1-ATPase in reconstituted membranes using atomic force microscopy. *FEBS Letters* **1996,** *392* (2), 110-113.
47. Mohraz, M.; Yee, M.; Smith, P. R., Novel crystalline sheets of Na,K-ATPase induced by phospholipase A2. *Journal of Ultrastructure Research* **1985,** *93* (1–2), 17-26.
48. Apell, H.-J.; Colchero, J.; Linder, A.; Marti, O.; Mlynek, J., Na, K-ATPase in crystalline form investigated by scanning force microscopy. *Ultramicroscopy* **1992,** *42–44, Part 2* (0), 1133-1140.
49. Karyakin, A. A.; Presnova, G. V.; Rubtsova, M. Y.; Egorov, A. M., Oriented Immobilization of Antibodies onto the Gold Surfaces via Their Native Thiol Groups. *Analytical Chemistry* **2000,** *72* (16), 3805-3811.
50. Lu, B.; Smyth, M. R.; O'Kennedy, R., Tutorial review. Oriented immobilization of antibodies and its applications in immunoassays and immunosensors. *Analyst* **1996,** *121* (3), 29R-32R.
51. Dekeyser, C. M.; Buron, C. C.; Mc Evoy, K.; Dupont-Gillain, C. C.; Marchand-Brynaert, J.; Jonas, A. M.; Rouxhet, P. G., Oligo(ethylene glycol) monolayers by silanization of silicon wafers: Real nature and stability. *Journal of Colloid and Interface Science* **2008,** *324* (1–2), 118-126.
52. Walkey, C. D.; Olsen, J. B.; Guo, H.; Emili, A.; Chan, W. C. W., Nanoparticle Size and Surface Chemistry Determine Serum Protein Adsorption and Macrophage Uptake. *Journal of the American Chemical Society* **2011,** *134* (4), 2139-2147.
53. Samanta, D.; Sarkar, A., Immobilization of bio-macromolecules on self-assembled monolayers: methods and sensor applications. *Chemical Society Reviews* **2011,** *40* (5), 2567-2592.
54. Matharu, Z.; Bandodkar, A. J.; Gupta, V.; Malhotra, B. D., Fundamentals and application of ordered molecular assemblies to affinity biosensing. *Chemical Society Reviews* **2012,** *41* (3), 1363-1402.
55. Lofas, S.; Johnsson, B., A novel hydrogel matrix on gold surfaces in surface plasmon resonance sensors for fast and efficient covalent immobilization of ligands. *Journal of the Chemical Society, Chemical Communications* **1990,** (21), 1526-1528.
56. Jung, Y.; Kang, H. J.; Lee, J. M.; Jung, S. O.; Yun, W. S.; Chung, S. J.; Chung, B. H., Controlled antibody immobilization onto immunoanalytical platforms by synthetic peptide. *Analytical Biochemistry* **2008,** *374* (1), 99-105.
57. Johnsson, B.; Löfås, S.; Lindquist, G., Immobilization of proteins to a carboxymethyldextran-modified gold surface for biospecific interaction analysis in surface plasmon resonance sensors. *Analytical Biochemistry* **1991,** *198* (2), 268-277.
58. Green, N. M., Avidin. In *Advances in Protein Chemistry*, C.B. Anfinsen, J. T. E.; Frederic, M. R., Eds. Academic Press: 1975; Vol. Volume 29, pp 85-133.
59. Chilkoti, A.; Stayton, P. S., Molecular Origins of the Slow Streptavidin-Biotin Dissociation Kinetics. *Journal of the American Chemical Society* **1995,** *117* (43), 10622-10628.
60. Block, H.; Maertens, B.; Spriestersbach, A.; Brinker, N.; Kubicek, J.; Fabis, R.; Labahn, J.; Schäfer, F., Chapter 27 Immobilized-Metal Affinity Chromatography

(IMAC): A Review. In *Methods in Enzymology*, Richard, R. B.; Murray, P. D., Eds. Academic Press: 2009; Vol. Volume 463, pp 439-473.

Chapter Two:

Techniques and Methods Employed

2. Overview

Typical information desired from protein-surface interactions includes the amount, conformation, orientation, shape, and dynamics of protein adsorption. To achieve this information, techniques for investigation of protein-surface interactions must be surface sensitive, capable of resolving shapes of molecules and substructures within the proteins, capable of measuring submonolayer amounts, and have sufficient time resolution. Ideally these techniques would also be label-free, allow for solution flow and exchange, inexpensive, and reproducible. Realistically, one technique might not have all these characteristics, but by using a combination of techniques the desired information, such as shape, amount, size, orientation, and conformation, may be achieved.

Proteins range from a few to hundreds of nanometers in size. To directly study the conformation and orientation at the surface, one must be able to visualize the protein adsorbed to the surface. Thus, a technique capable not only of imaging but also of resolving features on the nanometer size scale is imperative. Additionally, incorporation of a way to mimic natural physiological environment(s) of proteins such as in fluid would be ideal. To study adsorption and desorption rates, a technique which is capable of monitoring interactions at the surface while enabling solution exchange in real-time with a time resolution faster than the binding and dissociation rate of the analyte is necessary. Techniques capable of at least a 0.1 nanometer resolution and up to 100 nanometers or more are desired for studying adsorbed protein structure. Techniques capable of measuring at sub-second to at most minutes,

depending on the protein system are required for dynamic measurements. Studies capable of monitoring interactions without altering the protein or conditions are desirable. Label-free techniques are advantageous for monitoring natural protein-surface interactions without alteration of components, such that the original state of the protein is not disrupted.

Common techniques for study of protein-surface interactions include physical techniques such as Fourier transform infrared spectroscopy[1] (including infrared spectroscopy attenuated total reflectance (FTIR-ATR),[2-4] infrared reflection-absorption spectroscopy (IRAS),[5] polarization modulation infrared reflection absorption spectroscopy (PM-IRRAS),[6] time-of-flight secondary ion mass spectrometry (ToF-SIMS),[7] total internal reflection fluorescence (TIRF),[8, 9] atomic force microscopy (AFM),[10-15] surface plasmon resonance (SPR),[16-21] fluorescence microscopy,[22] ellipsometry,[1, 23] and quartz crystal microbalance,[16, 24] sum frequency generation (SFG),[25] circular dichroism (CD), among others[26-28] as well as more typical biochemical methods such as ELISA and solution depletion.[26] FTIR provides data about the amide I and amide II bands of the protein which give information about the conformation of the protein after adsorption to the surface. TIRF provides information about protein kinetics and relative spatial coverage of the protein on the surface via fluorescence intensity measurements. AFM provides an image of the molecule and the surface. SPR provides a label-free measurement via monitoring changes in refractive index for measurements of affinity, specificity, concentration, and kinetic information about protein surface interactions in real time. Ellipsometry

uses changes in elliptically polarized light to determine thin film thicknesses. QCM uses a change in resonance frequency of a quartz crystal to determine the amount and kinetics of protein adsorption to surfaces. Most likely one technique will not be sufficient for a complete picture of protein binding, and a combination of techniques may be required. This will be the strategy adopted in this thesis.

This chapter describes the following techniques utilized in this thesis to study surfaces and/or protein-surface interactions: ellipsometry, goniometry, AFM, SPR, and fluorescence microscopy. Ellipsometry and goniometry provide details about the surface and surface modifications for characterization purposes. AFM provides images of protein conformation(s) on surfaces as well as allows modification to surfaces. SPR complements AFM with bulk measurements on similar surfaces. Fluorescence serves as a series of control tests to confirm the chemistry utilized in engineering the protein patterning at the surface. For most of these techniques, precise surface preparation is a key factor in obtaining surfaces suitable to meet the requirements of the techniques.

2.1. Surface Preparation

To study these protein surface interactions, substrates suitable for AFM and SPR studies were required. Requirements for AFM include flat and uniform surfaces. Stable surfaces or thin films are desired. If the surfaces can be modified or tuned via surface chemistry, that is even better. Requirements for SPR include a metal with excitable surface plasmons and properties of surfaces desired include tunability, stability, and flexibility. Surfaces investigated include gold, silicon, graphite, and

mica, along with modifications thereof. Gold and silicon are relatively flat surfaces that can be modified by covalently linking molecules to the surface with different terminal groups. Gold is relatively inert, durable, well-studied for functionalization, and is metallic, which provides surface plasmons available for excitation. Therefore, gold substrates can be used for direct comparison for the AFM and SPR data. Self assembled monolayers (SAMs) of alkane thiols can be readily formed on gold to tune surface chemistry.[29, 30] However, SAMs of alkyl silanes or alkenes are more robust and stable, so silicon oxide and hydrogen terminated silicon surfaces are also ideal surface substrate candidates. Silicon is also a flat surface, relatively easy to work with, and inexpensive. Mica and graphite are both atomically flat and as such ideal hydrophilic and hydrophobic surfaces, respectively and as such are good model surfaces for investigations of protein conformation. Additionally, both mica and graphite are layered materials which are cleavable to expose clean atomically smooth surfaces immediately prior to the experiment. Typical surface preparations are detailed below.

2.1.1. Gold Preparation

Types of gold utilized include commercially available gold (Platypus, Agilent, and BiaCore gold), house gold, template stripped gold (TSG), and flame annealed gold. A variety of gold sources is needed to achieve specific goals for different experiments. Characteristics of gold samples include gold thickness, grain size, and optical properties. Thicknesses of gold films on surfaces used in these experiments generally range from 50-350 nanometers. Gold coated onto silicon or glass included

an adhesion layer of chromium or titanium. Unlike mica and graphite, gold is not atomically flat. Gold films are also not single crystalline, which results in grain boundaries. Even single crystals have steps and terraces just like graphite. Grain size can vary from tens of nanometers to microns in size (Figures 2.1 and 2.3). Thickness of the gold depends on coating conditions and use. Optically transparent films are needed for some studies, thus the gold films for these experiments must be thinner (~50 nm). SPR requires the gold thickness to be about 50 nanometers. For opaque gold, about 150-300 nanometers of gold was sufficient. Optical properties of gold include both the refractive index (real and imaginary components or n and k values, as addressed in section 2.3.1) and the reflectivity of the surface.

Commercially available Platypus gold samples are relatively rough and have small grain sizes (30-50 nm with a few grains as large as about 80 nanometers), but have decent thickness and are suitable for ellipsometry and goniometry measurements. Agilent gold was flame annealed and had larger grains but was relatively expensive. BiaCore gold chips are also rough with small grains; so it has the same drawbacks of Platypus gold, but are specialized sensor chips for the SPR instrument.

House gold is less expensive, but can still be rough and contain small grains. Template-stripped gold and flame-annealed gold are variations of the house gold that have been modified to improve quality and thus both have large grain sizes.

2.1.1.1. Commercially Available Gold

Platypus gold is a commercially available type of gold obtained from Platypus Technologies (product code AU.1000.SLI). Gold is electron beam evaporated unto silicon wafers coated with a titanium adhesion layer. Specifications include 100 nm of gold on four inch diameter silicon wafers with a 5 nm adhesion layer of titanium. Gold roughness was not included on the website, but a Platypus substrate brochure indicated a root mean square (RMS) roughness of 1.73 nm with a contact angle for freshly evaporated gold of 25-40°.[31, 32] A 2.00 μm^2 AFM height image and corresponding cross-section of Platypus gold confirms that this surface is rough (RMS roughness over a 2 μm^2 area of 1.5 nanometers) and contains small grain sizes of approximately 30-60 nanometers in diameter (Figure 2.1a).

Agilent gold is commercially available gold obtained from Agilent Technologies (part number N9807A-FG). Au(111) substrates via Agilent are gold substrates epitaxially grown to a minimum of 150 nanometers thick on cleaved mica and flame annealed. Flame annealing produces reconstructed gold grains or terraces are as large as 280,000 μm^2.[33] A 2.00 μm^2 AFM height image and corresponding cross-section of Agilent flame annealed gold confirms that this surface contains large grains (340-1000 nanometers in diameter) that are relatively flat across these terraces but have deep boundaries between the grains (RMS roughness over a 2 μm^2 area of 2.5 nanometers) (Figure 2.1b).

SPR chips bought from the manufacturer (BiaCore now GE Healthcare, order code BR-1004-05) are referred to as “BiaCore gold”. BiaCore SPR gold chips consist

of thin glass cover slips, strength No. 3 (0.28-0.32 mm), standard dimensions 18 mm by 18 mm, with an adhesion layer and about 50 nanometer thick gold which contains peaks and troughs less than 5 nm.[34] A 2.00 μm^2 AFM height image and corresponding cross-section of BiaCore gold sensor chip confirms that this surface, much like the Platypus gold, is rough (RMS roughness over a 2 μm^2 area of 1.5 nanometers) and contains small grain sizes (40-140 nanometers in diameter) (Figure 2.1c).

Table 2.1 compares image root mean square (RMS) roughness and grain size ranges for quantitative comparisons and Figure 2.1a-c represents typical AFM images of commercially available gold for qualitative comparison. Objects higher above the surface (tops of gold grains) are brighter in color, those deeper (grain boundaries) are darker in color. Cross sections were taken across the images to provide another view of grain sizes and roughness. Since the RMS roughness taken over the entire two micron by two micron image area takes into account all variations within the heights, this value is not always as reasonable as it should be for surfaces like gold with deep grain boundaries. Additionally, not all grains are on the same level. Therefore, another RMS roughness for each type of gold was taken across individual gold grains to provide a better picture of roughness across terraces of grains. Platypus gold is fairly rough with small grain sizes that are at a fairly uniform height across the surface. Agilent gold has been flame-annealed and thus has very large grains with less roughness across the gold grains. The RMS over the larger area is larger than either the Platypus or BiaCore SPR gold chip due to the deep grain boundaries. SPR

chips are much like Platypus gold with a rough surface and small grain sizes. Experimental goals dictated which gold was best suited. For SPR studies, SPR chips (or specialized samples) must be utilized as they are the right size and thickness to fit within the instrument. For ellipsometry measurements and FTIR, Platypus gold was most suited due to its thickness. For studying protein adsorption via AFM, something like Agilent gold was most valuable due to its large and flat grains.

Table 2.1: Characteristics of Commercial Gold (RMS roughness and range of grain sizes)

Commercial Gold	RMS roughness (nm) over a 2 μm^2 area	Average RMS (nm) over Gold Grain	Range of Grain Sizes (nm)
Platypus	1.5	0.6	30-60
Agilent flame annealed	2.5	0.2	340-1000
BiaCore SPR Chip	1.5	0.4	40-140

a) Platypus gold

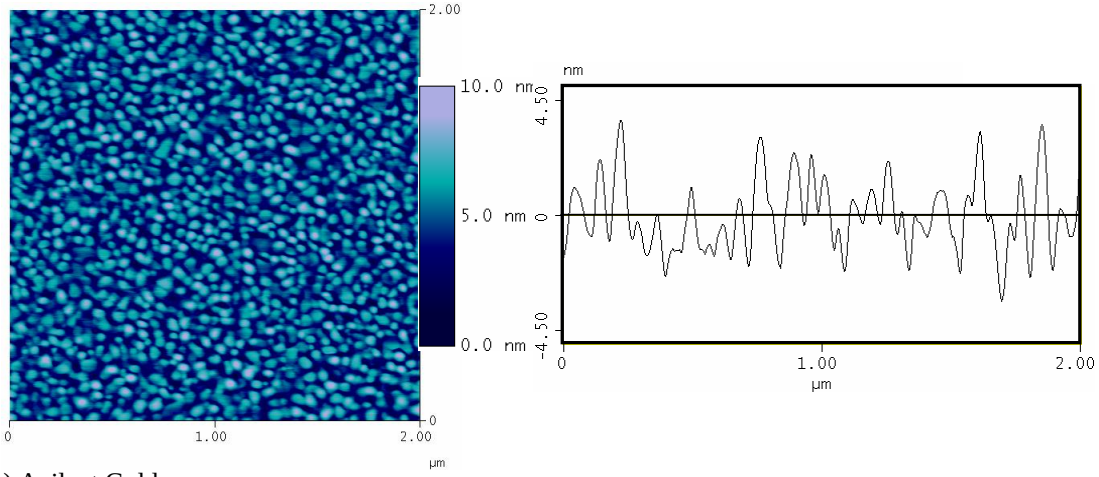

b) Agilent Gold

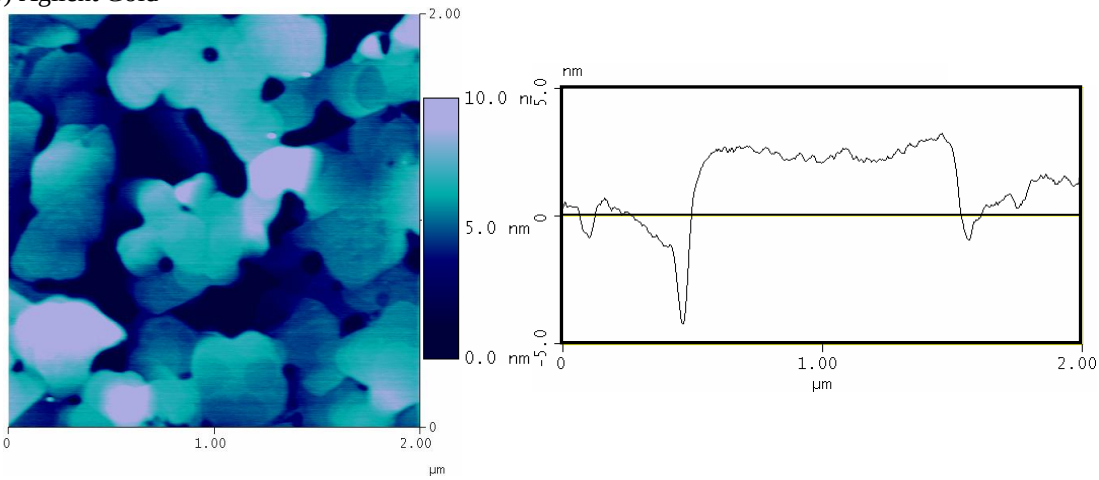

c) BiaCore gold (SPR chip)

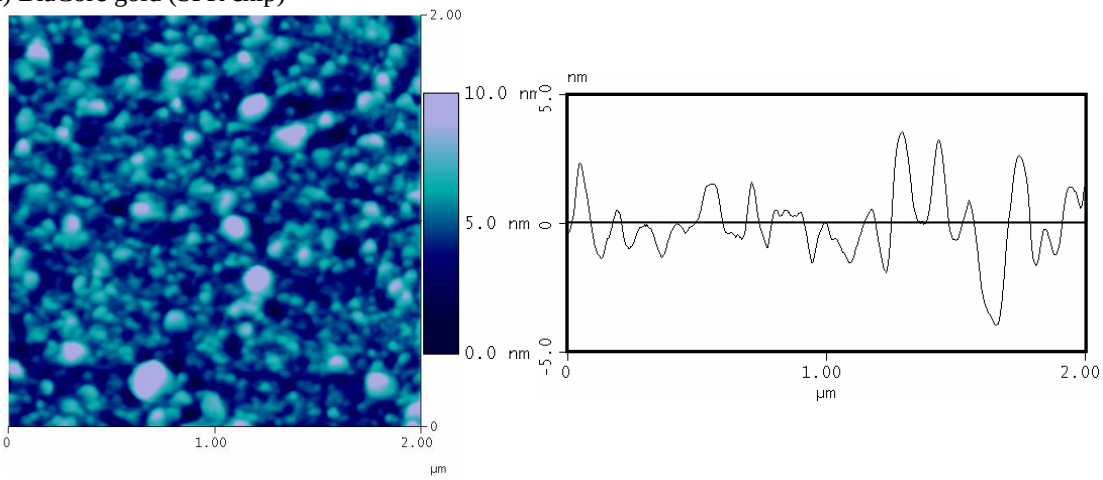

Figure 2.1: 2.00 µm x 2.00 µm AFM height images with a 10.0 nm height scale and corresponding cross sections of commercially available gold a) Platypus, b) Agilent flame-annealed gold, and c) BiaCore gold SPR chip.

2.1.1.2. Evaporation of Gold onto Mica

An Edwards Auto 306 Vacuum Evaporator was utilized to coat gold onto mica or glass. Mica was first mechanically cleaved with tweezers to expose a fresh, clean surface. Mica was secured to the sample plate via bars and screws. The sample plate was then secured within the evaporator and rotated during evaporator operation. A piece of gold wire (Alfa Aesar 0.5mm diameter, Premion®, 99.9985% CAS#7440-57-5) was coiled into a ball via tweezers and placed within the Tungsten wire sample basket. The shutter was placed over this gold in the basket. The chamber was sealed and pumped down to a pressure of about 1-1.5 x 10^{-6} Torr (as monitored by a Penning gauge) while cooling with liquid nitrogen. The chamber was heated by a halogen lamp until the pressure rose to 2-5 x 10^{-6} Torr, at which time the lamp was turned off and the pressure was allowed to drop back down to 1-1.5 x 10^{-6} Torr. This heat cycle continued until the temperature was as high as possible (100-300ºC) as measured by a thermocouple. Once the chamber was at a high temperature and low pressure (typically 5-8 x 10^{-7} Torr to 1 x 10^{-6} Torr), coating was started. A quartz crystal microbalance (QCM) was used to monitor the coating process by measuring the thickness of gold evaporated. A current was applied through the sample basket, heating the gold. Once the gold started evaporating (as evidenced by a rise in pressure), the shutter was moved. Once about 200-300 nanometers of gold were coated (according to the QCM), the current was decreased and turned off and the shutter was replaced. Typically, the gold was allowed to anneal for 1-3 hours with the lamp heating the system. The lamp was then turned off, the chamber was allowed

to cool until reaching room temperature, vented to atmospheric pressure, and then opened. The sample plate was removed, and gold on mica was removed from the plate and stored under nitrogen until use. Note, depending on the placement of components within the system, actual temperatures and thicknesses may have varied from measured values. Evaporation rate and rotating sample plate are critical to smoothness of samples and grain sizes as well as the evenness of the coating. A slow evaporation rate is advantageous because it allows molecules to move around and achieve lowest energy state. Ideally this rate is at 0.5 to 1 Å/s,[35, 36] although consistency of evaporation rate can be difficult to precisely control.

Characterization of the gold was performed before analysis via visualization (held up to light to determine if transparent or opaque and to check reflectivity and also to check the color – golden hue desired), ellipsometry (to determine optical properties), contact angles to confirm cleanliness, and AFM (Figure 2.3a) to determine grain sizes and roughness. The grains were fairly small at about 40 to 90 nanometers in diameter and the RMS roughness was 3.7 nanometers over a 2.00 square micron area, which is fairly rough. If need be, modifications to the gold were performed via template-stripping or flame annealing as described in the following sections.

2.1.1.3. Template Stripping Gold Preparation

Since evaporated gold on mica can have small grain sizes, a couple of methods were employed to increase the size of these grains. Large grains are desired for patterning and biological imaging via AFM. Bigger and flatter areas allow facile

separation of surface topography from surface chemistry and ease of distinguishing features of molecules adsorbed on surface from surface roughness. One technique employed was template stripping the gold[35, 37] (Figure 2.2) and another (section 2.1.1.4.) was flame annealing the gold.[33] Template stripped gold exposes the first layer of gold coated on mica. Since mica is atomically flat and gold grows epitaxially on the mica, the gold grains first coated onto the mica are typically the flattest.

In order to expose this initial deposition layer, epoxy from Epoxy Technology EPO-TEK (parts A and B) was used. To prepare epoxy, equal volumes (obtained via marked glass pipettes) of epoxy parts A and B were combined in a centrifuge tube, capped, and mixed via vortexing for about one minute. The solution was allowed to rest about one hour to thicken and polymerize. An oven was set to 150ºC and allowed to heat to that temperature. A glass slide was divided into ten half-inch by half-inch pieces using a ruler and sharpie to mark the sections and a scribe to cut the glass along those marks. The glass pieces were cleaned with acetone and rinsed with water. The previously evaporated gold on mica was cut into small sample sizes. The coated gold was placed gold side up, mica side down onto a tray. Using the round bottom of a cotton-tipped applicator, a small drop of epoxy was placed on the gold side of the sample. The glass piece was placed on top of the gold side of the gold on mica. Tweezers were used to gently press the glass/epoxy/gold/mica together and to squeeze out any air bubbles. These template strip precursors (glass/epoxy/gold/mica) were then placed in the oven for either two hours or 24-48 hours. After this time, the oven was turned off and allowed to cool before precursors were removed from the

oven, allowed to equilibrate to room temperature, and stored until needed. When needed, the mica was removed from the template stripped precursor by either mechanical or chemical means to expose the gold surface. Mechanical preparation of gold surfaces from precursors was performed by using tweezers to first gently press on the precursor sandwich followed by a gentle peeling of the mica from the glass-epoxy-gold portion. Occasionally, some mica was left behind on the freshly exposed gold surface. Chemical stripping to prepare gold surfaces from precursors involved placing the precursors into tetrahydrofuran (THF) and waiting approximately one to five minutes.[35] After waiting, the mica was usually disassociated from the other portion and the gold surface was exposed. Unfortunately, the mechanism of this separation is not well known and a few issues may arise including failure of mica to separate from the gold and delamination issues of the gold from the glass surface at later points. AFM was used to determine grain sizes to be about 100 to 500 nanometers in diameter and roughness RMS value of 0.8 nanometers of a 2.00 square micron area (Figure 2.3b). The grains were larger and the roughness smoother than the initial evaporated gold. Ellipsometry was used to obtain optical properties (Table 2.3) and goniometry was used to obtain contact angles.

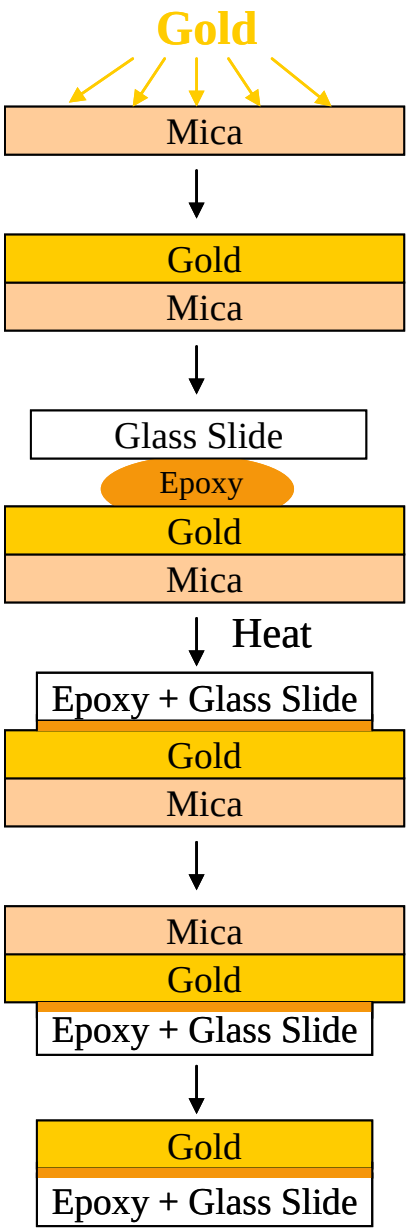

Figure 2.2: Schematic of gold modification: Template-strip precursor methods. Gold was deposited onto mica via evaporation to form a gold mica substrate, a small amount of epoxy was added to the gold and a piece of glass slide was added and secured to sandwich, this sandwich was heated and subsequently flipped, the mica was then removed from the template stripped precursor to reveal a gold surface on the epoxy glass slide substrate.

2.1.1.4. Flame Annealing Gold Preparation

Another technique for increasing the size of the gold grains was flame-annealing the gold.[33, 38] After coating, the gold coated mica surface was heated via a hydrogen flame. Basically, a piece of gold coated mica was removed from the evaporator or desiccator. The gold was placed onto a thick sheet of mica. The hydrogen flame apparatus was setup. This included a hydrogen gas tank, regulator, flashback arrestor, and a quartz tube narrowing to a sharp tip as a torch. The lights were turned off and the gas was ignited with a striker. The gas adjusted to about a four centimeter long flame and was allowed to burn a few minutes until it turned colorless. Once the hydrogen flame was lit and void of impurities (the flame became colorless), it was raster scanned across the mica base for a few minutes. Then, the flame was raster scanned across the gold surface a few times (for a total of 30-90 seconds) at an angle of about 30º. Care must be taken to not burn the gold. The flame was then extinguished and the regulator turned off. After annealing, the gold was allowed to cool briefly and then stored in a desiccator backfilled with nitrogen until needed.

Raising the temperature allows gold atoms on the surface to diffuse to more favorable sites and therefore creates larger grain sizes and reduction in the number of defects. The flame annealed gold was allowed to cool to room temperature and was either used immediately or stored under nitrogen until needed. AFM was used to characterize the surface (Figure 2.3c). Like the Agilent gold, the grains were fairly large and flat ranging from about 200 to 600 nanometers and RMS of 2.5 nanometers

over a two micron square area. This roughness is greater than that of the TSG, but this arises from the flame-annealed surface being less uniform, as although the grains were flat and large, they were not on same plane, as compared to template-stripped gold. And, the average RMS across gold grains was much lower than the evaporated gold at 0.2 nanometers compared to 0.7 nanometers. Ellipsometry was used to obtain optical properties (Table 2.3) and goniometry was used to obtain contact angles.

Table 2.2: Characteristics of House Gold (RMS roughness and range of grain sizes)

House Gold	RMS roughness (nm) over a 2 μm^2 area	Average RMS (nm) over Gold Grain	Range of Grain Sizes (nm)
Evaporated	3.7	0.7	40-90
Template-stripped	0.8	0.1	100-500
Flame annealed	2.5	0.2	200-600

Comparing values obtained for RMS roughness in Table 2.2 to reported literature values, the template-stripped gold RMS of 0.8 nanometers was slightly better than that by Semenza who reported an RMS roughness of less than 2 angstroms over a 2.25 μm^2 area for template-stripped gold.[35] Reported values for a 1 x 1 μm^2 roughness of 77.7 Å for unannealed and 2.7 Å for annealed gold,[36] calculated values for evaporated gold were lower and for flame-annealed gold were higher, so better and slightly worse, respectively (note, values calculated for 1 by 1 μm^2 area were approximately equivalent to values obtained on a 2 by 2 μm^2 area reported in Table 2.2. For template stripped gold, literature values are less than one nanometer in roughness,[35] comparable to values obtained with house template-stripped gold. Literature values reported gold grain sizes for evaporated gold of 50 nanometers in diameter at a deposition temperature of 20ºC and 500 nanometers in diameter at a

deposition temperature of 300ºC as measured via STM,[35] or 45-60 nanometers.[39] Values for gold grains in evaporated gold were closer to the lower temperature range. This confirms if large terraces are desired, coating should be performed hot rather than cold.[35] Wanunu reported values for gold grains with and without an annealing procedure to be small grains at 0.1 μm and deep grain boundaries of about 60 nanometers and a ten-fold increase in grain size to 1.0-1.5 μm, respectively, both of which are slightly bigger than the grain sizes achieved by our evaporation and flame-annealing.[36] A review paper[29] reported that these metal films are polycrystalline with grains ranging from 10 to 1000 nanometers. The structure of these gold grains depends on the deposition conditions and additional annealing processes.[29]

a) Evaporated gold onto mica

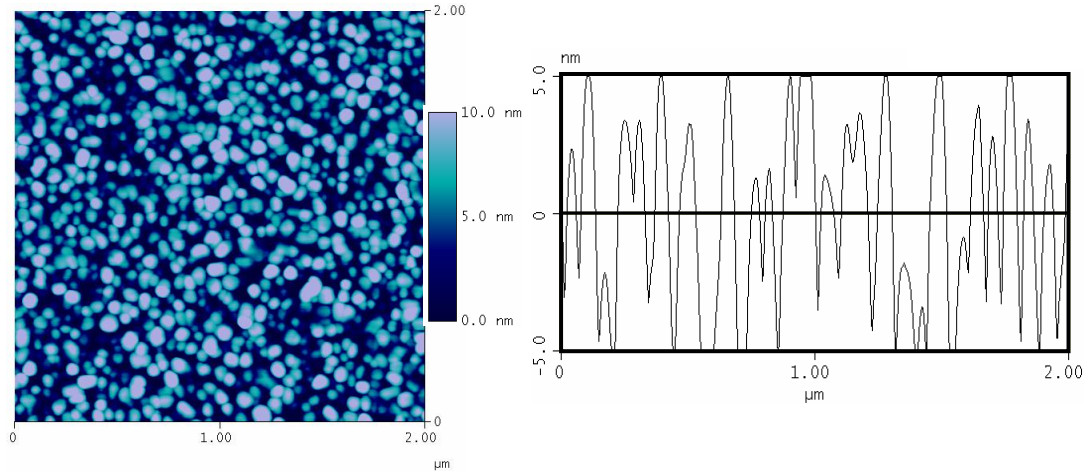

b) Template-stripped gold

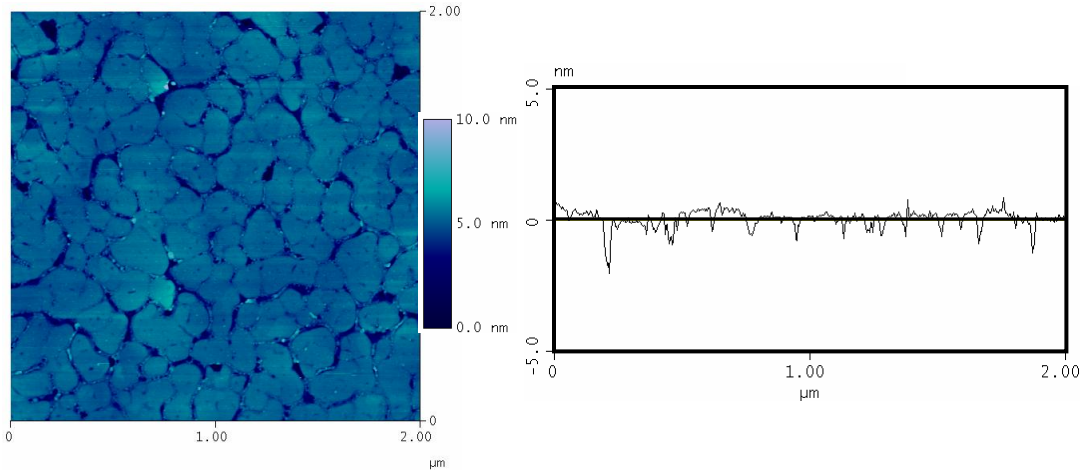

c) Flame-annealed gold

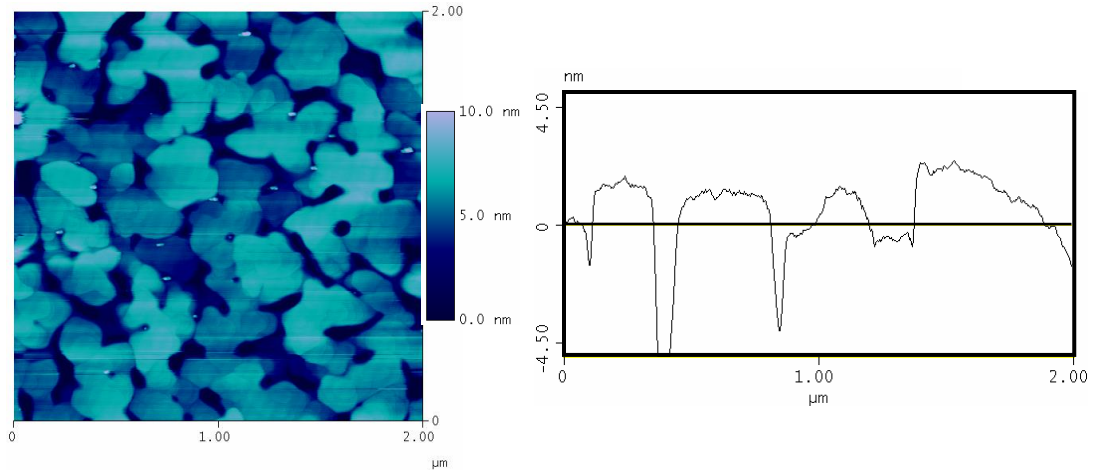

Figure 2.3: 2.00 µm x 2.00 µm AFM height images with a 10.0 nm height scale and corresponding cross sections of house gold of a) Evaporated gold onto mica, b) Template-stripped gold, and c) Flame-annealed gold.

2.1.2. Silicon

Silicon wafers, Si(100) or Si(111), were ordered from Virginia Semiconductor, Inc. Samples were cut to approximately the size of an AFM puck (mms) via a diamond tipped scribe. Wafers pieces were then rinsed with water, dried with nitrogen gas, and cleaned via piranha to remove organic contaminants. Freshly cleaned silicon oxide is hydrophilic with a contact angle of $<10^{o}$ and is fully wettable. Silicon is a nice flat surface as observed via AFM (Figure 2.4). Analysis of this 2.00 μm x 2.00 μm AFM image of silicon with a ten nanometer height scale resulted in a RMS roughness of 0.059 nanometers across the 2.00 μm^2 area. Piranha solution was prepared by placing about 15 milliliters of hydrogen peroxide into a beaker and slowly adding about 35 milliliters of sulfuric acid (30:70 solution of H_2O_2:H_2SO_4). The solution was heated to boiling and wafer pieces were placed in solution for 10-30 minutes before removing with Teflon tweezers and thoroughly rinsing with water. *Warning – piranha solution can be explosive when exposed to organics!* Additionally, piranha should not be stored in a closed container and should be neutralized by adding water, sodium bisulfite until bubbling decreases, and then sodium bicarbonate until pH reaches seven, prior to disposal.

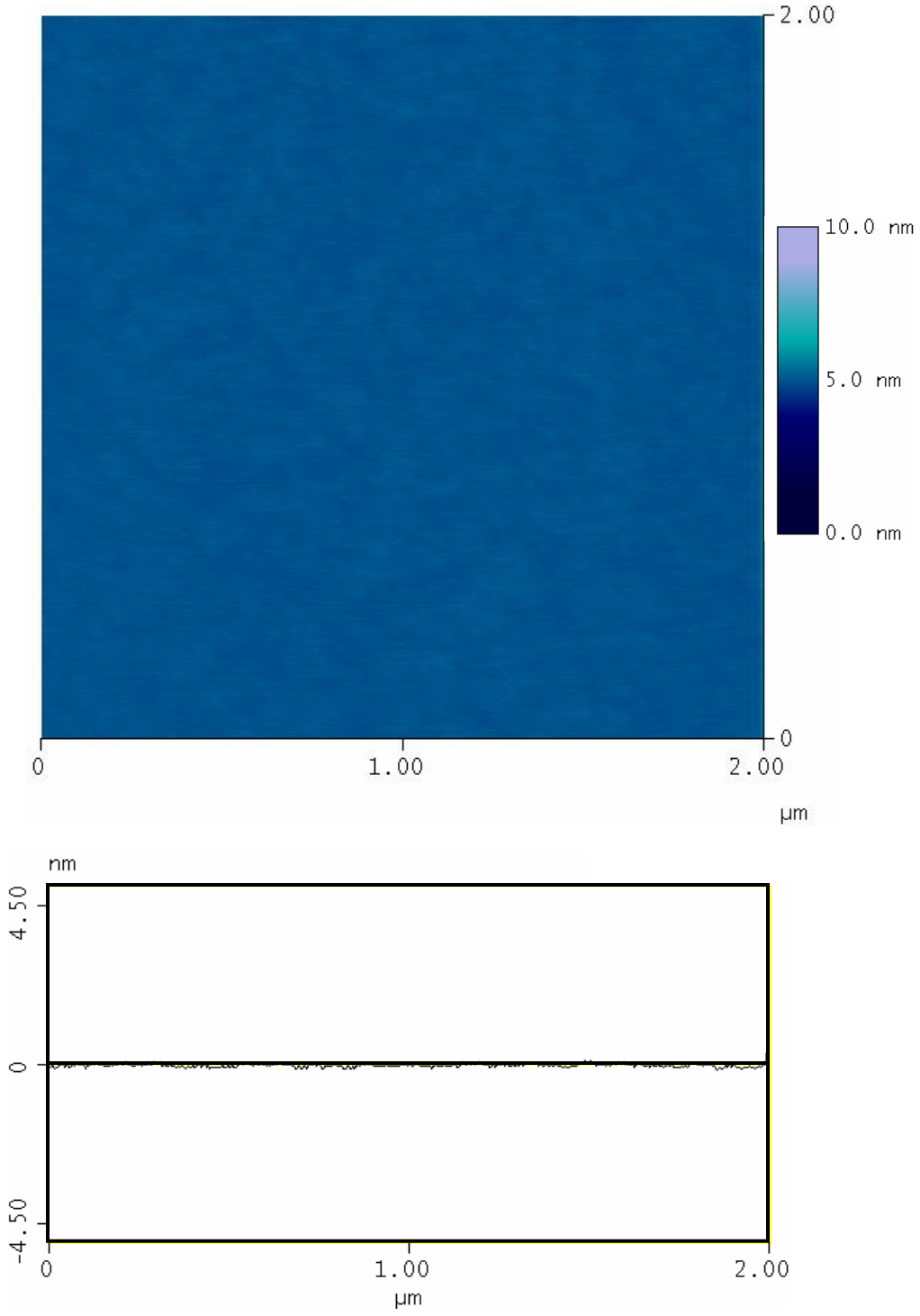

Figure 2.4: 2.00 µm x 2.00 µm AFM height image of silicon surface with a 10.0 nanometer height scale and corresponding cross section.

2.1.3. Mica and Graphite Preparation

Two models surfaces, mica and graphite, were utilized for their atomically flat characteristics. Mica (size 3 V1 Ruby block mica) was acquired from Lawrence & Co. Mica, a hydrophilic, atomically flat surface was utilized for nonspecific adsorption studies for both fibrinogen (Figure 3.2-4a) and F_1-ATPase (Figure 4.6-7). Muscovite mica [$H_2KAl_3(SiO_4)_3$] contains a low density of terminal hydroxyl groups and thus was negatively charged under the conditions of these experiments. Mica was prepared for use by mechanical cleavage with tape. Cleavage resulted in a freshly exposed surface that was free of contaminants. Freshly cleaved mica was hydrophilic and fully wettable with a contact angle of <10º. Graphite, highly-oriented pyrolytic graphite (HOPG), grade ZYH was bought from Veeco (now Bruker). Graphite contains sheets of sp^2 hybridized carbon atoms, in fused 6-membered rings, creating a hydrophobic surface. Graphite was also mechanically cleaved by tape to reveal a fresh, clean surface. Freshly cleaved graphite was hydrophobic with large contact angles. Characterization of these surfaces was performed via AFM. Mica was flat and smooth with an RMS roughness of 0.050 nm over a 2 μm^2 area or 0.072 nm ± 0.004 nm over a 5 μm^2 area (RMS roughness from n=9 AFM images) (Figures 2.5a). Graphite contains terraces that are flat and smooth but with step edges separating terraces with an RMS roughness of 0.160 nm over a 2 μm^2 area or 0.361 nm over 5 μm^2 area (Figure 2.5b). Atomic images of both mica and graphite were obtained by imaging a small area (about 5 nm^2) at a fast scan rate (about 30 Hz) in order to obtain atomic level images (Figure 2.6a and 2.6b, respectively). Analyses of

these two images show that mica and graphite differ in terms of lattice structures with a calculated distances similar to literature values of 5.3 Å between molecules for mica[40] and a smaller spacing of 2.5 Å for those in graphite.[40, 41]

a)

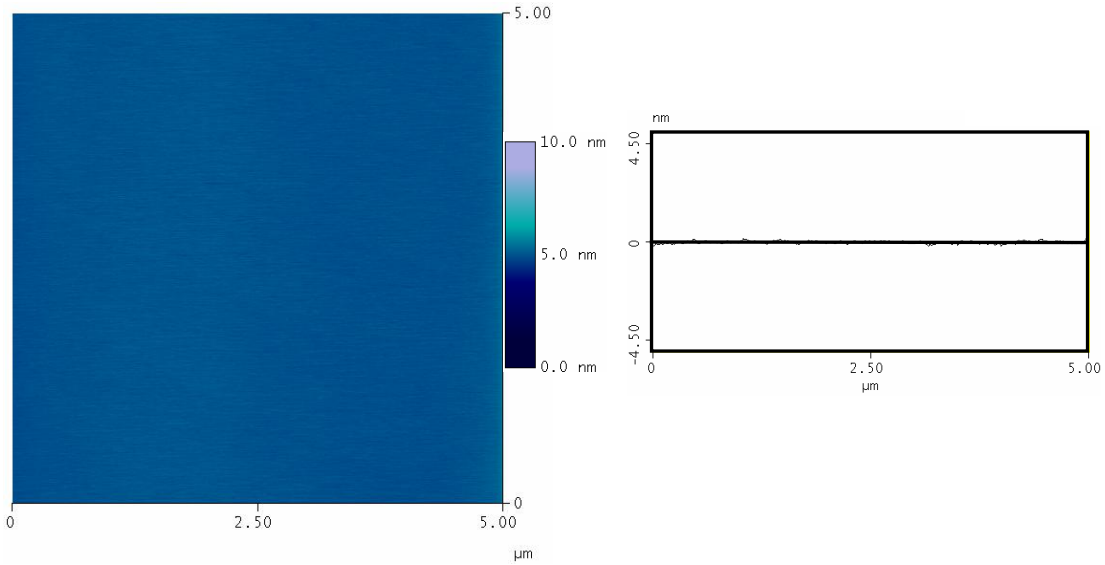

b)

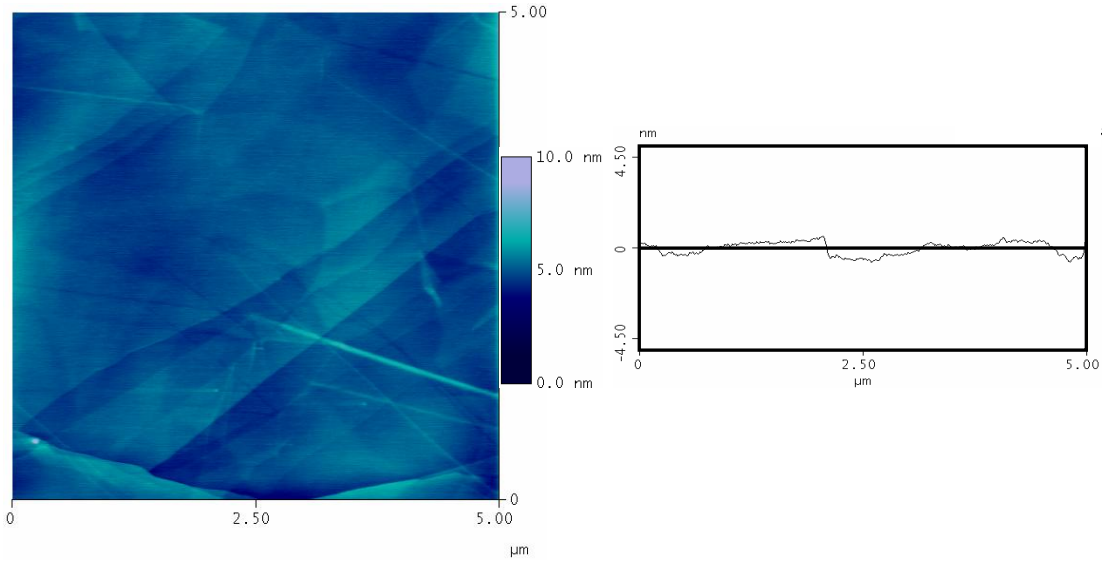

Figure 2.5: 5.00 µm x 5.00 µm AFM height images and corresponding cross sections of a) mucosiva mica and b) graphite with a 10.0 nm height scale.

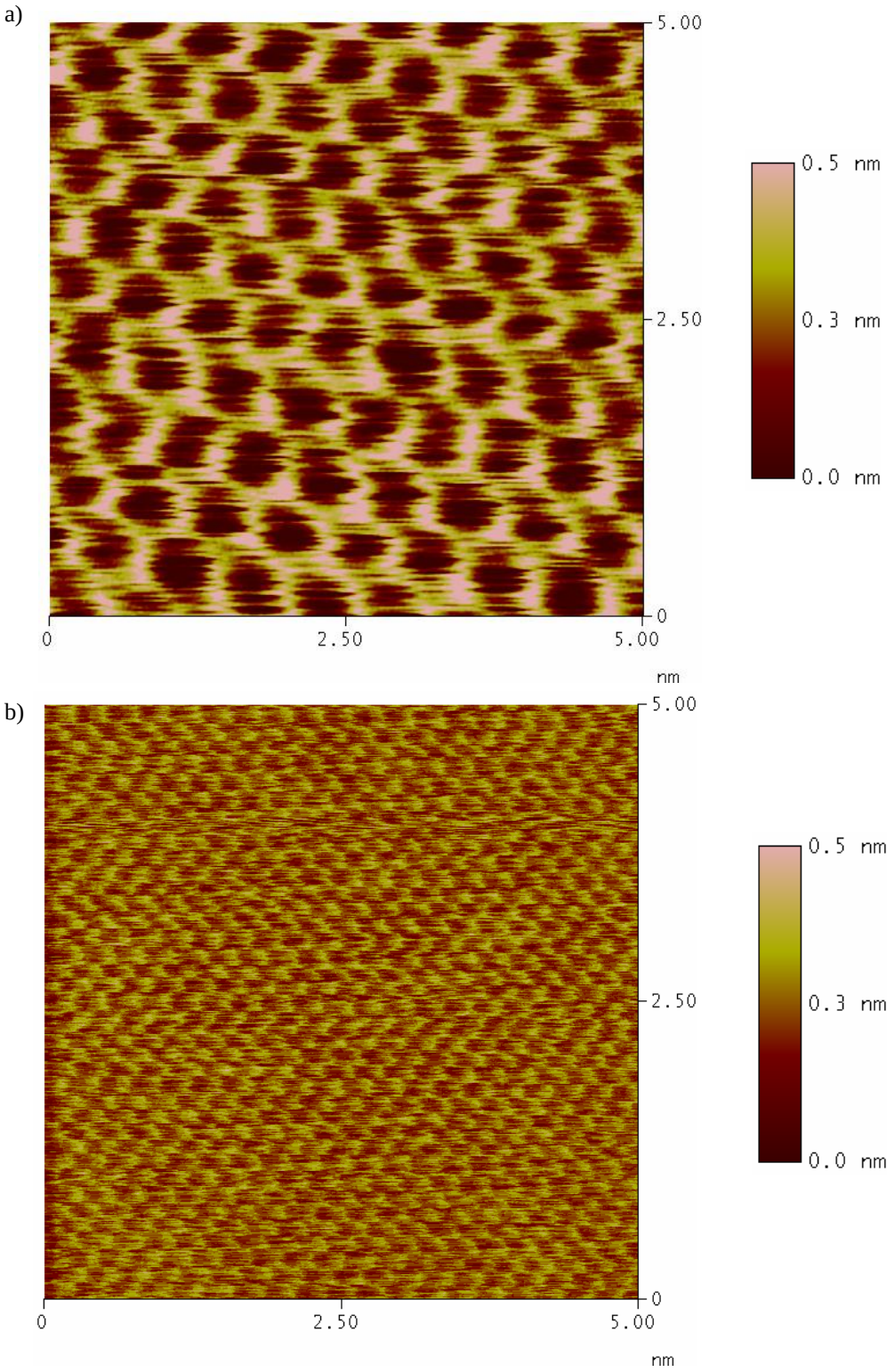

Figure 2.6: 5.00 nm x 5.00 nm AFM height images of a) mucosiva mica and b) highly-oriented pyrolytic graphite with a 0.5 nm height scale. Images courtesy of Cindy Berrie, University of Kansas.

2.2. Self-assembled monolayer Preparation

In addition to employing various bulk surfaces, some of these surfaces can be utilized further by tuning these surfaces by adding a layer of organic molecules with different terminal groups to form a monolayer.[42] In this manner, self-assembled monolayers (SAMs) are model surfaces in which the terminal chemistry can be tuned to the desired chemistry.[43] These are useful model surfaces which are well ordered and characterized.[29] Types of organic molecules used to form SAMs include alkane thiols, alkyl silanes, and alkenes. Alkane thiols bind to gold surfaces while alkyl silanes bind to silicon oxide or mica surfaces and alkenes bind to hydrogen terminated silicon surfaces. Thiols are somewhat easier to form and manipulate than organic monolayers on silicon, but can oxidize and deteriorate over time.[44-46] Monolayers on silicon are more stable over time and more robust than thiols on gold but are less well-ordered. Techniques such as SPR require surfaces that have available plasmons and so only the gold thiol monolayers are useful. All SAMs mentioned here are compatible with AFM and FTIR, alkanethiolates on BiaCore gold SPR chips are compatible with SPR.

2.2.1. General technique

The SAM formation process is a relatively straightforward but elegant process (Figure 2.7a-c) via spontaneous vapor or liquid deposition.[29, 47] The focus of this dissertation is with the latter. SAMs were formed by placing a clean substrate into a solution of molecules. These molecules have one end (α - highlighted in green in Figure 2.7a) which specifically binds to the surface that are typically connected to a

carbon chain, $(CH_2)_x$ (region between green and red in Figure 2.7a), and a terminal functional group (ω – highlighted in red in Figure 2.7a), where surface reactive groups include thiols, pi bond of olefins, and silicon-chloride groups for alkane thiols, alkenes, and silanes, respectively. After the reactive group binds to the surface, and as more molecules bind to the surface, they self assemble and align via van der Waals interactions amongst the hydrocarbon chains and stand up on the surface. Hydrocarbon chain length can vary from about 3-18 carbons, with an increase in stability as increase chain length due to increased van der Waals interactions.[42] Over time, more molecules attach to the surface and fill in holes and defects until a decent monolayer is formed. This process of binding to the surface and aligning of the molecules occurs spontaneously for thiols and silanes (on gold and silicon, respectively). For thiols, this occurs with molecules at a 27^o angle to the surface normal.[48] At maximum coverage, density of thiols on gold is about 4.5×10^{14} molecules/cm^2.[49] A well-formed monolayer can be achieved in 18-24 hours for most molecules, with only millimolar solutions required (Figure 2.7a). Molecules such as alkenes require a hydrogen terminated surface and heat to initiate the self-assembly process as depicted in Figure 2.7b.

This formation process leaves the terminal functional groups aligned at the opposite end from the surface reactive groups. The functional group can consist of any number of moieties, ranging from simple R-CH_3, R-COOH, R-OH, R=CH_2, R-NH_2, and halogens, to more complicated groups such as maleimides,[50] esters, carbohydrates, azulenes,[51] ligands, etc.[29, 52] The exposed surface chemistry can thus

be tuned according to the molecule initially utilized in the self-assembly process. Additionally, by having two different types of thiols in solution, a mixed SAM film can be produced. SAMs to resist nonspecific protein adsorption such as polyethylene glycols (PEGs) may also be utilized. Furthermore, additional modification of this terminal group may be conducted, either by charge in the cases of R-COOH or R-NH_2 or by additional chemical steps such as oxidation of double bonded or methyl terminal groups.

Thiols react with gold to form a stable RS-Au bond with 40-44 kcal/mol.[48, 49] Thiols can also react with silver, palladium, or copper to form SAMs.[29] Silicon-chloride undergoes hydration to form Si-O which then binds to silicon oxide surfaces with a bond energy of 130 kcal/mol.[53] Alkyl silanes also react with Si-O groups on mica and glass or aluminum oxides.[48] And olefin pi bonds undergo reduction to form a C-Si bond to hydrogen-terminated silicon with a bond energy of 70 kcal/mol.[53] The following sections detail any modifications made to these processes along with some specific surface control and preparation.

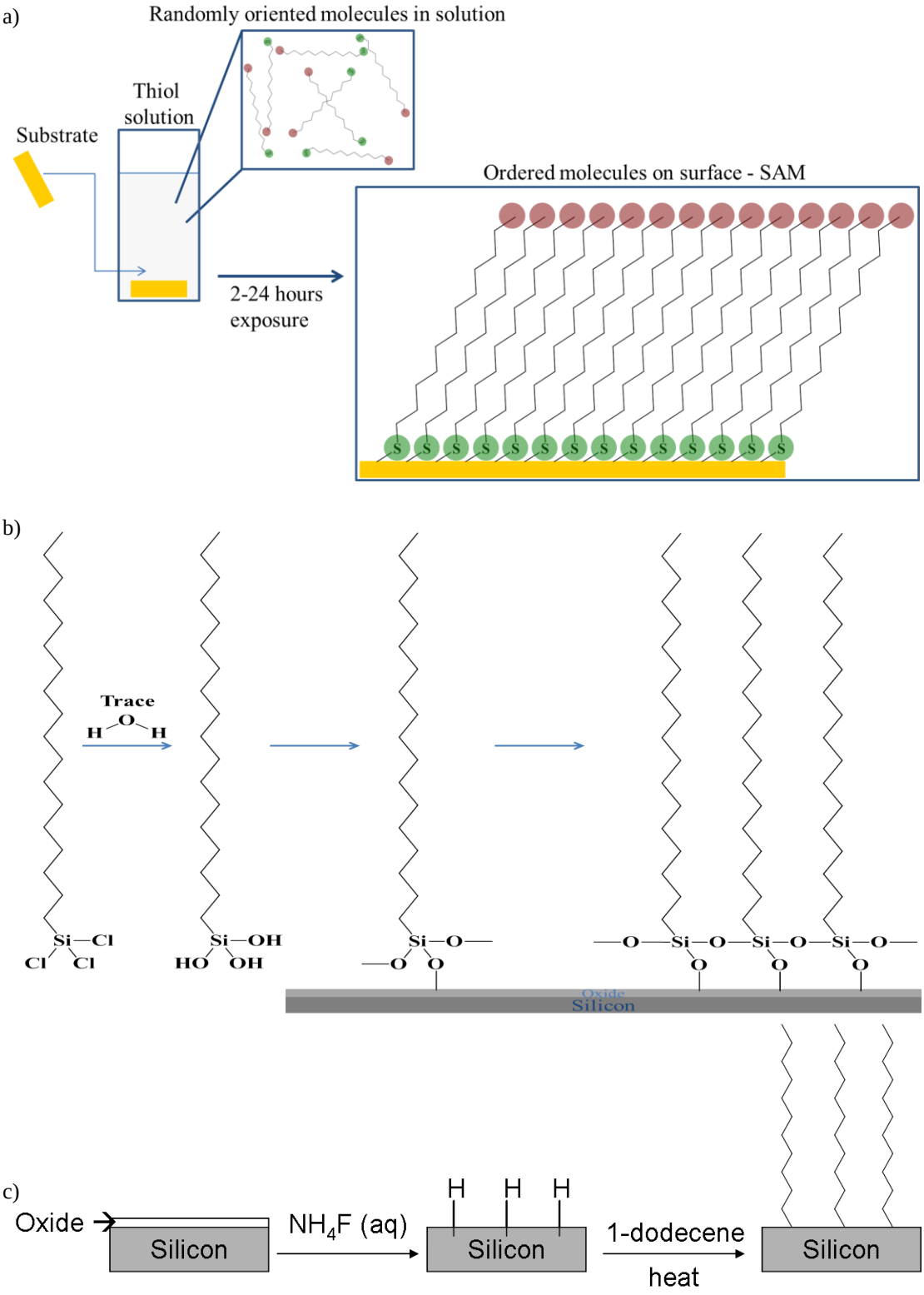

Figure 2.7: SAM formation of a) Alkane thiols (1-dodecanethiol) on gold, b) Alkyl silanes (octadecyltrichlorosilane) on silicon, and c) Alkenes (1-dodecene) on hydrogen terminated silicon.

2.2.2. Alkane Thiols on Gold

SAMs were prepared by placing clean gold (either via piranha cleaning or solvent rinsing) into solutions of generally 1-5 millimolar thiol in ethanol solutions for 18-24 hours or longer (Figure 2.12a).[29, 54] For dithiols, the concentration was typically higher at about 20 to 500 micromolar in ethanol. The terminal thiols specifically react with the gold to form bonds, tethering the molecules to the surface in a well-ordered manner. Samples were removed from the thiol solution and the SAMs were then rinsed with chloroform, acetone, and ethanol, and dried with nitrogen gas. Additional steps for R-COOH and R-NH_2 SAMs included addition of 2% by volume of trifluoroacetic acid to thiol ethanol solution and an extra rinsing step. This extra rinsing step helps to disrupt any double layered molecules that may have formed from hydrogen bonds between SAM molecules and solution molecules.[55, 56] This ensures that the resulting surface is the desired monolayer as opposed to a bilayer. SAMs were characterized via ellipsometry, goniometry, and AFM to confirm quality. Various names and corresponding structures of thiols utilized can be found in Figure 2.8.

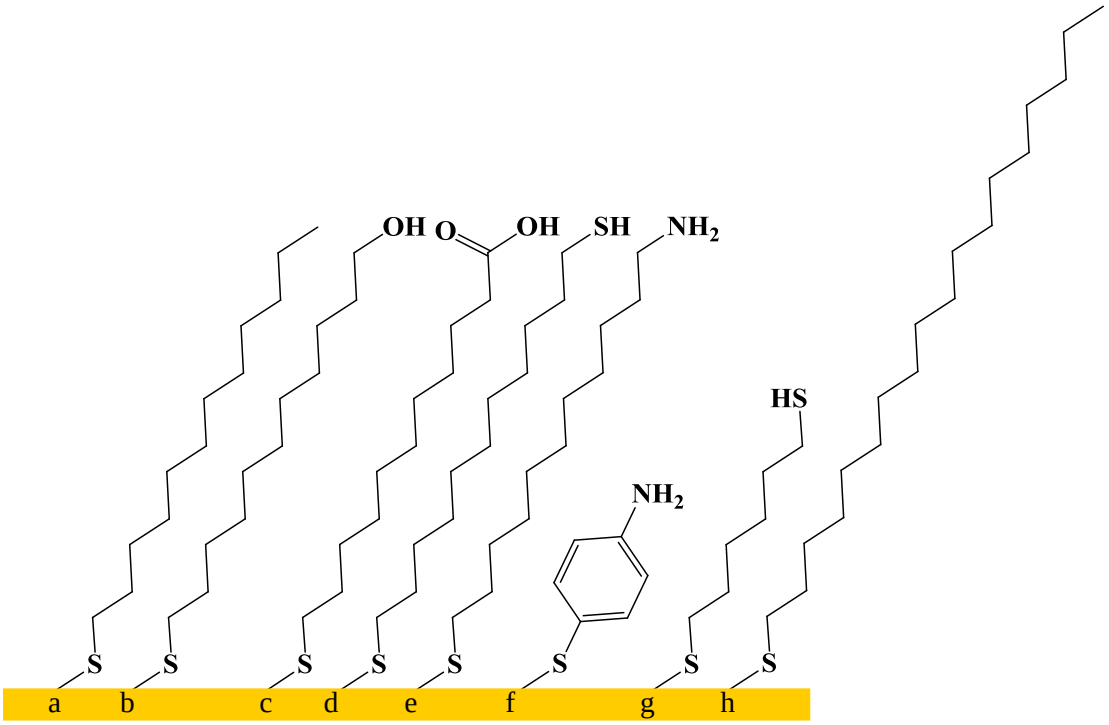

Figure 2.8: Various thiols for SAM formation: a) 1-dodecanethiol, b) 11-mercapto-1-undecanol, c) 11-mercaptoundecanoic acid, d) 1,11-undecanedithiol, e) 11-amino-1-undecanethiol, f) 4-aminothiophenol, g) 1,6-hexanedithiol, and h) 1-octadecanethiol.

These various thiols shown in Figure 2.8 were utilized in SAMs or grafting patterns to tune the surface chemistry and/or molecule length. 1-dodecanethiol and 1-octadecanethiol are methyl terminated molecules which are hydrophobic; the two molecules differ in length. Thiols with a hydroxyl, carboxylic acid, thiol, or amine terminal group (11-mercapto-1-undecanol, 11-mercaptoundecanoic acid, 1,11-undecanedithiol, 11-amino-1-undecanethiol, 4-aminothiophenol, and 1,6-hexanedithiol) are all hydrophilic. The carboxyl and amine terminated thiols have the advantage of charge tunability with solution conditions (negative or positive, respectively). Many of these terminal groups have the capability of additional chemistry after SAM formation,[29] but only the dithiol terminal functional group will be exploited in this fashion. These various thiol SAMs were characterized via ellipsometry and goniometry after formation.

2.2.3. Alkyl Silanes on Silicon

Formation of SAMs of alkyl silanes on silicon were performed as follows (Figure 2.7b).[57] Piranha cleaned silicon wafer pieces were rinsed with Milli-Q, dried with nitrogen gas, and placed in 2-5 millimolar solution of silanes (such as octadecyltrichlorosilane or octadecyldimethylchlorosilane) in hexane:chloroform (1:4) or in toluene (preferred solvent), capped, parafilmed, and left in solution for at least 2-48 hours. Substrates were removed from solution and the SAMs were then rinsed with toluene and water and dried with nitrogen gas. For alkyl silanes, trace amounts of water must be present for the reaction to initiate. Alkyl silanes have at least one chlorine group attached to the silane, these chlorine groups must be removed

and replaced by a hydroxide group. Then, the hydroxide group of the silane and the hydroxide group of the surface silicon oxide can react in a condensation reaction to form a silicon-oxide-silicon bond. If the alkyl silane contains multiple chlorine substituents, each of these may interact with water to form hydroxides. Thus, in the schematic shown in Figure 2.7b, the silane can interact with the surface and neighboring silanes to form multiple silane oxide bonds. This stabilizes the interactions and forms a more stable and uniform monolayer than silanes with only one or two surface active groups. SAMs were characterized via ellipsometry, goniometry, and AFM to confirm quality. These samples were either characterized and used immediately or stored under nitrogen until needed.

2.2.4. Alkenes on Hydrogen-Terminated Silicon

SAM formation of alkenes on hydrogen-terminated silicon was executed as follows (Figure 2.7c).[58-60] Piranha cleaned silicon wafer samples were hydrogen terminated by placing the wafers into a 40% ammonium fluoride water solution for about one to two minutes. The samples were rinsed with water and dried with nitrogen gas. Hydrogen-terminated silicon surfaces were then heated (~200ºC) or sonicated in neat alkene (either 1-dodecene or 1-octadecene) while purging with nitrogen gas for about two hours. The solution was allowed to cool to room temperature before samples were removed with tweezers. Samples were then rinsed with chloroform and dried with nitrogen gas. Samples were placed into sample vials, backed-filled with nitrogen, capped, and parafilmed until needed. Prior to use, SAMs

were then rinsed with toluene and water and dried with nitrogen gas. SAMs were characterized via ellipsometry, goniometry, and AFM to confirm quality.

2.3. Surface Characterization Techniques

Once a monolayer was formed, the properties of that SAM were confirmed by determining the thickness via ellipsometry, the hydrophobicity via goniometry, and the topography via AFM. A visual check of samples was also performed. In some cases, surface-enhanced infrared spectroscopy was performed to confirm terminal functional groups of SAMs on the surface. Other groups have used x-ray photoelectron spectroscopy (XPS) to confirm that SAMs are oriented upright on the surface with the terminal group exposed at the monolayer-air interface.[61] This section details these characterization techniques utilized to determine the quality of SAM formation.

2.3.1. Thickness Measurements via Ellipsometry

Surface characterization techniques typically began with a determination of self-assembled monolayer thickness via ellipsometry.[42] Ellipsometry works by shining elliptically polarized light (from a HeNe laser and polarizer) onto a surface (Figure 2.9a).[23] The change in polarization of the light that is reflected off the surface is detected. A general schematic (Figure 2.9a) is as follows: a laser light source (i) emits red light (λ = 632.8 nm) which passes through a polarizer (ii) to become polarized. Then, a quarter-wave plate (iii) converts this light into elliptically polarized light. The light (about 1 mm^2 in diameter)[5] hits the sample surface (iv) on the stage and is reflected (v). The light goes through an analyzer (vi) and finally into

a detector (vii). The changes in the angles (Del and psi) of elliptically polarized light are determined. Combined with knowledge about the optical properties of the substrate and monolayer, the thickness of the monolayer can be determined from these angle measurements. Comparing that thickness to literature values and the length of the molecule allows determination of monolayer formation. A well-ordered monolayer had a thickness close to literature values and the length of the molecule (as long as the tilt angle of the molecule is taken into account). Ellipsometry measurements have an accuracy of 0.1 Å or better.[5]

Thin samples (transparent or partially transparent) are less useful for ellipsometry measurements than opaque samples. If the light passes through the substrate to the underlying surface instead of through the monolayer and into the substrate, then the change in polarization of the light may be due to more than just the monolayer. The optical properties of the underlying surface such as epoxy, titanium, or glass may differ from the bulk gold properties. Therefore, since both the gold layer and glass components of BiaCore gold chips are thin and somewhat transparent, they are less suitable for ellipsometric measurements.

Table 2.3 contains typical optical constants different types of gold surfaces studied. In order to determine the thickness of the SAM films, a value for the refractive index, n=1.45 was assumed for this organic layer.[42] The angle (Phi) measured at was 70 degrees. Ellipsometry measurements employed different program methods, depending on the properties of the sample to be characterized. Sample methods included one for the calibration standard with silicon with thermally

grown oxide of about 1036 Å, one for determination of optical properties of substrate, one for monolayer thickness determination on a single layer substrate, and another one for double film on silicon substrates (oxide 15 Å and monolayer). Optical properties for silicon are 3.858 for n and 0.018 for k, where n and k are the real and imaginary components, respectively, of the refractive index of the substrate. The different models provided fitting of DELTA and PSI angles to extract either optical constants or a thickness depending on the sample. The optical properties of gold surface utilized are indicated in Table 2.3. These samples are not bulk gold, since they are only thin films with 50-350 nanometers of gold, and therefore the films behave differently, resulting in a variation of n and k values which are not too far from the expected values of 0.15 and 3.5 for n and k, respectively.

Table 2.3: Optical properties for all types of gold

Type of Gold	Optical Properties	
	N value	***K value***
Platypus (n=167)	0.163 ± 0.006	3.475 ± 0.023
Agilent (n=34)	0.156 ± 0.008	3.448 ± 0.099
BiaCore (n=83)	0.423 ± 0.073	3.385 ± 0.062
Evaporated (n=7)	0.137 ± 0.003	3.102 ± 0.045
Template stripped (n=62)	0.171 ± 0.088	3.541 ± 0.049
Flame annealed (n=7)	0.176 ± 0.006	3.413 ± 0.071

Utilizing these substrate and film optical properties, the various monolayers were characterized via ellipsometry to determine thicknesses (Table 2.4).

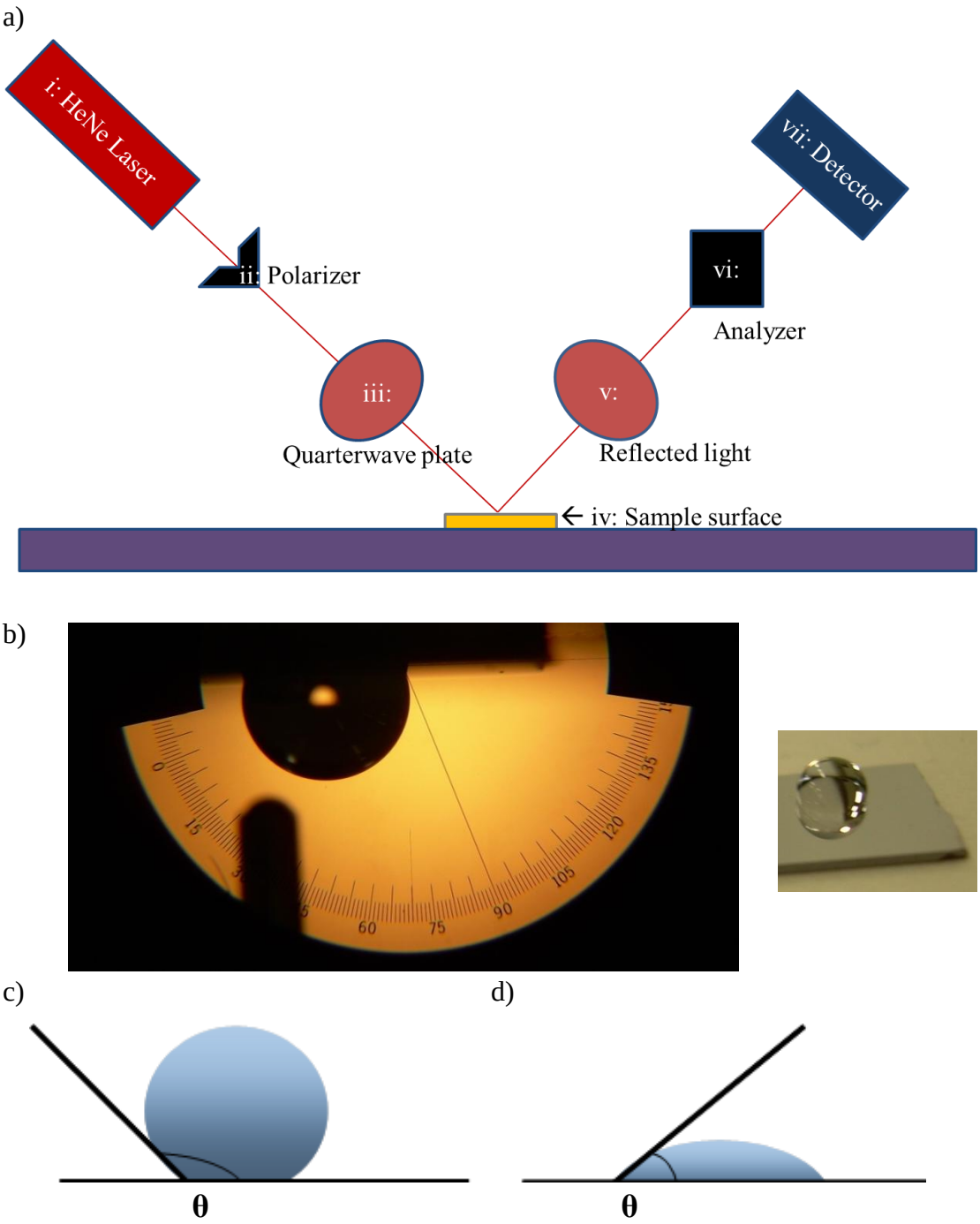

Figure 2.9: SAM Characterization Techniques. a) Ellipsometer Schematic with (i) HeNe laser, (ii) polarizer, (iii) quarter-wave plate, (iv) sample surface, (v) reflected light, (vi) analyzer, and (vii) detector.[23] b) Goniometer view and water droplet on methyl-terminated silane SAM on silicon, c) water droplet balled up on a hydrophobic surface, and d) water spreads out on a hydrophilic surface.

2.3.2. Surface Energy Measurements via Goniometry

Goniometry, a technique used to determine static contact angles of Milli-Q water on surfaces, provides an indication of surface hydrophobicity (Figure 2.9b-d).[62] Both chemistry and topography play a role in the way water sits on a surface. A water droplet beads up on a hydrophobic surface, (Figure 2.9b-c) resulting in contact angles above 90 degrees, with 110 degrees as a typical contact angle for a well ordered hydrophobic surface such as methyl-terminated SAM films. Contact angles between 30-90 degrees were indicative of a mixed degree of hydrophobicity/philicity. A hydrophilic surface was fully wettable or had a low contact angle (0-30 degrees as in Figure 2.9d). Gold was generally 40-60 degrees depending on how clean it is (unclean samples have a higher contact angle due to hydrocarbon contamination). Typical contact angles for the samples studied can be found in Table 2.4. The gold substrate had a contact angle of 41 degrees, which was hydrophilic. As expected, all the hydrophilic SAMs had low contact angles since water will spread out on a hydrophilic surface. The methyl terminated SAM was hydrophobic, as such, the water droplet balled up on the surface and produced a high contact angle as expected.

Wettability can be a good indication of a well-formed monolayer.[61] If the contact angle matches expected values, this is a good indication of a densely packed monolayer with the terminal groups exposed at the monolayer-air surface. If the contact angle is lower than it should be for hydrophobic monolayers on gold, this may be an indication of low packing density as the water droplet may see the surface.[42, 61] If the contact angle is higher for hydrophilic monolayers, this may be an indication of

low packing density with chains tilted over at a greater angle, where the methylene groups within the chain impede the water spreading. As long as the surface is smooth, roughness should not significantly impact the surface interaction with the water droplet. However, if roughness is a factor, than the true contact angle is related to the observed by the following equation: $\cos \theta_{observed} = r \cos \theta_{true}$.[61] Therefore, for hydrophobic surfaces roughness may increase the apparent or observed contact angle and for hydrophilic surfaces may decrease the apparent contact angle.

Table 2.4: Ellipsometry and Goniometry Results for SAMs.

Terminal Group Structure	***Literature Thickness (Å)***	***Experimental Thickness (Å) (n=7)***	***Literature Contact Angle (°)***	***Experimental Contact Angle (°) (n=6)***
Au	n/a	n/a	25-40[32]	41 ± 2
HS-$(CH_2)_{11}$-**COOH**	15 ± 3[63]	13.9 ± 4.6	<10,[55 a1] 35 ± 2,[55 a2] 8-29[64 b]	28 ± 3
HS-$(CH_2)_{11}$-**OH**	16.0 ± 1.0[65]	16.3 ± 7.4	13,[66] 34.2 ± 2.9,[65] 29 ± 3[64]	33 ± 3
HS-$(CH_2)_6$-**SH**	7[67]	9.5 ± 0.6	40-50[68]	37 ± 2
HS-C_6H_4-**NH_2**	8[69]	6.9 ± 1.9	57 ± 5[70 c]	70 ± 2
HS-$(CH_2)_{11}$-**NH_2**	18[71]	20.4 ± 4.7	28 ± 2,[55 a3] 43 ± 5,[55 a2] 25-42[64 b]	35 ± 4
HS-$(CH_2)_{17}$-**CH_3**	28-29,[72] 25.3 ± 0.5[73]	24.0 ± 7.2	108 ± 2[70 c]	108 ± 1
HS-$(CH_2)_{11}$-**CH_3**	20,[72] 17 ± 1[74]	16.5 ± 0.3	110,[70] 110 ± 2[64]	110 ± <1
Cl_3Si-$(CH_2)_{17}$-**CH_3**	25[75]	31.4 ± 0.9	114 ± 2[75]	106 ± 1
H_2C=HC-$(CH_2)_9$-**CH_3**	13[59]	20.5 ± 0.9	110 ± 3[59 c]	97 ± 2

Notes: a) Contact angles for SAMs prepared under different solvent conditions a1) ethanol with 2% CF_3COOH, a2) ethanol, or a3) ethanol with 3% $N(CH_2CH_3)_3$., b) Contact angles were pH dependent, and c) Contact angle values were calculated by averaging the advancing and receding contact angles; errors were calculated via propagation of errors.

Results of characterization of these various thiol, silane, and alkene SAMs found in Table 2.4 and for the most part match well with literature values.

2.3.3. Surface Structure Analysis via Atomic Force Microscopy and Visual Inspection

AFM characterization was utilized to determine topography of surfaces or molecules on surfaces. Grain sizes of gold and roughness of surfaces and monolayers were measured and calculated with contact mode AFM. SAMs were also subsequently characterized and modified via AFM. General AFM technique information can be found in section 2.4.

A visual inspection of samples was performed. For gold samples made in-house, the transparency was checked. Samples that were transparent had only a very thin a gold layer and as such did not generally produce meaningful ellipsometry data. Gold samples with decent thickness were generally opaque. With silanes, any cloudiness or roughening of the surfaces was generally indicative of polymerization of molecules and monolayer formation was compromised. Samples which failed to exhibit acceptable characteristics were rejected and not used in further studies.

2.4. Atomic Force Microscopy

AFM is a powerful tool for studying features at the nanoscale.[76] With this technique, it is possible both to image and to modify surfaces at size scales needed both to investigate and to control protein surface interactions without moving the sample. As detailed later, AFM can be used to study biological molecules under pseudo-physiological conditions. AFM has wide flexibility in terms of experimental

operating conditions (dry or fluid) and the types of surfaces employed. AFM provides the ability in a single experiment to create model structures, image those surfaces, adsorb protein directly to that pattern, and image the protein without ever having to expose the surface to another interface (air-water) or switch instruments. For AFM to be an amenable technique, flat surfaces must be employed to be able to resolve and distinguish protein features from surface features. Surfaces should be uniform with low roughness, and robust.[77] Advantages of gold and silicon are that they exhibit these requirements and allow modification to these surfaces via SAMs. Thus, it is possible to eliminate one variable (the type of surface), but still vary the chemistry at the surface. The ability of AFM to resolve features down to a few nanometer length scales (proteins are tens of nanometers in size) in realistic conditions (fluid with physiological conditions) makes the technique amenable to monitoring protein-surface interactions. The structure and conformation of proteins adsorbed to surfaces can be determined without use of labeling (which could interfere with natural adsorption modes). Additionally, AFM is capable not only of creating patterns of the same or different chemistries but also characterizing these, allowing determination of the effect of topography and/or chemical functionalities on protein adsorption characteristics. AFM provides flexibility in terms of the types of functionality and shapes and spatial location of patterns down to molecular sizes with impressive resolution.

2.4.1. Technique Description

Atomic Force Microscopy (AFM) is a surface technique that provides surface topography, friction, force, and phase images. A schematic of a typical AFM system is shown in Figure 2.10. The typical output is a topographical map of the surface and any components adsorbed to the surface. AFM works by raster scanning a sharp tip on a cantilever across the surface. As the tip encounters features on the surface, the cantilever deflects vertically. By aligning a laser on the back of a cantilever this deflection can be monitored, magnified, and recorded as the laser light hits a four quadrant photodiode detector. The laser is also aligned within the center of this detector. As a function of position, a map or topographical profile of the surface features is constructed. AFM modes include contact mode, tapping mode, friction, or force – volume imaging, among others. The scanner is calibrated with a commercially available standard sample.

An AFM chip is a long substrate with one or more cantilever beams (rectangular or triangular in shape) at one end. At the end of these beams is a pyramidal shaped portion known as the tip (Figure 2.10b-c), which is used to image the surface. Force constant, resonance frequency and tip radius of curvature are key qualities of AFM cantilevers. Depending on the experiment, different tips are required. The force constant provides insight into tip sturdiness (typical force constants are tip dependent and range from 0.06 N/m to 14 N/m). Higher force constants are indicative of sturdier cantilevers and lower force constants, more flexible cantilevers. Depending on the surface and goal of the experiment, different

force constants are desired. For etching or robust surfaces, a higher force constant is desired; for softer surfaces, a lower force constant is desired. Resonance frequency is the inherent frequency at which the tip oscillates (typical values range from 10 kHz to 315 kHz depending on the stiffness of the tip). Tips with low spring constants are useful for imaging in fluid, while tips with a high spring constant are useful for dry imaging. Tip curvature describes the shape and size of the tip; typically, the sharper the tip, the better the resolution (typical values are less than 10 or 20 nanometers).

For our AFMs, the sample size needs to be about the size of an AFM puck (about one and a half centimeters in diameter) or smaller. Samples were adhered to a magnetic puck via sticky tabs to secure in place onto the piezo on the instrument. Sample movement during imaging is undesirable. Resolution and noise in the system depends on the rigidity of the microscope. Relative movement causes a decrease in resolution.

Adjustable AFM parameters include scan controls such as scan size, scan dimensions, scan angle, scan speed, lines per scan, and feedback controls such as gains, and deflection setpoint force or setpoint amplitude. Scan size is the area of the scan desired (nanometers to micrometers). Scan dimensions or aspect ratio involves control over the length and width of images and is adjustable from 1:1 to 256:1 where the first number is the width and the second the length (so a box or rectangles of decreasing length). Scan angle or the direction in which the sample moves under the tip is adjustable from 0 to 360 degrees. This means patterns can be made in a greater variety of shapes (stars, letters, and vs, versus just bars, boxes, or ts). Samples/line or

lines per scan is a factor of the data points collected during the scan (for our purposes this is set at the maximum, 512 lines per scan). Scan speed or rate is how fast the tip moves across the surface. Typical scan rates for imaging in contact mode are 1-5 Hz, and in tapping mode are 1-2 Hz, and adjusted as needed. Gains (both integral and proportional) deal with how well the tip tracks the surface and can be adjusted as need be. Deflection setpoint determines how hard you are pressing into the surface or the force applied to the surface. Typically, if simply scanning a surface this value is set as low as possible (0.1-1 volts), to minimize imaging forces which could disturb the sample. The greater the voltage, the greater force the tip applies to the sample. This can be calibrated to determine the amount of force applied. In tapping mode, the feedback parameter is the amplitude of oscillation, which decreases as the tip approaches the sample.

Image options utilized include height, deflection, friction, or phases with adjustable height or voltage scales. For the types of samples investigated in this work, height scales were typically set to ten nanometers. These scales are color coded, with a gradual decrease in the color shade indicative of higher points on the image (brighter spots are higher off the surface; darker spots are deeper on the surface). Voltage settings are similar in that a color gradient represents different voltage values. Images can be obtained in the trace or retrace scan direction. This feature enables a check to ensure the image is same both directions. This helps to disregard or eliminate artifacts (somewhat) and is a key element in obtaining useful friction images.

a)

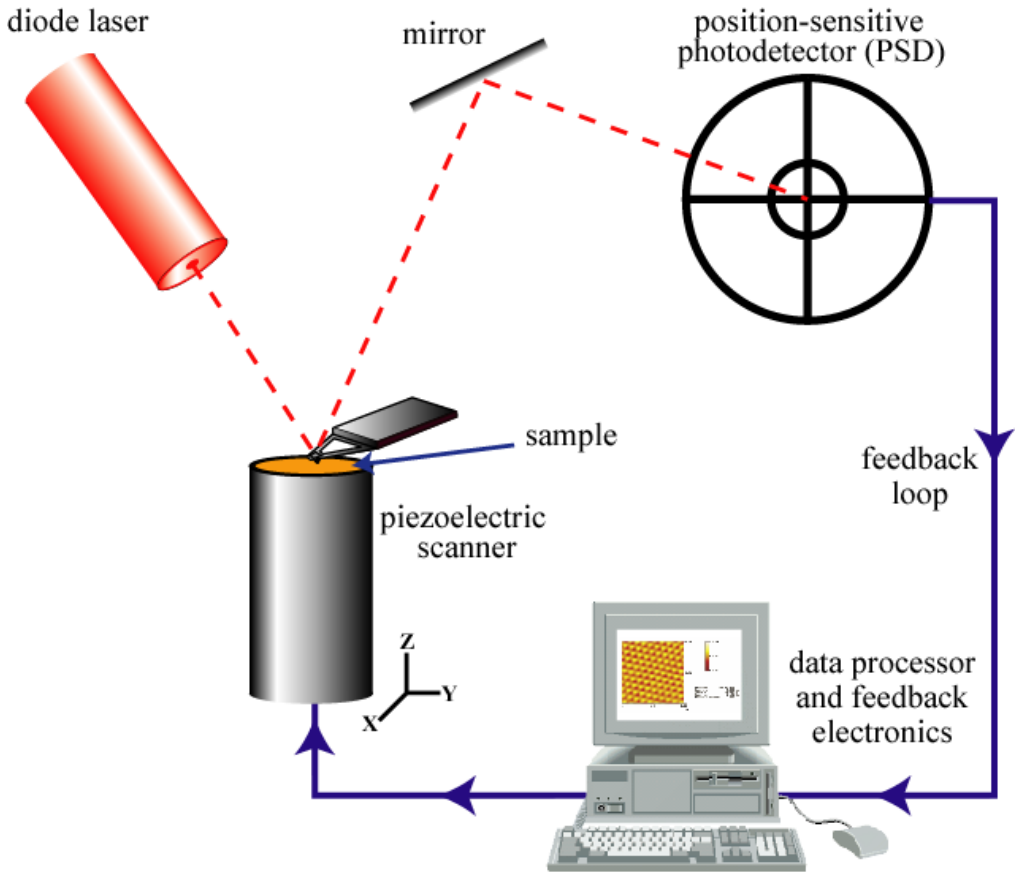

b)

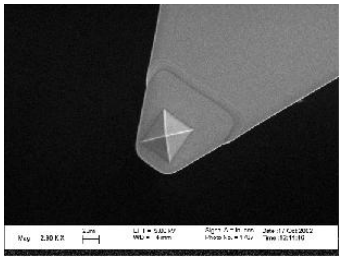

c)

Figure 2.10: a) AFM Schematic, b) SEM top-down image of AFM cantilever and tip (Courtesy of Dr. Jill E. Headrick, University of Kansas), and c) Magnified side-view picture of AFM cantilever and tip (with assistance from Gregory J. Smith).

2.4.1.1. Contact Mode

Contact mode AFM involves simply bringing the tip into contact with the surface and then raster scanning the tip along the surface. Tip is in contact with the surface and closely tracks surface features via software that controls the deflection voltage to match the setpoint voltage. The laser signal from the top two quadrants of the photodetector minus the bottom two quadrants (vertical deflection) is monitored. The output is a topographical map of surface features and anything adsorbed on the surface. This topography is viewed with a height scale bar where a color variation indicates surface features; the lighter the color, the higher the feature and the darker the color the lower the feature. A completely flat surface exhibits little to no color variation, as exemplified in a 2.00 μm by 2.00 μm contact mode AFM image of atomically flat mica (Figure 2.11). The dimensions of the surface and/or adsorbent features can be measured. In contact mode, since the tip is in contact with the surface, a lateral force is applied to the surface and anything adsorbed on the surface.

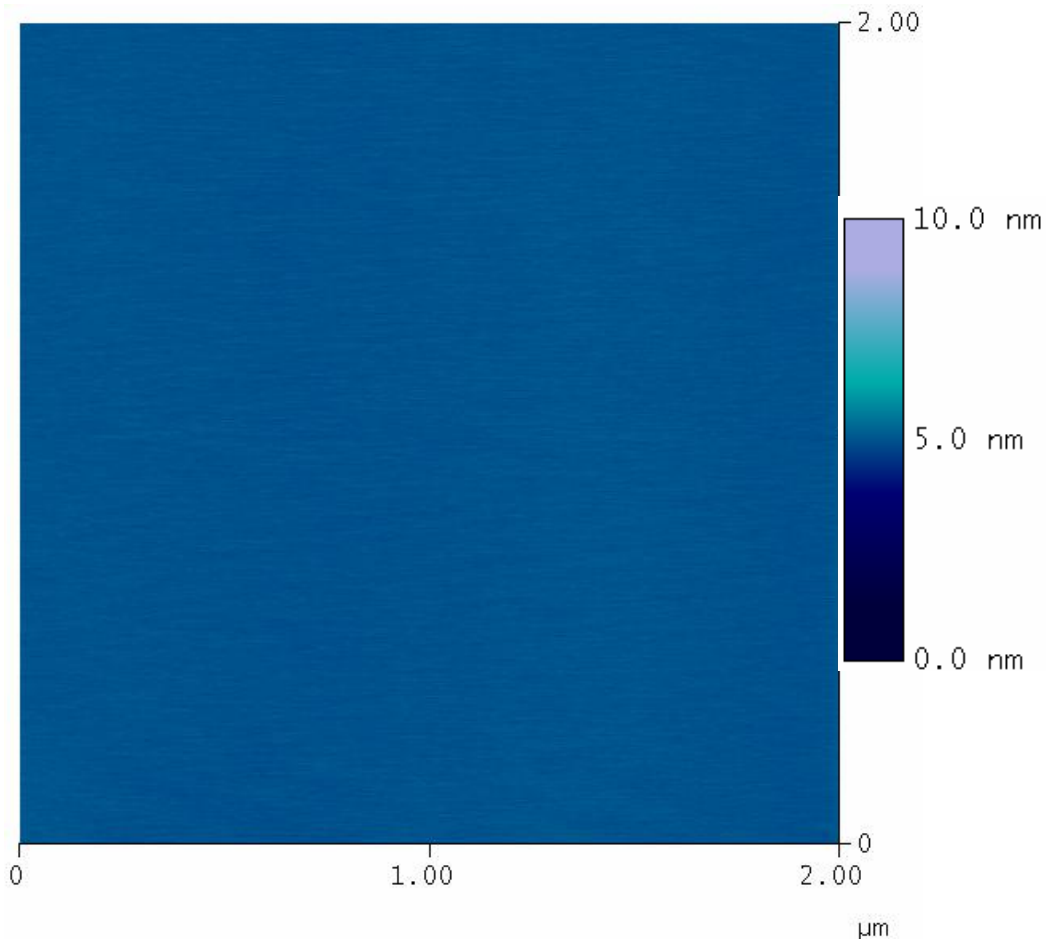

Figure 2.11: AFM height image of atomically flat mucosiva mica 2.00 µm x 2.00 µm scan area with a 10.0 nm height scale.

2.4.1.2. Tapping Mode

The lateral force applied by the AFM tip in contact mode can sometimes be too much for soft samples such as proteins. For example, fibrinogen was allowed to absorb onto mica and the surface was rinsed and dried. A 2.00 micron by 2.00 micron area was subsequently imaged in contact mode (Figure 2.12a). After adsorbing protein to a surface and imaging via AFM in contact mode, no protein appeared to be bound. Only a constant color was observed, the image lacked bright spots that would have indicated fibrinogen adsorption (the surface was flat with no variation); the image was very similar to the initial mica surface (Figure 2.11). Then, tapping mode was utilized to image an expanded 5.00 micron by 5.00 micron area at the same spot (Figure 2.12b). Fibrinogen molecules were observed on the surface (brighter spots) except in the 2.00 micron by 2.00 micron area previously scanned in contact mode where the protein molecules were pushed out of the imaging area by the lateral force of the tip as evidenced by the buildup of proteins at the edge of the scanned area (See Figure 2.12b). This is because contact mode AFM applied too much lateral force from the tip to the adsorbed proteins, causing the proteins to be moved (cleared) from the scan. This is visible upon zooming out and switching to tapping mode (a gentler imaging mode).

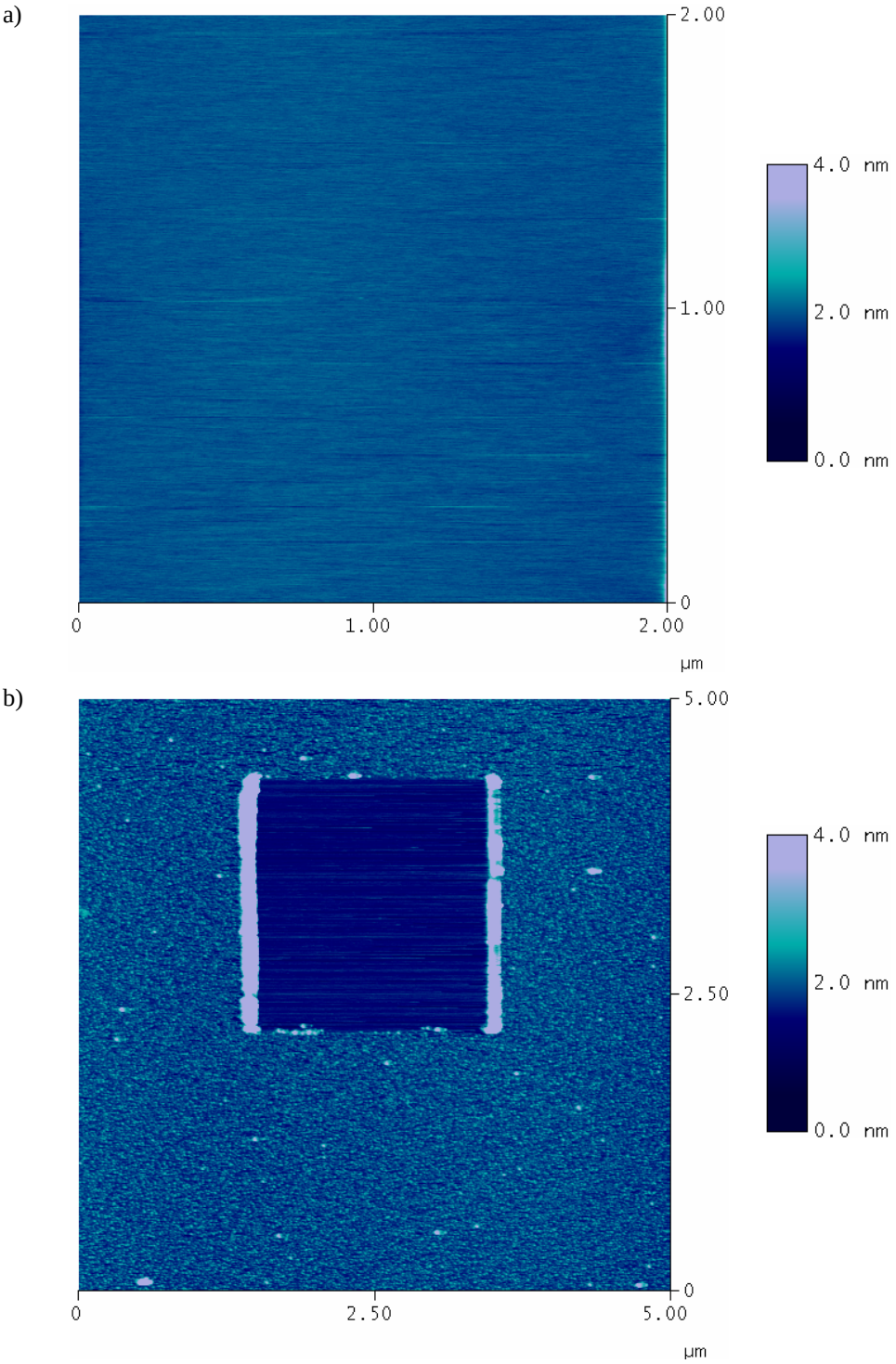

Figure 2.12: Importance of Tapping Mode for Soft Samples. a) 2.00 µm x 2.00 µm contact mode AFM height image of fibrinogen adsorbed onto mica imaged with a 4.0 nm height scale; no evidence of protein adsorption observed. b) 5.00 µm x 5.00 µm tapping mode AFM height image of same area with a 4.0 nm height scale; the area previously scanned is free of protein because the lateral force of the AFM tip pushed the protein molecules across the surface to the edge of the scan area.

Tapping mode relies on properties of the cantilever. In tapping mode, the cantilever is tuned to a value close to the resonance frequency, 10-80 kHz or 120-405 kHz depending on the cantilever set used. In fluids, this tuning value is much lower (10s of kHz). Then, the cantilever is oscillated while it scans across the surface and is intermittently in contact with the surface. The setpoint tip amplitude is related to the force applied to the sample. The change in amplitude of this oscillation is monitored. As the tip hits a feature on the surface, the amplitude is dampened. This produces a topographical map of the surface and anything adsorbed to it, as in contact mode. However, tapping mode applies less lateral force to the sample than contact mode, enabling imaging of soft materials such as proteins.

2.4.1.3. Friction

AFM is typically used to obtain topographical information, but often additional information that goes beyond topography is desired. To gain further information about the surface features, another mode, friction, can be employed simultaneously with contact mode. Friction mode allows the determination of different chemistries at the surface, even when the heights of such features are the same. One example of this, a 1,11-undecanedithiol star shape (approximately 10 μm long by 2 μm wide bars at 45º, 90º, and 315º) was patterned into a 1-dodecanethiol SAM resist matrix shows that the heights are roughly equivalent (one-dimension schematic in Figure 2.13a). The resulting AFM image shows no variation in height within the star pattern region (Figure 2.13b). Just by viewing the height image, it is

not possible to discern successful patterning. Thus another mode of imaging, friction, was necessary to view this pattern.[78]

a)

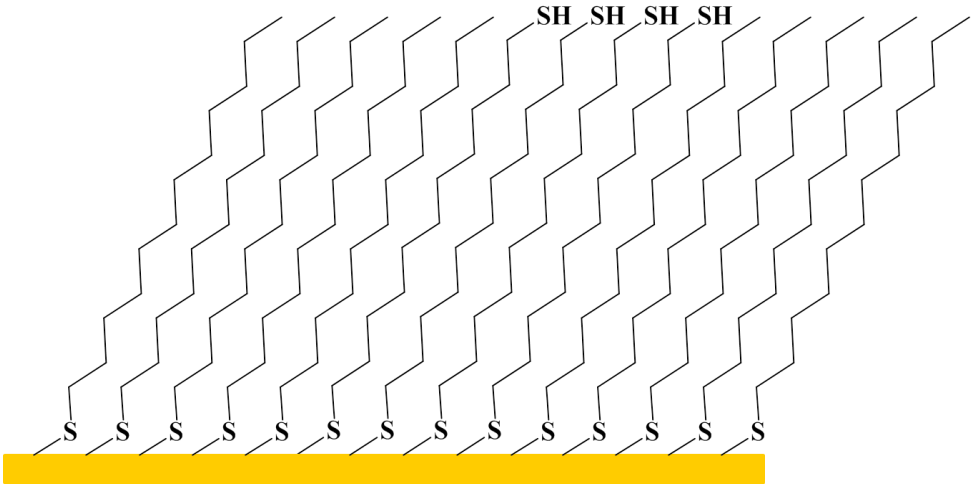

b)

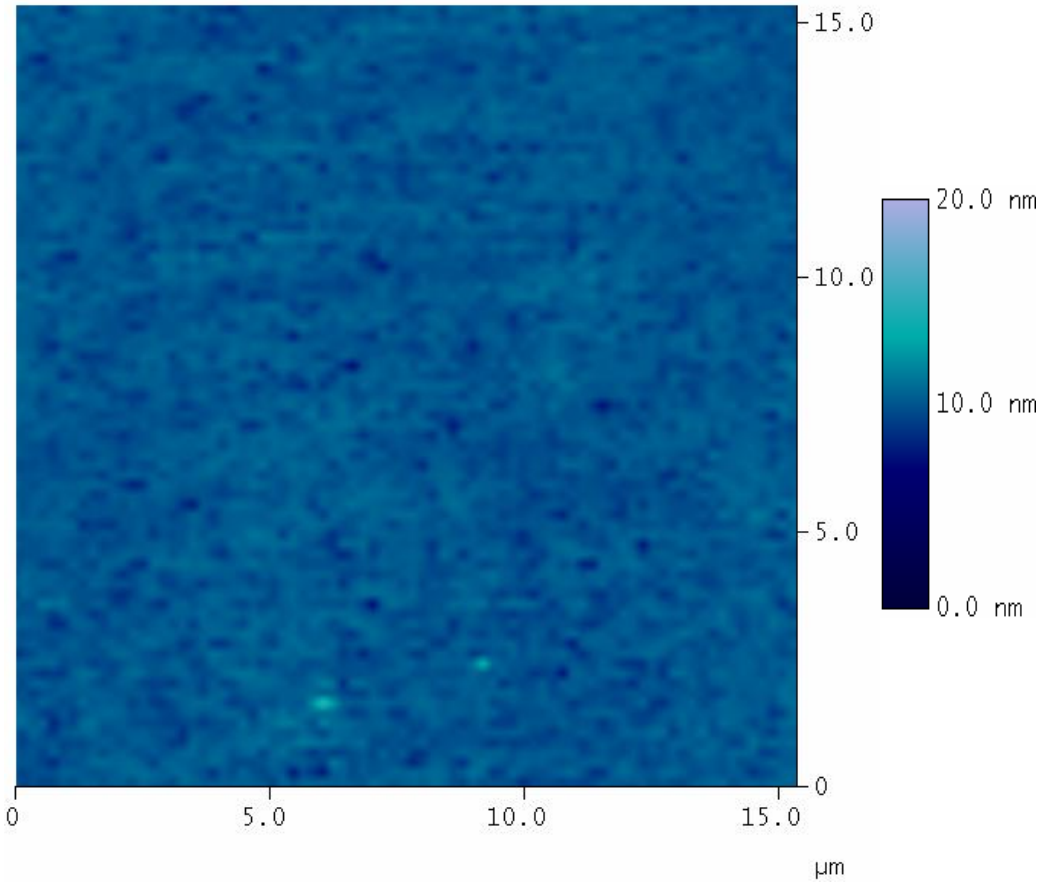

Figure 2.13: a) Schematic of 1,11-undecanedithiol grafted into 1-dodecanethiol matrix SAM on gold. b) 15.0 µm x 15.0 µm AFM height image of 1,11-undecanedithiol star patterned into 1-dodecanethiol resist matrix on gold with a 20.0 nanometer height scale.

Friction mode is performed at a scan angle of 90 degrees and works by the cantilever twisting as it moves across the surface. The laser light detected on the photodiode in the left two quadrants minus the right two quadrants (horizontal deflection) is monitored. Friction mode images are the result of attractive forces of the tip to the surface. This attractive force depends on the type of chemistry on the surface and thus changes with a change in chemistry or functional group(s) on the surface. The AFM tip used is generally silicon nitride, which is hydrophilic. As such, the tip has a greater affinity for hydrophilic surfaces than hydrophobic surfaces. Thus as the tip scans, it will be more attracted to hydrophilic features and less so to hydrophobic features. If the surface is of uniform chemistry, the friction will be uniform. However, as the tip scans a hydrophobic surface with a hydrophilic pattern, the friction will be low on the hydrophobic surface and once it reached the hydrophilic pattern, the magnitude of the friction will increase until it reaches another hydrophobic portion were it pulls off. The cantilever twists in one direction in trace scan and the other direction in retrace scan. Mapping out this difference between the two trace scans results in a friction plot or image. This phenomenon is opposite in the trace and retrace direction of scanning and thus a contrast between the two is observed (see Figures 2.14). The friction images example is a 15.0 micron by 15.0 micron image of a star 1,11-undecanedithiol (hydrophilic) pattern into a 1-dodecanethiol (hydrophobic) resist matrix. The trace image (2.14a) has a dark star compared to the matrix background while the retrace image star is lighter (2.14b).

Thus, according to the friction images, the chemistry within the pattern differs from that outside the pattern as expected and grafting was successful.

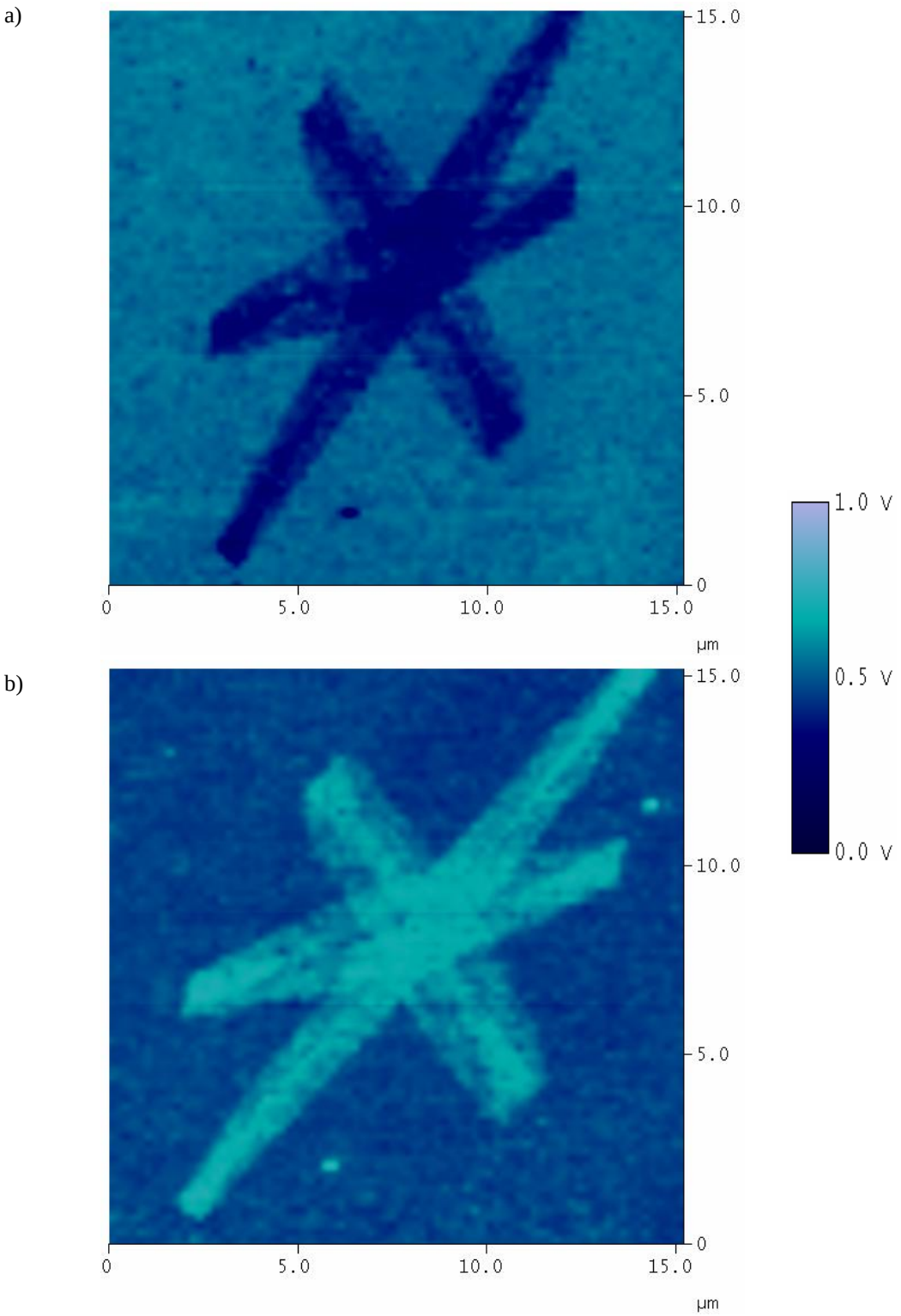

Figure 2.14: 15.0 µm x 15.0 µm AFM friction images of a) trace and b) retrace of a 1,11-undecanedithiol star patterned into a 1-dodecanethiol background matrix on Platypus gold with a 1.0 voltage scale.

2.4.1.4. Imaging Conditions (Dry versus Fluid)

AFM measurements can be performed in dry (ambient air or vacuum) or in fluid environments. Dry measurements are standard and involve a regular tip holder with ambient lab conditions. No special precautions are necessary for dry measurements. Dry imaging offers a flexible, quick, and facile set up. The sample is merely adhered to a puck and placed on the piezo. The tip is placed into the tip holder and set into the AFM. Then the laser is aligned, the laser signal maximized, and centered on the photodiode. Then one can engage and image a surface. Additionally, with dry imaging, surface modification(s) is (are) feasible. Additionally, dry imaging often provides better resolution than fluid imaging. Unfortunately, issues with dry imaging exist, especially in the case of biological samples because this removes them from their native environment.

Fluid measurements are performed using a fluid cell. Fluid measurements are performed when the sample and/or the surface are sensitive to air, when solution exchange is desired, or in order to carry out reactions. Proteins can be denature and/or dry out upon exposure to air. Solution exchange allows for systematic testing of different buffers or buffer conditions with the same surface or introduction of new components to the system. Additional reactions including grafting or chemical/biological reactions may be performed as well, which typically involves fluid exchange. Fluid cell measurements involve securing the sample to the fluid cell via an o-ring and vacuum grease. This creates a chamber containing a portion of the sample and the tip where fluid can be introduced. The piezo scanner is sensitive to

fluid (will be damaged if gets wet) thus, special precautions and checks to ensure fluid does not leak. Fluid cell experiments allow surface and sample imaging without exposing either to the air-water interface. The type of fluid introduced to cell can vary greatly and is limited by adverse interactions with fluid cell, sample, or o-ring. Some fluids are better for imaging than others. The fluid cell is sensitive (may dissolve the o-ring) to harsh organic solvents such as chloroform. Buffer solutions are usually compatible provided that they are clean and filtered as salts can deposit from or crash out of solution onto the surface, which may complicate data analysis. Also some surfaces are easier to image in fluid than others. For example, hydrophobic surfaces are sometimes harder to image in fluid due to the appearance of nanobubbles (image a small air bubble instead of surface or adsorbents).[79] Weak resonance of cantilevers in fluid can lead to difficulty tuning. Additionally, some cantilevers have a resonant frequency, which falls in audible range (8-20Hz) and can be ear-piercing.

Despite these drawbacks, fluid measurements are often crucial for success of experimental objectives. Dry modifications are incapable of patterning thiols because simply etching of a thiol on gold dry does not work because the thiol molecules fill back into the spot.[80] Fluid experiments are also necessary when grafting thiols into thiol SAMs on gold. Additionally, imaging in fluid allows one to view the same spot and monitor changes over time. Advantages of fluid imaging include ability to modify surfaces and mimic physiological conditions.

2.4.2. Biological Imaging

Biological imaging provides insight into the conformation or orientation of the adsorbed molecule. In the case of proteins, this can provide information on the degree of denaturation and spreading of the protein on the surface after adsorption. Additionally, this can determine potential functionality, for example addition of antibody to determine if binds to its antigen,[81, 82] or DNA hybridization,[83] or addition of thrombin to see if polymerization occurs,[84] protein oligomerization,[10] or bacterial shape changes upon antibiotic treatments,[76] or rotation in the case of ATPase,[85] etc. Tapping mode is typically essential for imaging biological samples such as proteins. As seen earlier (Figure 2.12) the lateral force in contact mode can move soft samples such as proteins out of the imaging area. Dry imaging may be performed to get a general idea of protein shape on the surface and typically yields better resolution of the protein. However, fluid measurements often mimic the protein environment better and have the advantage of not exposing the sample and proteins to the air/water interface. This may be needed to maintain the protein in pseudo-native environment, perhaps lessening the likelihood of the protein to denature. Immobilization strategies play a critical role in the ability to image proteins with AFM.[86] A wide array of proteins systems and other biological molecules adsorbing to surfaces have been studied. These include but are not limited to DNA,[87] purple membrane surfaces,[88] c-ring of ATPase,[89, 90] proteins,[12] and antibodies,[91, 92] among others. Protein changes have been observed as well, including conformational changes,[93] polymerization,[94] and subsequent binding events.[95] Figure 2.15 shows an example AFM height image

(~150 nm by 150 nm) of two fibrinogen molecules on a graphite surface. The bent trinodular structure of these molecules is clearly evident.

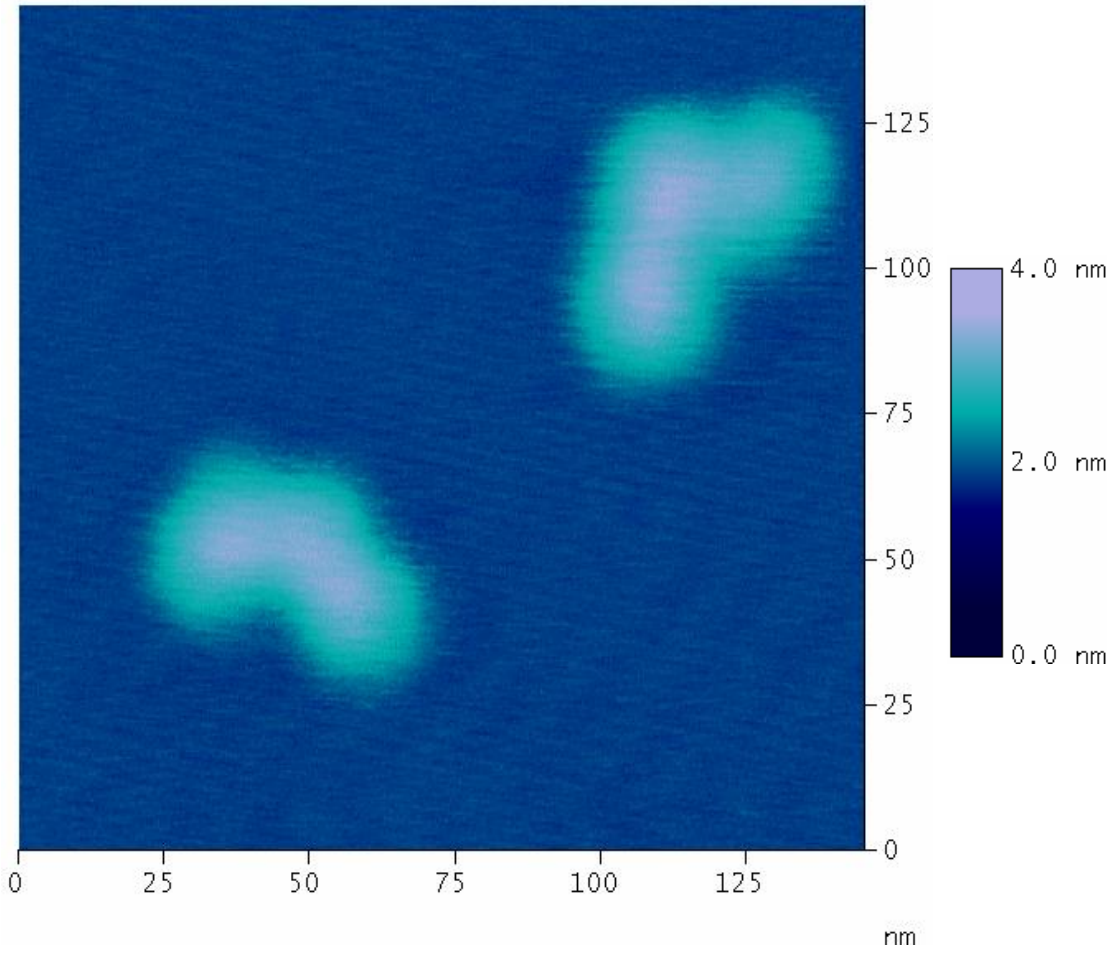

Figure 2.15: 150 nm x 150 nm AFM height image of fibrinogen adsorbed onto graphite with a 4.0 nm height scale.

2.4.3. Patterning via AFM

AFM is also useful for surface modification or patterning at the micron scale and even down to the nanoscale. The size and shape of patterns depends on the range of the scanner and the creativity of the user. The maximum scan size (for a single pattern) depends on the range of scanner used; NanoScope® IIIa and NanoScope® E have a maximum scan size of 13.2 and 17.2 square-micrometers respectively, while a NanoScope® J has a maximum scan size of 100 square-micrometers. The minimum pattern size is limited by the size of the tip; typical radius of curvature for tips is less than 10 nanometers.[96] Pattern shape is controlled by modifying the dimensions and scan angles to suit desired pattern. Patterns range from simple boxes or line to more complex patterns of letters, words, stars, and other shapes, to even more sophisticated and elaborate patterns such as symbols, networked systems, scribes and even a school seal (UC Davis Seal[97]) An example patterned image, a 1.00 μm by 1.00 μm AFM height image of the letters "K" and "U" etched into a monolayer to form KU, school initials for the University of Kansas, is shown below (Figure 2.16). Patterns can be created either via direct methods or automated with control over the sizes of patterns, both length and width. Additionally, either individual patterns or arrays of patterns (with a multiple cantilevers) can be created with AFM. Applications of AFM patterning include wire fabrication, protein and/or cell patterning, and devices fabrication. Patterns have been created using AFM that range as small as 10 nanometers to as large as one micron,[82] and J scanners can get up to tens of microns.

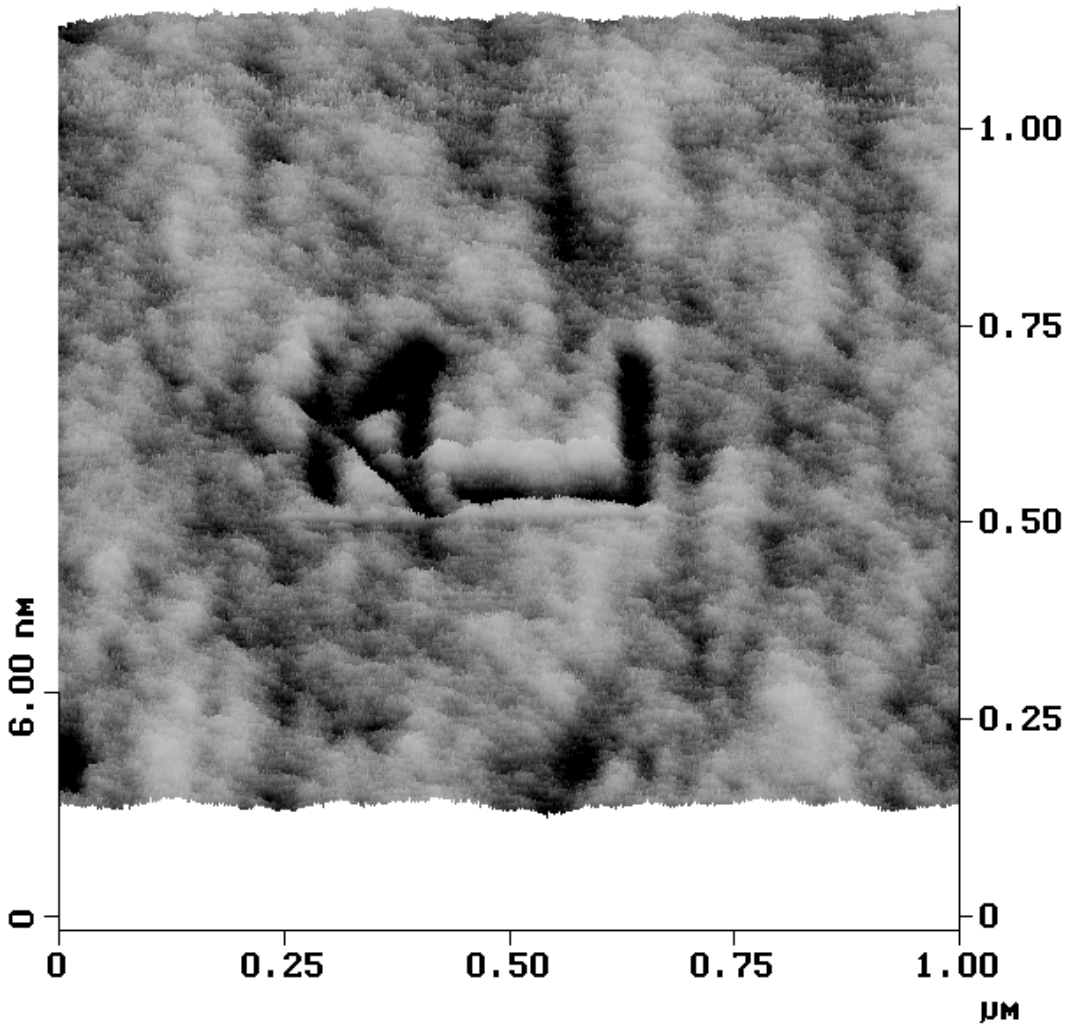

Figure 2.16: 1.00 µm x 1.00µm AFM image of KU etched into monolayer. Image courtesy of Dr. Jill E. Headrick, University of Kansas.

For types of surfaces and films, see sections 2.2.1.1 and 2.4-2.6. Typical surface modifications include etching[98] or grafting[99, 100] (Figures 2.17-2.18). Etching involves mechanically scratching either the surface itself or removing part of a self-assembled monolayer and exposing the underlying surface or film. To etch a sample, a greater force is applied to the sample (compared to the force needed to just image the surface). Typically this deflection setpoint is between 5.0-9.5V, which is equivalent to applying a greater force to the sample. It is often useful to also increase the scan speed (typically from 2 kHz to about 5 kHz) while etching. Typically, the surface is imaged, the scan size is reduced by zooming in and then an etch pattern is made. To check that etching worked, the force is reduced back down and the sample is imaged on a bigger scale. An example of this is shown in Figure 2.17b, where four 400 nanometer by 400 nanometer boxes were etched into a 1-dodecene SAM and then imaged at a lower setpoint voltage to obtain a 5.00 micron by 5.00 micron AFM image of these patterns. The boxes were measured and each was about the intended 400 nm^2 area with approximately 11 nanometer depth. This depth is through the monolayer and into the underlying silicon substrate. Therefore, the monolayer was selectively removed within the etched areas.

a)

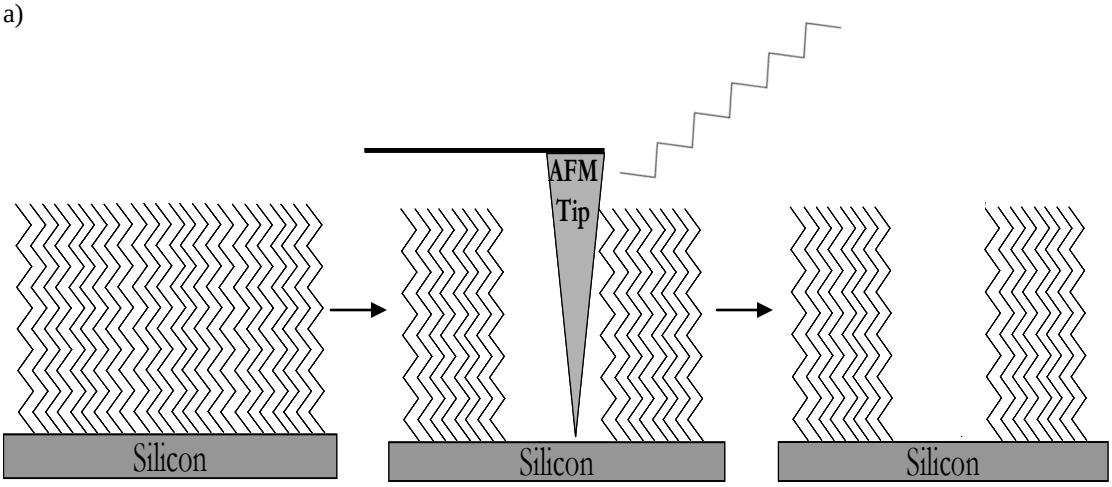

b)

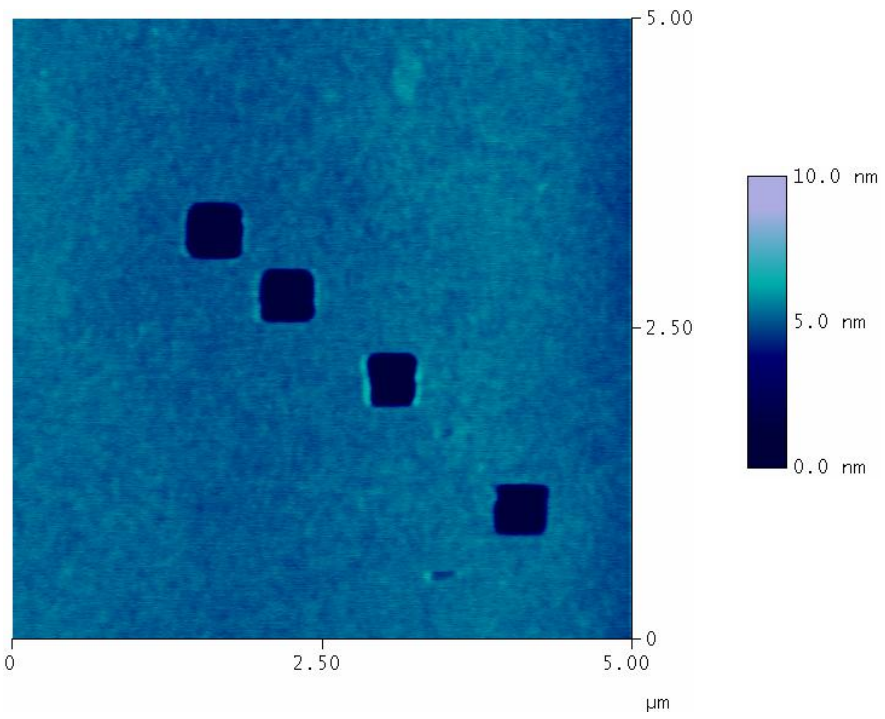

Figure 2.17: a) Etching schematic. Left is 1-dodecene SAM on Silicon. Middle shows that by applying more force at a faster scan rate with the AFM tip, the monolayer of scanned area is selectively removed. And the right image shows the etched area. By decreasing the force and scan rates, the monolayer with the etched area may be imaged. b) 5.00 µm x 5.00 µm AFM height image of etched pattern with a 10.0 nm height scale. Four 400 nm x 400 nm boxes etched into 1-dodecene SAM on silicon, the monolayer of scanned area was selectively removed within the patterns.

Grafting involves a two step process where first the SAM is removed as in the etching procedure above with faster scan rate and higher force and then another SAM (or set of molecules) fills in the space.[97, 100-103] For thiols, grafting must be performed in fluid solution of the grafting thiol in ethanol because if performed dry, the removed molecules will readsorb to the surface and fill in the etch space.[80] An example of this is shown in Figure 2.18b, where a 500 nanometer by 500 nanometer area (box) of 1-octadecanethiol was grafted into a 1-dodecanethiol SAM and then imaged at a lower setpoint voltage to obtain a 5.00 micron by 5.00 micron AFM image of this pattern. The box was measured to be about the intended 500 nm^2 area with approximately 0.9 nanometer height increase over the matrix monolayer. This increase is comparable to the expected height difference of 0.76 nanometers for 12 to 18 alkanethiol and even closer to the value of 0.8-0.9 nanometers per difference between ellipsometric measurements of comparable SAMs and was highlighted in the cross-section image.[72] The rest of the monolayer was intact and of even height. Therefore, the monolayer was selectively removed and replaced within the grafted area.

a)

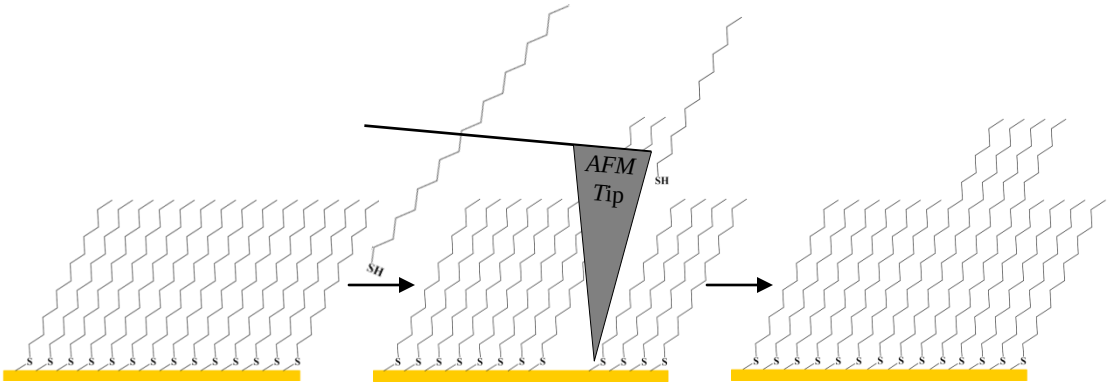

b)

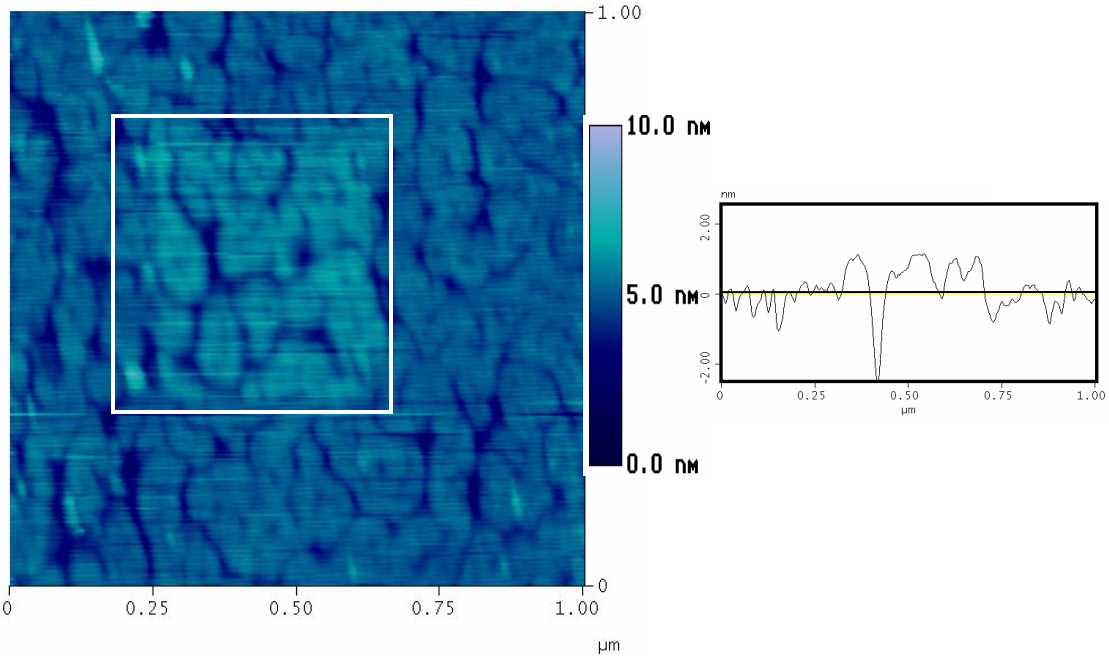

Figure 2.18: a) Grafting schematic. The left schematic shows a 1-dodecanethiol SAM on gold. The middle schematic shows that by applying more force at a faster scan rate with the AFM tip, the monolayer of scanned area is selectively removed and by performing this in a solution of another thiol (1-octadecanethiol in this case), that new thiol is grafted into the area. The right schematic shows the grafted area within the initial SAM matrix. By decreasing the force and scan rates, the monolayer with the grafted area may be imaged. b) 1.00 µm x 1.00 µm AFM height image with a 10.0 nm height scale of 1-dodecanethiol SAM matrix on gold with grafted 1-octadecanethiol (500 nm x 500 nm) box, outlined with a white box frame for clarity and corresponding cross-section across pattern to highlight height difference.

Challenges in both etching and grafting include the following. Drift may be an issue, as such, typically it is beneficial to scan the area to be patterned before and after etch or graft to minimize this drift and improve pattern. For etching, sometimes even if the force is substantially increased, it is not possible to remove all of the monolayer.[104] The ability to etch into and through a monolayer on a surface depends on the attachment chemistry of monolayer on surface. For example, with alkyl silanes on silicon, depending on the surface active groups at the binding end of the molecule, this may be more or less difficult. If the alkyl silane contains a trichloro- versus a monochloro- end group, then a significant difference in both cross-linking to other molecules and surface packing. If SAM molecules are cross-linked to each other as well as bound to the surface as in the trichloro case, it is more difficult to penetrate the layer and completely remove the monolayer. Figure 2.19a depicts an example of this with a 6.00 μm by 6.00 μm AFM height image of four boxes (of increasing size down and to the left) partially etched into an octadecyltrichlorosilane monolayer. The cross-section shows a section of the top three boxes (red, green, and black lines correspond to the boxes starting from the top of the image, respectively). All boxes are consistent in depth, about 0.4 nanometers deeper than the background matrix. Since the height of the monolayer was about 2.5 nanometers, these etches did not successfully remove all of the monolayer. If the SAM molecules are not cross-linked and bound to the surface simultaneously as in the case of octadecyldimethylchlorosilane molecules with one chlorine and two methyl end group molecules, than the monolayer is more easily disrupted due to an increased

number of defect sites and molecules are easier to remove as less bonds need be to be broken. Figure 2.19b depicts an example of this with a 6.00 μm by 6.00 μm AFM height image of two 500 nm by 500 nm boxes etched into an octadecyldimethylchlorosilane monolayer. The cross-section shows a line section through approximately the center of both boxes (red line for top box and green line for bottom box). The depth of both boxes was consistent at about 13 nanometers into the monolayer. Since the height of the monolayer is about 1.0 nanometers, these etches did successfully remove all of the monolayer and went into the silicon oxide substrate beneath the monolayer as well. Etching capability depends on the attachment chemistry of the monolayer to the surface. When the bond energy is greater or the monolayer is cross-linked within itself, etching is more difficult. On the other end of the spectrum, it is also possible with some films on some surfaces to etch away not only the monolayer, but also into the surface beneath, as was the case with alkene silanes (Figure 2.17b). Additionally, etches may be incomplete where part of the pattern etched and another part only partially etched. This can occur if the tip dulls during etching. However, with some SAMs (1-alkenes on hydrogen terminated silicon) it is possible to control the depth of these etches by varying the applied load or the number of etching passes at a high load.[98] Figure 2.17 was an example of such an alkene pattern in which the applied load and number of scans were high. By adjusting these parameters, etches of different depths could have been achieved. This etching variation can be further evaluated by comparing bond energy differences between the monolayer and the substrate. The relative bond strengths are

highest for the alkyl silanes, followed by the alkene silanes, and then the alkane thiols. Thus, it makes sense that it is easier to etch into and through an alkene silane over an alkyl silane.

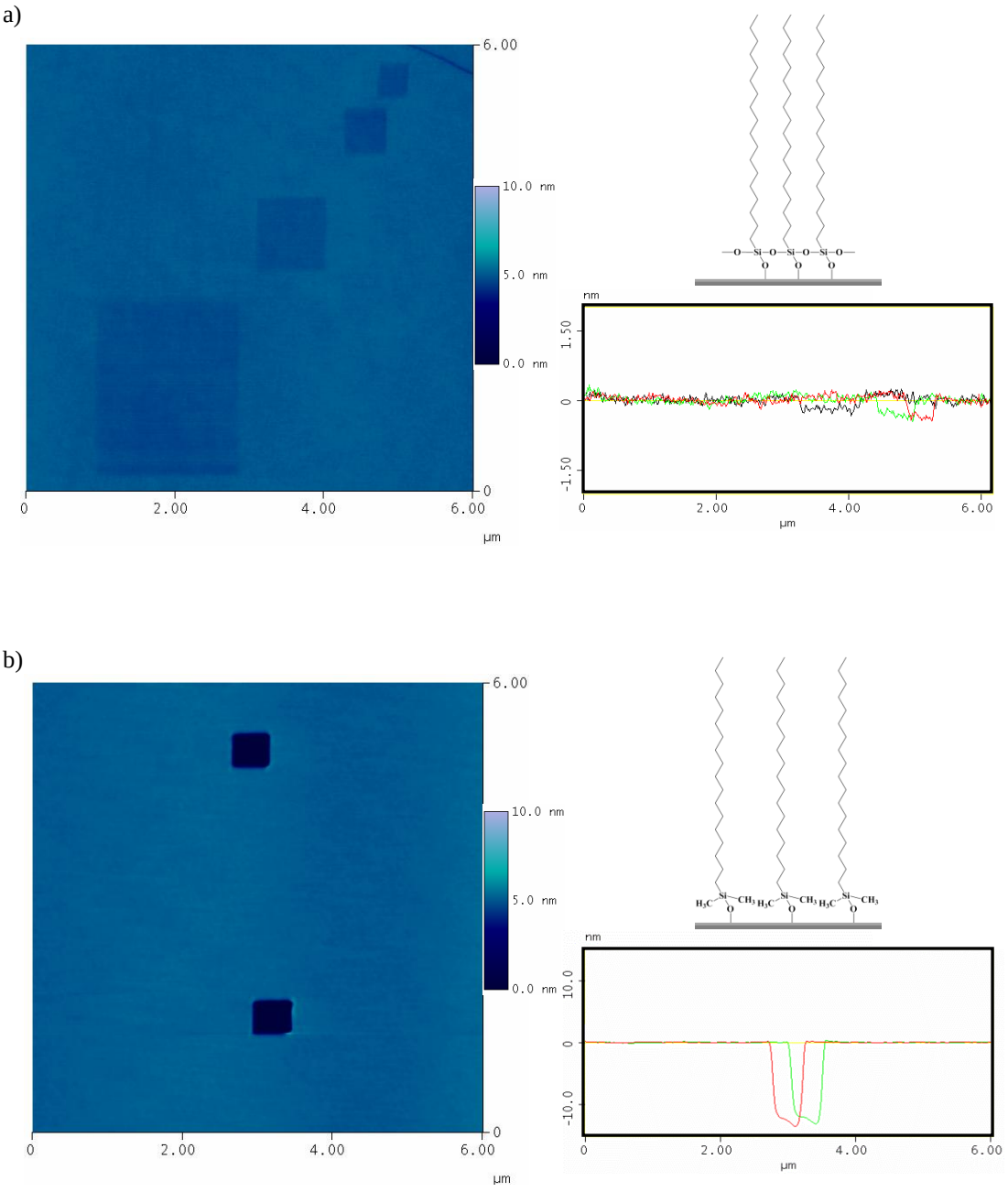

Figure 2.19: 6.00 µm x 6.00 µm AFM height images with a 10.0 nm height scale and corresponding cross sections of a) Four boxes partially etched into an octadecyltrichlorosilane monolayer and b) Two boxes etched into an octadecyldimethylchlorosilane monolayer (Image courtesy of Jill E. Koehler).

With grafting, because this is performed in solution of another thiol, that thiol can insert itself into defect sites within the monolayer.[105, 106] Often the concentration of the grafting thiol solution can be critical to the successful incorporation of these molecules and controlling single versus multilayer formation.[101] Solution compatibility and rinse steps to change solutions are imperative as well. Thus, functional molecules or building blocks may be at random areas outside as well as inside the patterned area. Both etching and grafting may have issues with drift. If the AFM scanner drifts during the scan, then the pattern will be stretched larger than intended.

Advantages of these surface modification techniques include the ability to both modify and image the surface with the same tip without moving the sample. If moving the sample is required, markers placed on the sample allow for relocation of the same spot later for reimaging, for further analysis, and/or additional modification(s). Remarkably, monolayers on silicon and etched patterns remain intact even after long periods of time, sometimes years.[98]

2.4.4. Limitations of AFM

AFM images can be topographic, friction, deflection, or phase, among others. In the case of AFM producing a topographical map of the surface, a variation in height may be evident, but what produces that variation is not. Thus, careful controls are essential. Solutions containing only molecules of interest are desirable since contamination (such as buffer salts) will interfere if it adsorbs to the surface. An AFM image may show that something has adsorbed to the surface, but not what that

something is. Anything that adsorbs to surface may have a height difference from the surface, but one cannot readily distinguish adsorbents without prior knowledge. With friction, a contrast between the trace and retrace and inside/outside a feature in the friction images is observed, but it is not possible to definitively say that the chemistry has changed within that area. Rearrangement of molecules can also cause this friction contrast. Friction contrast provides evidence that the surface was successfully modified, but is inconclusive as to the absolute change. Again, control tests such as FTIR, attachment of a dye and fluorescence microscopy, or attachment of something else such as gold nanoparticles and height change monitoring with AFM can be performed to confirm the success of any chemical modification. Control over parameters, conditions, and solutions are thus imperative for decent AFM images.

The resolution achievable by AFM is limited by the size and shape of the tip. If the tip is wider or bigger than the surface feature, broadening occurs. If the tip is damaged, surface features may be convoluted. Typically, the image shows evidence of tip damage via doubling. For example, if the image has repeating features and a check by changing the scan angle to 90 degrees to see if the features were still repeating but in other direction confirms this, then the tip is probably damaged. The tip can become contaminated by adsorbing material from the sample. This results in a decrease in contrast of the image, or smearing across the image, either of which can be fixed by removing the material from the tip and reimaging. In both of these cases, the tip can sometimes be restored by setting a small scan size (10-100nm), a higher

force (5-9V), and a faster scan speed (~5 Hz), and scanning up and down a number of times.

Another limitation of AFM is that surfaces or substrates used must be uniform (flat) and clean (free of contaminants) such that one can distinguish adsorbed proteins from the surface background. Imaging in fluid can help overcome the cleanliness issue. Additionally, within fluid it is possible to monitor the same area and thus overcome some surface feature variation because can see same spot and any changes over time and thus distinguish between surface features and adsorbent features. Model surfaces such as graphite, mica, and self-assembled monolayers offer this flatness while still offering the ability to tune the hydrophobicity and even chemistry at the surface for insight into fundamental protein adsorption characteristics. These manipulations are limited by the attachment chemistry at the surface. Additionally, when specific surface structure is required, one can manufacture a surface with pits or patterns to mimic certain types of structures. AFM is somewhat slow, making kinetic analysis difficult. Additionally, AFM is critically dependent upon scanning parameters, which may limit novice users in their productivity. Despite these limitations, with proper controls AFM imaging allows one to gain valuable insight into the structure of both the surface and the adsorbed molecules. While AFM is an excellent tool for studying individual molecules, the time scale is slow. Thus, to complement these studies, a method utilizing bulk studies on a faster time scale is desired to provide a more complete picture of not only the conformation on different surface but also the dynamics of these protein-surface interactions.

2.5. Surface Plasmon Resonance

Surface Plasmon Resonance (SPR) is a technique in which the binding of molecules to surfaces can be monitored label-free, in real time, in pseudo-physiological conditions. This is a powerful technique for getting information about kinetics, which is difficult to get from AFM, so these two techniques are complimentary. Properties such as specificity, binding affinity, as well as rates of adsorption and desorption can be determined for nonspecific or specific binding of molecules such as proteins to a variety of surfaces have been elucidated with SPR. SPR has utilized for interactions of small molecules with surfaces,[107, 108] DNA hybridization,[109] and drug interactions with liposomes,[110-112] among others.[113] Additionally, SPR has been employed to study protein surface adsorption onto SAMs,[21, 114-116] and polymer surfaces,[117] or for competitive protein adsorption,[118] antibody screening,[119] and protein-drug interactions.[120, 121]

2.5.1. Technique Description

Figure 2.20a shows a typical schematic of the SPR instrument, a BiaCore3000. Briefly, the technique involves probing a sensor surface with p-polarized light and sensing the change in refractive index of the surface using the evanescent field generated at the surface of the metal. Light from a near-infrared light-emitting diode is sent through a prism onto the sample from the backside. At angles of incidence of the light greater than or equal to the critical angle, the light is totally internally reflected. The intensity and angle of this totally internally reflected light is measured by the detector. When this light is in resonance with the energy of

the surface plasmons of the gold, the plasmons can absorb the energy from the light, giving minimum peak intensity of the reflected light at the angle that corresponds to this resonance. The plasmon resonance frequency is dependent on the refractive index. The evanescent field that senses the refractive index of the sample, decays exponentially away from the surface with a decay length of about 200 nm, making this technique sensitive to surface activity. As the refractive index near the surface changes, the angle at which a minimum occurs shifts because of this resonance condition. Because the surface plasmons have momentum parallel to the surface, p-polarized light is required for their excitation. This phenomenon follows these equations:

$$k_{parallel} = (2\pi/\lambda)n_{prism}\sin\theta \qquad k_{plasmon} = (2\pi/\lambda)\sqrt{n_{gold}^2 n_s^2/n_{gold}^2 + n_s^2}$$

@ resonant angle: $k_{parallel} = k_{plasmon}$

$$(2\pi/\lambda_{light})n_{prism}\sin\theta = (2\pi/\lambda_{plasmon})\sqrt{n_{gold}^2 n_s^2/n_{gold}^2 + n_s^2}$$

where k is the momentum of the wave vector, λ is the wavelength, n is the refractive index, and θ is the angle. These equations show that in order for surface plasmons to be excited, the momentum of the photon parallel to the surface must match the momentum of the surface plasmons. As the refractive index near the surface changes, the momentum of the surface plasmon changes, this means that the angle of the minimum intensity shifts. This shift in angle can be monitored to 0.00001^{o}.[122] Because this technique relies on the excitation of surface plasmons, materials with free electrons that support plasmons are required as substrates (gold, silver, and others).

Two modes of monitoring this change involve either following the shift of the angle of the minimum in the intensity versus wavelength, or monitoring the change in intensity at a fixed angle. The former is used in the following set of experiments. This shift in the angle of minimum intensity can be displayed in a response versus time plot known as a sensorgram (Figure 2.20b-c). As molecules bind to the surface, the refractive index of the surface changes, typically increasing, causing the minimum in the intensity curve to shift. This change in SPR angle is converted to a change in response units, which are the typical units for an SPR plot. The higher the molecular weight of the adsorbent, the greater the change in refractive index at the surface and the greater the response (RU) from the SPR. Monitoring this change over time produces a sensorgram from which the adsorption and desorption properties of analyte binding can be elucidated. By carrying out experiments at a number of analyte concentrations, one can fit the traces to obtain the adsorption and desorption rate constants with appropriate models for the binding. In addition, by comparing the adsorption on different surfaces, information about the relative affinity can be obtained. The amount of analyte bound to the surface can be determined from the change in refractive index (from initial baseline) after dissociation. The specificity of an interaction can be determined by varying the analyte and/or ligand and determining if a binding event occurs or not.

SPR parameters include detection, flow path, flow rate, and injection options, among others. Each integrated fluidic cartridge (IFC) system contains four flow cells through with liquid can be introduced. This IFC seals to the sensor surface. A

method was constructed to fit experimental goals. A BiaCore3000 has four different channels that can use; either one or two of these channels can be used as reference channels to enable subtraction of any change in response associated with or due to nonspecific binding or difference in refractive index between solutions. Detection can be on any of the four flow cells or various combinations of channels. Detection can also automatically subtract out a reference cell from the sample cell. Flow path can be through one cell or multiple cells. Injection options utilized included regular injections or kinjections. Regular injections are typical injections for method development or control injections, while kinjections offer more a precise injection segment and control over association and dissociation times and are important for kinetic studies. Flow rate can be anywhere from zero to one-hundred microliters per minute. Flow rate is important for overcoming mass transport limitations. Sample injection volume is limited to five to 250 or 325 microliters depending on the type of injection.[122]

Several methods of analyzing systems can be accomplished with SPR. In the experiments presented in this dissertation, both nonspecific and specific binding of proteins to surfaces were investigated. Clearly, using a reference cell to subtract out the contribution from binding and refractive index changes in the case of nonspecific adsorption is not possible, and complicates the analysis slightly. In nonspecific adsorption studies, the protein of interest is injected unto a surface. The adsorption of the protein to the surface is monitored over time. The terminal chemistry at this surface can be tuned to study nonspecific adsorption on a variety of surface

chemistries. In specific adsorption studies, a specific component of the analyte is targeted for binding to the ligand on the surface. More details of nonspecific and specific adsorption characteristics are provided in sections 2.5.2.1 and 2.5.2.2, respectively.

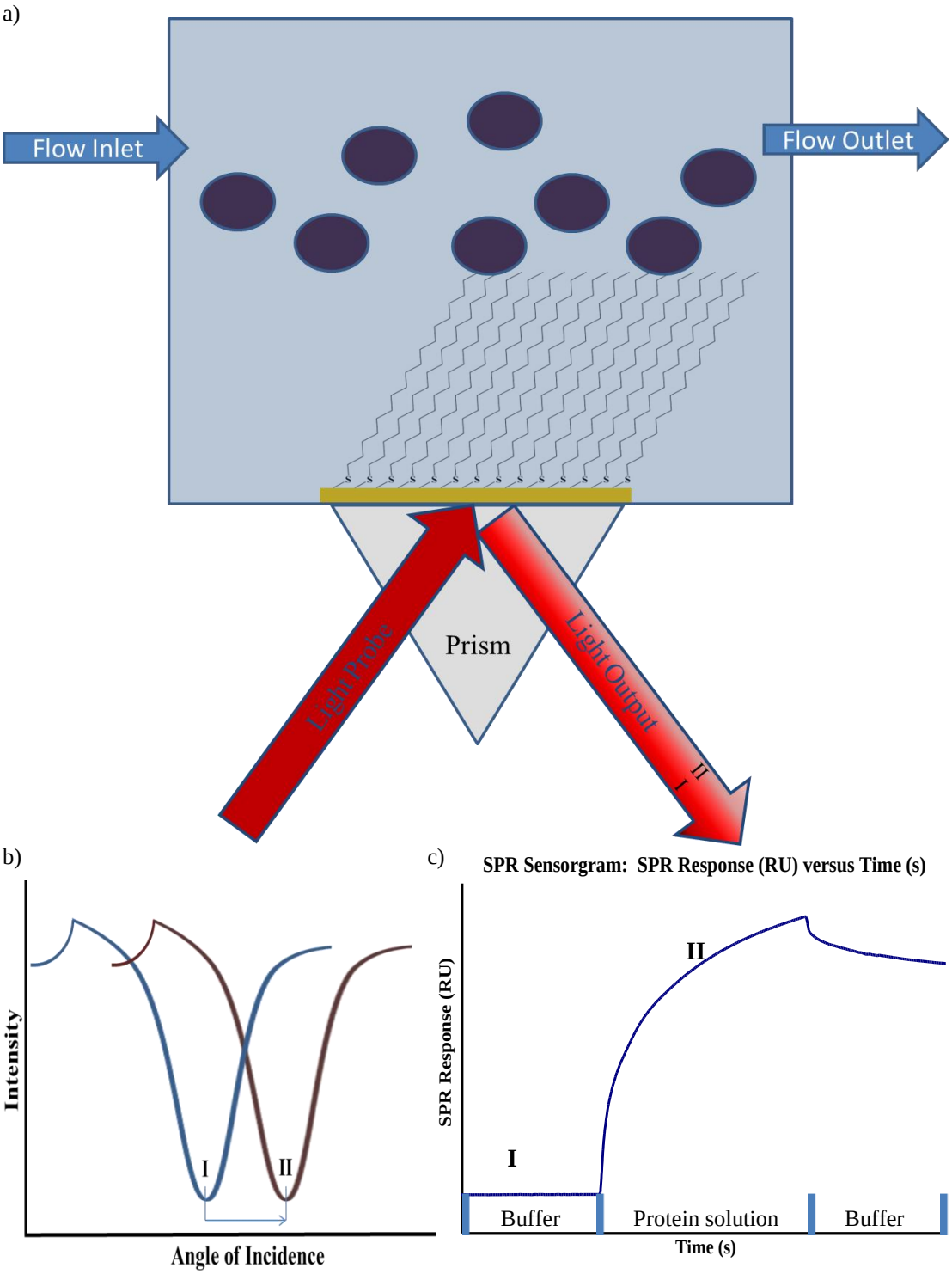

Figure 2.20: a) SPR schematic. b) Plot of Intensity versus Angle of Incidence with changes from I to II indicated. c) Typical Sensorgram with regions of solutions and changes from I to II indicated.

2.5.1.1. Surfaces

Chemistries utilized for nonspecific adsorption studies include bare gold surfaces (2.4.1.1) and alkane thiol monolayers (2.5.2) of various terminal chemistries (1-octadecanethiol $\mathbf{CH_3}(CH_2)_{17}SH$, 1-dodecanethiol $\mathbf{CH_3}(CH_2)_{11}SH$, 4-aminothiophenol $\mathbf{NH_2}C_6H_4SH$, 11-amino-1-undecanethiol, hydrochloride $Cl^-\ ^+\mathbf{H_4N}(CH_2)_{11}SH$, 11-mercapto-1-undecanol $\mathbf{OH}(CH_2)_{11}SH$, 11-mercaptoundecanoic acid $\mathbf{HOOC}H(CH_2)_{11}SH$, 1,6-hexanedithiol $\mathbf{SH}(CH_2)_6SH$ or 1,11-undecanedithiol $\mathbf{SH}(CH_2)_{11}SH$, etc.) on gold. These surfaces were chosen to allow sufficient variety in terminal chemistry properties to elucidate binding affinity and kinetics behavior. This potentially allows determination of factors important in controlling protein-surface interactions. Specific chemistry studies include use of an NTA chip and His-tagged proteins. This allowed for verification that the chemistry utilized in AFM patterning studies was functional and specific. It also will allow for kinetics determination. Further details will be discussed in section 4.3.2.

2.5.1.2. Sensorgram Details

A sensorgram displays the output or results of an SPR experiment (Figure 2.20c). Sensorgrams are plots of SPR response (RU) versus time (seconds). Initially, the system is allowed to equilibrate until a flat baseline is observed. When sample is injected, an increase in response will occur if molecules bind to the surface. If this response levels off during binding, equilibrium is reached where molecules are adsorbing and desorbing to the surface at the same rate. When buffer is reintroduced to the system, some or all of those molecules desorb (come off the surface), and a

decrease in response is observed. If the response does not return to the baseline level, some of the protein or ligand is left on the surface. To repeat measurements or inject a different analyte concentration, the surface must be regenerated so that the response has returned to baseline level. A regeneration solution is injected with interacts with the molecules of interest to remove them from the surface. In some cases this is a straightforward and simple disruption and in others this is more difficult or possibly not achievable. Regeneration solutions range from simple salt solutions to solutions of different pH, to surfactants, to dilute organic solvents, to competitive ligands, and to other solutions. In some experiments, regeneration is facile and by simply injecting a competing ligand a known interaction is disrupted. In cases where the surface interaction is unknown or multifaceted, this tends to be a more difficult or even insurmountable task. If regeneration is not feasible and additional studies with increasing concentrations of analyte are desired without a new surface (kinetic titrations,[123] it may be imperative to take into account that the number of available binding sites on the surface may have changed (decreased) and consider this when fitting data.

A reference cell is often used in SPR experiments with specific adsorption in which the surface is not activated in that cell but is activated within the sample cell. This allows for any change in refractive index of sample solution from buffer to be subtracted from the sample cell. Additionally, any nonspecific analyte binding will also be removed by subtracting reference cell data from sample cell data. The advantage of this is that the final sensorgram contains only information pertaining to

the analyte response to the surface. Sensorgrams can provide information on affinity, kinetics, specificity, and concentration of analyte interactions with the surface.

2.5.2. SPR for Protein Adsorption

SPR has several advantages for protein surface interaction studies. As a label-free technique, proteins can be studied without a label potentially disrupting or altering its adsorption properties. Since the mechanism involves flow, samples are held in an aqueous environment without exposure to air. Thus, proteins are kept in pseudo-physiological conditions. This enables real time monitoring of protein adsorption and extraction of adsorption and desorption rate constants. Variations of conditions are easily achieved by simply changing the buffer or the flow rate. This allows for multiple tests to be performed, allowing for further analysis on the same surface to determine reproducibility as well as elucidation of kinetics details of binding. The substrate can be changed to measure interactions based on surface hydrophobicity or chemistry. Nonspecific and specific methods of study for investigating protein surface interactions were performed to study protein adsorption and desorption. Nonspecific methods allow for a more general idea of protein adsorption to be studied with a variation to surfaces studied as in the fibrinogen studies (Section 3.3.2). Specific methods allow for determination of success of specific interactions as in the case with ATPase-His and a nickel ion – NTA surface (Section 4.3.2.1).

2.5.2.1. Nonspecific binding

One atypical method of monitoring protein-surface interactions with SPR is to monitor the nonspecific adsorption of proteins to surfaces. This method involves an injection of protein over the surface and observing the adsorption behavior. By controlling the chemistry at the surface as well as the solution conditions, adsorption properties can be analyzed. Potential interactions of nonspecific adsorption include hydrophobic, hydrophilic, and electrostatic. Analyses of sensorgrams provide details about the affinity of the protein for the surface, the strength of that adsorption, as well as the rates of adsorption and desorption of the protein from a variety of surfaces. This would allow elucidation of important components required to promote or inhibit binding or potentially even for disruption of binding. Knowledge of fundamental properties involved in protein adsorption should enable more accurate control in design of materials to selectively bind or inhibit protein adsorption and provides methods of protein removal from surface if it was undesirably adsorbed.

2.5.2.2. Specific binding

A more typical method of monitoring protein-surface interactions with SPR involves monitoring the specific adsorption of proteins to surfaces. In this case, typically a ligand is bound to the surface. The target analyte is then introduced to the flow cell and allowed to bind to the ligand. Then buffer is reintroduced into the system to remove any unbound analyte. A regeneration solution may be applied to disrupt the specific interaction and regenerate the surface (return the baseline response back to the initial level). To make analysis simpler, a reference cell is

employed in which the ligand is either blocked or not introduced to the cell. In this case, the change in the refractive index between the analyte solution and buffer as well as any potential nonspecific adsorption of the protein to the surface can be monitored. Subtraction of the sensorgram of the reference cell from the sample cell results in a sensorgram containing only the response from specific protein-surface interactions. Determination of the specificity and strength of binding can be elucidated from the resulting sensorgram.

2.5.3. Extraction of Kinetics Parameters via SPR

Kinetic fits using specific binding models allow determination of the rate of adsorption (k_a) and rate of desorption (k_d) for the analyte interaction with the surface. Depending on the interaction studied, different binding models need to be applied. The typical methods are 1:1 Langmuir binding, heterogeneous binding, and others. The 1:1 Langmuir binding states that one analyte binds to one spot on the surface. The heterogeneous binding model involves the analyte binding independently to multiple binding sites on the surface. Other binding models take into account other situations as well. These models provide one versus two sets of binding constants that take into account one versus multiple different attachment sites. Detailed information about kinetic fits and equations involved have been reviewed and includes factors such as occupied binding sites, maximum response at equilibrium, concentration, and rates of adsorption and desorption.[17, 124-126]

The shape of the curves provides information about the binding properties of the analyte to the surface. The steeper the initial slope, the quicker the molecules are

adsorbing to the surface and the fewer molecules are desorbing from the surface. If adsorption and desorption of molecules reaches an equilibrium, the curve will flatten off at the top. Upon buffer exchange, molecules can desorb or be removed from the surface. Some or all of the adsorbed molecules will desorb upon introduction of buffer to the system. The steeper the slope of this desorption part of the curve, the more readily the molecules desorb and the less tightly the molecules were bound to the surface. After switching back to buffer and allowing time for desorption, some molecules may remain bound to the surface. This allows for determination of analyte concentration on the surface. Analyte affinity for the surface can be determined by both the adsorption and desorption properties.

2.5.4. Limitations of SPR

Similar to AFM studies, SPR will show a response whenever anything binds to the surface. The response is not specific to one particular analyte. Any adsorption to the surface will produce a response. SPR detects a change in refractive index, which can be caused by adsorption of any species and even from just changes in the solution composition. Therefore, careful control and calibration is required to ensure that the response is really due to the solution of interest. The purity of the protein solution was critical in these experiments. Other limitations include baseline drift, which is usually minimal if solutions have been equilibrated to room temperature. For kinetics, mass transport limitations must be taken into consideration. If the arrival of the protein to the surface is limited by mass transport, then the observed rates are not the true kinetic rates. SPR has a limit to the molecular weights

measurable. The response of a larger analyte is much larger than a small molecule, therefore it is preferable to attach the small molecule ligand to the surface and measure the binding of the larger protein molecule. Experimental design is critical. Carryover, or transfer of sample either between sequential injections, flow cells, or vials, may be an issue, extra clean and other steps can be taken to avoid this. Refractive index changes of the solution can dominate the signal due to binding of the analyte if the composition of the buffer and adsorption solution are very different. Competitive reactions require additional controls. The response in a SPR experiment depends sensitively on distance, and therefore very thin samples are required, due to the decay of the evanescent field of about 200 nm. Solutions used must be compatible with the BiaCore parts, including the IFC, tubing, etc. Therefore, primarily aqueous solutions are used, depending on the instrument. Combinations of solutions are important too, if something precipitates out on the system, the IFC may become clogged; solution compatibility should be determined before injecting into the system. Routine maintenance is critical for optimal instrument performance to maintain pristine flow channels. SPR instruments are expensive to upkeep, partially due to clogging of the small channels within IFC, which requires IFC replacement.

Despite these limitations, SPR is a valuable tool for protein – surface interaction studies, especially when analyte is scarce. SPR provides bulk measurements of analyte surface interactions including affinity, concentration, specificity, and kinetics of binding, both nonspecific and specific. SPR studies have been performed for such diverse applications in order to elucidate binding targets for

drugs,[108] to study immunoassays,[127, 128] to study interactions between biotin and streptavidin,[129] to determine histidine-tagged protein adsorption,[130] and to determine potential protein resistant surfaces.[21]

2.6. Fluorescence Microscopy

One way to verify that a functional group (such as a thiol) is exposed on a surface or within a pattern is to attempt to specifically or covalently attach a fluorescent molecule to that moiety and observe the resulting fluorescence via fluorescence microscopy. If the sample or region of the pattern exhibits enhanced fluorescence, than there is evidence that the moiety was accessible to attach / bind to the fluorescent molecule. Positive and negative control studies with a full-coverage reactive thiol-terminated or resist methyl-terminated monolayer can be performed to check this specificity and confirm results. Common types of reactive moieties on dyes include maleimide, thiol, active ester, amine, carboxylic acid, isothiocyanate, alkynes, among others.[131] These react with chemical groups such as amines, thiols, ketones, carboxylic acids, aldehydes, azides, among others, on the analyte or the surface.[131]

Fluorescence microscopy works by irradiating a sample with light and recording the light emitted. After initial excitation of an electron in a conjugated dye molecule by the incident light, the electron relaxes back to the ground state through the emission of light (fluorescence). The wavelength of excitation and emission is dependent upon the dye molecule probed in the experiment.

2.6.1. Dye Molecules

Control studies to confirm availability of terminal thiol with dithiol SAMs as well as interaction with maleimide functionality were performed with maleimide fluorescent dyes. Each of these dyes has a maleimide functional group attached to a conjugated ring system. Successful attachment of fluorescent dye to terminal thiol will result in fluorescence under appropriate conditions.

Dye molecules utilized included Texas Red® C_2-maleimide ($C_{37}H_{36}N_4O_8S_2$), Alexa Fluor® 488 C_5-maleimide ($C_{30}H_{25}N_4NaO_{12}S_2$), fluorescein-5-maleimide ($C_{24}H_{13}NO$), and Oregon Green® 488 maleimide ($C_{24}H_{11}F_2NO_7$) from Invitrogen (catalog numbers T6008, A10254, F150, and O6034, respectively).[131]

Excitation for Texas Red is green at 582 nm and emission is brilliant red at 600 nm. Excitation for Alexa Fluor 488 is blue at 493 nm with green emission at 516 nm. For fluorescein and Oregon Green® 488 Maleimide, the excitation is blue at 492 nm with green emission at 515 nm. During emission, these wavelengths are all shifted to longer wavelengths than the excitation wavelengths due to loss of energy from molecular vibrations when the fluorophore is within the excited states before relaxing back to the ground state energy levels. This red shift in wavelength is termed the Stokes shift and the magnitude of this shift is determined by the electronic structure of the fluorophore. The excitation and emission wavelengths reported here are the maximum where the efficiency is the highest. As shown in the spectra below (Figure 2.21), both excitation and emission have a broad wavelength range over which energy is adsorbed or emitted.

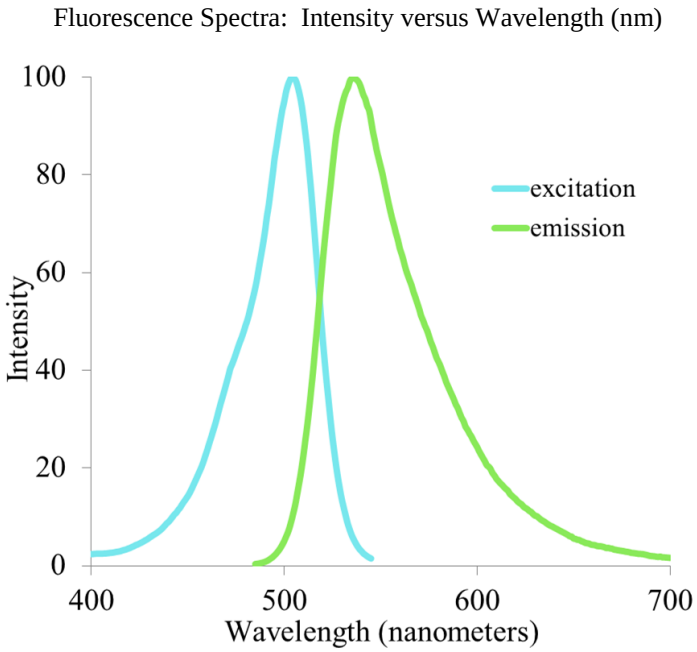

Figure 2.21: Example Fluorescence Spectra of Oregon Green.[131]

2.6.2. Attachment Strategies

For the fluorescence microscopy studies, all fluorescent molecules contained a maleimide moiety. Therefore, for these maleimide fluorescent molecules, maleimide thiol chemistry was utilized. The double bond in the maleimide group reacted with the thiol to form a covalent bond (Figure 2.24). However, before this step can occur, it is imperative to ensure that free thiols are available. Disulfide bonds can occur between neighboring dithiols bound to the surface, or between a dithiol bound to the surface and one that was free in solution (Figure 2.22). If a disulfide bond is present, those thiols are not available for reaction with the maleimide group. Therefore, the maleimide reaction was performed after incubating the surface in a solution of tris(2-carboxyethyl)phosphine (TCEP) to break any such disulfide bonds (Figure 2.23). The purpose of these fluorescent studies was to confirm that a thiol terminal group

was available for further chemical reaction (with maleimide-NTA), which is why this specific moiety (maleimide) was chosen.[132]

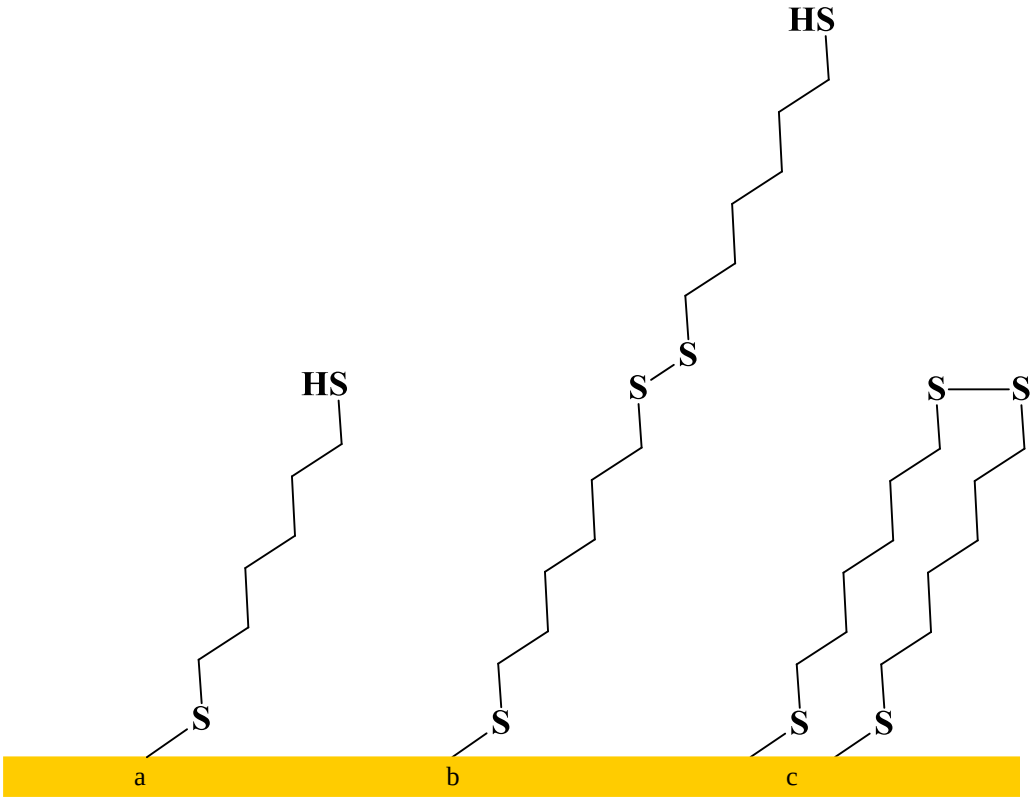

Figure 2.22: Schematic of 1,6-hexanedithol adsorption to gold film. a) Ideal SAM formation of single monolayer, b) 1,6-hexanedithiol bound to the surface with disulfide bond to a free dithiol in solution, c) two 1,6-hexanedithiol molecules bound to the surface with a disulfide bound between the terminal thiols.

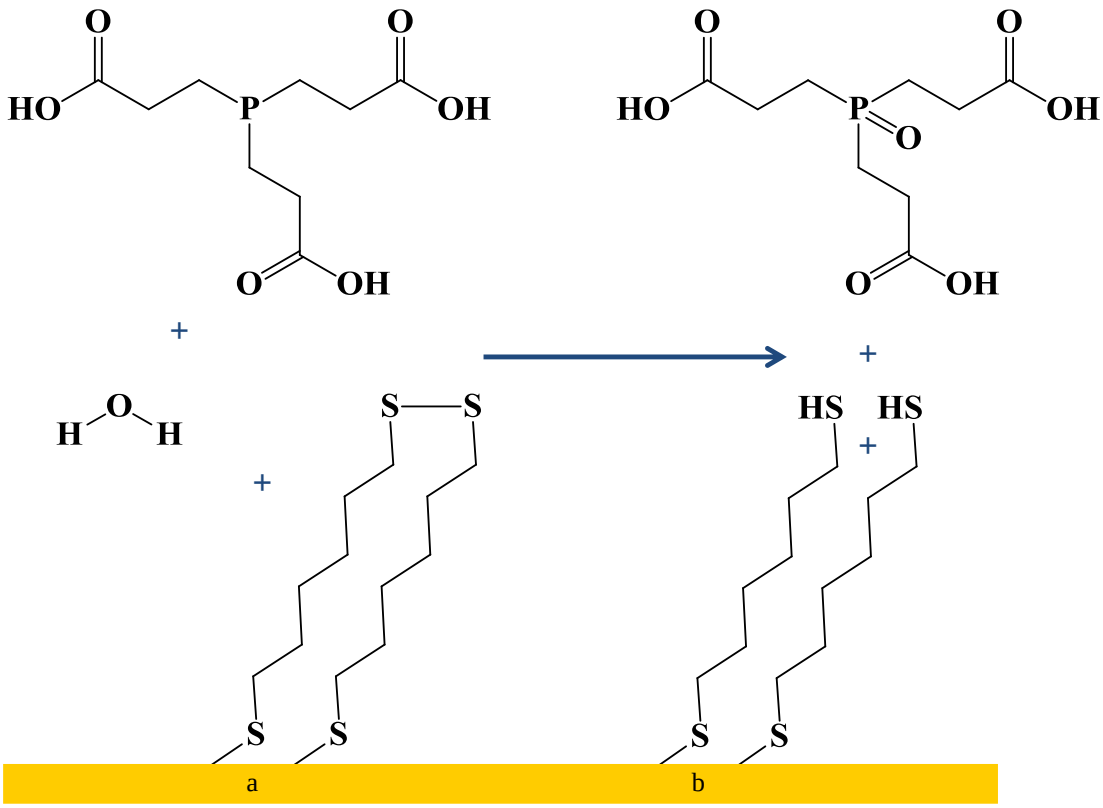

Figure 2.23: Schematic of TCEP reaction with disulfide bonds. a) TCEP, water, and two 1,6-hexanedithiol molecules bound to the surface with a disulfide bound between the terminal thiols, and b) After reaction TCEP is oxidized and the disulfide bond between the two 1,6-hexanedithiol molecules on the surface has been reduced yielding free terminal thiols.

The fluorescent dye was dissolved in buffer with a small amount of TCEP. Note, after TCEP addition it is crucial to test the pH of the solution and adjust if need be to back within a pH range of 7.0 to 7.5.[131] This is critical in maintaining an environment in which the maleimide remains reactive. Buffers with pHs above or below this pH range will result in low or minimal dye reaction with available thiols and thus a false negative. After about an hour or two of dye solution incubation at room temperature or overnight at 2-8ºC, the sample was removed and rinsed thoroughly with buffer and water and dried with nitrogen gas before imaging. All

solutions were protected from light by wrapping containers in aluminum foil and working in the dark.

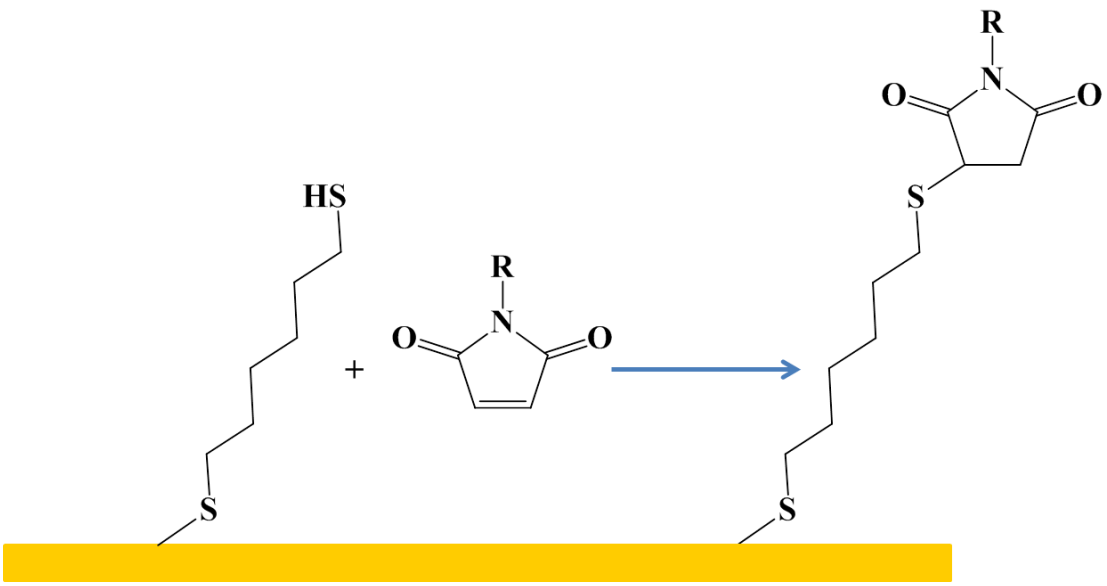

Figure 2.24: 1,6-hexanedithiol molecule on gold surface, after addition of maleimide-dye a thioester bond has formed between the terminal thiol and the maleimide group.

Additional fluorescence microscopy studies were performed with protein samples as another test to confirm protein was successfully bound to the surface and within patterned region. For these studies, F_1-ATPase-his protein was modified to include a Rop armature ($\alpha_{3\text{-His}}\beta_3\gamma$Rop) with an available cysteine group to fluorescently label the protein via the same maleimide-thiol chemistry. For the attachment of fluorescein to the cysteine on the Rop, a similar attachment strategy was utilized via thiol – maleimide chemistry. Steps taken to achieve this labeling can be found in section 2.7.2.2. The protein was then specifically bound to nickel-nitrilotriacetic acid bound to the entire surface or within a patterned region and imaged via AFM and fluorescence microscopy.

2.6.3. Limitations of Fluorescence Microscopy

While fluorescence microscopy can be an advantageous technique for study and confirmation of available functional groups or patterning success, some limits exist. Fluorescence from nonspecific adsorption of dyes to surfaces can lead to conflicting results. If the protein of interest does not naturally fluoresce, a fluorescent label must be attached to observe the protein, which may affect the protein's adsorption properties. Any thiol in the protein (in a cysteine amino acid) could be labeled with the maleimide dyes utilized. It this is an issue, it is generally possible to engineer out these cysteines for a nonreactive amino acid to eliminate any extra cysteines if this is an issue. However, most proteins have less than two percent cysteines, so this is not typically an issue or necessary action.

Additionally, dyes may be quenched or photobleached upon exposure to reactive molecular oxygen and light dyes. This means that prior to the emission of fluorescence, the excited energy state transfers energy to oxygen or light and thus has none left for fluorescence. Sometimes if a fluorophore is too close to a surface, the surface can steal the excited energy from the fluorophore, quenching the signal. Another pathway of decay which eliminates observed fluorescence is photobleaching, in which the molecular structure of the molecule changes such that it cannot adsorb additional excitation light energy.[133] This means that even if the dye is attached to the surface or protein, it may not be observed via fluorescence microscopy. This necessitates control studies to ensure that the dye is still active. Other technical difficulties complicate the process. One of these is that the size of the fluorescence

pattern matters. Any patterns created need to be fairly large, greater than hundreds of nanometers or even microns, to detect. If a large surface (millimeters) is used in the study, even if the pattern is large (microns), locating this pattern could be like trying to locate a needle in a haystack. One way this was overcome laborious search was to make visual landmarks near the pattern of interest as a reference point in order to zone in on the area of the pattern.

Even with these limitations, fluorescence microscopy offers confirmation of chemistries and patterning and serves as a valid control system. With the added advantage of a low background signal, this technique provides not only high sensitivity but also high selectivity.

2.7. Sample Preparation

Protein samples and corresponding solutions were prepared per details in the following subsections.

2.7.1. Fibrinogen

Fibrinogen (bovine) was ordered through Sigma-Aldrich and stored at -20ºC. Fibrinogen solutions were prepared by dissolving 0.0010 grams of fibrinogen into 10 milliliters of 50 mM phosphate buffer (pH experimentally controlled at either pH 7.4, 4.0, or 5.8), creating stock solution one (100 μg/mL). Fibrinogen was dissolved, inverted to mixed and filtered through a 0.22 μm filter. One milliliter of stock solution one was combined with 49 milliliters buffer to create stock solution two (2 μg/mL). Finally, two milliliters of stock two was combined with 18 milliliters of buffer to create a 0.2 μg/mL fibrinogen solution. Further dilutions were made as

necessary. Alternatively, 0.0020 grams of fibrinogen was combined with fifty milliliters of buffer, mixed, filtered through a 0.22 μm filter, and degassed for 40 μg/mL fibrinogen solutions for use in SPR studies. Additional dilutions for SPR studies were made using the BiaCore3000. Fibrinogen solutions were stored at 2-8ºC and equilibrated to room temperature before use. However, fibrinogen solutions were typically prepared on the day of usage.

Additionally, bulk preparation of a higher fibrinogen concentration (about three milligrams per milliliter was prepared, aliquoted, and frozen. Aliquots were diluted to desired concentration in desired buffer conditions.[28]

2.7.2. F_1-ATPase

F_1-ATPsynthase (F_1-ATPase), F_1-ATPase-His, F_1-ATPase-His-Rop, and F_1-ATPase-His-Rop-fluorescein were diluted with Tris-HCl buffer as necessary from stock solutions provided from the Richter lab. The Richter lab purified ATPase (alpha3-beta3-gamma) before providing samples, which were prepared with two millimolar ATP (for stability) in 50 millimolar Tris-HCl, pH 8.0 buffer and additives of 20 percent glycerol for cold storage and one millimolar ethylene diamine tetraacetic acid (EDTA, Sigma-Aldrich) for sample preservation.

2.7.2.1. Recombinant F_1-ATPase Preparation

F_1-ATPase was isolated from the chloroplasts of spinach by the Richter group.[134, 135] Cloned or recombinant F_1-ATPase subunits (alpha, beta, and gamma) were produced by inserting the genes to encode for the individual subunit into plasmids. These plasmids are then placed into bacteria, which are induced to over-

express the DNA for these subunits. The result is protein in an insoluble form, which is then solubilized with urea and folded via a dialysis method. The folding and assembling of the complex occurs in one step and is followed by purification with size-exclusion chromatography. The success was verified with sodium dodecyl sulfate polyacrylamide gel electrophoresis and phosphate assay activity studies. Protein concentration was determined via the Bradford method with UV-VIS spectroscopy.[136]

2.7.2.2. Modifications to F_1-ATPase

The ATPase protein utilized in experiments was initially the $\alpha_3\beta_3\gamma$ or a majority of the F_1 portion. Modifications to this protein included incorporation of poly-histidine tags into the α-subunits and then the addition of Rop protein to the gamma subunit. Additionally, sometimes proteins were engineered such that any external cysteines were replaced by serines. This form of the protein can be purified with a nickel affinity column via the histidine tags and eluted with imidazole. Additional purification step(s) were performed to remove imidazole. The Rop serves as an armature extending from the gamma subunit. Additionally, reengineered proteins from mixed systems from Richter's group were utilized.

To fluorescently label the protein, the histidine $\alpha_3\beta_3\gamma$-His-Rop protein was combined with 20 μM fluorescein-5-maleimide for ten minutes, followed by one mM dithiothreitol (DTT) to terminate the reaction. The final protein solution provided to the Berrie lab included about six mg/mL protein, 50 mM Tris-HCl buffer, pH 8.0, two mM adenosine triphosphate, and one mM DTT. The Rop contained a cysteine to

react with the maleimide of the dye to produce fluorescently labeled ATPase with histidine tags.

2.7.3. Protocol for Buffers and Dilutions

This section provides a brief protocol for buffers, protein samples studied, and dilutions.

Solution Preparation for AFM experiments:

$NiCl_2$ solution

A fifty millimolar nickel chloride solution was prepared by combining approximately 0.59 grams nickel chloride (green crystals) with fifty milliliters of water or buffer. Note, ethanol in not a suitable solvent as the pH is too low to enable coordination of the nickel ion to NTA. This solution is then mixed to dissolve crystals (sonicated about 5 minutes if necessary) and filtered through a 0.22 micron filter. This solution was stored at 2-8ºC and equilibrated to room temperature before use.

Maleimide-NTA solution

Per Vogel *et al.*,[137, 138] a 0.2 mg/mL solution of maleimide-nitrilotriacetic acid (maleimide-NTA or M-NTA) was prepared by weighing two milligrams M-NTA and combining that with 10 mL of either water or buffer and mixing. Alternatively, a 0.1 mg/mL solution of M-NTA was prepared. These solutions were stored at 2-8ºC and equilibrated to room temperature before use.

TCEP solution

Five mM tris(2-carboxy-ethyl)phosphine hydrochloride (TCEP) was prepared with TCEP from Sigma. To make a 5 mM solution, approximately 0.0143 grams of TCEP (crystals) was combined with 10 mL of buffer (either Tris HCl or HEPES buffers with pH adjusted to 7.0-7.5) and dissolved. Solution was stored at 2-8ºC and equilibrated to room temperature before use.

Dye solution(s)

For fluorescently labeled ATPase, see previous section (2.6.2 and 2.7.2.2). For Texas Red dye, about 5 mM dye solution was prepared in HEPES buffer with TCEP, pH 7.4. Dye solution was protected from light by wrapping vial in aluminum foil. Dye solution was added to surface after a five minute incubation in TCEP and allowed to react for two hours or overnight at 2-8ºC, protected from light at all times. After dye incubation, the surface was removed, rinsed with buffer and water, dried with nitrogen gas, and imaged via fluorescence microscopy.

Solution Preparation for SPR Experiments:

Phosphate buffer pH adjustment

Phosphate buffer, 50 mM pH 7.0, was adjusted with sodium hydroxide or hydrochloric acid to increase or decrease pH as needed while stirring and monitoring the pH with a pH probe. Solution was filtered through a 0.22 μm filter. Solution was stored at 2-8ºC and equilibrated to room temperature and degassed if needed before use.

The SPR experiment with a NTA chip required the following solutions: HEPES running buffer, $NiCl_2$ solution, $MgSO_4$ solution, regeneration solution, imidazole solution, and ATPase-His protein dilutions.

HEPES running buffer

HEPES running buffer for SPR experiments contained 0.01M HEPES, 0.15M NaCl, 50 μM EDTA, and 0.005% Surfactant p20 at pH 7.4. To prepare HEPES running buffer, a 500 mL volumetric flask was obtained. A small amount of deionized water was added to the flask. Approximately 1.192 grams of HEPES was weighed and added to the flask. Sodium chloride, 4.383 grams, and 0.01131 grams of EDTA were also individually weighed and added to the flask. The flask was swirled to dissolve the components and then filled to volume and capped and inverted to mix. The solution was transferred to a 1000 mL beaker with a stir rod. A pH meter was calibrated and the pH of the buffer was measured. Sodium hydroxide (0.75 M) was added until the pH was 7.40. The solution was filtered through a 0.22 μm filter, degassed, and about 25 microliters of P20 surfactant (BiaCore, now GE Healthcare) was added. Running buffer was stored at 2-8ºC until needed and then equilibrated to room temperature and degassed as needed.

$NiCl_2$ solution

A 500 μM nickel chloride solution was prepared in a fifty milliliter volumetric flask by combining approximately 0.0119 grams of nickel chloride (green crystals) with distilled water. The solution was mixed to dissolve the crystals and filled to

volume. Then the solution was filtered through a 0.22 μm filter, degassed, and stored at 2-8ºC until needed and then equilibrated to room temperature.

$MgSO_4$ solution

A 1.6 millimolar magnesium sulfate solution was prepared in a 10 mL volumetric flask by combining approximately 0.0039 grams of magnesium sulfate with distilled water. The solution was mixed to dissolve the crystals and filled to volume. Then the solution was filtered through a 0.22 μm filter, degassed, and stored at 2-8ºC until needed and then equilibrated to room temperature. This solution was used as a control solution to check if magnesium ions bind to the NTA groups of the reference cell and thus potentially interfered with histidine-tag protein binding analysis.

Regeneration solution

Regeneration solution for the ATPase-His interaction with NTA-nickel ions consists of 0.01M HEPES buffer, 0.15M NaCl, 0.35M EDTA, 0.005% Surfactant p20 at pH 8.3. To prepare this regeneration solution, the following steps were employed. For a 100 milliliter solution, 0.2383 grams of HEPES was combined with 0.8766 grams of sodium chloride, and 15.827 grams of EDTA in a 100 mL volumetric flask containing a small amount of distilled water. The flask was swirled to dissolve the components and filled to volume with distilled water. Then the pH was adjusted to 8.3 with 4 M HCl. The solution was filtered through a 0.22 μm filter and degassed. Lastly, 5 μL of surfactant p20 was added and the solution was gently mixed. Solution was stored at 2-8ºC until needed and then equilibrated to room temperature.

Imidazole solution

To prepare a 500 millimolar imidazole solution, approximately 1.702 grams of imidazole (pale yellow, large flaky crystals) were combined with fifty milliliters of water, mixed, and filtered through a 0.22 micron filter, capped and parafilmed. To protect solution from light, a brown bottle was used. This solution was stored at 2-8ºC and equilibrated to room temperature before use.

2.8. Summary

Preparation and characterization of surfaces and self-assembled monolayers was important in determination of their quality and characteristics to evaluate their suitability for experiments. AFM, SPR, and fluorescence microscopy in conjunction with surface and sample preparation techniques serve as valuable assets in the analysis of protein surface interactions. Finally, solution preparation is a vital component contributing to the success of any experiment. Through employing these techniques and characterization methods, model substrates can be prepared and characterized for use as well-defined substrates in protein-surface adsorption experiments. Furthermore, AFM enables not only surface characterization, but also surface modification to fabricate nanostructured materials to perform more sophisticated investigations. For details of the experiments and analysis of protein surface interactions investigated, see chapter three for fibrinogen studies and chapter four for F_1-ATPase investigations.

2.9. References

1. Hair, M. L., *Infrared spectroscopy in surface chemistry*. M. Dekker: 1967.
2. Tamm, L. K.; Tatulian, S. A., Infrared spectroscopy of proteins and peptides in lipid bilayers. *Quarterly Reviews of Biophysics* **1997,** *30* (04), 365-429.
3. Lu, D. R.; Park, K., Effect of surface hydrophobicity on the conformational changes of adsorbed fibrinogen. *Journal of Colloid and Interface Science* **1991,** *144* (1), 271-281.
4. Liley, M.; Keller, T. A.; Duschl, C.; Vogel, H., Direct Observation of Self-Assembled Monolayers, Ion Complexation, and Protein Conformation at the Gold/Water Interface: An FTIR Spectroscopic Approach. *Langmuir* **1997,** *13* (16), 4190-4192.
5. Tengvall, P.; Lundström, I.; Liedberg, B., Protein adsorption studies on model organic surfaces: an ellipsometric and infrared spectroscopic approach. *Biomaterials* **1998,** *19* (4–5), 407-422.
6. Desroches, M. J.; Chaudhary, N.; Omanovic, S., PM-IRRAS investigation of the interaction of serum albumin and fibrinogen with a biomedical-grade stainless steel 316LVM surface. *Biomacromolecules* **2007,** *8* (9), 2836-2844.
7. Wagner, M. S.; Castner, D. G., Analysis of adsorbed proteins by static time-of-flight secondary ion mass spectrometry. *Applied Surface Science* **2004,** *231–232* (0), 366-376.
8. Wertz, C. F.; Santore, M. M., Effect of Surface Hydrophobicity on Adsorption and Relaxation Kinetics of Albumin and Fibrinogen: Single-Species and Competitive Behavior. *Langmuir* **2001,** *17* (10), 3006-3016.
9. Wertz, C. F.; Santore, M. M., Adsorption and Reorientation Kinetics of Lysozyme on Hydrophobic Surfaces. *Langmuir* **2002,** *18* (4), 1190-1199.
10. Waner, M. J.; Gilchrist, M.; Schindler, M.; Dantus, M., Imaging the Molecular Dimensions and Oligomerization of Proteins at Liquid/Solid Interfaces. *The Journal of Physical Chemistry B* **1998,** *102* (9), 1649-1657.
11. Santos, N. C.; Castanho, M. A. R. B., An overview of the biophysical applications of atomic force microscopy. *Biophysical Chemistry* **2004,** *107* (2), 133-149.
12. Karrasch, S.; Hegerl, R.; Hoh, J. H.; Baumeister, W.; Engel, A., Atomic Force Microscopy Produces Faithful High-Resolution Images of Protein Surfaces in an Aqueous Environment. *Proceedings of the National Academy of Sciences of the United States of America* **1994,** *91* (3), 836-838.
13. Marchin, K. L.; Berrie, C. L., Conformational Changes in the Plasma Protein Fibrinogen upon Adsorption to Graphite and Mica Investigated by Atomic Force Microscopy. *Langmuir* **2003,** *19* (23), 9883-9888.
14. Gettens, R. T. T.; Bai, Z.; Gilbert, J. L., Quantification of the kinetics and thermodynamics of protein adsorption using atomic force microscopy. *Journal of Biomedical Materials Research Part A* **2005,** *72A* (3), 246-257.
15. Tsapikouni, T. S.; Missirlis, Y. F., pH and ionic strength effect on single fibrinogen molecule adsorption on mica studied with AFM. *Colloids and Surfaces B: Biointerfaces* **2007,** *57* (1), 89-96.
16. Liu, Y.; Jaiswal, A.; Poggi, M. A.; Wilson, W. D., Surface Plasmon Resonance and Quartz Crystal Microbalance Methods for Detection of Molecular Interactions. In *Chemosensors*, John Wiley & Sons, Inc.: 2011; pp 329-344.
17. Green, R. J.; Frazier, R. A.; Shakesheff, K. M.; Davies, M. C.; Roberts, C. J.; Tendler, S. J. B., Surface plasmon resonance analysis of dynamic biological interactions with biomaterials. *Biomaterials* **2000,** *21* (18), 1823-1835.

18. Schuck, P., Use of Surface Plasmon Resonance to Probe the Equilibrium and Dynamic Aspects of Interactions Between Biological Macromolecules. *Annual Review of Biophysics and Biomolecular Structure* **1997,** *26* (1), 541-566.
19. Liedberg, B.; Nylander, C.; Lundström, I., Biosensing with surface plasmon resonance -- how it all started. *Biosensors and Bioelectronics* **1995,** *10* (8), i-ix.
20. Myszka, D. G., Kinetic analysis of macromolecular interactions using surface plasmon resonance biosensors. *Current Opinion in Biotechnology* **1997,** *8* (1), 50-57.
21. Mrksich, M.; Sigal, G. B.; Whitesides, G. M., Surface Plasmon Resonance Permits in Situ Measurement of Protein Adsorption on Self-Assembled Monolayers of Alkanethiolates on Gold. *Langmuir* **1995,** *11* (11), 4383-4385.
22. Kim, K. H.; Kim, J. D.; Kim, Y. J.; Kang, S. H.; Jung, S. Y.; Jung, H., Protein Immobilization Without Purification via Dip-Pen Nanolithography. *Small* **2008,** *4* (8), 1089-1094.
23. Tompkins, H. A., *A User's Guide to Ellipsometry* Academic Press, Inc.: San Diego, 1993.
24. Hu, Y.; Liu, G. Y.; Mrksich, M.; Vanderah, D. J.; Vanderlick, T. K.; Scoles, G. In *Comparative AFM study of compressibility and friction of unmodified and PEG-modified alkane thiol SAMS on Au(111) using nanografting*, 2003; pp 251-COLL.
25. Le Clair, S. V.; Nguyen, K.; Chen, Z., Sum Frequency Generation Studies on Bioadhesion: Elucidating the Molecular Structure of Proteins at Interfaces. *The Journal of Adhesion* **2009,** *85* (8), 484-511.
26. Hlady, V.; Buijs, J.; Jennissen, H. P.; Ronald, W., [26] Methods for studying protein adsorption. In *Methods in Enzymology*, Academic Press: 1999; Vol. Volume 309, pp 402-429.
27. Nakanishi, K.; Sakiyama, T.; Imamura, K., On the adsorption of proteins on solid surfaces, a common but very complicated phenomenon. *Journal of Bioscience and Bioengineering* **2001,** *91* (3), 233-244.
28. Jung, S.-Y.; Lim, S.-M.; Albertorio, F.; Kim, G.; Gurau, M. C.; Yang, R. D.; Holden, M. A.; Cremer, P. S., The Vroman Effect: A Molecular Level Description of Fibrinogen Displacement. *Journal of the American Chemical Society* **2003,** *125* (42), 12782-12786.
29. Love, J. C.; Estroff, L. A.; Kriebel, J. K.; Nuzzo, R. G.; Whitesides, G. M., Self-assembled monolayers of thiolates on metals as a form of nanotechnology. *Chem. Rev.* **2005,** *105* (4), 1103-1169.
30. Laibinis, P. E.; Whitesides, G. M.; Allara, D. L.; Tao, Y. T.; Parikh, A. N.; Nuzzo, R. G., Comparison of the structures and wetting properties of self-assembled monolayers of n-alkanethiols on the coinage metal surfaces, copper, silver, and gold. *Journal of the American Chemical Society* **1991,** *113* (19), 7152-7167.
31. Platypus Au Website. http://www.platypustech.com/goldsubstrates.html (accessed January 21, 2012).
32. Platypus Gold Coated Substrates. http://www.amsbio.com/presentation/GoldCoatedSubstrates.pdf (accessed June 18, 2012).
33. Agilent Agilent Technologies Website_Hydrogen Flame Annealing. http://www.home.agilent.com/agilent/editorial.jspx?cc=FR&lc=fre&ckey=914989&id=914989 (accessed June 1, 2012).
34. VanScyoc, W. A. S., Biacore, Inc.), BiaCore Slides. Settle, J., Ed.

35. Hegner, M.; Wagner, P.; Semenza, G., Ultralarge atomically flat template-stripped Au surfaces for scanning probe microscopy. *Surface Science* **1993,** *291* (1–2), 39-46.
36. Nogues, C.; Wanunu, M., A rapid approach to reproducible, atomically flat gold films on mica. *Surface Science* **2004,** *573* (3), L383-L389.
37. Cacciafesta, P.; Humphris, A. D. L.; Jandt, K. D.; Miles, M. J., Human Plasma Fibrinogen Adsorption on Ultraflat Titanium Oxide Surfaces Studied with Atomic Force Microscopy. *Langmuir* **2000,** *16* (21), 8167-8175.
38. SPI Molecular Imaging Picosubstrates™_Instructions for flame annealing and use. http://www.2spi.com/catalog/gold-sub2.html (accessed June 1, 2012).
39. Love, J. C.; Wolfe, D. B.; Haasch, R.; Chabinyc, M. L.; Paul, K. E.; Whitesides, G. M.; Nuzzo, R. G., Formation and Structure of Self-Assembled Monolayers of Alkanethiolates on Palladium. *Journal of the American Chemical Society* **2003,** *125* (9), 2597-2609.
40. Lin, F.; Meier, D. J., Atomic-Scale Resolution in Atomic Force Microscopy. *Langmuir* **1994,** *10* (6), 1660-1662.
41. Albrecht, T. R.; Quate, C. F., Atomic resolution imaging of a nonconductor by atomic force microscopy. *Journal of Applied Physics* **1987,** *62* (7), 2599-2602.
42. Ulman, A., *An Introduction to Ultrathin Organic Films: From Langmuir-Blodgett to Self-Assembly*. Academic Press: 1991.
43. Schreiber, F., Structure and growth of self-assembling monolayers. *Progress in Surface Science* **2000,** *65* (5–8), 151-257.
44. Willey, T. M.; Vance, A. L.; van Buuren, T.; Bostedt, C.; Terminello, L. J.; Fadley, C. S., Rapid degradation of alkanethiol-based self-assembled monolayers on gold in ambient laboratory conditions. *Surface Science* **2005,** *576* (1-3), 188-196.
45. Yang, G. H.; Amro, N. A.; Starkewolfe, Z. B.; Liu, G. Y., Molecular-level approach to inhibit degradations of alkanethiol self-assembled monolayers in aqueous media. *Langmuir* **2004,** *20* (10), 3995-4003.
46. Schlenoff, J. B.; Li, M.; Ly, H., Stability and Self-Exchange in Alkanethiol Monolayers. *Journal of the American Chemical Society* **1995,** *117* (50), 12528-12536.
47. Reed, M. A.; Tour, J. M., Computing with molecules. *Sci Am* **2000,** *282* (6), 86-93.
48. Ulman, A., Formation and Structure of Self-Assembled Monolayers. *Chem. Rev.* **1996,** *96* (4), 1533-1554.
49. Dubois, L. H.; Nuzzo, R. G., Synthesis, Structure, and Properties of Model Organic Surfaces. *Annual Review of Physical Chemistry* **1992,** *43* (1), 437-463.
50. Houseman, B. T.; Gawalt, E. S.; Mrksich, M., Maleimide-Functionalized Self-Assembled Monolayers for the Preparation of Peptide and Carbohydrate Biochips†. *Langmuir* **2003,** *19* (5), 1522-1531.
51. Neal, B. M.; Vorushilov, A. S.; DeLaRosa, A. M.; Robinson, R. E.; Berrie, C. L.; Barybin, M. V., Ancillary nitrile substituents as convenient IR spectroscopic reporters for self-assembly of mercapto- and isocyanoazulenes on Au(111). *Chemical Communications* **2011,** *47* (38), 10803-10805.
52. Devaraj, N. K.; Miller, G. P.; Ebina, W.; Kakaradov, B.; Collman, J. P.; Kool, E. T.; Chidsey, C. E. D., Chemoselective Covalent Coupling of Oligonucleotide Probes to Self-Assembled Monolayers. *Journal of the American Chemical Society* **2005,** *127* (24), 8600-8601.
53. Kluth, G. J.; Sander, M.; Sung, M. M.; Maboudian, R. In *Study of the desorption mechanism of alkylsiloxane self-assembled monolayers through isotopic labeling and high resolution electron energy-loss spectroscopy experiments*, San Jose, California (USA), AVS: San Jose, California (USA), 1998; pp 932-936.

54. Nuzzo, R. G.; Allara, D. L., Adsorption of bifunctional organic disulfides on gold surfaces. *Journal of the American Chemical Society* **1983,** *105* (13), 4481-4483.
55. Wang, H.; Chen, S.; Li, L.; Jiang, S., Improved Method for the Preparation of Carboxylic Acid and Amine Terminated Self-Assembled Monolayers of Alkanethiolates. *Langmuir* **2005,** *21* (7), 2633-2636.
56. Inc., A. Self-Assembing Molecules_Variations in the Assembly Protocol for Carboxy- and Amine-Terminated Alkanethiols. www.asemblon.com (accessed April 1, 2009).
57. Wasserman, S. R.; Tao, Y. T.; Whitesides, G. M., Structure and reactivity of alkylsiloxane monolayers formed by reaction of alkyltrichlorosilanes on silicon substrates. *Langmuir* **1989,** *5* (4), 1074-1087.
58. Linford, M. R.; Chidsey, C. E. D., Alkyl monolayers covalently bonded to silicon surfaces. *Journal of the American Chemical Society* **1993,** *115* (26), 12631-12632.
59. Linford, M. R.; Fenter, P.; Eisenberger, P. M.; Chidsey, C. E. D., Alkyl Monolayers on Silicon Prepared from 1-Alkenes and Hydrogen-Terminated Silicon. *Journal of the American Chemical Society* **1995,** *117* (11), 3145-3155.
60. Sung, M. M.; Kluth, G. J.; Yauw, O. W.; Maboudian, R., Thermal Behavior of Alkyl Monolayers on Silicon Surfaces. *Langmuir* **1997,** *13* (23), 6164-6168.
61. Bain, C. D.; Troughton, E. B.; Tao, Y. T.; Evall, J.; Whitesides, G. M.; Nuzzo, R. G., Formation of monolayer films by the spontaneous assembly of organic thiols from solution onto gold. *Journal of the American Chemical Society* **1989,** *111* (1), 321-335.
62. Erbil, H. Y., *Surface Chemistry of Solid And Liquid Interfaces*. Blackwell Pub.: 2006.
63. Mendoza, S. M.; Arfaoui, I.; Zanarini, S.; Paolucci, F.; Rudolf, P., Improvements in the Characterization of the Crystalline Structure of Acid-Terminated Alkanethiol Self-Assembled Monolayers on Au(111). *Langmuir* **2007,** *23* (2), 582-588.
64. Evans-Nguyen, K. M.; Schoenfisch, M. H., Fibrin Proliferation at Model Surfaces: Influence of Surface Properties. *Langmuir* **2005,** *21* (5), 1691-1694.
65. Frutos, A. G.; Brockman, J. M.; Corn, R. M., Reversible Protection and Reactive Patterning of Amine- and Hydroxyl-Terminated Self-Assembled Monolayers on Gold Surfaces for the Fabrication of Biopolymer Arrays. *Langmuir* **1999,** *16* (5), 2192-2197.
66. Pan, W.; Durning, C. J.; Turro, N. J., Kinetics of Alkanethiol Adsorption on Gold. *Langmuir* **1996,** *12* (18), 4469-4473.
67. Kohli, P.; Taylor, K. K.; Harris, J. J.; Blanchard, G. J., Assembly of Covalently-Coupled Disulfide Multilayers on Gold. *Journal of the American Chemical Society* **1998,** *120* (46), 11962-11968.
68. Colvin, V. L.; Goldstein, A. N.; Alivisatos, A. P., Semiconductor nanocrystals covalently bound to metal surfaces with self-assembled monolayers. *Journal of the American Chemical Society* **1992,** *114* (13), 5221-5230.
69. Valerio, E.; Abrantes, L. M.; Viana, A. S., 4-Aminothiophenol Self-Assembled Monolayer for the Development of a DNA Biosensor Aiming the Detection of Cylindrospermopsin Producing Cyanobacteria. *Electroanalysis* **2008,** *20* (22), 2467-2474.
70. Ruths, M., Boundary Friction of Aromatic Self-Assembled Monolayers: Comparison of Systems with One or Both Sliding Surfaces Covered with a Thiol Monolayer. *Langmuir* **2003,** *19* (17), 6788-6795.
71. Watanabe, M.; Kajikawa, K., An optical fiber biosensor based on anomalous reflection of gold. *Sensors and Actuators B: Chemical* **2003,** *89* (1–2), 126-130.

72. Porter, M. D.; Bright, T. B.; Allara, D. L.; Chidsey, C. E. D., Spontaneously organized molecular assemblies. 4. Structural characterization of n-alkyl thiol monolayers on gold by optical ellipsometry, infrared spectroscopy, and electrochemistry. *Journal of the American Chemical Society* **1987,** *109* (12), 3559-3568.
73. Han, T.; Beebe, T. P., Scanning Probe Microscopy Depth Measurements of Self-Assembled Monolayer Structures on Gold. *Langmuir* **1994,** *10* (8), 2705-2709.
74. Kondo, T.; Yanagida, M.; Shimazu, K.; Uosaki, K., Determination of Thickness of a Self-Assembled Monolayer of Dodecanethiol on Au(111) by Angle-Resolved X-ray Photoelectron Spectroscopy. *Langmuir* **1998,** *14* (19), 5656-5658.
75. Parikh, A. N.; Allara, D. L.; Azouz, I. B.; Rondelez, F., An Intrinsic Relationship between Molecular Structure in Self-Assembled n-Alkylsiloxane Monolayers and Deposition Temperature. *The Journal of Physical Chemistry* **1994,** *98* (31), 7577-7590.
76. Braga, P. C.; Ricci, D., *Atomic Force Microscopy: Biomedical Methods and Applications*. Humana Press: 2004.
77. Pattier, B.; Bardeau, J.-F.; Edely, M.; Gibaud, A.; Delorme, N., Cheap and Robust Ultraflat Gold Surfaces Suitable for High-Resolution Surface Modification. *Langmuir* **2008,** *24* (3), 821-825.
78. Xu, S.; Miller, S.; Laibinis, P. E.; Liu, G.-y., Fabrication of Nanometer Scale Patterns within Self-Assembled Monolayers by Nanografting. *Langmuir* **1999,** *15* (21), 7244-7251.
79. Ishida, N.; Inoue, T.; Miyahara, M.; Higashitani, K., Nano Bubbles on a Hydrophobic Surface in Water Observed by Tapping-Mode Atomic Force Microscopy. *Langmuir* **2000,** *16* (16), 6377-6380.
80. Liu, G.-y.; Salmeron, M. B., Reversible Displacement of Chemisorbed n-Alkanethiol Molecules on Au(111) Surface: An Atomic Force Microscopy Study. *Langmuir* **1994,** *10* (2), 367-370.
81. Browning-Kelley, M. E.; Wadu-Mesthrige, K.; Hari, V.; Liu, G. Y., Atomic Force Microscopic Study of Specific Antigen/Antibody Binding. *Langmuir* **1997,** *13* (2), 343-350.
82. Wadu-Mesthrige, K.; Xu, S.; Amro, N. A.; Liu, G.-y., Fabrication and Imaging of Nanometer-Sized Protein Patterns. *Langmuir* **1999,** *15* (25), 8580-8583.
83. Liu, M.; Liu, G.-Y., Hybridization with Nanostructures of Single-Stranded DNA. *Langmuir* **2005,** *21* (5), 1972-1978.
84. Evans-Nguyen, K. M.; Fuierer, R. R.; Fitchett, B. D.; Tolles, L. R.; Conboy, J. C.; Schoenfisch, M. H., Changes in Adsorbed Fibrinogen upon Conversion to Fibrin. *Langmuir* **2006,** *22* (11), 5115-5121.
85. Uchihashi, T.; Iino, R.; Ando, T.; Noji, H., High-Speed Atomic Force Microscopy Reveals Rotary Catalysis of Rotorless F1-ATPase. *Science* **2011,** *333* (6043), 755-758.
86. Wagner, P., Immobilization strategies for biological scanning probe microscopy. *FEBS Letters* **1998,** *430* (1–2), 112-115.
87. Hansma, H. G.; Vesenka, J.; Siegerist, C.; Kelderman, G.; Morrett, H.; Sinsheimer, R. L.; Elings, V.; Bustamante, C.; Hansma, P. K., Reproducible Imaging and Dissection of Plasmid DNA Under Liquid with the Atomic Force Microscope. *Science* **1992,** *256* (5060), 1180-1184.
88. Müller, D. J.; Sass, H.-J.; Müller, S. A.; Büldt, G.; Engel, A., Surface structures of native bacteriorhodopsin depend on the molecular packing arrangement in the membrane. *Journal of Molecular Biology* **1999,** *285* (5), 1903-1909.
89. Seelert, H.; Poetsch, A.; Dencher, N. A.; Engel, A.; Stahlberg, H.; Muller, D. J., Structural biology: Proton-powered turbine of a plant motor. *Nature* **2000,** *405* (6785), 418-419.

90. Stahlberg, H.; Muller, D. J.; Suda, K.; Fotiadis, D.; Engel, A.; Meier, T.; Matthey, U.; Dimroth, P., Bacterial Na+-ATP synthase has an undecameric rotor. *EMBO Reports* **2001,** *2* (3), 229-233.
91. Tan, Y. H.; Liu, M.; Nolting, B.; Go, J. G.; Gervay-Hague, J.; Liu, G.-y., A Nanoengineering Approach for Investigation and Regulation of Protein Immobilization. *Acs Nano* **2008,** *2* (11), 2374-2384.
92. Chen, S.; Liu, L.; Zhou, J.; Jiang, S., Controlling Antibody Orientation on Charged Self-Assembled Monolayers. *Langmuir* **2003,** *19* (7), 2859-2864.
93. Müller, D. J.; Schoenenberger, C.-A.; Schabert, F.; Engel, A., Structural Changes in Native Membrane Proteins Monitored at Subnanometer Resolution with the Atomic Force Microscope: A Review. *Journal of Structural Biology* **1997,** *119* (2), 149-157.
94. Ta, T. C.; Sykes, M. T.; McDermott, M. T., Real-Time Observation of Plasma Protein Film Formation on Well-Defined Surfaces with Scanning Force Microscopy. *Langmuir* **1998,** *14* (9), 2435-2443.
95. Li, L.; Chen, S.; Oh, S.; Jiang, S., In Situ Single-Molecule Detection of Antibody−Antigen Binding by Tapping-Mode Atomic Force Microscopy. *Analytical Chemistry* **2002,** *74* (23), 6017-6022.
96. MikroMasch Main Page and AFM Probes. http://www.spmtips.com/main/ (accessed March 2012).
97. Yu, J.-J.; Ngunjiri, J. N.; Kelley, A. T.; Garno, J. C., Nanografting versus Solution Self-Assembly of α,ω-Alkanedithiols on Au(111) Investigated by AFM. *Langmuir* **2008,** *24* (20), 11661-11668.
98. Headrick, J. E.; Armstrong, M.; Cratty, J.; Hammond, S.; Sheriff, B. A.; Berrie, C. L., Nanoscale Patterning of Alkyl Monolayers on Silicon Using the Atomic Force Microscope. *Langmuir* **2005,** *21* (9), 4117-4122.
99. Xu, S.; Liu, G.-y., Nanometer-Scale Fabrication by Simultaneous Nanoshaving and Molecular Self-Assembly. *Langmuir* **1997,** *13* (2), 127-129.
100. Liu, G.-Y.; Xu, S.; Qian, Y., Nanofabrication of Self-Assembled Monolayers Using Scanning Probe Lithography. *Accounts of Chemical Research* **2000,** *33* (7), 457-466.
101. Kelley, A. T.; Ngunjiri, J. N.; Serem, W. K.; Lawrence, S. O.; Yu, J.-J.; Crowe, W. E.; Garno, J. C., Applying AFM-Based Nanofabrication for Measuring the Thickness of Nanopatterns: The Role of Head Groups in the Vertical Self-Assembly of ω-Functionalized n-Alkanethiols. *Langmuir* **2010,** *26* (5), 3040-3049.
102. Amro, N. A.; Xu, S.; Liu, G.-y., Patterning Surfaces Using Tip-Directed Displacement and Self-Assembly. *Langmuir* **2000,** *16* (7), 3006-3009.
103. Xu, S.; Laibinis, P. E.; Liu, G. Y., Accelerating the kinetics of thiol self-assembly on gold - A spatial confinement effect. *Journal of the American Chemical Society* **1998,** *120* (36), 9356-9361.
104. Torres-Gavosto, R.; Berrie, C. L., In Preparation. **2012**.
105. Fuchs, D., J.; Weiss, P. S., Insertion of 1,10-decanedithiol in decanethiolate self-assembled monolayers on Au{111}. *Nanotechnology* **2007,** *18* (4), 1-7.
106. Dunbar, T. D.; Cygan, M. T.; Bumm, L. A.; McCarty, G. S.; Burgin, T. P.; Reinerth, W. A.; Jones, L.; Jackiw, J. J.; Tour, J. M.; Weiss, P. S.; Allara, D. L., Combined Scanning Tunneling Microscopy and Infrared Spectroscopic Characterization of Mixed Surface Assemblies of Linear Conjugated Guest Molecules in Host Alkanethiolate Monolayers on Gold. *The Journal of Physical Chemistry B* **2000,** *104* (20), 4880-4893.

107. Davis, T. M.; Wilson, W. D., Determination of the Refractive Index Increments of Small Molecules for Correction of Surface Plasmon Resonance Data. *Analytical Biochemistry* **2000,** *284* (2), 348-353.
108. Myszka, D. G.; Rich, R. L., Implementing surface plasmon resonance biosensors in drug discovery. *Pharmaceutical Science & Technology Today* **2000,** *3* (9), 310-317.
109. Okahata, Y.; Kawase, M.; Niikura, K.; Ohtake, F.; Furusawa, H.; Ebara, Y., Kinetic Measurements of DNA Hybridization on an Oligonucleotide-Immobilized 27-MHz Quartz Crystal Microbalance. *Analytical Chemistry* **1998,** *70* (7), 1288-1296.
110. Baird, C. L.; Courtenay, E. S.; Myszka, D. G., Surface plasmon resonance characterization of drug/liposome interactions. *Analytical Biochemistry* **2002,** *310* (1), 93-99.
111. Balon, K.; Riebesehl, B. U.; Müller, B. W., Drug Liposome Partitioning as a Tool for the Prediction of Human Passive Intestinal Absorption. *Pharmaceutical Research* **1999,** *16* (6), 882-888.
112. Danelian, E.; Karlén, A.; Karlsson, R.; Winiwarter, S.; Hansson, A.; Löfås, S.; Lennernäs, H.; Hämäläinen, M. D., SPR Biosensor Studies of the Direct Interaction between 27 Drugs and a Liposome Surface: Correlation with Fraction Absorbed in Humans. *Journal of Medicinal Chemistry* **2000,** *43* (11), 2083-2086.
113. Karlsson, R., SPR for molecular interaction analysis: a review of emerging application areas. *Journal of Molecular Recognition* **2004,** *17* (3), 151-161.
114. Huang, Y.-W.; Gupta, V. K., A SPR and AFM study of the effect of surface heterogeneity on adsorption of proteins. *The Journal of Chemical Physics* **2004,** *121* (5), 2264-2271.
115. Vutukuru, S.; Bethi, S. R.; Kane, R. S., Protein Interactions with Self-Assembled Monolayers Presenting Multimodal Ligands: A Surface Plasmon Resonance Study. *Langmuir* **2006,** *22* (24), 10152-10156.
116. Evans-Nguyen, K. M.; Tolles, L. R.; Gorkun, O. V.; Lord, S. T.; Schoenfisch, M. H., Interactions of Thrombin with Fibrinogen Adsorbed on Methyl-, Hydroxyl-, Amine-, and Carboxyl-Terminated Self-Assembled Monolayers†. *Biochemistry* **2005,** *44* (47), 15561-15568.
117. Green, R. J.; Davies, J.; Davies, M. C.; Roberts, C. J.; Tendler, S. J. B., Surface plasmon resonance for real time in situ analysis of protein adsorption to polymer surfaces. *Biomaterials* **1997,** *18* (5), 405-413.
118. Green, R. J.; Davies, M. C.; Roberts, C. J.; Tendler, S. J. B., Competitive protein adsorption as observed by surface plasmon resonance. *Biomaterials* **1999,** *20* (4), 385-391.
119. Canziani, G. A.; Klakamp, S.; Myszka, D. G., Kinetic screening of antibodies from crude hybridoma samples using Biacore. *Analytical Biochemistry* **2004,** *325* (2), 301-307.
120. Rich, R. L.; Day, Y. S. N.; Morton, T. A.; Myszka, D. G., High-Resolution and High-Throughput Protocols for Measuring Drug/Human Serum Albumin Interactions Using BIACORE. *Analytical Biochemistry* **2001,** *296* (2), 197-207.
121. Stenlund, P.; Frostell-Karlsson, A.; Karlsson, O. P., Studies of small molecule interactions with protein phosphatases using biosensor technology. *Analytical Biochemistry* **2006,** *353* (2), 217-225.
122. *BiaCore 3000 Instrument Handbook*. October 2003 (Version AE) ed.
123. Karlsson, R.; Katsamba, P. S.; Nordin, H.; Pol, E.; Myszka, D. G., Analyzing a kinetic titration series using affinity biosensors. *Analytical Biochemistry* **2006,** *349* (1), 136-147.

124. O'Shannessy, D. J.; Brigham-Burke, M.; Karl Soneson, K.; Hensley, P.; Brooks, I.; Michael, L. J. a. L. B., [15] Determination of rate and equilibrium binding constants for macromolecular interactions by surface plasmon resonance. In *Methods in Enzymology*, Academic Press: 1994; Vol. Volume 240, pp 323-349.
125. Morton, T. A.; Myszka, D. G.; Chaiken, I. M., Interpreting Complex Binding Kinetics from Optical Biosensors: A Comparison of Analysis by Linearization, the Integrated Rate Equation, and Numerical Integration. *Analytical Biochemistry* **1995,** *227* (1), 176-185.
126. Önell, A.; Andersson, K., Kinetic determinations of molecular interactions using Biacore—minimum data requirements for efficient experimental design. *Journal of Molecular Recognition* **2005,** *18* (4), 307-317.
127. Fägerstam, L. G.; Frostell, Å.; Karlsson, R.; Kullman, M.; Larsson, A.; Malmqvist, M.; Butt, H., Detection of antigen—antibody interactions by surface plasmon resonance. Application to Epitope Mapping. *Journal of Molecular Recognition* **1990,** *3* (5-6), 208-214.
128. Daniels, P. B.; Deacon, J. K.; Eddowes, M. J.; Pedley, D. G., Surface plasmon resonance applied to immunosensing. *Sensors and Actuators* **1988,** *15* (1), 11-18.
129. Morgan, H.; Taylor, D. M.; D'Silva, C., Surface plasmon resonance studies of chemisorbed biotin-streptavidin multilayers. *Thin Solid Films* **1992,** *209* (1), 122-126.
130. Sigal, G. B.; Bamdad, C.; Barberis, A.; Strominger, J.; Whitesides, G. M., A Self-Assembled Monolayer for the Binding and Study of Histidine-Tagged Proteins by Surface Plasmon Resonance. *Anal. Chem.* **1996,** *68* (3), 490-497.
131. Johnson, I. D.; Technologies, L.; Haugland, R. P.; Spence, M. T. Z., *The Molecular Probes Handbook: A Guide to Fluorescent Probes and Labeling Technologies, 11th Edition*. Life Technologies: 2010.
132. Scientific, T. Instructions TCEP*HCl. http://www.piercenet.com/Products/Browse.cfm?fldID=02051012&WT.mc_id=go_TCEP_TCEP_pf&gclid=CPyCmt_r6a0CFUcCQAod5T678g (accessed May 1, 2012).
133. Atkins, P.; De Paula, J.; Friedman, R., *Quanta, Matter and Change: A Molecular Appraoch to Physical Change*. W. H. Freeman: 2008.
134. Binder, A.; Jagendorf, A.; Ngo, E., Isolation and composition of the subunits of spinach chloroplast coupling factor protein. *Journal of Biological Chemistry* **1978,** *253* (9), 3094-3100.
135. Richter, M. L.; Snyder, B.; McCarty, R. E.; Hammes, G. G., Binding stoichiometry and structural mapping of the .epsilon. polypeptide of chloroplast coupling factor 1. *Biochemistry* **1985,** *24* (21), 5755-5763.
136. Bradford, M. M., A rapid and sensitive method for the quantitation of microgram quantities of protein utilizing the principle of protein-dye binding. *Analytical Biochemistry* **1976,** *72* (1–2), 248-254.
137. Kröger, D.; Liley, M.; Schiweck, W.; Skerra, A.; Vogel, H., Immobilization of histidine-tagged proteins on gold surfaces using chelator thioalkanes. *Biosensors and Bioelectronics* **1999,** *14* (2), 155-161.
138. Rigler, P.; Ulrich, W.-P.; Hoffmann, P.; Mayer, M.; Vogel, H., Reversible Immobilization of Peptides: Surface Modification and In Situ Detection by Attenuated Total Reflection FTIR Spectroscopy. *ChemPhysChem* **2003,** *4* (3), 268-275.

CHAPTER THREE:

Fibrinogen Adsorption on Model Surfaces: Investigations of Nonspecific Adsorption

3. Overview

The plasma protein fibrinogen is a key component in thrombosis or blood clotting. Thus, understanding its adsorption at surfaces is important to improving both biocompatibility and biosensing capabilities. However, to date a detailed description of fibrinogen adsorption to surfaces is still lacking. This section describes studies which investigated fibrinogen adsorption on different model surfaces, including self-assembled monolayers, using both atomic force microscopy (AFM) and surface plasmon resonance (SPR). AFM images were obtained both dry and in pseudo-physiologically relevant conditions with tapping mode in order to determine the conformation and structure of the surface bound protein film. Individual and sequential injections of increasing fibrinogen concentration were performed on different surfaces and used to study nonspecific fibrinogen adsorption to surface via SPR to determine affinity and kinetics data. Differences in the maximal uptake of fibrinogen on different surfaces measured by SPR were correlated with changes in the conformation observed in AFM height images. The comparison of the SPR and AFM data allows for a more complete description of the dynamic nature of fibrinogen adsorption to a variety of surfaces.

3.1. Fibrinogen Background

Fibrinogen is an important plasma protein with a critical role in blood clotting cascade or thrombosis. Typically this role is advantageous, for example, if a person is cut and bleeding, a clot is desired to stop the bleeding. This process saves lives; people with blood clotting disorders are at risk for bleeding to death. However, with

implants, this clotting can lead to incompatibility and even rejection of the implant if a clot encapsulates it. Additionally, if a blood clot formed around the outside of a biosensor, this could render biosensor useless, as the analyte would be blocked from the detection site.

Fibrinogen is the third most prevalent plasma protein, behind albumin and immunoglobulins.[1] The typical fibrinogen concentration in blood is approximately 3 mg/mL.[2] When an injury occurs, signals are released to initiate conversion of prothrombin to thrombin. Thrombin then cleaves fibrinogen into fibrin which then polymerizes to form fibrils and ultimately, upon combination of red blood cells and other components, results in a blood clot.

Fibrinogen is a large plasma protein (340 kDa) with an isoelectric point of approximately 5.8.[3] As seen in the crystal structure (Figure 3.1a), fibrinogen consists of three globular domains connected by alpha-helical coiled-coil domains. These globular subunits of fibrinogen are labeled, D, E, and D with attached arms ending in alpha-C domains. The globular domains are hydrophobic while the arms and connecting regions and the alpha-C arms are hydrophilic (Figure 3.1b). Crystal structure measurements of fibrinogen report 45-50 nanometers for its length.[4, 5] The charge distribution across fibrinogen (which is determined by the amino acid sequence and pH) is positive on the alpha C domains and arms and negative on the globular domains at a pH of ~7.4.[6] Fibrinogen is known to bind strongly to a variety of surfaces. Fibrinogen contains a multitude of potential attachment sites that afford multiple chemical interactions for surface coordination. However, details of binding

are still not well understood and thus remain elusive. Studies have shown that there are differences on fibrinogen binding on different surfaces that have been attributed to conformational changes, but direct measurements are lacking. The mechanism and nature of this conformational change still need to be resolved. The effects of surface chemistry on dynamic behavior and kinetics of fibrinogen adsorption have so far proven inconclusive. The relative role of different interactions under different conditions remains critical for materials design and is not well-understood.

Surface used in biodevices and implants range from simple metals (titanium or platinum), to ceramics, to polymers [poly(urethane), poly(dimethylsiloxane), poly(ethylene)], depending on the device application.[7, 8] The properties (wettability, morphology, charge state) of these surfaces vary. Most of these materials were not designed for biomedical applications. Improving the design of these materials requires knowledge of the types of surfaces that are biocompatible (nontoxic) and will either resist nonspecific protein adsorption (such as fibrinogen) or protect it from an undesired physiological response, either of which will endanger the lifetime of the device or implant.

a)

b)

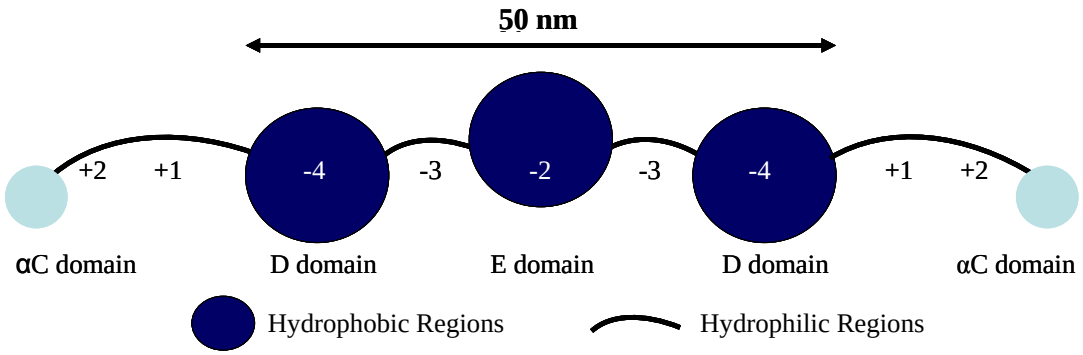

Figure 3.1: Fibrinogen Structure. a) Crystal structure (PDB: 1DEQ) [5] b) Schematic with charge distribution.[6]

3.1.1. Previous Investigations

This next set of sections details the previous investigations into fibrinogen adsorption to surfaces, including conformation and kinetic studies. Conformation of fibrinogen refers to the way fibrinogen adsorbs to surfaces. Typical conformations include a balled up form, "globular", or an extended form, "trinodular" (either linear or bent). Kinetics of fibrinogen adsorption to surfaces describes both the relative affinity of fibrinogen for surfaces as well as the ease with which fibrinogen is removed from the surface. A myriad of techniques (independently or in combination) have been utilized to investigate fibrinogen adsorption to surfaces including electron microscopy,[4, 9, 10] scanning transmission electron microscopy (STEM),[11] sum frequency generation vibrational spectroscopy,[12] ellipsometry,[13, 14] optical waveguide lightmode spectroscopy,[14] quartz crystal microbalance,[2, 14-16] atomic force microscopy,[3, 16-25] surface plasmon resonance,[24, 26-28] attenuated total reflection infrared spectroscopy,[12, 25, 29] radio labeling,[30] solution depletion,[31] and total internal reflectance spectroscopy.[32-34]

3.1.1.1. Conformations of Fibrinogen

Some conflicting evidence exists as to the conformation of fibrinogen on different surfaces, partially due to inconsistencies in solution, preparation, and imaging conditions. One study determined via AFM that fibrinogen was globular with a length of 28 nm on the silicon oxide surface and trinodular with a length of 47 nm on the hydrogen-terminated surface (both surfaces are hydrophilic with low contact angles, but they reported that the hydrogen-terminated surface had a lower

contact angle).[25] However, the concentration and time of protein adsorption varied greatly for the two measurements (incubation of a 0.2 μg/mL fibrinogen solution for 10 minutes and 20 μg/mL fibrinogen solution for 60 minutes, respectively).[25] Other studies[33] have shown that adsorption time influences spreading and denaturation of proteins, so the resultant comparison between these two surfaces may have not have been ideal.

Santore *et al.* studied the fibrinogen adsorption to a variety of surfaces via TIRF.[33] Three different surfaces, hydrophilic (N-(3-triethoxysilylpropyl)-4-hydroxybutyramide), hydrophobic (hexadecyltrichlorosilane), and superhydrophobic (1H,1H,2H,2H-perfluorodecyltrichlorsilane), were utilized to study fibrinogen adsorption to surfaces. The average footprint (or area covered by a fibrinogen molecule) as a function of the time to reach 75% coverage (a measure of how fast the protein was delivered to the surface) was monitored. This is determined by TIRF in which the intensity of fluorescence (from fluorescently labeled fibrinogen) was determined and then the number of molecules on the surface was back calculated and divided by the surface area to determine the footprint. Their data showed that initially, the footprint of fibrinogen is small, no matter what surface it was adsorbed onto. As fibrinogen adsorption time was increased, they observed that on the hydrophilic surface, the footprint did not grow much. However, on both the hydrophobic and superhydrophobic surfaces, as more adsorption time was allowed, the footprint of the protein increased significantly. Thus, on larger time scales, the footprint of fibrinogen was larger on the hydrophobic versus hydrophilic surface.

While these results are indicative of probable differences in protein conformation upon adsorption, these studies did not directly measure the protein conformation.

Missirlis *et al.* studied fibrinogen adsorption to mica via tapping mode AFM after thirty minute buffer incubation followed by sixty minute protein immersion then rinsing, and determined relative adsorption as a function of pH and ionic strength.[3] The three pHs studied were 3.5, 5.8 (isoelectric point of fibrinogen), and 7.4. Fibrinogen was found to have the greatest adsorption at pH 5.8, followed by pH 7.4, with the least amount of adsorption at pH 3.5. This was due to the decrease in electrostatic interactions and subsequent increase in hydrogen bonding and van der Waals forces which lead to an increase in adsorption near the isoelectric point. In terms of ionic strength, relative fibrinogen adsorption was highest at 150 mM (physiological value), followed by 15 mM, and then 500 mM. In this case, ions can screen the electrostatic repulsion so proteins can get closer to the surface and adsorb via van der Waals forces, thus a decrease in lateral electrostatic repulsions resulted in an increased amount of fibrinogen on the surface.

McDermott *et al.* studied fibrinogen adsorption to graphite and mica via scanning force microscopy in real-time, to study the growth mechanism of the resultant films.[22] They found that the morphology of fibrinogen adsorption is dependent upon the substrate.[22] They saw aggregates on graphite but no evidence of aggregates on mica.[22] They proposed a model for how fibrinogen adsorbs to the two different surfaces (through hydrophobic domains on graphite and the hydrophilic alpha-C arms on mica) and the resultant effect on film formation.[22]

Cremer *et al.* studied the displacement of fibrinogen from silica substrates with several techniques including AFM, vibrational sum frequency spectroscopy, immunochemical assays, and fluorescence microscopy.[6] They determined that fibrinogen adsorbed through the alpha-C domains via electrostatic interactions with the surface can be easily displaced by other proteins.[6] However, upon acidic pH cycling the conformation on the surfaces changes to a more elongated structure and the adsorption through van der Waals interactions causes a significant decrease in the ability of other proteins to displace fibrinogen.[6] Thus, fibrinogen adsorption to the surface and the resultant conformation may play a key role in subsequent interactions with other proteins and thus should influence the blood clotting cascade.[6]

For descriptions of other fibrinogen adsorption studies to surfaces via AFM, please see a review by Schoenfisch.[17] Briefly, a myriad of surfaces, solution conditions, incubation times, and imaging conditions result in a library of data that is not necessarily directly comparable.

3.1.1.2. Kinetics of Fibrinogen Adsorption

Another study by Santore's group resulted in TIRF data of the initial rate of adsorption of fluorescently labeled fibrinogen molecules as a function of fibrinogen concentration.[33] Their data analysis indicated that the initial rate of fibrinogen adsorption on the hydrophilic, hydrophobic, and superhydrophobic surface did not vary significantly, and thus was not surface dependent. And, as the fibrinogen concentration increases, so in a linear fashion did the initial rate of adsorption for all surfaces.

An AFM study of fibrinogen kinetics on mica versus graphite conducted by Gilbert's group revealed that adsorption to mica was fully reversible while adsorption to graphite was irreversible.[35] Kinetics of adsorption were similar on the two surfaces (k_a of 2.7 x 10^{-4} $mL \cdot \mu g^{-1} s^{-1}$ for mica versus 2.2 x 10^{-4} $mL \cdot \mu g^{-1} s^{-1}$ for graphite), but the kinetics of desorption was slower on the graphite surface (k_d of n/a or fully reversible for mica compared to 8.3 x 10^{-5} s^{-1} for graphite).[35]

Hu's group studied kinetics of fibrinogen adsorption via quartz crystal microbalance (QCM).[36] They advanced the study of fibrinogen kinetics by adding in a term for the conformational change or denaturation of fibrinogen after adsorption. They determined the following for kinetics of fibrinogen adsorption to a quartz surface, k_a of (8.03 ± 0.92) x 10^3 $M^{-1}s^{-1}$, k_d of (6.76 ± 0.76) x 10^{-3} s^{-1}, and a k_f of (5.32 ± 0.21) x 10^{-4} s^{-1}, where k_a was the association constant, k_d was the dissociation constant, and k_f was the irreversible adsorption constant. These constants were determined to be estimates of the true constants. Although they included an extra step in the kinetics model (in addition to the Langmuir model constraints) to account for an irreversible state possibility, their model may still be too simplistic for the complicated process of protein kinetics due to potential conformational changes upon adsorption and random orientations associated with nonspecific adsorption.[36]

Qualitative studies of relative protein adsorption to SAMs were performed via SPR. Schoenfisch determined via SPR that fibrinogen adsorption was greater on amine-terminated, followed by methyl-terminated, carboxyl-terminated, and finally hydroxyl-terminated SAMs.[15]

3.1.1.3. Current Investigation Goals

Previous investigations have both directly and indirectly determined fibrinogen adsorption characteristics.[37] For example, Santore studied fibrinogen adsorption to three different surfaces, a hydrophilic, hydrophobic, and superhydrophobic surface.[33] By monitoring adsorption through fluorescent tags on proteins using TIRF, they discovered that the initial adsorption rate is surface independent. The surface hydrophobicity did affect the footprint (or size) of the protein on the surface with a larger footprint on hydrophobic surfaces compared to hydrophilic surfaces. And, the more time fibrinogen was allowed to adsorb to the surface, the larger the footprint became on the hydrophobic surface while the fibrinogen footprint on the hydrophilic surface remained small even after longer adsorption times.[33]

While Santore's data suggested that the behavior of the fibrinogen footprint is surface dependent, this was determined via an indirect method and did not reveal what the difference was between fibrinogen adsorption to the different surfaces. They provided some evidence that surface matters, but did not answer what it was that caused this difference. Their data did not provide molecular scale details. Thus, one goal of my studies was to provide molecular scale details via AFM and well defined model surfaces to better understand these differences. More specifically, the goal of this section of the dissertation is to further investigate these phenomena using a direct method, AFM, to study the conformation of fibrinogen on a variety of

surfaces and then correlate that data with an indirect method, SPR, to determine if conformation of adsorbed protein can be correlated with observed kinetic properties.

Thus goals for this fibrinogen work include determining nonspecific adsorption and desorption kinetics as well as relative surface affinity via SPR and correlation of this data to conformation of protein on different surfaces determined from AFM. Various surface chemistries and conditions were tested to determine fibrinogen binding characteristics.

Nonspecific adsorption of fibrinogen was studied on a variety of surfaces via both AFM and SPR. Initially, studies on graphite and mica were used to represent model hydrophobic and hydrophilic surfaces, respectively. Later, self assembled monolayers (SAMs) were utilized as model surfaces containing hydrophobic, hydrophilic, neutral, positively, and negatively charged moieties [R-CH_3, R-OH, R-SH, R-(phenol)-NH_2, R-(CH_3)-NH_2, R-COOH, respectively]. When formed on smooth gold surfaces, these SAMs provide model surfaces while also enabling modification or tuning of charges via pH adjustment below, at, and above the isoelectric point (pI) of fibrinogen (pHs of 4, 5.8, 7.4). This adjustment of pH affects not only the overall charge on fibrinogen, but also the charge on the surface if the surface chemistry is ionizable.

The conformation of fibrinogen after adsorption to the surface could impact the accessibility of thrombin cleavage sites. Fibrinogen molecules can also aggregate. Whether aggregation happens in solution or on the surface is a question. Determination of the surface coverage also provides details as to the relative affinity

of fibrinogen to different surfaces. The amount of fibrinogen adsorbed to the surface may influence its subsequent mitigation of the coagulation cascade. The conformation of fibrinogen after adsorption to the surface may strongly influence the activity. If the fibrinogen is adsorbed in such a conformation that the thrombin cleavage site is inaccessible, the protein will not be cleaved. This would decrease the number of fibrin molecules, potentially hindering the polymerization events in the clotting cascade. Therefore understanding the conformation and dynamics is critical to the design of new materials.

AFM studies provide several advantages, including but not limited to structural information, high resolution images, single molecule imaging, pseudo-physiological conditions, and label-free. However, AFM disadvantages include cumbersome data analysis, a lack of specificity, and a slower timescale.

Conversely, SPR provides real time quantitative information about binding affinity and kinetics in pseudo-physiological conditions also without requiring labeling. This technique is sometimes automated, very sensitive, utilizes only microgram quantities of protein, and provides association and dissociation constants for mechanistic studies and the capability to regenerate surface under certain conditions. However, SPR analyses, probe the entire surface simultaneously and do not provide molecular level details of the conformation of binding. Additionally, SPR data may contain artifacts (refractive index change and temperature changes), be subject to interferences (non-specific binding), relies on modeling interactions, requires very careful control of parameters and one generally requires that one of the

binding partners is immobilized on the surface, which may change the interactions observed.

Thus, as a complementary technique to AFM, SPR analysis of fibrinogen adsorption to surfaces was also performed. Via kinetic titrations, sequential injections of increasing amounts of fibrinogen were allowed to adsorb to different surfaces. Study of the resulting sensorgrams and the shapes of the curves provided information on affinity and kinetics of fibrinogen adsorption to the SAMs listed previously.

The goal of this project is to build upon what is already known about fibrinogen adsorption to surfaces via diverse techniques to both complement the existing data and elucidate additional key factors to assist in the development of a more complete mechanistic understanding of the properties involved in fibrinogen adsorption to different surfaces. The hope is that the nature of these experiments, direct visual information about protein conformation and kinetic data will improve the current understanding of adsorption to ultimately enable control over fibrinogen adsorption to such materials as implants and sensors. Correlating kinetics with conformation by performing complementary tests via SPR and AFM on similar model surfaces should assist in these goals. Additionally, this work may provide insight into factors controlling nonspecific binding of proteins in general and lead to a better understanding of this type of protein-surface interactions.

3.2. Experimental

A multimode AFM with a NanoScope® IIIa controller by Digital Instruments (now Bruker) in contact mode, friction mode, and tapping mode was utilized for these studies. Cantilevers included Bruker NP-S10 composed of non-conductive silicon nitride with four v-shaped cantilevers/tips with following sets of force constants and resonant frequencies: 0.350 N/m and 50-80 kHz; 0.12 N/m with 16-28 kHz; 0.24 N/m with 40-75 kHz, and 0.06 N/m with 12-24 kHz. For patterning and tapping mode imaging, μmasch NSC35 / Si_3N_4 / AIBS with 3 rectangular cantilevers: 7.5 N/m with 210 kHz, 14 N/m with 315 kHz, and 4.5 N/m with 150 kHz were utilized. In fluid, the frequency used in tapping mode is much lower (5-20 kHz).

Substrates included Platypus gold, house gold on mica, house template-stripped gold, house flame-annealed gold, and silicon (see chapter 2 section 2.1.1, subsections thereof, and 2.1.2 for descriptions). Rinse solutions included chloroform, acetone, and ethanol. Drying was performed with nitrogen gas. SAM formation and modifications utilized ethanol, thiols (4-aminothiolphenol, 1-octadecanethiol, 1,11-mercaptoundecanol, 1,11-mercaptoundecanoic acid, 1-dodecanethiol, 11-amino-1-undecanethiol, hydrochloride), octadecyltrichlorosilane, and buffers (see sections 2.2.2 and 2.2.3 for preparation details). Surface and SAM characterization were performed with a Rudolph Research (now Entrepix) AutoEL ellipsometer for substrate optical properties and monolayer thickness determination, and a Ramé-hart, Inc. NRL C.A. goniometer (Model 100-00) for static contact angle measurements with three droplets of water (six measurements) for each surface. After measuring

contact angles, the surfaces were rinsed with chloroform, acetone, and ethanol and dried with nitrogen gas.

Bovine fibrinogen (Product Number F8630-1G, type 1-S, 71% protein; 85% clottable protein) was ordered from Sigma-Aldrich. Fibrinogen was diluted in buffer from lyophilized protein. Phosphate buffer, 50mM, pH 7.0 from Fisher Scientific was adjusted to pH of 4.0, 5.8, or 7.4, (with hydrochloric acid or sodium hydroxide) for surface equilibration and protein dilutions.

For SPR studies and kinetics, a BiaCore (now GE Healthcare) 3000 SPR (COBRE Center in Protein Structure and Function, KU CORE facilities), and BiaCore gold chips as well as chemically modified gold SPR chips were utilized. Regeneration solutions such as 0.5% sodium dodecyl sulfate from Sigma-Aldrich were utilized in SPR studies. SPR studies were performed at a flow rate of 100 μL/min to avoid mass transport limitations. A series of protein dilutions were prepared via the SPR. Injections included a 100 μL of 15% sucrose solution before and after protein injections to check chip performance. For protein injections, either individual or sequential 100 μL protein kinjections with 300 second dissociation periods (in which the buffer was allowed to flow over the surface) with a long wait time at the end were performed. Sometimes, injection(s) of regeneration solution were made. A reference flow cell was not used because it was inapplicable since the intention of the experiment was to study nonspecific adsorption to surfaces.

3.3. Results and Discussion

The following sections explain the results and the information acquired from these studies of fibrinogen adsorption to a variety of surfaces via AFM and SPR. First, AFM studies of nonspecific fibrinogen adsorption to mica, graphite, gold, and various SAMs provided information on fibrinogen structure or conformation on the surfaces. Then, SPR studies of fibrinogen adsorption to gold and various SAMs provided information on the relative binding affinity and kinetics of fibrinogen adsorption.

3.3.1. Nonspecific Conformation (or Orientation) of Fibrinogen Adsorption via AFM

Conformation(s) of fibrinogen nonspecifically adsorbed to a variety of surfaces (model atomically flat and chemically controlled surfaces) were studied using tapping mode AFM. These different surfaces were chosen for their unique characteristics. SAMs on gold were utilized due to their tunability. The following sections will discuss the different surfaces utilized to study nonspecific fibrinogen adsorption.

3.3.1.1. Mica and Graphite (Atomically Smooth Substrates)

Mica and graphite are both atomically smooth substrates utilized for initial fibrinogen adsorption studies. Mica is a smooth hydrophilic surface with some negative charge under the conditions of these experiments. Mica was freshly cleaved and incubated in 50 mM phosphate buffer pH 7.4 for approximately 10 minutes. A 0.1 μg/mL fibrinogen solution was added to the surface and allowed to adsorb for

approximately 20 minutes. The surface was then rinsed thoroughly with buffer and Milli-Q water and dried with nitrogen gas. The sample was adhered to an AFM puck with a sticky tab. AFM images (2.00 μm by 2.00 μm) show that the surface coverage on mica was evenly distributed throughout surface and dependent on fibrinogen solution concentration (Figure 3.2a). By zooming in on groups or individual molecules, the conformation of the individual fibrinogen molecules was observed on mica via AFM image and cross-sectional analysis and was found to be globular (Figure 3.3a). A three-dimensional representation of this 150 nanometer by 150 nanometer image highlights this globular conformation (Figure 3.4a). This makes sense as in solution (a hydrophilic environment) fibrinogen is globular and maintains that formation after adsorption to a hydrophilic surface. Since both the substrate surface and protein surface were hydrophilic, the protein had no need to unfold to minimize the energy of the interaction, and thus fibrinogen remained balled up on the surface. The α-C arms are thought to be wrapped around the hydrophobic domains of the protein and adsorbed to the surface. It was more favorable for the protein to adsorb through these arms rather than the more hydrophobic portions. Additionally, mica is a negatively charged surface, so charge distribution along the protein may have played a significant role in this adsorption mechanism (arms are positively charged and globular domains are negatively charged). The width of this molecule was measured to be about 30 nanometers (smaller than the extended form) and the height was about two nanometers. Little to no aggregation was evident on the mica substrate; the molecules adsorbed individually and remained separate. This agrees

with results from the McDermott group.[22] The fibrinogen molecules were evenly distributed across the mica substrate.

Graphite is a flat model hydrophobic surface. Protein adsorption was performed as per the preparation of the mica sample. Initial analysis of 2.00 μm by 2.00 μm AFM images of fibrinogen to graphite showed that aggregation was evident upon adsorption to the graphite surface (Figure 3.2b), which agrees with previous studies.[22] Typically, about three fibrinogen molecules were observed per aggregate at pH 7.0. Additionally, fibrinogen exhibited mobility on the graphite surface as molecules were closer to step edges and distribution across surface was nonuniform, inconsistent with a random distribution of proteins. By zooming in on individual molecules via AFM imaging and cross-sections, the conformation of fibrinogen on graphite was found to be mostly trinodular (bent or linear), with some globular molecules as well (Figure 3.3b). The cross-section only shows two (instead of three) domains because the molecule was bent instead of linear thus, the middle domain is not in line with the cross-section so was missed. A three dimensional representation of this 150 nanometer by 150 nanometer AFM image highlights this trinodular bent conformation (Figure 3.4b). Since in solution fibrinogen is globular, this indicated a conformational change in the protein upon surface adsorption. Looking at the fibrinogen domains, this makes sense because the large hydrophobic domains would rather interact with the surface than the hydrophilic arms, causing the molecule to spread out on the surface. The length of the linear proteins was about 50 nanometers as expected for the extended form of the protein.

This more extended conformation on graphite than mica (hydrophobic versus hydrophilic surface) provides direct evidence that fibrinogen adsorption is surface dependent. Additionally, this was congruent with Santore's data that increasing surface hydrophobicity increased the footprint of fibrinogen on the surface.[33]

Initial AFM studies were expanded to include a variation in pH. On graphite, decreasing the pH to 4 resulted in a higher amount of protein aggregation on the surface (Figure 3.5). This aggregation may be due to a change in the charge distribution across the protein as well as an alteration in protein conformation as a result of pH change, which would change the interactions between protein molecules.[3]

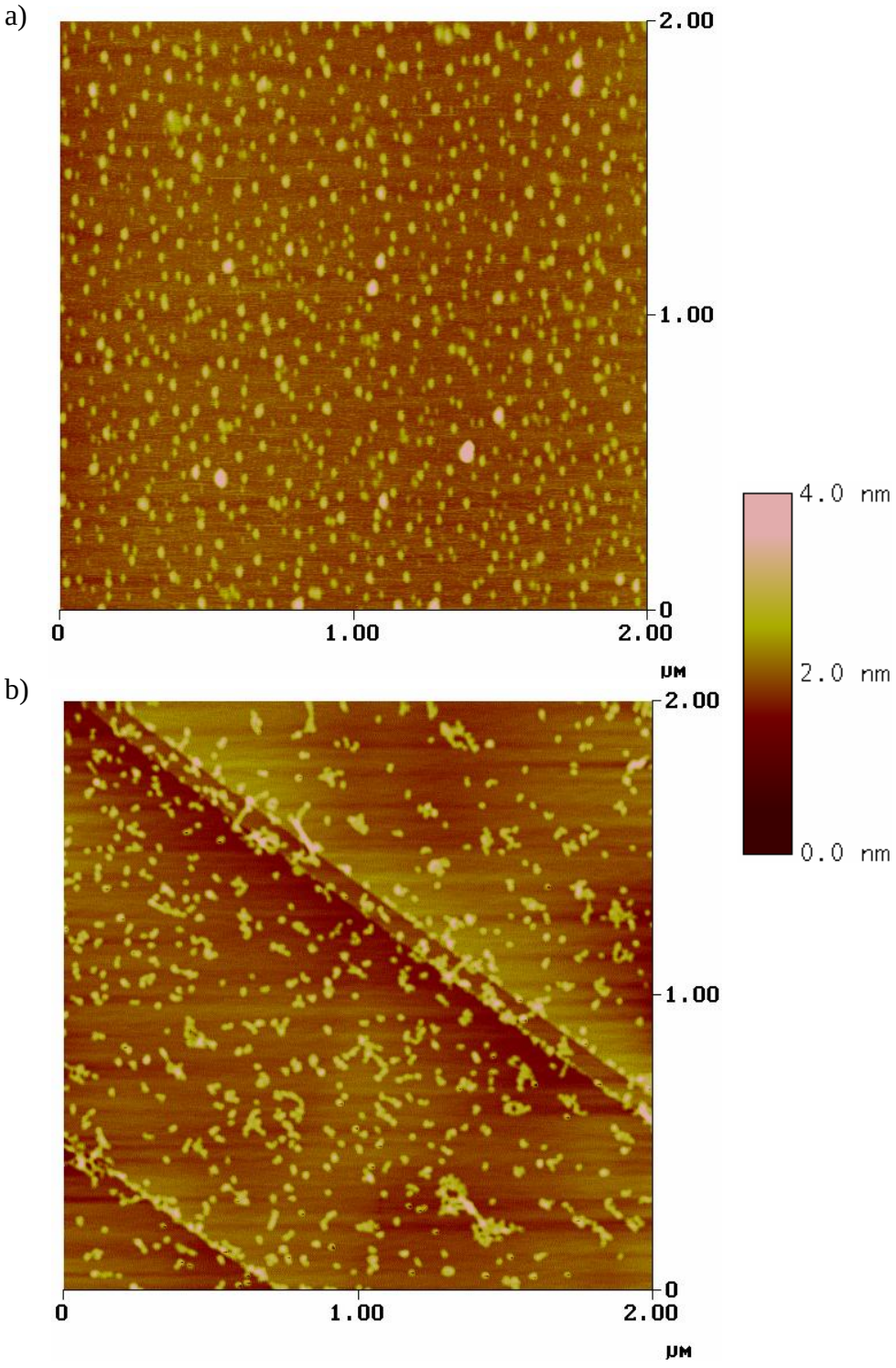

Figure 3.2: 2.00 µm x 2.00 µm AFM height images of Fibrinogen Adsorption to a) Mica and b) Graphite with 4.0 nm height scales.

a)

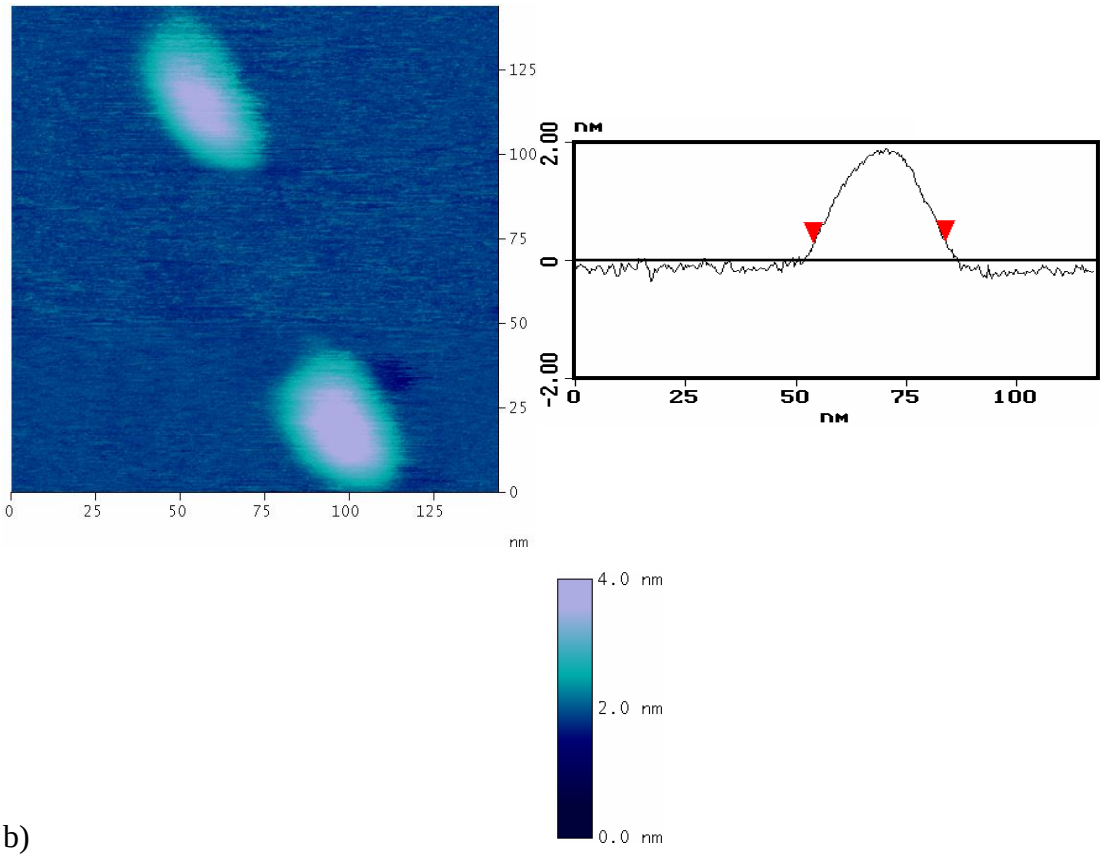

b)

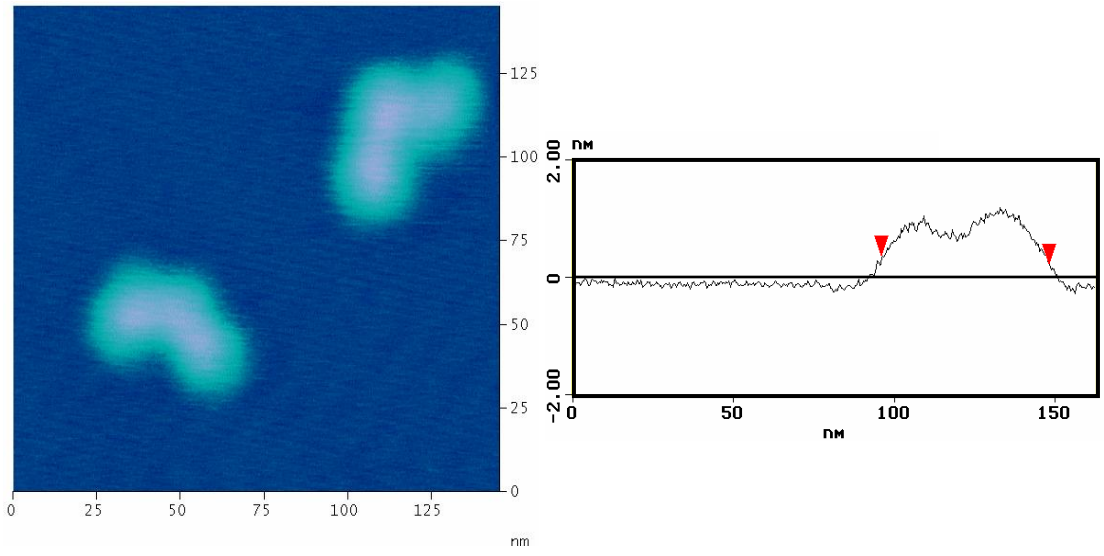

Figure 3.3: Zoomed in AFM height images (~150 nm x 150 nm) of Fibrinogen Adsorption to a) Mica and b) Graphite with 4.0 nm height scales.

a) Fibrinogen on Mica

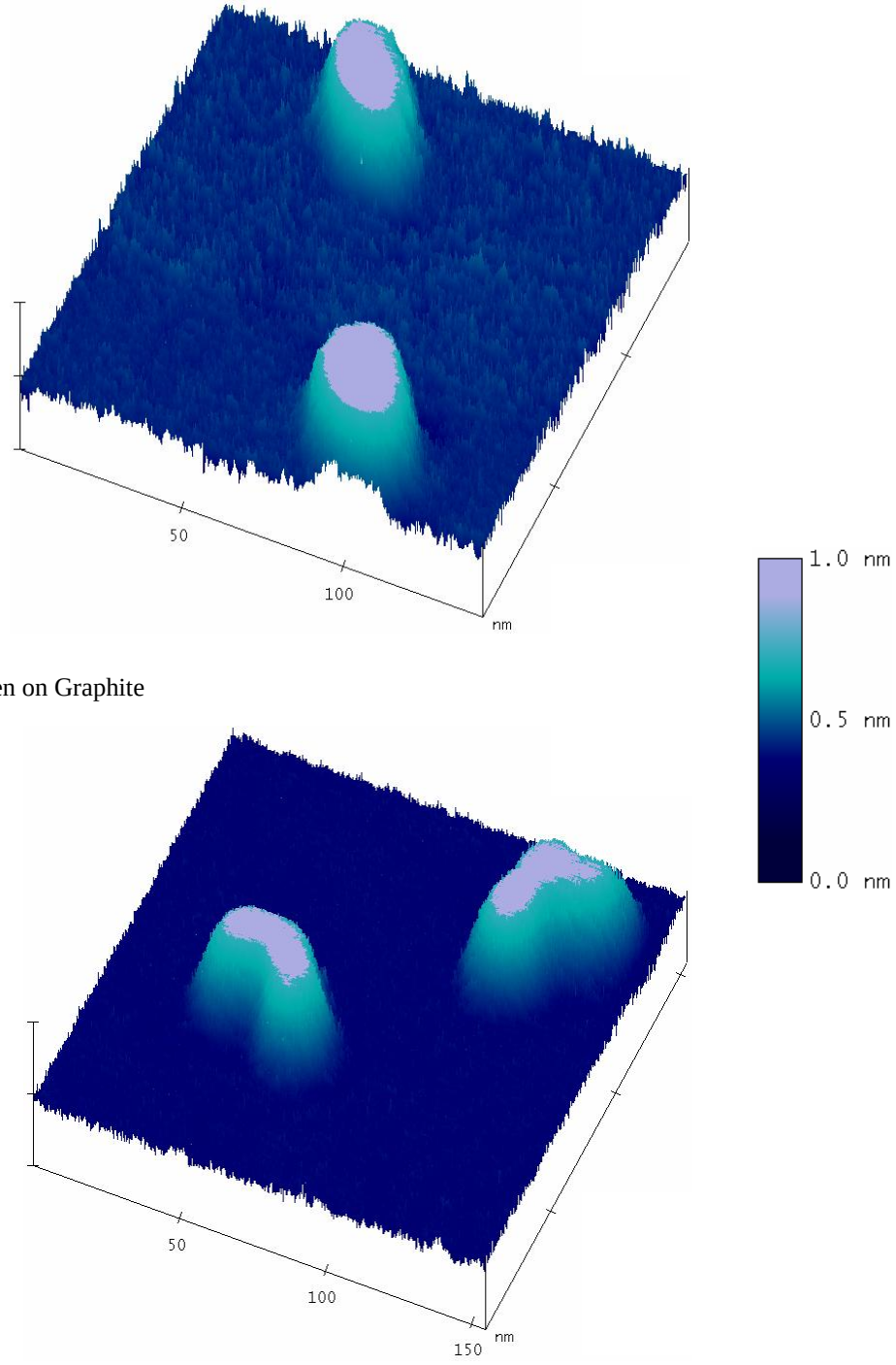

b) Fibrinogen on Graphite

Figure 3.4: 3D AFM images (~150 nm x 150 nm) of Fibrinogen Adsorption to a) Mica and b) Graphite with 1.0 nm height scales.

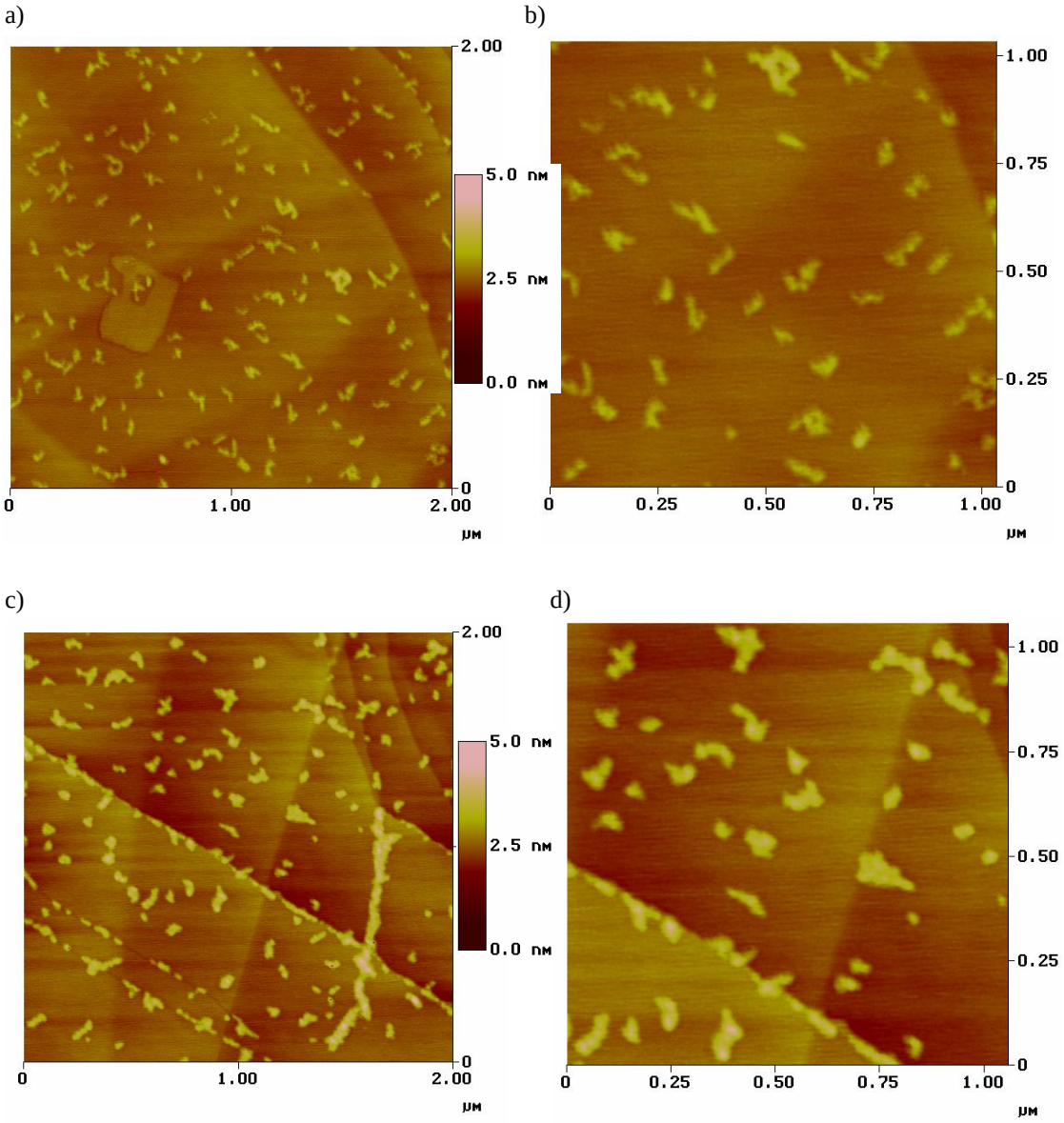

Figure 3.5: AFM height images (a & c 2.00 µm x 2.00 µm or b & d 1.00 µm x 1.00 µm) of 0.1 µg/mL Fibrinogen Adsorption to Graphite with 5.0 nm height scales at pH 7 buffer (a-b) and pH 4 buffer (c-d).

3.3.1.2. Au, SAMs, Silicon (Chemical Control of Substrate)

For tunable surfaces, gold substrates were first utilized. Then a silicon surface with a SAM of octadecyltrichlorosilane was utilized. Fibrinogen conformation, aggregation, and surface coverage were all analyzed on these different surfaces after nonspecific adsorption. For each study, first the gold or silicon and then the monolayer surfaces were imaged, and imaged again after protein adsorption.

Template stripped gold surfaces have large grain sizes with adequate areas of flat regions that are large enough to study protein adsorption (distinguish protein from surface roughness). Before protein adsorption, the gold surface was smooth and flat (with deeper areas indicative of grain boundaries or pits) and mainly a consistent hue in the AFM image (Figure 3.6a). After protein adsorption (Figure 3.6b), the gold grains were still visible and the fibrinogen adsorbed to the surface could be analyzed. This 1.00 μm by 1.00 μm AFM image revealed that much like fibrinogen adsorption to the mica substrate, the fibrinogen adsorbed to the hydrophilic gold substrate was evenly distributed and round in conformation.

Fibrinogen was also adsorbed to an amine-terminated SAM on a template-stripped gold surface. Initially this surface was similar to the plain gold surface with large grains and low roughness, a consistent hue was observed in the AFM height image (Figure 3.7a). After protein adsorption (Figure 3.7b), analysis of the 1.00 μm by 1.00 μm AFM height image showed that similar to the adsorption of fibrinogen to mica and gold substrates, an even distribution and round in conformation were observed. In some areas the observed heights and lengths were larger than expected

(4.2 ± 0.7 nm and 42 ± 10) for a single molecule and was possibly due to protein aggregation. These areas still maintained the globular structure. The smaller set of molecules observed were globular with heights of 1.8 ± 0.3 nm and lengths of 25 ± 7 nm, consistent with single molecule dimensions.

Another substrate, silicon, was utilized for its low surface roughness, which was also ideal for the study protein adsorption. Before protein adsorption, the silicon with the octadecyltrichlorosilane surface was smooth and flat and mainly a consistent hue in the AFM height image (Figure 3.8a). This provided a model hydrophobic terminated SAM film for protein adsorption studies to determine protein conformation. After protein adsorption (Figure 3.8b), the conformation of adsorbed fibrinogen on the surface could be analyzed. This 1.00 μm by 1.00 μm AFM image revealed that much like fibrinogen adsorption to the graphite substrate, the fibrinogen adsorbed to the hydrophobic monolayer on silicon in an extended conformation with much aggregation and cross-linking.

a) Before

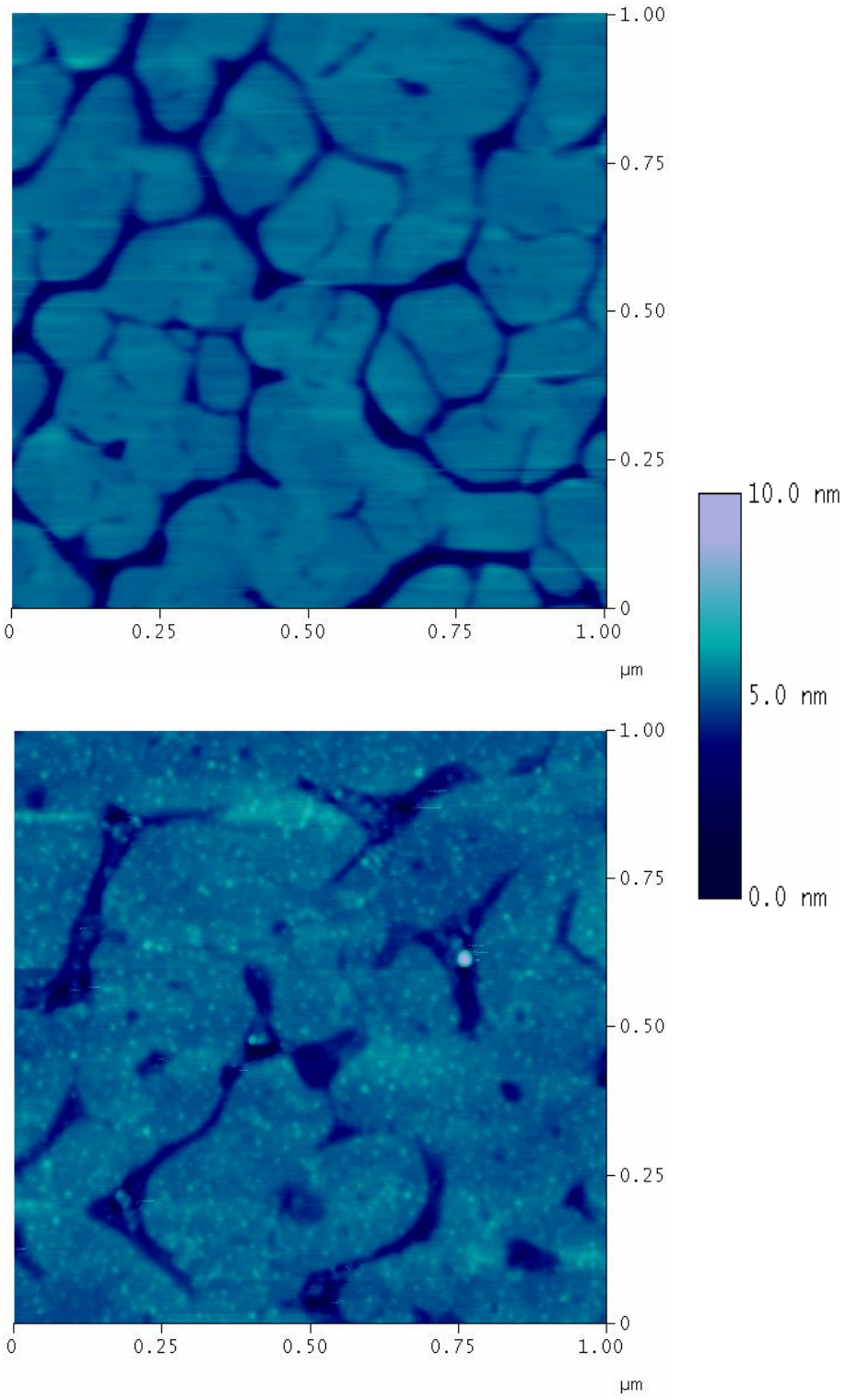

b) After

Figure 3.6: 1.00 µm x 1.00 µm AFM images of a) gold and b) fibrinogen adsorbed onto template-stripped gold with 10.0 nm height scales.

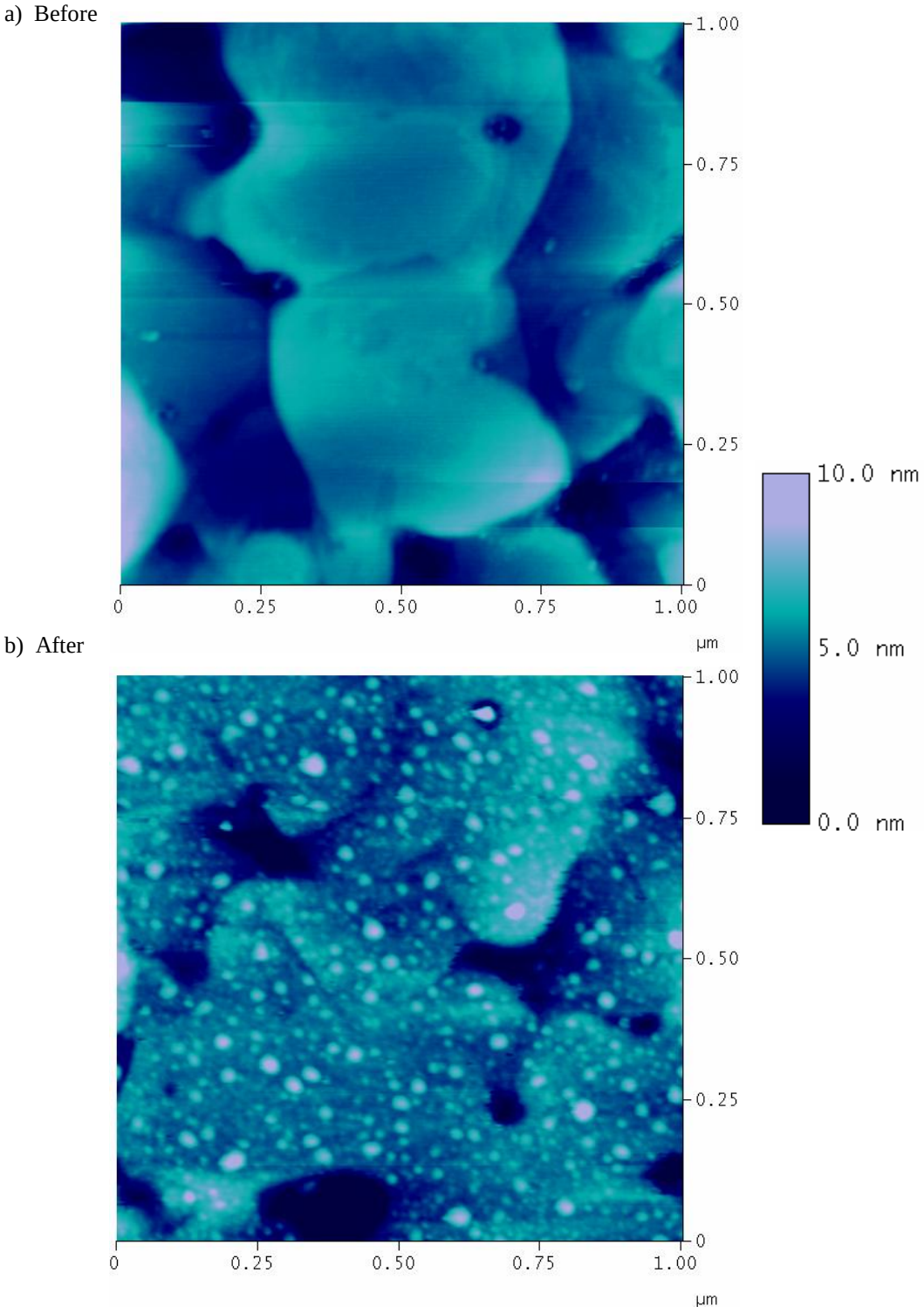

Figure 3.7: 1.00 µm x 1.00 µm AFM images of a) amine-terminated SAM on gold and b) fibrinogen adsorbed onto an amine-terminated SAM on template-stripped gold with 10.0 nm height scales.

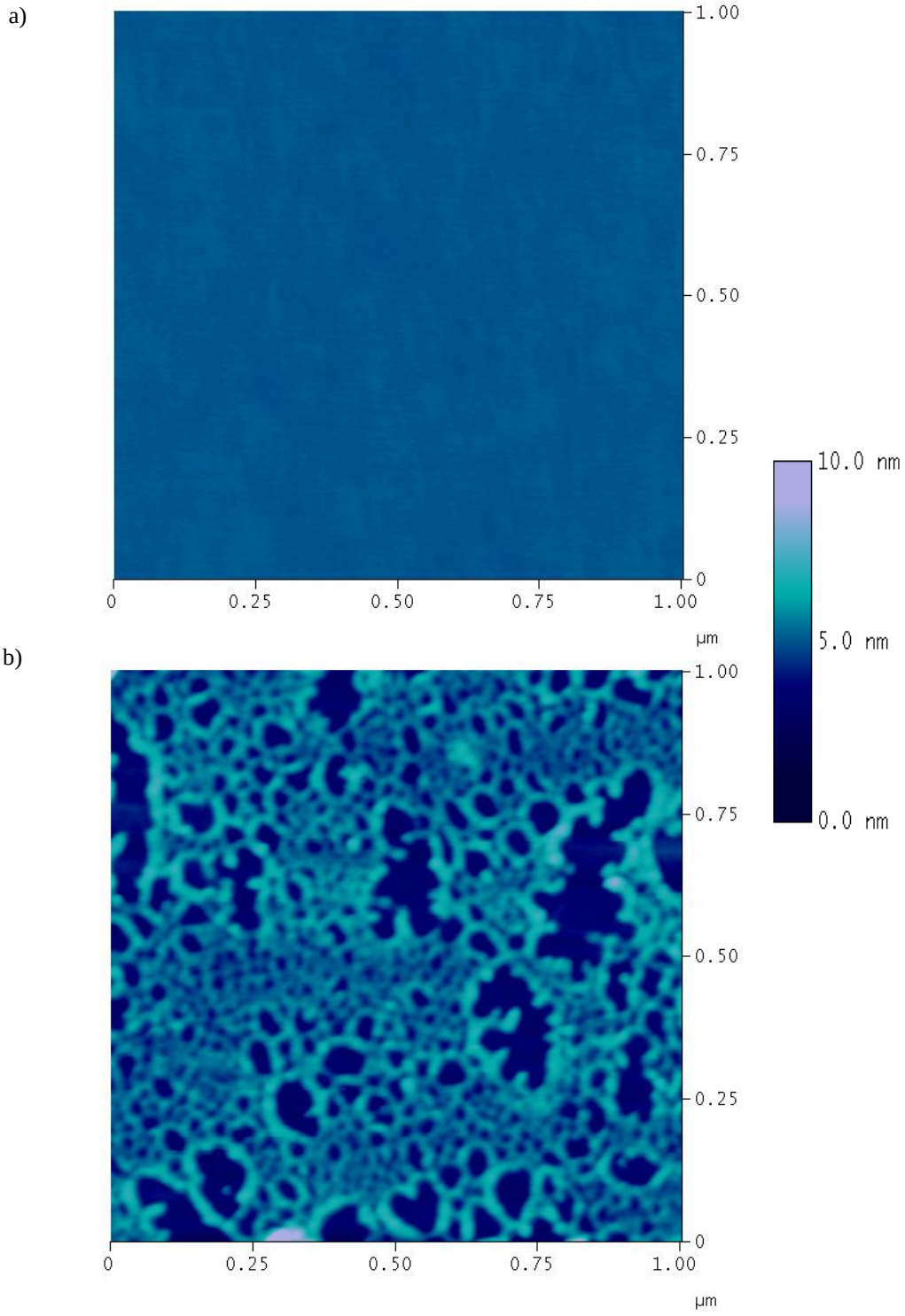

Figure 3.8: 1.00 µm x 1.00 µm AFM images of a) silicon with octadecyltrichlorosilane SAM and b) fibrinogen adsorption to octadecyltrichlorosilane SAM on silicon with 10.0 nm height scales.

3.3.2. Nonspecific Adsorption of Fibrinogen via SPR

SPR studies were performed to complement the AFM conformation data with information about kinetics and adsorption affinity. Initially, individual injections of fibrinogen were performed on different surfaces. Analysis of SPR sensorgrams for fibrinogen adsorption to the methyl versus amine terminated surfaces (Figure 3.9), confirmed that the initial rate is the same and surface independent as was the case in Santore's experiments.[33] In both cases, the concentration of fibrinogen was high and so the total response from fibrinogen adsorption was also high (~2500-2900 RU). Fibrinogen is sticky and as such adsorbed at high coverages to both surfaces. Slightly more fibrinogen adsorbed to the methyl terminated over the amine terminated surface. This corresponds to fibrinogen affinity being higher on hydrophobic versus hydrophilic surfaces, as suggested in the literature. After the fibrinogen injection, upon return to buffer, little fibrinogen desorbed from the surface as seen by the slight drop in response. Again, most of the fibrinogen once adsorbed remained on the surface as expected. The strength of this adsorption was further evaluated by attempting to regenerate the surface. This means that one injects a solution which may disrupt the binding of fibrinogen to the surface, thereby removing it from the surface and returning the surface to one free of protein and the response (RU) would return to the initial level. Learning about what types of solutions disrupt binding of fibrinogen to surfaces will help elucidate the binding characteristics.

A wide variety of regeneration solutions was tested and none were found to be both suitable and system compatible for all surfaces (Table 3.1). These regeneration

solutions were chosen based on their properties that might disrupt protein-surface interactions such as different ionic strength (electrostatic interactions), different pHs (change charge distribution and hydrogen bonding), surfactants (hydrophobic interactions). After buffer equilibration, fibrinogen was injected onto an amine-terminated and a methyl-terminated surface (Figure 3.9). On both surfaces, fibrinogen adsorbed to a great extent (the baseline increased and leveled off at a high response). Then, a regeneration solution was injected and the resultant sensorgram was analyzed. Initially, on the methyl terminated surface, the surface was nearly regenerated with 0.5% sodium dodecyl sulfate (SDS) as seen by the drop in response back close to the initial baseline after the regeneration injection (about 7% of initial protein adsorbed still remained on the surface). This means that there was very little protein still bound to the surface after the regeneration step. This was not the case with the amine terminated surface as the response dropped a little, but did not return to baseline, indicative of a good percentage, roughly 67%, of the protein still bound to the surface after the regeneration. Thus, fibrinogen was removed with 0.5% SDS more efficiently from the methyl-SAM (hydrophobic) than from the amine-SAM (hydrophilic). This indicated a difference in binding and interactive forces involved in fibrinogen adsorption on the two surfaces. Probable interaction of fibrinogen with SDS was hydrophobic forces; the fibrinogen was more strongly attracted to the long hydrophobic chain of the surfactant than to the methyl-terminated surface, and so it desorbed from surface. On the amine-terminated surface, it is possible that these hydrophobic groups were buried and so did not interact with the SDS. Thus, for the

most part fibrinogen remained bound to the amine-terminated surface even after the surfactant injection. Unfortunately 0.5% SDS was not compatible with the IFC in the SPR as fibrinogen and 0.5% SDS produced a precipitate under some conditions and lower concentrations of SDS were unsuccessful at completely regenerating even the methyl-terminated surface.

Typically, it is not as easy to regenerate the surface if adsorption is via nonspecific interactions unless something is known about the forces that are active in the binding of the protein to the surface. If electrostatic forces were in play, then one could use a change in salt concentration to disrupt the interactions. If hydrophobic or hydrophilic forces are involved, then SDS or cetyltrimethylammonium bromide (CTAB) could be utilized. With these regeneration solutions it is imperative to ensure that the solutions are compatible with the SPR system and do not form a precipitate upon interaction with the protein or surface. To date successful regeneration of fibrinogen has not been feasible. This is not surprising because it is consistent with fibrinogen being a very sticky, difficult protein to work with, that fouls a variety of surfaces. Learning about what might desorb adsorbed fibrinogen from the surface might help elucidate some of the important binding characteristics involved.

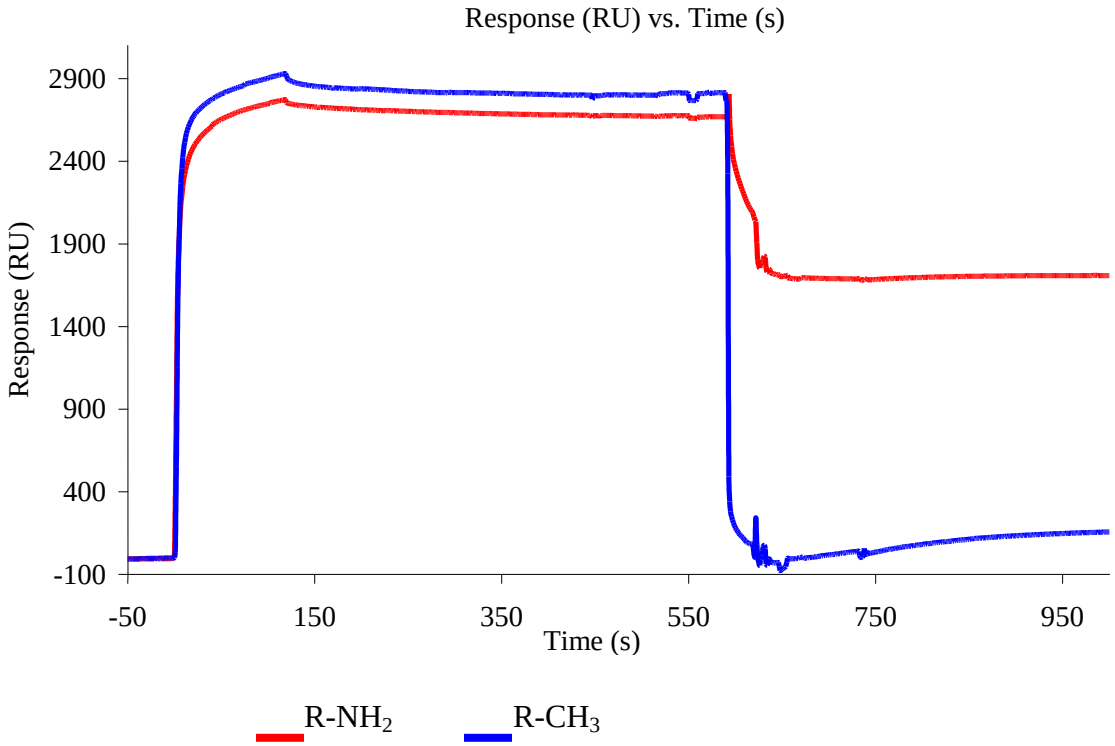

Figure 3.9: SPR Sensorgrams of phosphate buffer, pH 7 followed by fibrinogen injection (100 µg/mL of 0.1 mg/mL fibrinogen) at 0 seconds, return to buffer at about 100 seconds for desorption until 600 seconds when subsequent regeneration attempt with 0.5% SDS on amine (red R-NH_2) and methyl (blue R-CH_3) terminated SAMs. Fibrinogen is removed with 0.5% SDS more efficiently from the Methyl-SAM (hydrophobic) than from the Amine-SAM (hydrophilic). This is indicates a difference in binding and interactive forces involved in fibrinogen adsorption on the two surfaces.

Table 3.1: Regeneration solutions tested

50 mM Phosphate Buffer, pH 7.4
0.5% Sodium Dodecyl Sulfate
0.05% Sodium Dodecyl Sulfate
1 M Sodium Chloride
3M Sodium Chloride
100 mM Hydrochloric Acid
100 mM Phosphoric Acid
100 mM Sodium Hydroxide
250 mM Sodium Hydroxide
100 mM Sodium Hydroxide + 3 M Sodium Chloride
10 mM Glycine-HCl pH 2.5
100 mM Sodium Hydrogen Carbonate pH 8.14
200 mM Sodium Carbonate pH 11.22
70 % Formic Acid
25 % Ethanol
70 % Ethanol
50 % Ethylene Glycol pH 2.04
20 % Acetonitrile pH 7.25
20 % Acetonitrile + 100 mM Sodium Hydroxide pH 12.94

3.3.2.1. Nonspecific Affinity Analysis of Fibrinogen Adsorption via SPR

Fibrinogen was absorbed to a number of different SAM surfaces via SPR. Table 3.2 provides characterization data for the various SAM films with experimental data that match well with literature values (see Table 2.4), indicative of decent SAM formation. For structure of these various thiols, see Figure 3.12.

Table 3.2: Characterization of SAMs

Terminal Group Structure	***Experimental Thickness (Å) (n=7)***	***Experimental Contact Angle (°) (n=6)***
Au	n/a	41 ± 2
HS-$(CH_2)_{11}$-**COOH**	13.9 ± 4.6	28 ± 3
HS-$(CH_2)_{11}$-**OH**	16.3 ± 7.4	33 ± 3
HS-C_6H_4-**NH_2**	6.9 ± 1.9	70 ± 2
HS-$(CH_2)_{11}$-**NH_2**	20.4 ± 4.7	35 ± 4
HS-$(CH_2)_{17}$-**CH_3**	24.0 ± 7.2	108 ± 1

Typical kinetic analyses require at least four injections of analyte at different concentrations. Since regeneration of the SAM surface after fibrinogen adsorption was not currently feasible, the experimental procedure outlined above was altered. Single injections of fibrinogen on the surface were not practical since all of the protein could not be removed from the surface so different chips would be required in order to obtain enough data for kinetic analysis. This is undesirable because of the variability amongst different chips. Thus, instead of single fibrinogen injections upon the surface, sequential injections of increasing concentrations of analyte were performed.[38] The idea behind this is to inject low concentrations of analyte such that the surface sites were not significantly diminished between each injection. The

advantage of this approach was regeneration (which is not feasible in this case) was not needed to obtain sufficient information for kinetic analysis. Figure 3.10 depicts an example sensorgram of fibrinogen adsorption to a hydroxyl-terminated SAM with this sequential injection scheme. First, the surface was equilibrated with buffer to obtain a stable baseline. Then, 0.1 μg/mL fibrinogen was injected (a rise in the SPR response was observed). After the injection, buffer was introduced into the system to allow for dissociation (a decrease in response was observed). Then this process was repeated with fibrinogen solutions of increasing concentrations (0.3 μg/mL, 0.8 μg/mL, 2.0 μg/mL, 7.0 μg/mL). Finally, the stock solution of 40 μg/mL was injected three times in this same manner. This resulted in a serial increase in response. A greater initial response was observed after each protein injection as the protein concentration increased. Eventually the surface began to saturate and little to no further adsorption was observed.

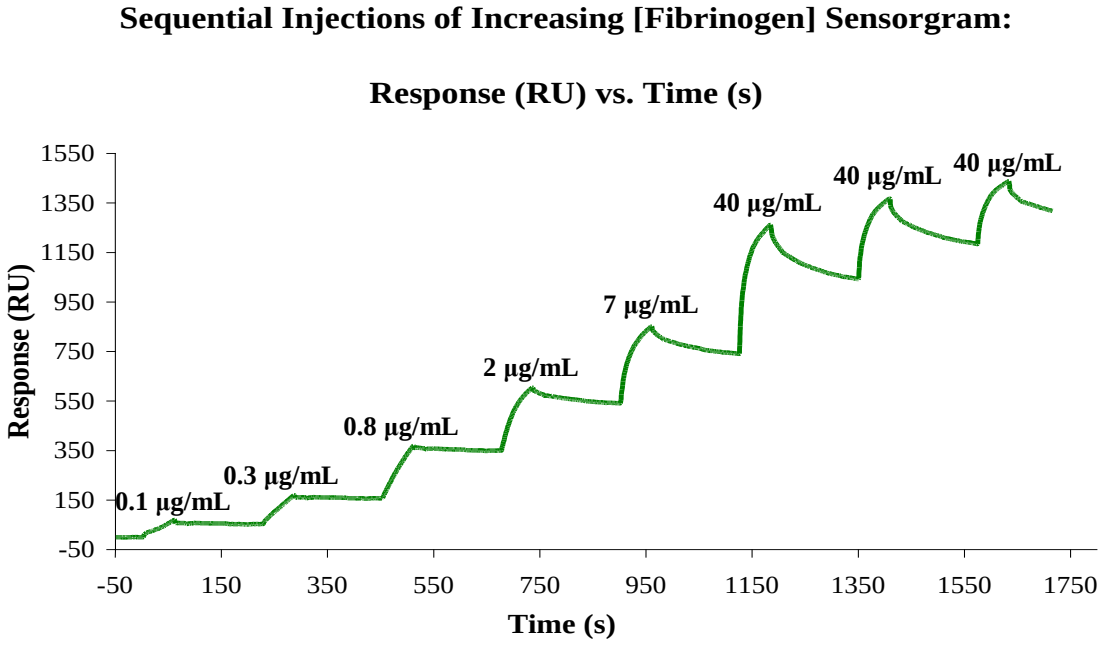

Figure 3.10: SPR sequential sensorgram of fibrinogen adsorption to a hydroxyl-terminated SAM.

This sensorgram can be analyzed for both affinity and kinetic information. A series of these sequential injection schemes were performed on the various SAM films (Figure 3.11).

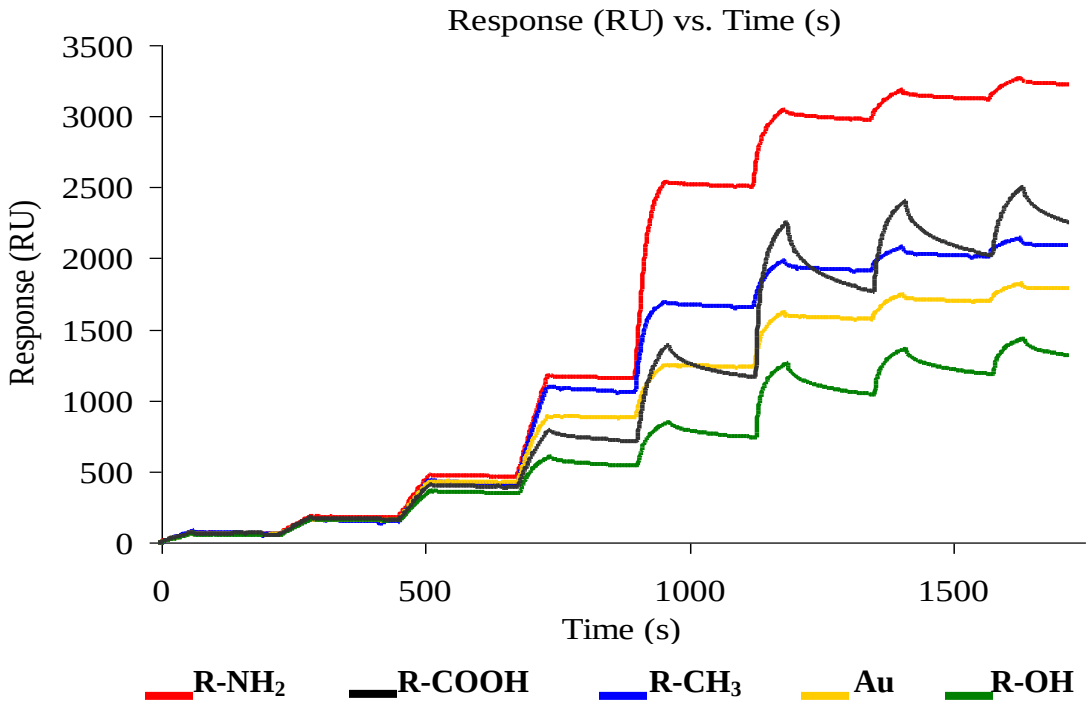

Figure 3.11: SPR sequential sensorgrams of fibrinogen adsorption to various SAMs.

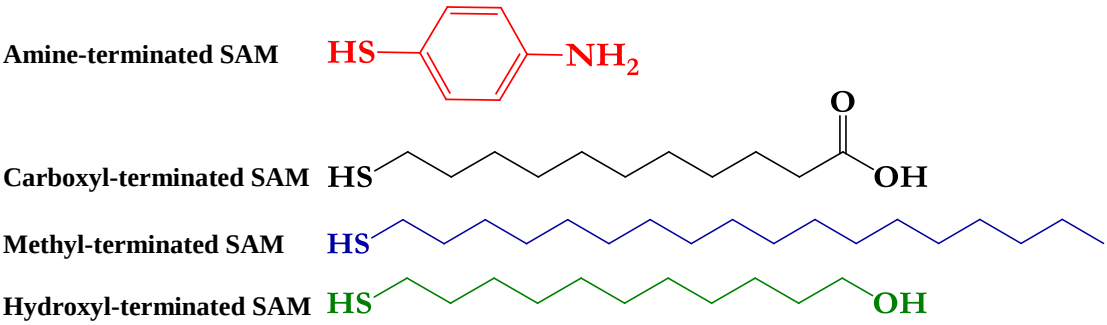

Figure 3.12: Structures of various SAM thiols.

The following trends were observed for the nonspecific adsorption affinity of fibrinogen to various surfaces, at a pH of 7.4, from comparison of the point (response level) at which each sensorgram leveled off at the end of the sequence. The amine terminated SAM exhibited the highest overall response, and thus had the highest affinity. This was followed by the methyl, the hydroxyl, and carboxylic acid terminated SAMs, respectively. Plain gold had a response in between the methyl and hydroxyl terminated SAMs. The relative amounts of fibrinogen adsorption to the surfaces (highest to lowest) was found to be the amine, carboxyl, methyl, gold, hydroxyl terminated SAMs, as determined from the level of response at the end of the sequential injection series. And the relative desorption amounts (highest to lowest) was determined to be carboxyl, hydroxyl, methyl, gold, amine, as determined by the relative shape of the desorption curves (the steeper the slope, the larger the desorption). In terms of previous studies, a qualitative analysis via examination of the shapes of the adsorption and desorption curves from the sensorgrams reported by Schoenfisch *et al.* yielded similar results for the highest and lowest adsorption surfaces, but the middle carboxyl and methyl surfaces were opposite in order.[15] The responses for their methyl and carboxyl terminated SAMs were close, and perhaps if my sensorgrams had a longer desorption time, the carboxyl curve with a higher desorption slope would have leveled out to a response below the response of the methyl and match their results. Also, in terms of the desorption curve slopes, results here match up with their desorption results with the exception that the amine was highest for them and lowest for this data.[15] The difference in the order of the amine

terminated SAM in terms of desorption curves may be due to issues with preparing a decent amine-terminated film or differences in the packing. They utilized a long chain amine, while my results were from a short phenol amine thiol. This amine issue will be discussed in more detail later. Additionally, the differences in the overall order of these results may be due to different binding conditions. This group performed injections of larger protein concentrations over a longer time frame at a slower flow rate, all parameters which can influence adsorption and desorption properties. While these studies observed the adsorption and desorption curves from sensorgram data on different surfaces, only one concentration of fibrinogen was tested. Thus, only qualitative information about binding dynamics could be assessed; kinetic analysis was not performed.

An issue arose with the consistency of phenol amine-terminated SAM sensorgrams. Some experiments resulted in a high response (as in Figure 3.11 and red sensorgram in Figure 3.13) and others resulted in a much lower response (grey sensorgram in Figure 3.13).

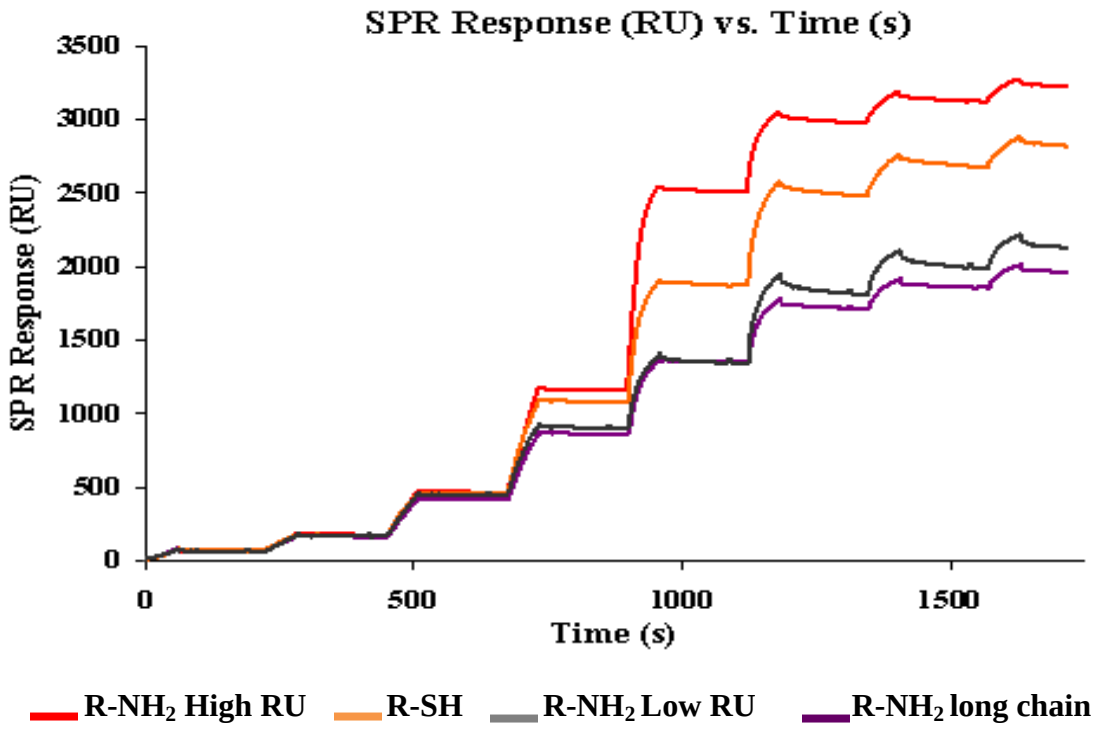

Figure 3.13: Overlay of SPR sensorgrams of sequential injections of increasing fibrinogen concentrations for amine-terminated SAM investigations. The red trace is the initial high response for the phenol amine-terminated SAM, the orange trace is a dithiol SAM, the grey trace is the lower response from the phenol amine-terminated SAM, and the purple trace is a long-chain amine-terminated SAM.

This deviation was potentially due to either the formation a mixed layer of amine terminal groups (intended) or thiol groups (double layer from hydrogen bonding)[39, 40] to which the protein was exposed. Due to the similarity of contact angles of these surfaces as well as difficulties in measurements of thickness with ellipsometry in these very thin metal films for SPR analysis, results were inconclusive and did not distinguish if either a single or multi-layer formation was occurring. Further tests were performed with a long chain amine and controlling the pH of the thiol solutions to try to disrupt hydrogen bonding. The long chain amine sensorgram was very similar to the low phenol amine sensorgrams (Figure 3.13, purple

sensorgram). Additionally, a dithiol SAM was prepared and tested via sequential fibrinogen injections to try to resolve this issue (orange sensorgram Figure 3.13). The dithiol monolayer sensorgram shapes and final response were closer to the high phenol amine sensorgrams. This suggests that at least some of the responses observed from the high phenol amine sensorgrams may be attributed to full or partial bilayer formation. Other possibilities for the differences in these amine terminated sensorgrams may be attributed to differences in packing density, monolayer formation, and charge. We are still working to resolve these issues with the variability in fibrinogen adsorption to the amine-terminated SAMs. SPR responses from other surfaces were very consistent.

3.3.2.2. Nonspecific Kinetics Analysis of Fibrinogen Adsorption via SPR

The shapes of SPR curves of fibrinogen adsorption to various SAMs on gold provided insight into the adsorption and desorption kinetics of nonspecific binding of fibrinogen to a variety of surfaces (Figure 3.11). The initial rises in response for the different SAMs were the same, which is in agreement with work by Santore *et al.*[33] Following the initial slope, the curves started to deviate from each other on the different surfaces. The desorption curves resulted in even more distinctive shapes amongst the various surfaces. Specifically, the slope of the desorption curves for the carboxyl and hydroxyl terminated SAM appear qualitatively larger than those of the other SAMs.

While a qualitative assessment of the curve shapes is interesting, a quantitative approach was also performed to yield more concrete comparisons. The

individual sensorgrams were cut into individual injections of fibrinogen concentrations and overlaid (Figure 3.14).

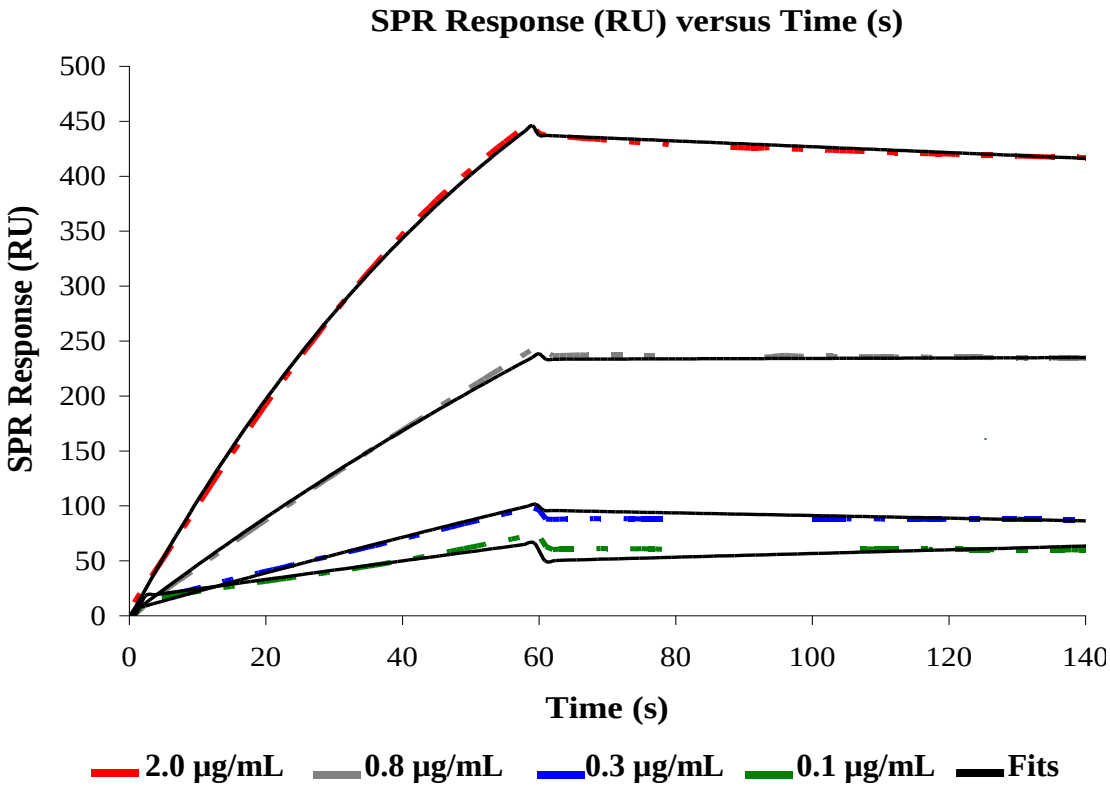

Figure 3.14: Example SPR sensorgram data of fibrinogen adsorption to hydroxyl-terminated SAM (colored lines) and kinetic fits (black lines).

The fitting model initially chosen was the simple 1:1 Langmuir binding model. This model accounts for one analyte binding to one site on the surface. $P + S \leftrightarrow PS$, where P stands for protein, S for the surface site, and PS for the protein adsorbed to the surface. This model was not ideal for this sequential injection experiment because it does not take into account a potential change (decrease) in available surface sites with each additional injection, but was adequate to obtain an estimate of kinetic parameters. A correction factor for conformational changes in the protein after adsorption was also not integrated into this kinetic model. Due to

constraints within the model and the way the data collection had to be done (starting with a reasonably covered surface is bad), the fits were only performed on the first four injections at the lowest concentrations. The sensorgrams were cut to isolate individual injections such that an overlay of the various concentrations was feasible. Although the fitting model was not ideal, as seen in an example sensorgram array with sample data and fits for the amine-terminated SAM (Figure 3.14), the fits matched closely with the experimental data. This analysis was performed for each surface tested to provide kinetic adsorption and desorption rate constants (Figures 3.15 and 3.16 and Table 3.3). Note, the large error bars are mostly due to differences between SPR chips. The sensorgrams between the four flow cells on one chip were consistent. The data was compiled from individual flow cell sensorgrams from different chips to provide an n of 12 for the gold, methyl, and carboxyl terminated SAM, 4 for the amine terminated SAM, and 7 for the carboxyl SAM. In addition to the adsorption and desorption parameters, a K_D was also determined for all surfaces. The association rate constants were similar for the hydroxyl and carboxyl terminated SAMs. The association rate constants for the amine and methyl terminated SAMs were similar. With the large error bars, the gold surface association constant was not distinguishable from any of the SAM surfaces, possibly due to the fact that the gold surface is more variable as it is more susceptible to contamination than the SAM surfaces are. The dissociation rate constants were similar for the hydroxyl and carboxyl terminated surfaces could be distinguished from the amine-terminated and gold surfaces, as they were much greater. Qualitatively, the shapes of the curves

were consistent with these fits. The desorption slopes of the carboxyl and hydroxyl terminated SAMs were much greater than the gold or the amine terminated SAM, so we would expect more protein to desorb from those surfaces and less from the gold and amine terminated SAM. While the general trend can be seen in the quantitative values, more drastic differences can be observed from the shapes of the curves, especially in the carboxyl terminated SAM. This may be due in part to the limited concentration range we were able to fit. Only the low concentrations (first four) were fit, decreasing the accuracy of the kinetic values. We are currently working to improve the kinetics model and the sequential injection method.

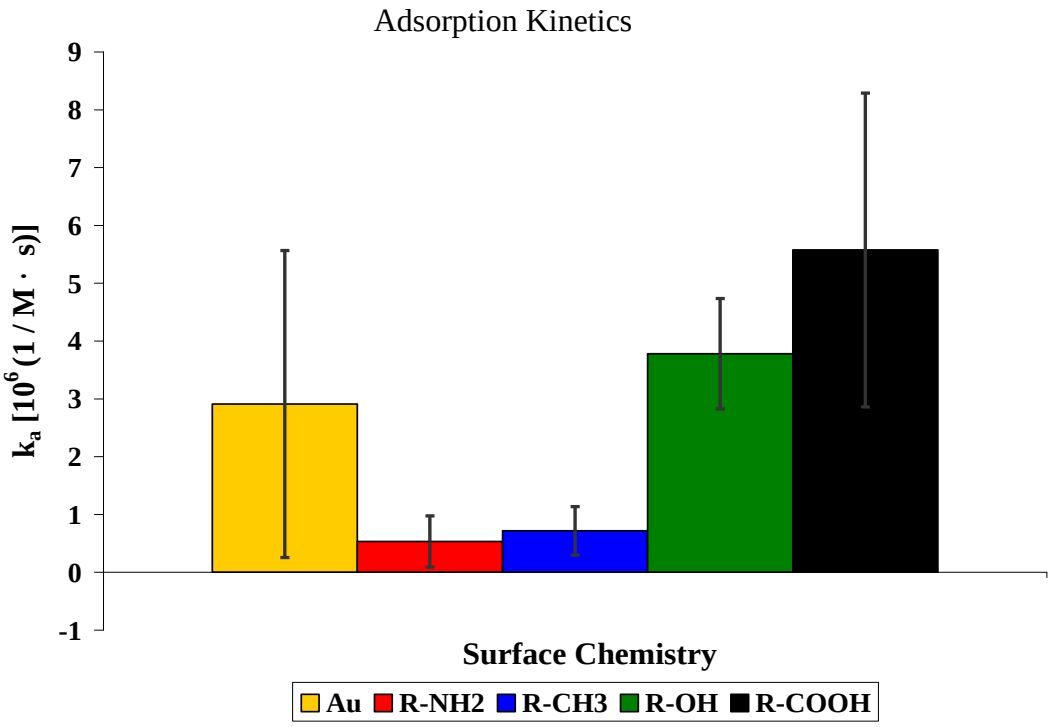

Figure 3.15: Bar graph of SPR sensorgram data for kinetic adsorption analysis of fibrinogen adsorption to various SAMs.

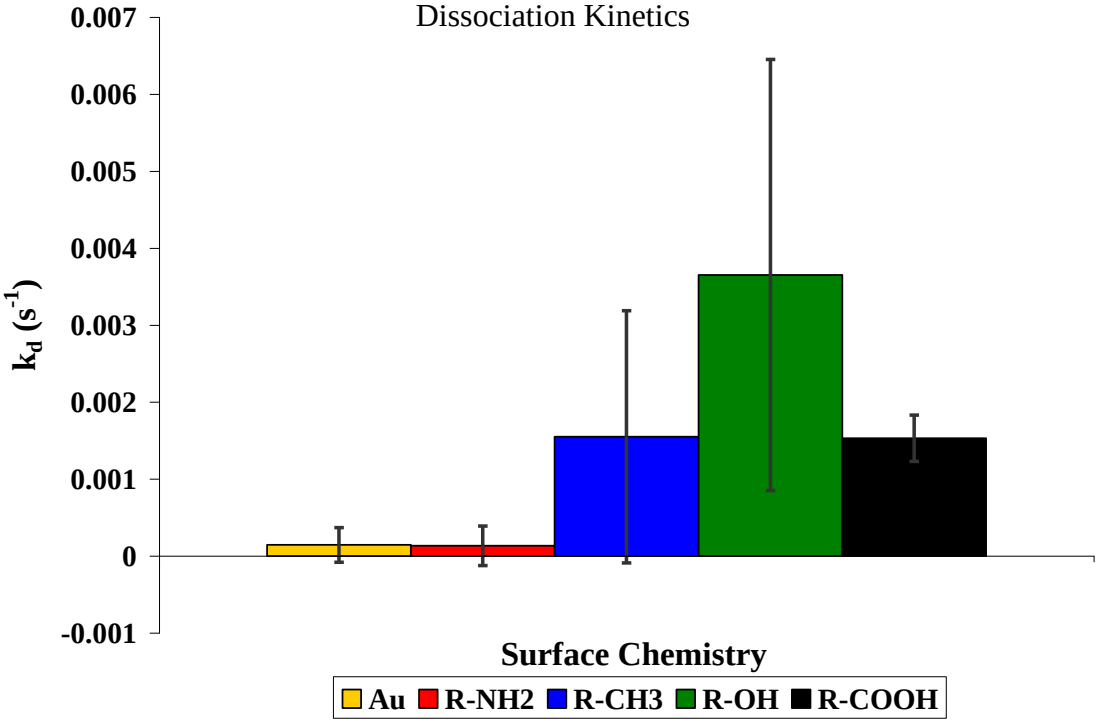

Figure 3.16: Bar graph of SPR sensorgram data for kinetic desorption analysis of fibrinogen adsorption to various SAMs.

Table 3.3: Summary of Kinetic Data of Fibrinogen Adsorption to SAMs

Terminal Surface Chemistry	*Adsorption Rate Constant (k_a)*	*Desorption Rate Constant (k_d)*	*Rate Constant (K_D)*
Au (n=12)	**$(3 \pm 3) \times 10^{6}$**	**$(1 \pm 2) \times 10^{-4}$**	**$(8 \pm 10) \times 10^{-11}$**
R-NH_2 (n=12)	**$(5 \pm 4) \times 10^{5}$**	**$(1 \pm 3) \times 10^{-4}$**	**$(3 \pm 6) \times 10^{-10}$**
R-CH_3 (n=12)	**$(7 \pm 4) \times 10^{5}$**	**$(2 \pm 2) \times 10^{-3}$**	**$(2 \pm 6) \times 10^{-8}$**
R-OH (n=16)	**$(4 \pm 1) \times 10^{6}$**	**$(4 \pm 3) \times 10^{-3}$**	**$(9.5 \pm 0.7) \times 10^{-10}$**
R-COOH (n=12)	**$(6 \pm 3) \times 10^{6}$**	**$(1.5 \pm 0.3) \times 10^{-3}$**	**$(3 \pm 1) \times 10^{-10}$**

3.4. Correlations of Nonspecific Fibrinogen Adsorption Results from AFM and SPR

AFM and SPR studies were performed on different surfaces. Different types of surfaces, such as a hydrophobic versus a hydrophilic surface, were different in adsorption conformation. Thus far, similar surfaces exhibited similar types of aggregation and protein conformation. Adsorption of fibrinogen to hydrophilic mica and hydrophilic gold surfaces resulted in a rounded or globular structure with even distribution across the surface. While fibrinogen adsorption to hydrophobic graphite or hydrophobic methyl-terminated SAM surfaces resulted in an elongated structure with much aggregation.

To correlate the two methods, AFM studies revealed that fibrinogen was more spread out on the hydrophobic than the hydrophilic surface, which makes sense with why the SDS worked better to desorb fibrinogen on hydrophobic versus hydrophilic surface. In terms of ultimate surface coverage via SPR, on hydrophilic surfaces, the fibrinogen balled up, therefore each molecule occupied less space and more molecules could be packed in per area and a greater amount of adsorption was observed via SPR with the amine-terminated SAM. AFM studies revealed that on the hydrophobic methyl-terminated SAM in which the molecules take up more space and thus, fewer molecules can be packed in per area and a lower adsorption was observed via SPR. However, other hydrophilic SAM surfaces had a lower adsorption via SPR than the methyl terminated surface, so conformation is not the only important factor in adsorption properties. Thus, surface chemistry has an effect on not only the amount of protein adsorbed but also the strength of protein binding (or the amount of protein that remains adsorbed).

3.5. Summary

AFM and SPR studies provided evidence that surface chemistry plays a critical role in the conformation of adsorbed fibrinogen as well as in the rates of adsorption and desorption of fibrinogen to various surfaces. AFM studies on smooth hydrophobic graphite substrate exhibited a trinodular structure and aggregation while on hydrophilic mica substrate the structure was balled or rounded and molecules were evenly distributed (little aggregation evident). On gold, a hydrophilic surface, fibrinogen molecules acted similarly to the mica substrate in that they were balled up

and evenly distributed. On the hydrophobic methyl-terminated silicon surface fibrinogen aggregated. SPR studies revealed that surface chemistry plays an important role in the binding kinetics of fibrinogen. The rates of adsorption and desorption were different on different surfaces. The effect was more than just a difference between a hydrophobic or hydrophilic surface. Several hydrophilic surfaces (plain gold as well as an amine, carboxyl, and hydroxyl terminated SAM) were tested and the resultant sensorgrams showed significant differences between these different surface chemistries. This indicates that the relative hydrophobicity is certainly not the only important factor in determining how the protein will bind. Fibrinogen is sticky and hard to get off of any surface and as such the SPR desorption rates were slow.

Protein-surface interactions were studied via tapping mode AFM. Surface chemistry affected the conformation of adsorbed proteins. SPR studies revealed that fibrinogen desorbs from surfaces to a different degree depending on the surface chemistry, changing the final level of adsorbed protein on the surface. The kinetics on different surfaces correlated with conformation of fibrinogen on the different surface. In addition to surface chemistry, pH plays are role in the aggregation and adsorption properties as it changes the charge distribution on the protein and can also change the charge at the surface for the amine and carboxyl terminated SAMs. By controlling the chemistry and structure at the surface, it may be possible to manipulate the adsorption of protein at the surface for the desired result. For instance, to improve biocompatibility, although it might not be possible to completely

eliminate fibrinogen adsorption to surface, it may be possible to minimize this adsorption based on surface chemistry. Alternatively, controlling the adsorption in such a way that the conformation was such that the thrombin cleavage site(s) were inaccessible, would also reduce chance of clot initiation and improve compatibility. Most likely, the balled up or globular conformation will be less susceptible to cleavage based on previous work. So the mica, gold, and amine terminated SAM might reduce polymerization more so than the methyl terminated SAM. Ideally, probably a surface with this conformation and a low amount of adsorbed protein to begin with, such as the amine terminated SAM, will be most suitable towards improved biocompatibility.

3.6. References

1. Horbett, T. A., Chapter 13 Principles underlying the role of adsorbed plasma proteins in blood interactions with foreign materials. *Cardiovascular Pathology* **1993,** *2* (3, Supplement), 137-148.
2. Roach, P.; Farrar, D.; Perry, C. C., Interpretation of Protein Adsorption: Surface-Induced Conformational Changes. *Journal of the American Chemical Society* **2005,** *127* (22), 8168-8173.
3. Tsapikouni, T. S.; Missirlis, Y. F., pH and ionic strength effect on single fibrinogen molecule adsorption on mica studied with AFM. *Colloids and Surfaces B: Biointerfaces* **2007,** *57* (1), 89-96.
4. Weisel, J.; Stauffacher, C.; Bullitt, E.; Cohen, C., A model for fibrinogen: domains and sequence. *Science* **1985,** *230* (4732), 1388-1391.
5. Brown, J. H.; Volkmann, N.; Jun, G.; Henschen-Edman, A. H.; Cohen, C. 1DEQ: The crystal structure of modified bovine fibrinogen (at ~4 angstrom resolution) from "The crystal structure of modified bovine fibrinogen.". http://www.rcsb.org/pdb (accessed November 2007).
6. Jung, S.-Y.; Lim, S.-M.; Albertorio, F.; Kim, G.; Gurau, M. C.; Yang, R. D.; Holden, M. A.; Cremer, P. S., The Vroman Effect: A Molecular Level Description of Fibrinogen Displacement. *Journal of the American Chemical Society* **2003,** *125* (42), 12782-12786.
7. Mrksich, M., Using self-assembled monolayers to understand the biomaterials interface. *Current Opinion in Colloid & Interface Science* **1997,** *2* (1), 83-88.
8. Ostuni, E.; Yan, L.; Whitesides, G. M., The interaction of proteins and cells with self-assembled monolayers of alkanethiolates on gold and silver. *Colloids and Surfaces B: Biointerfaces* **1999,** *15* (1), 3-30.
9. Fowler, W. E.; Erickson, H. P., Trinodular structure of fibrinogen: Confirmation by both shadowing and negative stain electron microscopy. *Journal of Molecular Biology* **1979,** *134* (2), 241-249.
10. Beijbom, L.; Larsson, U.; Kavéus, U.; Hebert, H., Structure analysis of fibrinogen by electron microscopy and image processing. *Journal of Ultrastructure and Molecular Structure Research* **1988,** *98* (3), 312-319.
11. Wall, J.; Hainfeld, J.; Haschemeyer, R. H.; Mosesson, M. W., ANALYSIS OF HUMAN FIBRINOGEN BY SCANNING TRANSMISSION ELECTRON MICROSCOPY*. *Annals of the New York Academy of Sciences* **1983,** *408* (1), 164-179.
12. Clarke, M. L.; Wang, J.; Chen, Z., Conformational Changes of Fibrinogen after Adsorption. *The Journal of Physical Chemistry B* **2005,** *109* (46), 22027-22035.
13. Vroman, L.; Adams, A. L., Findings with the recording ellipsometer suggesting rapid exchange of specific plasma proteins at liquid/solid interfaces. *Surface Science* **1969,** *16* (0), 438-446.
14. Höök, F.; Vörös, J.; Rodahl, M.; Kurrat, R.; Böni, P.; Ramsden, J. J.; Textor, M.; Spencer, N. D.; Tengvall, P.; Gold, J.; Kasemo, B., A comparative study of protein adsorption on titanium oxide surfaces using in situ ellipsometry, optical waveguide lightmode spectroscopy, and quartz crystal microbalance/dissipation. *Colloids and Surfaces B: Biointerfaces* **2002,** *24* (2), 155-170.
15. Evans-Nguyen, K. M.; Tolles, L. R.; Gorkun, O. V.; Lord, S. T.; Schoenfisch, M. H., Interactions of Thrombin with Fibrinogen Adsorbed on Methyl-, Hydroxyl-, Amine-, and Carboxyl-Terminated Self-Assembled Monolayers†. *Biochemistry* **2005,** *44* (47), 15561-15568.

16. Choukourov, A.; Grinevich, A.; Saito, N.; Takai, O., SPM analysis of fibrinogen adsorption on solid surfaces. *Surface Science* **2007,** *601* (18), 3948-3951.
17. Averett, L. E.; Schoenfisch, M. H., Atomic force microscope studies of fibrinogen adsorption. *Analyst* **2010,** *135* (6), 1201-1209.
18. Sit, P. S.; Marchant, R. E., Surface-dependent conformations of human fibrinogen observed by atomic force microscopy under aqueous conditions. *Thrombosis and haemostasis* **1999,** *82* (3), 1053-60.
19. Agnihotri, A.; Siedlecki, C. A., Time-Dependent Conformational Changes in Fibrinogen Measured by Atomic Force Microscopy. *Langmuir* **2004,** *20* (20), 8846-8852.
20. Xu, L.-C.; Siedlecki, C. A., Effects of surface wettability and contact time on protein adhesion to biomaterial surfaces. *Biomaterials* **2007,** *28* (22), 3273-3283.
21. Ishizaki, T.; Saito, N.; Sato, Y.; Takai, O., Probing into adsorption behavior of human plasma fibrinogen on self-assembled monolayers with different chemical properties by scanning probe microscopy. *Surface Science* **2007,** *601* (18), 3861-3865.
22. Ta, T. C.; Sykes, M. T.; McDermott, M. T., Real-Time Observation of Plasma Protein Film Formation on Well-Defined Surfaces with Scanning Force Microscopy. *Langmuir* **1998,** *14* (9), 2435-2443.
23. Sethuraman, A.; Han, M.; Kane, R. S.; Belfort, G., Effect of Surface Wettability on the Adhesion of Proteins. *Langmuir* **2004,** *20* (18), 7779-7788.
24. Huang, Y.-W.; Gupta, V. K., A SPR and AFM study of the effect of surface heterogeneity on adsorption of proteins. *The Journal of Chemical Physics* **2004,** *121* (5), 2264-2271.
25. Tunc, S.; Maitz, M. F.; Steiner, G.; Vázquez, L.; Pham, M. T.; Salzer, R., In situ conformational analysis of fibrinogen adsorbed on Si surfaces. *Colloids and Surfaces B: Biointerfaces* **2005,** *42* (3–4), 219-225.
26. Li, L.; Chen, S.; Zheng, J.; Ratner, B. D.; Jiang, S., Protein Adsorption on Oligo(ethylene glycol)-Terminated Alkanethiolate Self-Assembled Monolayers: The Molecular Basis for Nonfouling Behavior. *The Journal of Physical Chemistry B* **2005,** *109* (7), 2934-2941.
27. Green, R. J.; Davies, M. C.; Roberts, C. J.; Tendler, S. J. B., Competitive protein adsorption as observed by surface plasmon resonance. *Biomaterials* **1999,** *20* (4), 385-391.
28. Mrksich, M.; Sigal, G. B.; Whitesides, G. M., Surface Plasmon Resonance Permits in Situ Measurement of Protein Adsorption on Self-Assembled Monolayers of Alkanethiolates on Gold. *Langmuir* **1995,** *11* (11), 4383-4385.
29. Steiner, G.; Tunc, S.; Maitz, M.; Salzer, R., Conformational Changes during Protein Adsorption. FT-IR Spectroscopic Imaging of Adsorbed Fibrinogen Layers. *Analytical Chemistry* **2007,** *79* (4), 1311-1316.
30. Ward, C. A.; Stanga, D., Biological activity of fibrinogen adsorbed on synthetic materials. *Journal of Colloid and Interface Science* **1986,** *114* (2), 323-329.
31. Norde, W.; Anusiem, A. C. I., Adsorption, desorption and re-adsorption of proteins on solid surfaces. *Colloids and Surfaces* **1992,** *66* (1), 73-80.
32. Wertz, C. F.; Santore, M. M., Adsorption and Relaxation Kinetics of Albumin and Fibrinogen on Hydrophobic Surfaces: Single-Species and Competitive Behavior. *Langmuir* **1999,** *15* (26), 8884-8894.
33. Wertz, C. F.; Santore, M. M., Effect of Surface Hydrophobicity on Adsorption and Relaxation Kinetics of Albumin and Fibrinogen: Single-Species and Competitive Behavior. *Langmuir* **2001,** *17* (10), 3006-3016.

34. Wertz, C. F.; Santore, M. M., Fibrinogen Adsorption on Hydrophilic and Hydrophobic Surfaces: Geometrical and Energetic Aspects of Interfacial Relaxations. *Langmuir* **2002,** *18* (3), 706-715.
35. Gettens, R. T. T.; Bai, Z.; Gilbert, J. L., Quantification of the kinetics and thermodynamics of protein adsorption using atomic force microscopy. *Journal of Biomedical Materials Research Part A* **2005,** *72A* (3), 246-257.
36. Hu, J.; Yang, D.; Kang, Q.; Shen, D., Estimation the kinetics parameters for non-specific adsorption of fibrinogen on quartz surface from the response of an electrode-separated piezoelectric sensor. *Sensors and Actuators B: Chemical* **2003,** *96* (1–2), 390-398.
37. Balasubramanian, V.; Grusin, N. K.; Bucher, R. W.; Turitto, V. T.; Slack, S. M., Residence-time dependent changes in fibrinogen adsorbed to polymeric biomaterials. *Journal of Biomedical Materials Research* **1999,** *44* (3), 253-260.
38. Karlsson, R.; Katsamba, P. S.; Nordin, H.; Pol, E.; Myszka, D. G., Analyzing a kinetic titration series using affinity biosensors. *Analytical Biochemistry* **2006,** *349* (1), 136-147.
39. Wang, H.; Chen, S.; Li, L.; Jiang, S., Improved Method for the Preparation of Carboxylic Acid and Amine Terminated Self-Assembled Monolayers of Alkanethiolates. *Langmuir* **2005,** *21* (7), 2633-2636.
40. Inc., A. Self-Assembing Molecules_Variations in the Assembly Protocol for Carboxy- and Amine-Terminated Alkanethiols. www.asemblon.com (accessed April 1, 2009).

CHAPTER FOUR:

Towards Nanoscale Devices Incorporating the Molecular Motor F_1-ATPase

4. Overview

The previous chapter discussed fibrinogen experiments which were based on nonspecific protein adsorption. In this chapter, a different protein, F_1-ATP synthase, was investigated via both nonspecific and specific adsorption methods. F_1-ATPase is of particular interest due to both its size and its rotary motor capabilities. As devices are manufactured at smaller and smaller scales (from micron to nano), eventually fabrication of inorganic motors to power these devices will not be feasible with current technology. A small rotary molecular motor offers a unique solution for fabrication of such devices due to its small size (inherently nanometers in dimension). Incorporation of biomolecules into hybrid nanobiodevices requires control over both biomolecule placement and its orientation within the device. Investigation into nonspecific adsorption of the tiny motor, F_1-ATP synthase (ATPase), via tapping mode AFM was performed to study protein orientation(s) on the surface. For the immobilized protein to function properly within a device, precise orientation is required. Therefore, controlling this orientation is imperative for increasing the number of functional molecules, as other orientations will lead to inactive protein motors. Additionally, placement of the protein motor within the device is vital for device fabrication. Several techniques, including SPR and AFM, have been utilized to study and control this adsorption process. The chemistry involved in this controlled orientation process and the durability of immobilization have been studied via SPR. AFM was used to both create a landing pad with specific chemistry (to control placement within the device) and to control orientation of the individual

protein molecules. By coordinating these efforts with nanoelectrode construction, a functional hybrid nanobiodevice may be successfully engineered (Figure 4.6).

4.1. Introduction

Adenosine triphosphate (ATP) synthases synthesize ATP, the primary energy source for living organisms. ATP synthase (ATPase) is a tiny enzyme that synthesizes ATP from adenosine diphosphate (ADP) and inorganic phosphate. The ubiquitous F-ATPase can be found in plants, animals, and bacteria.[1] Figure 4.1 shows a general structure of ATPase.[2] F-ATPase is composed of two portions including the membrane bound F_o and the soluble F_1 portion. The hydrophobic F_o portion contains subunits labeled a, two subunits labeled b, as well as a ring of ten to fourteen c subunits ($c_{10\text{-}14}ab_2$) and is connected to the gamma and epsilon subunits.[3-5] The hydrophilic F_1 portion is primarily composed of the central gamma subunit (γ) and a symmetric hexameric barrel consisting of alternating alpha and beta subunits ($\alpha_3\beta_3$) as well as an epsilon and delta subunit ($\alpha_3\beta_3\gamma\varepsilon\delta$). The intact enzyme is really two coupled motors driven by the protein gradient across the membrane. Although both portions rotate, just part of the F_1 portion ($\alpha_3\beta_3\gamma$) will be the focus of this dissertation. This section of the F_1 portion is approximately 360 kDa, measuring 10 nm in diameter and 8 nm in height according to the crystal structure.[6] The radius of the gamma subunit is 1 nm.[7] F_1-ATPase is the smallest known molecular motor.[8]

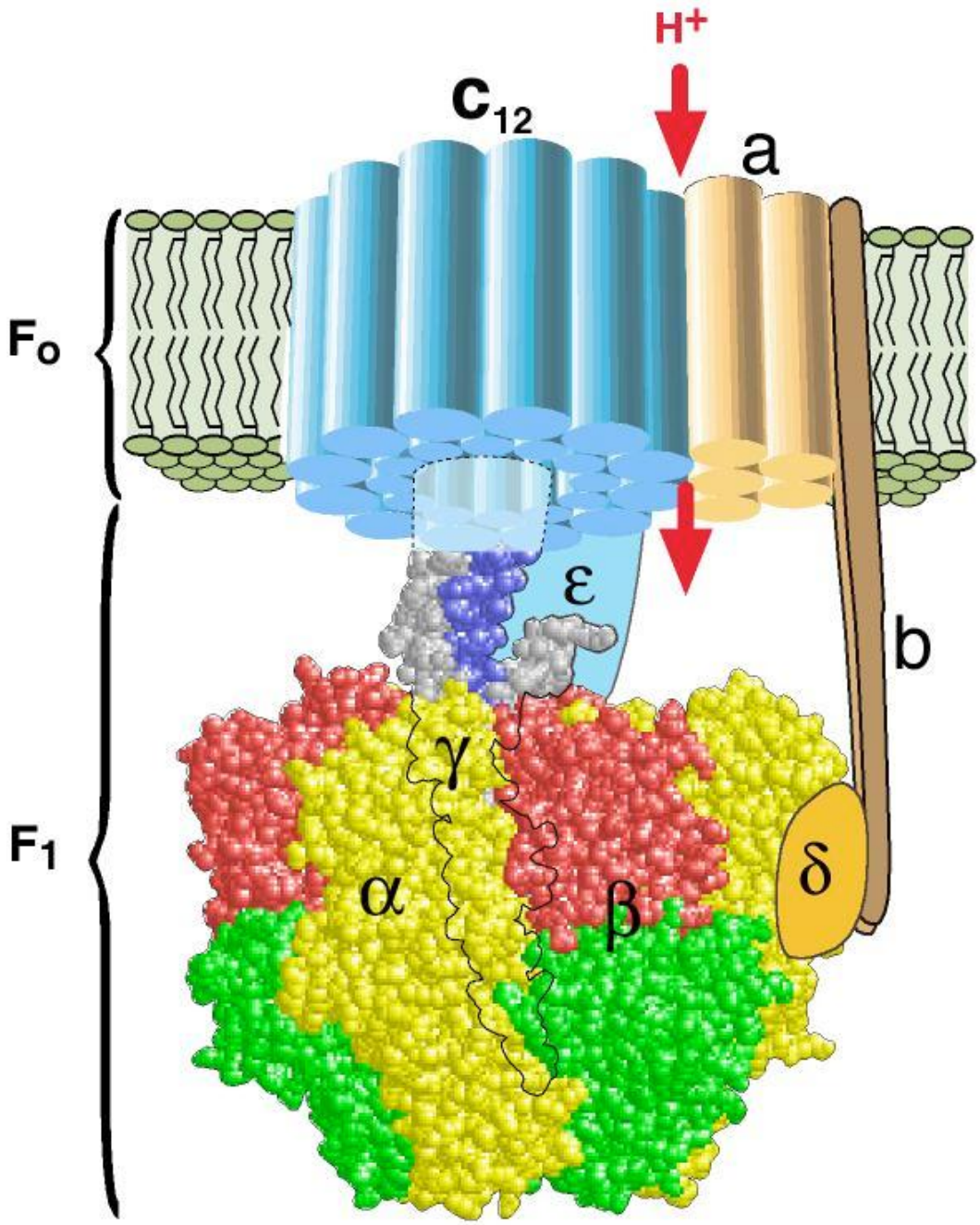

Figure 4.1: ATPase Structure courtesy of Oster, G.[2] Reprinted by permission from Macmillan Publishers Ltd: [Nature] (Wang, H.; Oster, G.; *Nature* **1998** *396*, 279-282), copyright (1998).

In addition to crystal structure experiments, previous investigations into the structure of ATPase via electron microscopy and AFM have mostly focused on either the whole complex (F_oF_1 ATPase from chloroplasts were studied by Dencher[9] and Seelert[3]), the bacterial F_oF_1 ATPase,[4,10] or just the F_o portion.[4]

Dencher used a lipid bilayer approach to adsorb chloroplast F_oF_1ATPase onto a mica surface and studied these films via cryoelectron microscopy and contact mode AFM in fluid and determined that the F_1 portion of the motor projected 10 nanometers above the lipid matrix with a diameter of about 28 nanometers.[9] By chemically or mechanically removing the F_1 portion, the F_o portion was studied and found to have ring-like structure with a divot in the middle and was about 0.4 nanometers above the matrix with a diameter of about 7 nanometers. The F_1 portion was estimated to be about 13 nanometers in diameter. Unfortunately, the resolution on these images was poor and distinct subunit information was unclear.[9]

Spinach chloroplast ATPase molecules were studied via AFM.[3] Height images distinctly display a ring-like structure with the fourteen subunits per rotor for this species (c_{14}).[3] In contrast, using a combination of contact mode AFM with a mica substrate and cryoelectron microscopy with carbon-coated copper grids, Dimroth determined that the c subunit bacterial Na^+-ATPase (a different species) to be undecameric (c_{11}).[4] An electron microscopy and tapping mode AFM study of bacterial F_o and F_oF_1-ATPase molecules in lipid membranes adsorbed unto a mica substrate revealed an F_1 sector of 90 Å diameter and F_oF_1 were observed to be pairs of spheres with a height of 100 Å, respectively. F_o structures were much smaller at less

than 10 Å with ring-like structures either with or without a hollowed center. However, the resolution of these studies was limited and substructure information was not obtained.[10] X-ray studies by Stock of yeast mitochondrial ATPase revealed only 10 subunits in the c ring (c_{10}).[5]

More extensive studies have been performed on the F_o portion due to the ease of sample preparation (merely adsorb a lipid bilayer with protein imbedded in it on the surface and image). This method of preparation results in protein packed within the bilayer such that the protein is confined and its movement is constricted, making imaging of this protein easier. To date, subunit resolved AFM images of the F_1-ATPase with the rotor ($\alpha_3\beta_3\gamma$) have not been reported.

Work on determining both structure and rotational mechanisms includes studies of conformational changes via electron microscopy[11] and high speed AFM.[12, 13] Electron microscopy was performed via negative staining. Their results show an uneven dumbbell shape with two spherical structures (one slightly larger than the other) connected by a rod shaped structures, corresponding to the F_1, the F_o, and the gamma subunit, respectively. The study was performed both in the absence and presence of nucleotide. With nucleotide, the F_o stayed the same while the F_1 changed slightly. These images provide a compelling structural picture of the ATPase complex.[11] A somewhat complementary study was performed with high speed AFM images where rotorless F_1-ATPase (so lacking the F_o and γ portions) without nucleotide were adsorbed onto mica and revealed six distinct sections in a ring, corresponding to the alternating alpha and beta hexameric barrel structures; the

catalytic beta subunits were higher than the alpha ones with a central hole (where gamma subunit is missing). After nucleotide addition, the structure changed a bit and revealed only one higher beta subunit. Upon addition of ATP, the brighter area was on one beta subunit and rotated around in a counterclockwise direction amongst the beta subunits. Quantitative measurements of the sizes of the molecules and subunits were not reported.[12] The fact that this conformation change was observed without the gamma subunit present is consistent with mutation studies where the gamma subunit has been sequentially shortened and rotation still occurs. These studies seem to contradict the current theory about the rotation mechanism involving interactions of the gamma subunit with the beta subunits. Further mechanistic investigations are required to elucidate the structure-function relationship within this enzyme.

Part of the ATP synthesis process involves the spinning of the γ (gamma) subunit.[14] When just the F_1 portion is studied, ATP hydrolysis occurs and observed spinning is in the counterclockwise direction (as viewed from the F_o side). Rotation studies with long filaments resulted in a 360º rotation with three 120º steps.[14] Each full rotation results in the hydrolysis of three ATP molecules to ADP and inorganic phosphate. Studies with smaller armatures (beads) with limiting ATP concentrations were able to elucidate discrete substeps within this rotation process of 80º and 40º or with 90º and 30º intermediate halts.[15,16] F_1-ATPase is thought to have three catalytic sites at the boundaries between the alpha and beta subunits. These sites are said to be in an open, closed, or intermediate state in which there is an empty site, ATP, or ADP bound to the beta subunit.[7] Calculated rotation speeds were about 130 revolutions per

second with a high energy efficiency.[16] This rotation generates a huge torque (ranging from 20 pN*nm to 80-100 pN*nm), meaning that this rotor may be useful for a variety of applications.[14,17] Potential applications include anything from delivery agents to powering motors for nanodevices to switches. If one wanted to use this motor as a switch, control over the spinning of the motor is critical. Thus, having the availability of a built in regulator to start and stop the motor (as is the case with the chloroplast ATPase which has a regulatory dithiol redox switch in the gamma subunit[18] or an integrated zinc switch[19]) to control the spinning is desired. Both the size and function of this protein are key attributes to be exploited. Most notably for this dissertation, ATPase will serve as a candidate for incorporation into a nanobiodevice as a molecular motor.

Previous experiments which provide evidence of rotation for this enzyme will be briefly explored. In one study, a fluorescent microsphere was attached to the tip of the gamma subunit and rotation was observed via a differential interferometer.[20] Itoh *et al.* performed rotation studies with 40 nanometer gold beads coated with biotinylated bovine serum albumin attached to the biotinylated gamma subunit via streptavidin, monitored via laser dark field microscopy, and captured with a charge-coupled device camera.[16] While these studies were compelling as to the possibility of rotation, some controversy exists. Since the beads were not much larger than the protein itself and placed almost directly above the protein, the motions captured were very tiny. It is possible that the observed movement was due to only Brownian motion and not from actual rotation of the gamma subunit. To more directly

determine rotation, one could extend movement away from central rotation. If rotation is still evident, then it is less likely to be Brownian motion. However, modifications to the protein that allow the rotation to be observed more off axis, would also be more likely to introduce drag and change the inherent motion of the motor.

Previous investigations by two groups, Yoshida (Figure 4.2) and Montemagno (Figure 4.3), have shown rotation of the gamma subunit by extending the length of the unit attached to it. Yoshida *et al.* demonstrated that a fluorescent actin filament attached to the gamma subunit rotates in the counterclockwise direction upon introduction of ATP. Montemagno's group visualized the rotation of a nickel rod nanopropeller attached to the gamma subunit rotating in the counterclockwise direction via a CCD camera.[17]

Noji, *et al.* pioneered the exploration of F_1-ATPase rotation experiments. In 1997, fluorescent measurements of this enzyme showed rotation of a two micrometer long fluorescent filament attached to the gamma subunit in the counterclockwise direction upon addition of ATP (Figure 4.2).[14]

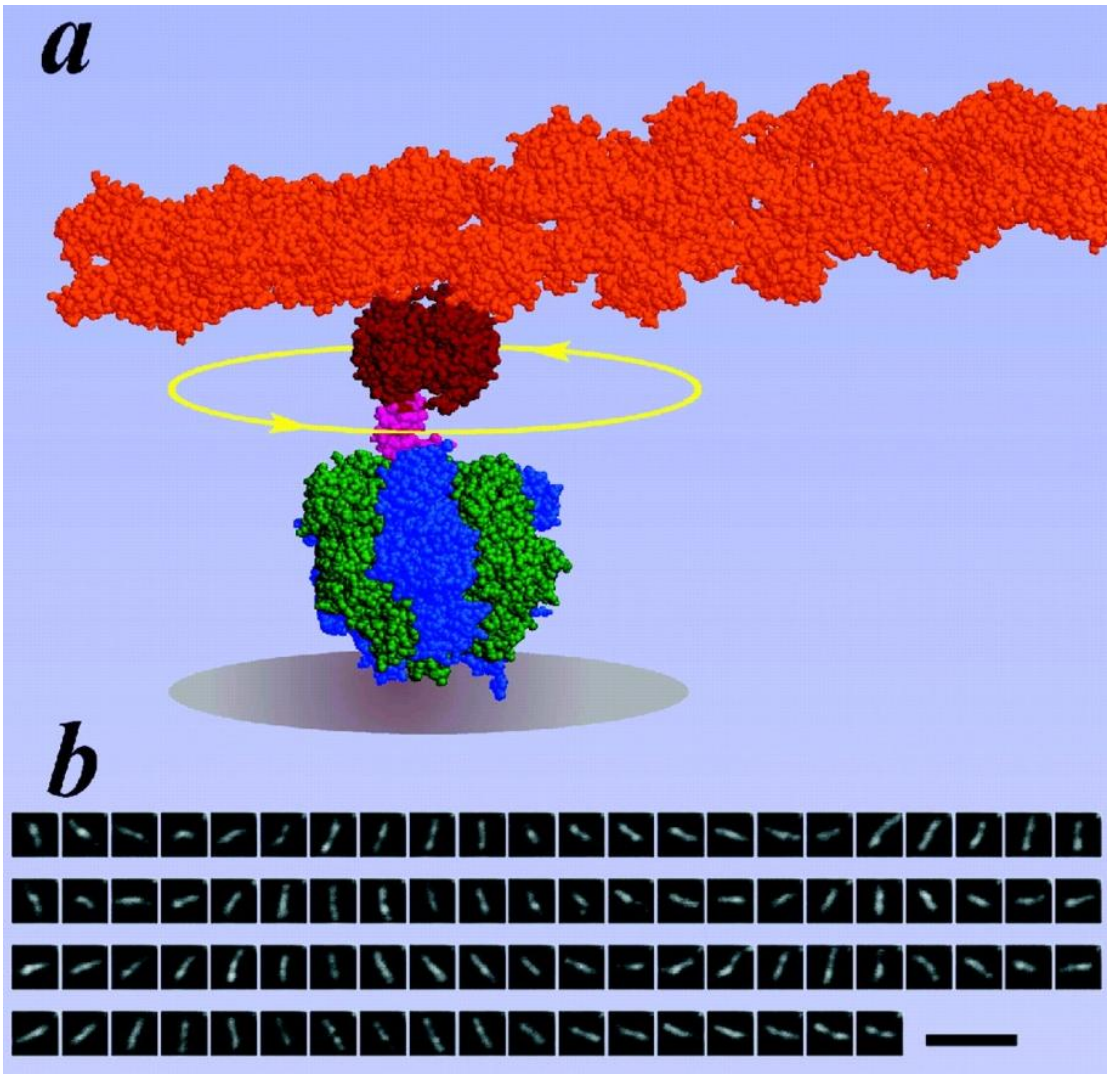

Figure 4.2: Evidence of ATPase rotation example 1.[14] Reprinted by permissions from FASEB Journal [Kazuhiko Kinosita, Jr.; *FASEB* **1999** *13*, S201-S208] & Macmillan Publishers Ltd: [Nature] (Noji, H; Yasuda, R.; Yoshida, M.; Kinosita, K.; *Nature* **1997** *386*, 299-302), copyright 1997.

In a second revolutionary visual example of ATPase rotation, Montemagno *et al.* used a charge-coupled device camera to monitor the rotation of nickel rods (nanopropellers) attached to the gamma subunit of F_1-ATPase (Figure 4.3).[17] These motors were attached to nickel posts that were 50 to 120 nm in diameter and 200 nanometers high via histidine tags incorporated into the β-subunit. The nanopropellers (150 nanometers in diameter and 750 to 1400 nanometers in length) were attached via streptavidin coupling, as both the gamma subunit and nanopropellers were biotinylated. Spinning of these nanopropellers was monitored and control studies were performed.

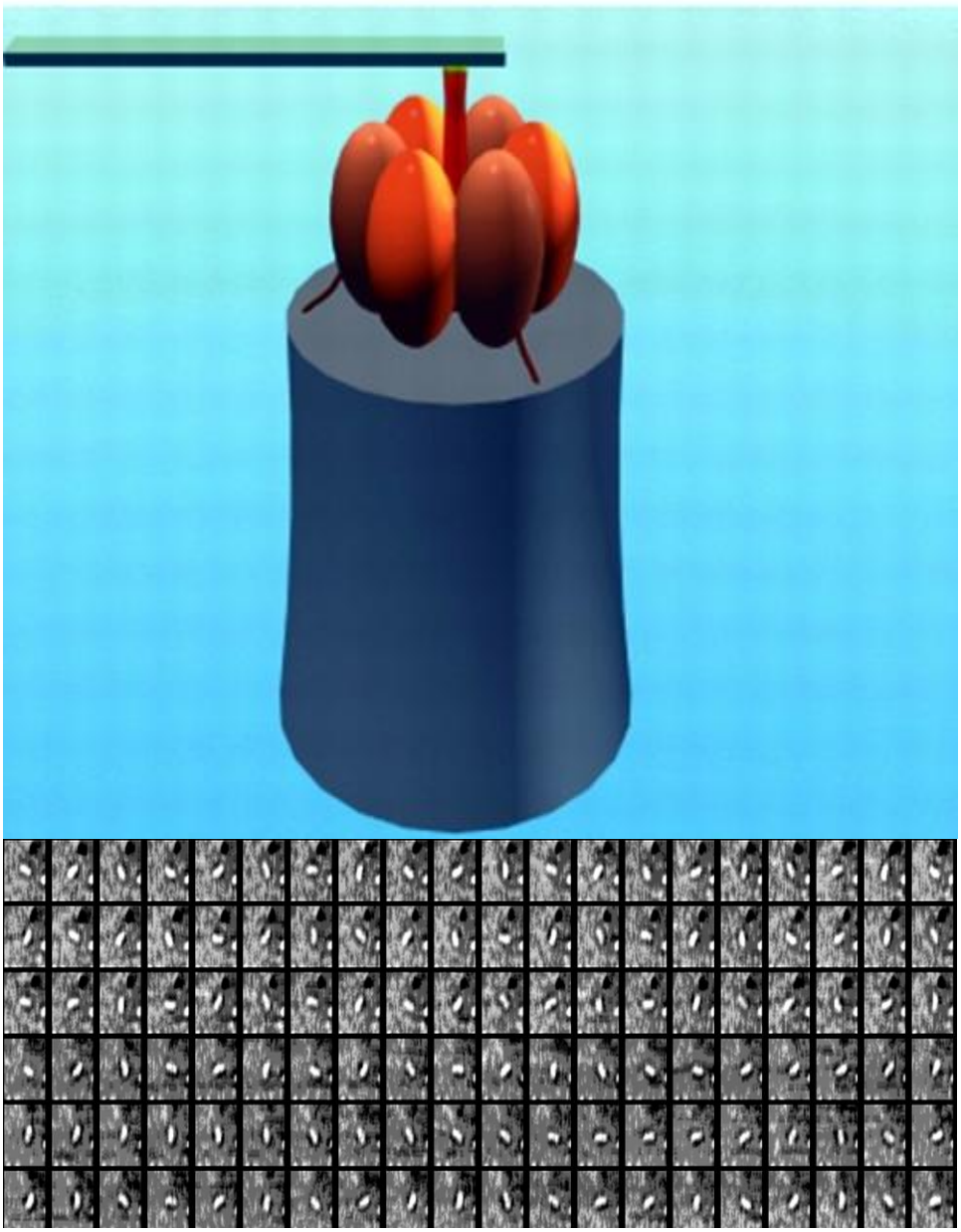

Figure 4.3: Evidence of ATPase rotation example 2.[17] From [Soong, R.K.; Bachand, G.D.; Neves, H.P.; Olkhovets, A.G.; Craighead, H.G.; Montemagno, C.D.; *Science* **2000** *290:5496*, 1555-1558]. Reprinted by permission from AAAS.

Both those examples exhibit the extraordinary power of the F_1-ATPase motor to spin a filament or rod around in a counterclockwise direction through ATP hydrolysis. What makes this so impressive is that these propellers are on the order of microns while the motor powering the rotation is only tens of nanometers. These examples of this protein spinning something so much larger than itself are true examples of the uniqueness of the torque of this motor. Unfortunately, in both rotation examples above, less than two percent of the motors were active. For Yoshida *et al.*, about only one out of 70 filaments were observed to rotate continuously in the counterclockwise direction.[14] In the case of Montemagno, only 5 of about 400 propellers rotated continuously in the counterclockwise direction and the device lasted for about 2.5 hours before the propeller broke away.[17]

In both cases, although histidine tags were used in an attempt to specifically attach and orient the proteins, some snags were evident in the protein immobilization strategies. For Yoshida's group, the substrate was a glass slide upon which horseradish peroxidase containing some nickel-nitrilotriacetic acid groups was adhered. While this was a reasonable plan, this surface turned out to not be ideal for the size scale of the protein investigated due to the roughness of the Ni-NTA layer.[21,22] Both the glass slide and the horseradish peroxidase surface components were rough. Previous members of the Berrie group constructed similar surfaces of cleaned glass slides and glass slides coated with horseradish peroxidase and observed this surface roughness (Figure 4.4).

a)

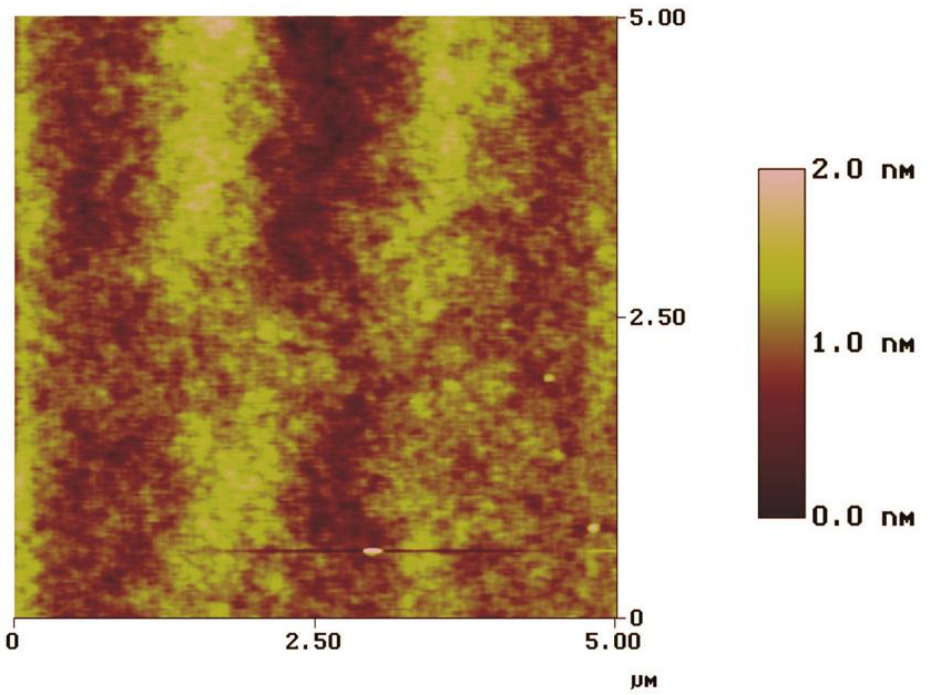

b)

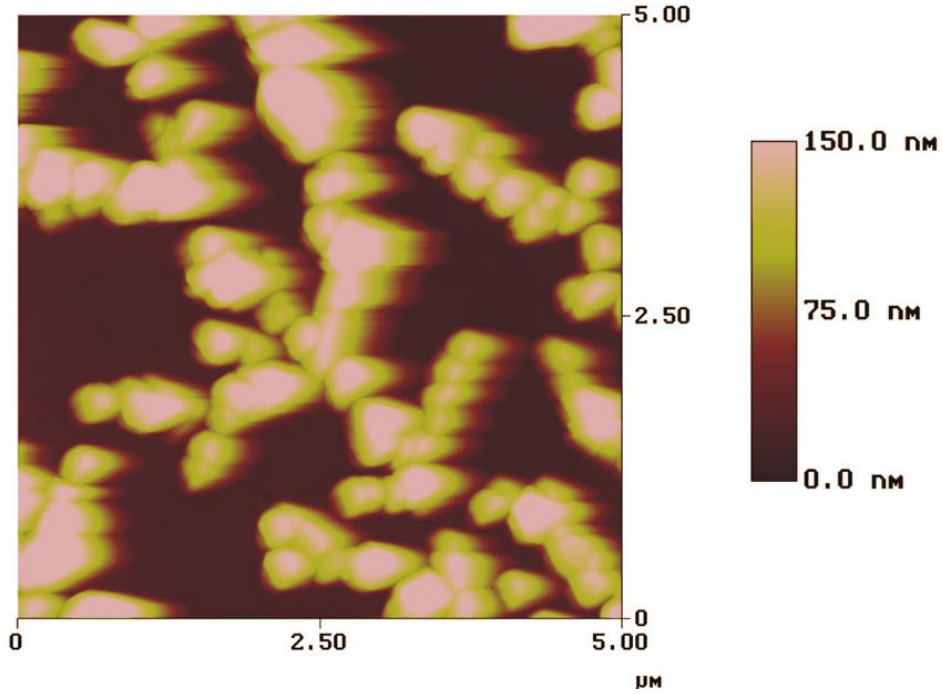

Figure 4.4: 5.00 µm by 5.00 µm AFM height images of a) glass slide with a 2.0 nm height scale and b) glass slide with horseradish peroxidase adsorbed with a 150.0 nm height scale.

Additional investigations by the Berrie group involved a mimic SAM NTA surface which was also very rough with a RMS roughness of about 1.573 nanometers over a 10 μm^2 area (Figure 4.5). The AFM height images show variations in the heights of the matrices; the surfaces were not a uniformly solid color across scan of image. This roughness means that there are some valleys where the histidine-tagged protein might reside which would inhibit the molecules spatially and thus cause them to be unable to spin or be observed. If the protein is trapped within matrix, then the arm cannot rotate freely because there is not enough room to spin. This decreases the overall percentage of functional molecules adsorbed to the surface. Additionally, orientation is a problem, if the surface chemistry is not uniform over the entire film. Nonspecific adsorption of F_1-ATPase could be an issue too. If the protein adsorbed to other unintended places on the surface, studies of rotation may be adversely compromised. And finally, denaturing of protein may also adversely impact the function or rotation after immobilization.

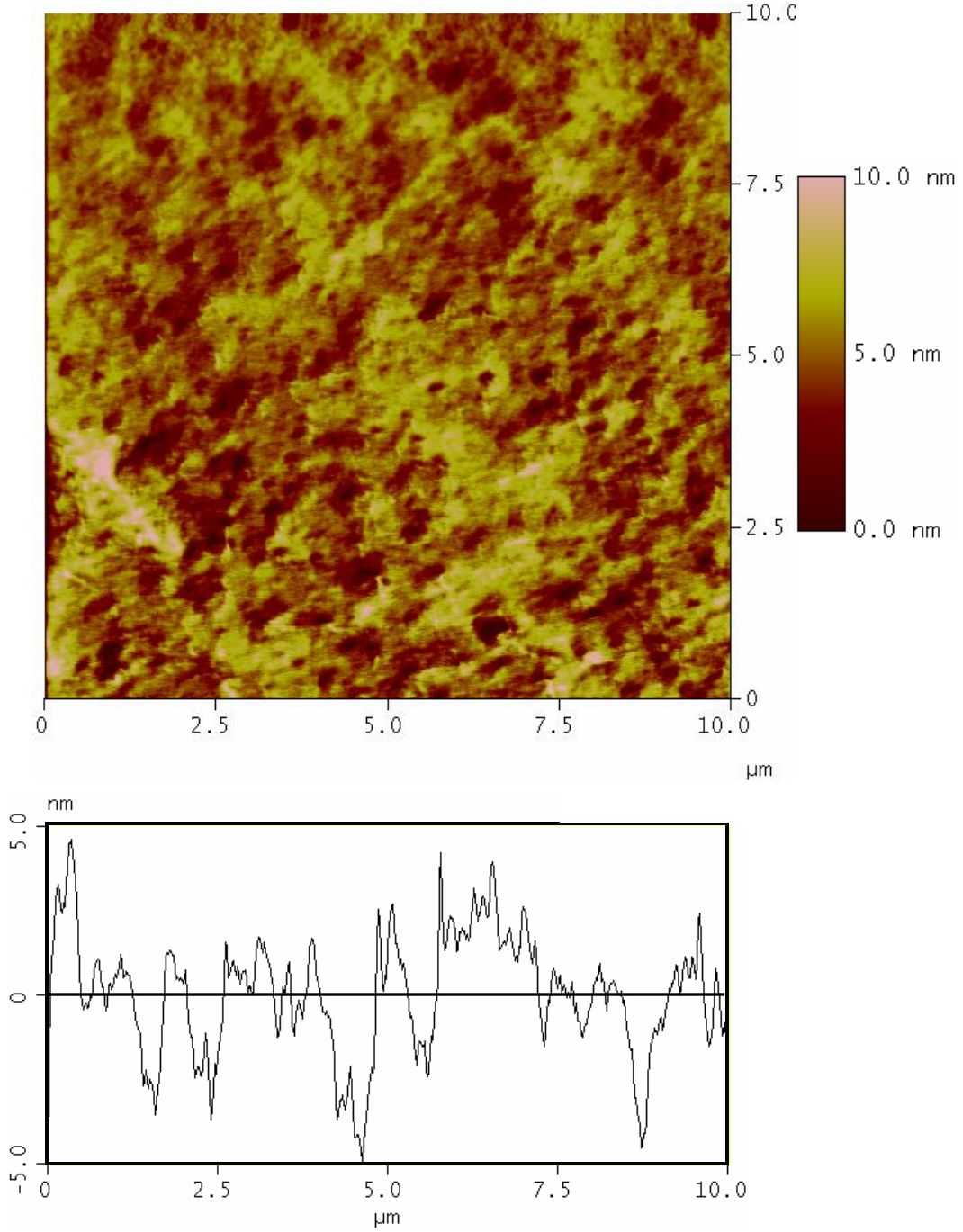

Figure 4.5: 10.0 µm by 10.0 µm AFM height image of NTA silane on silicon with a height scale of 10.0 nm and corresponding cross section. Surface is very rough and is not suitable for protein attachment. (Image courtesy of Dr. Jill E. Headrick)

For Montemagno's group, two main issues likely influenced the low percentage of functional spinning proteins. One was the use of nickel posts instead of nickel ions. Previous investigations[23] have shown that histidine tags have a lower affinity for nickel metal than nickel ions. A hard acids and soft bases argument also offers insight into this difference of affinity. Nickel metal is considered soft while the nickel ion is considered hard. Therefore, the nitrogen of histidine which is hard is more likely to more strongly coordinate with the hard nickel ion than the soft nickel metal. Soft atoms covalently bonds stronger to soft atoms and hard to hard. Soft atoms are more polarizable with a more diffuse electron cloud while hard atoms are the opposite, less polarizable with a tighter electron cloud. Thus, a charged metal surface improves the adhesion strength of hexahistidine coordination to nickel. Metal ions were found to be more "reliable and suitable" for protein immobilization within hybrid nanobiodevices.[23] Thus, protein molecules are less likely to coordinate to metal versus metal ions. Additionally, the attachment of nickel propellers was not specifically controlled in terms of where the propeller attached to the gamma subunit. This led to variation between molecules where some attached at the end of the propeller, some in the middle, and some other various positions. Not all propeller attachments were adequate for proper rotation. Yoshida *et al.* did not control the attachment of the filament either, as it was coated with biotin everywhere, so the filament could attach anywhere along the length which might hinder rotation. Also, with both groups, since the actin filament or propellers were so long (microns), there was a potential of drag, resulting in a slower rate of rotation. Although both groups

confirmed the unique capability of F_1-ATPase to spin, a combination of the above factors led to an inadequate number of functional molecules in both cases.

The motivation for this project, this tiny molecular motor, emerged from the idea to determine if we can utilize this motor in a practical fabricated hybrid nanobiodevice. This tiny molecular motor rotates counterclockwise when ATP is introduced into solution. Learning more about how it functions and how we can capitalize on this power in order to take advantage and harness what nature already provides, would be splendid. These studies should help to elucidate the mechanism of rotation through structure function relationships. Possible applications include motor to power micropumps or microgenerators, switching valves in nanofluidic devices, gears or levels within miniaturized analytical systems, controllable transporters, drug delivery system, cargo transport, nanostructuring or sorting protein assemblies, adaptive and self-healing materials, rotorooter, and more.[24-26] One application already in development is a polymer vesicle which contains the whole F_oF_1-ATPase complex and converts light to fuel for devices.[27] Despite somewhat extensive work into studying this protein motor, information is still lacking about structure-function relationships and how the motor spins. Some controversy exists about the mechanism of the rotation in ATPase. The role of the substeps is undefined. The nature of the possible contact sites of the gamma subunit within the alpha-beta barrel and potential conformational change is unclear. Additionally, there are some problems with placing this motor protein in a precise location within a device and with maintaining function of the motor after immobilization to the surface.

Thus, the goal of this portion of the dissertation is to improve upon the number of functional motors within a nanobiodevice by controlling the landing site chemistry and roughness, in hopes of increasing the number of functional protein molecules and controlling the background matrix to prevent, or minimize nonspecific adsorption. To determine the functionality within the device, nanoelectrodes will be constructed around the protein to monitor the current produced when ATP is added and a magnetic bead spins over the nanoelectrodes as the gamma subunit rotates. The proposed nanobiodevice is depicted in Figure 4.6. The focus of this work is the immobilization of the motor, but other work in the group is on investigation of wire fabrication. This hybrid nanobiodevice top down view shows immobilized F_1-ATPase motor in the center on a landing spot with the gamma subunit protruding (away from the surface) from the middle of the alpha-beta barrel. Attached to the gamma subunit is an armature with a magnetic bead on the end. Below the magnetic bead are u-shaped nanoelectrodes connected to microelectrodes. As ATP is added to the system, the gamma subunit should rotate, causing the magnetic bead to spin over the nanoelectrodes. As the bead spins, a current will be measured through the microelectrodes connected to the nanoelectrodes. Components other than a magnetic bead may be attached to the armature and alter the functionality of the device, such as a capsule that contains drugs, a fluorescent tag to monitor motion, or others. This structure would also be useful in driving the synthesis of ATP on demand by applying voltages across the electrodes sequentially. Development of this device should help us to determine the mechanism of rotation through structure function relationships.

Goals of the current work included determination and control over the orientation of ATPase at the surface, as well as control of the spatial locations of incorporation of the protein within the device. Immobilization of ATPase on the surface at desired location, in the desired concentration, with the correct orientation, while maintaining adequate functionality should drastically improve success in device fabrication.

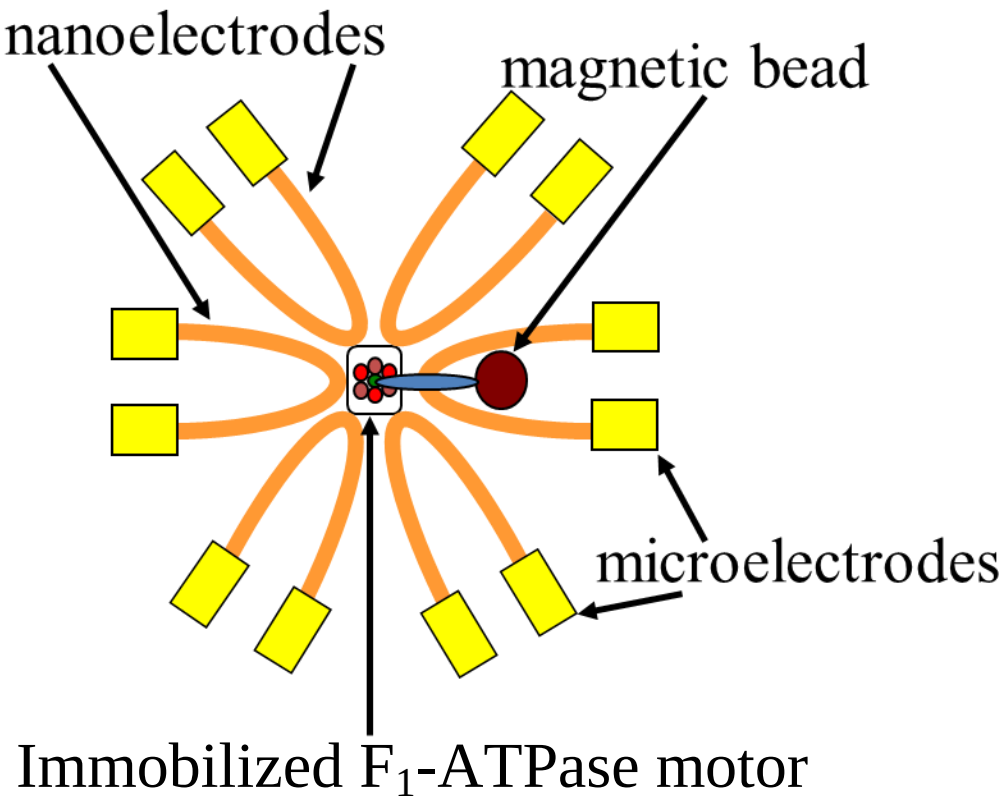

Figure 4.6: Proposed Hybrid Nanobiodevice.

4.2. Experimental

An AFM Multimode NanoScope® IIIa produced by Digital Instruments (now Bruker) in contact mode, friction mode, and tapping mode was utilized for these studies. A NanoScope® J (large scale) scanner was also utilized for larger micron grafting experiments while an "E" scanner (with a ~10 micron range) was used for the protein orientation investigations. Cantilevers used include Bruker NP-S10; Non-conductive silicon nitride; 4 v-shaped cantilevers/tips with following sets of force constants and resonant frequencies: 0.350 N/m and 50-80 kHz; 0.12 N/m with 16-28 kHz; 0.24 N/m with 40-75 kHz; and 0.06 N/m with 12-24 kHz. For surface engineering studies (patterning of SAM films), μmasch CSC37 / AIBS 3 rectangular cantilevers: 0.65 N/m with 41 kHz, 0.3 N/m with 21 kHz, and 0.35 N/m with 28 kHz were utilized. For patterning and tapping mode imaging, μmasch NSC35 with Si_3N_4 coating and an aluminum backside coating with 3 rectangular cantilevers: 7.5 N/m with 210 kHz, 14 N/m with 315 kHz, and 4.5 N/m with 150 kHz were utilized. In fluid, the tapping mode frequency used was much lower (5-20 kHz).

Substrates included Platypus gold, house gold on mica, house template-stripped gold, and house flame-annealed gold (see chapter 2 section 2.4.1 and subsections thereof for descriptions). Rinse solutions included chloroform, acetone, and ethanol. Drying involved nitrogen gas. A Rudolph Research (now Entrepix) AutoEL ellipsometer for substrate optical properties and monolayer thickness determination and a Ramé-hart, Inc. NRL C.A. goniometer (Model 100-00) for static contact angle measurements with three droplets of water (six measurements) for each

surface were utilized for SAM characterization. After measuring contact angles, the surfaces were rinsed with chloroform, acetone, and ethanol and dried with nitrogen gas.

SAM formation and modifications (see chapter 2 section 2.2.2 and 2.2.4) utilized ethanol, thiols (1-dodecanethiol, 1-octadecanethiol, 1,6-hexanedithiol, and 1,11-undecanedithiol from Sigma-Aldrich), or neat 1-dodecene, and Tris-HCl pH 8 buffer. Note, dithiol SAMs utilized higher concentrations of dithiols (~25mM) to crowd the surface with thiols to encourage upright binding of one thiol over adsorption of both thiols to the surface. Maleimide nitrilotriacetic acid (M-NTA) or [N-(5-(3-maleimidopropylamido)-1-carboxy-pentyl)iminodiacetic acid, disodium salt, monohydrate] was obtained from Dojinodo Molecular Technologies, Inc. Nickel (II) ion solution was prepared from nickel chloride from Mallinckrodt and buffer. Protein (F_1-ATPase) and modified versions were obtained from collaborators in the Richter lab (Molecular Biosciences, KU). Tris-HCl, pH 8 buffer was utilized for AFM studies. Two millimolar adenosine triphosphate and one millimolar ethylenediaminetetraacetic acid (EDTA) (Sigma) were added to protein buffer solution for protein stabilization. Concentration of proteins was determined using UV-VIS spectroscopy by the Richter lab. SDS PAGE gels were performed by the Richter lab to verify that all three components (alpha, beta, and gamma) of the enzyme were present.

For control studies of histidine binding to nickel ion-NTA surfaces and corresponding kinetic information, a BiaCore (now GE Healthcare) 3000 SPR

(courtesy of KU CORE facilities), and BiaCore NTA chips were utilized. HEPES buffer, pH 7.4 (0.01 M HEPES, 0.15 M NaCl, 50 μM EDTA, 0.005% Surfactant p20) was used as a running buffer. A 500 μM nickel chloride (Mallinckrodt) in HEPES buffer solution was used as a source for nickel ions. A 500 millimolar imidazole (Sigma-Aldrich) in water, regeneration solution (prepared in the same way as HEPES buffer, except with 0.35 M EDTA and pH 8.3), and 0.5% sodium dodecyl sulfate from Sigma-Aldrich were utilized in SPR studies as solutions to regenerate the NTA chip. SPR studies were performed at a flow rate of 20 μL per min based on previous literature and testing for mass transport limitations. A series of protein dilutions were prepared via the SPR. Injections were performed on a reference cell and sample cell as follows. Injections of 20 μL regeneration solution and 20 μL HEPES buffer on both cells were performed to clean the surface. A 60 μL nickel chloride solution was injected on the sample cell only, followed by a needle wash, a 250 μL buffer transfer, and a 20 μL buffer injection. A reference flow cell (without nickel chloride solution) was used in addition to the sample flow cell. Then on both flow cells, a 100 μL protein kinjection with 300 second dissociation was made. This was followed by a 20 μL buffer injection, 40 μL imidazole injection, 60 μL regeneration solution injection, and 100 μL SDS injection (at 100 μL/min flow) to regenerate the flow cells. An extraclean step was performed after all injections to help reduce carryover. This was required to eliminate cross contamination of subsequent injections.

Fluorescence studies for confirmation that the grafted thiol terminal group was available for additional chemistry utilized a Zeiss Axioplan 2 upright epifluorescence

microscope with Slide Book 5.0 and 1344 x 1024 Ocra ER CCD camera and 1.3 MP spot color camera (courtesy of KU MAI facilities).

4.3. Results and Discussion

This section provides details on the results and analysis. Specifically, section 4.3.1 will describe nonspecific adsorption studies of F_1-ATPase to mica surfaces via AFM. Section 4.3.2 includes SPR studies of specific immobilization chemistry and kinetics of binding to NTA chips. Section 4.3.3 describes the creation of a landing pad and details of fabrication of these nanoscale patterns and confirmation of protein binding on structure via AFM as well as provides evidence for successful immobilization of protein within pattern. Section 4.3.4 provides additional control studies for successful patterning steps via fluorescence. Together, these results demonstrate the controlled immobilization of the F_1-ATPase for use in future device applications. This has been a long standing problem in working with protein motors of this type.

4.3.1. Nonspecific Adsorption Studies ATPase/ATPase-His

In order to view things on a molecular scale such as imaging proteins and molecules on the surface, a technique such as AFM that is capable of resolution on that length-scale is needed. Nonspecific adsorption of ATPase to mica was studied both dry and in fluid via AFM in tapping mode. The ATPase utilized in these studies was only a portion of the F_1-ATPase ($\alpha_3\beta_3\gamma$). This should result in the protein with hexameric ring with the gamma subunit in the center, protruding from the ring. Nonspecific adsorption studies were performed in order to gain an understanding of

the interactions of ATPase with the surrounding SAM matrix and to determine whether the resolution required to image protein orientation would be achievable. This had not been previously demonstrated on this system, so was a critical prerequisite for the subsequent investigations. Nonspecific adsorption relies on physisorption rather than on chemisorption and is generally considered to involve weaker binding interactions. This means that properties such as hydrophobicity, van der Waals forces, and ionic interactions or electrostatic forces will be prevalent modes of binding as opposed to covalent bonding. These tests were performed under two different sets of conditions, dry and in fluid. Image resolution is typically better dry, but fluid imaging allows mimicking of pseudo-physiological conditions (typical protein conditions and environments).

4.3.1.1. Mica

Mica, a hydrophilic, atomically flat surface (Figure 4.7) was utilized for initial nonspecific ATPase adsorption studies. Ruby muscovite mica has some terminal hydroxyl groups and was negatively charged under the conditions of these experiments. Mica was prepared for use in studies by cleavage with tape. Cleavage resulted in a freshly exposed clean surface to which protein molecules were adsorbed.

4.3.1.1.1. Dry

The method for dry immobilization started with incubation of the mica surface in buffer solution (Tris-HCl, pH 8 with 1 mM EDTA and 1 mM ATP) for about ten minutes to equilibrate the surface to buffer conditions and then a one microgram per milliliter solution of protein was added to the surface and allowed to adsorb. After

about 15-20 minutes, the surface was rinsed with buffer and water and dried with nitrogen gas. The sample was then imaged via tapping mode AFM.

While this experimental design is relatively simple, conditions of experiment critical. Protein concentration must be low enough to image individual protein molecules; too high a concentration gives protein monolayers in which individual proteins are indistinguishable, while too low a concentration gives rise to time spent searching for immobilized proteins. After protein incubation, rinsing with buffer and then thorough rinsing with water is vital to ensure removal of salts. If salt is not removed, salt crystals will form upon drying, interfering with protein imaging (big clumps of crystals can obscure the much smaller protein molecules).

Once suitable imaging conditions are met, images can be analyzed. Mica is atomically flat, with an RMS roughness of about 0.072 nanometers over a 5.00 by 5.00 micrometers image. This provides a very uniform surface with very little contrast in AFM images (Figure 4.7).

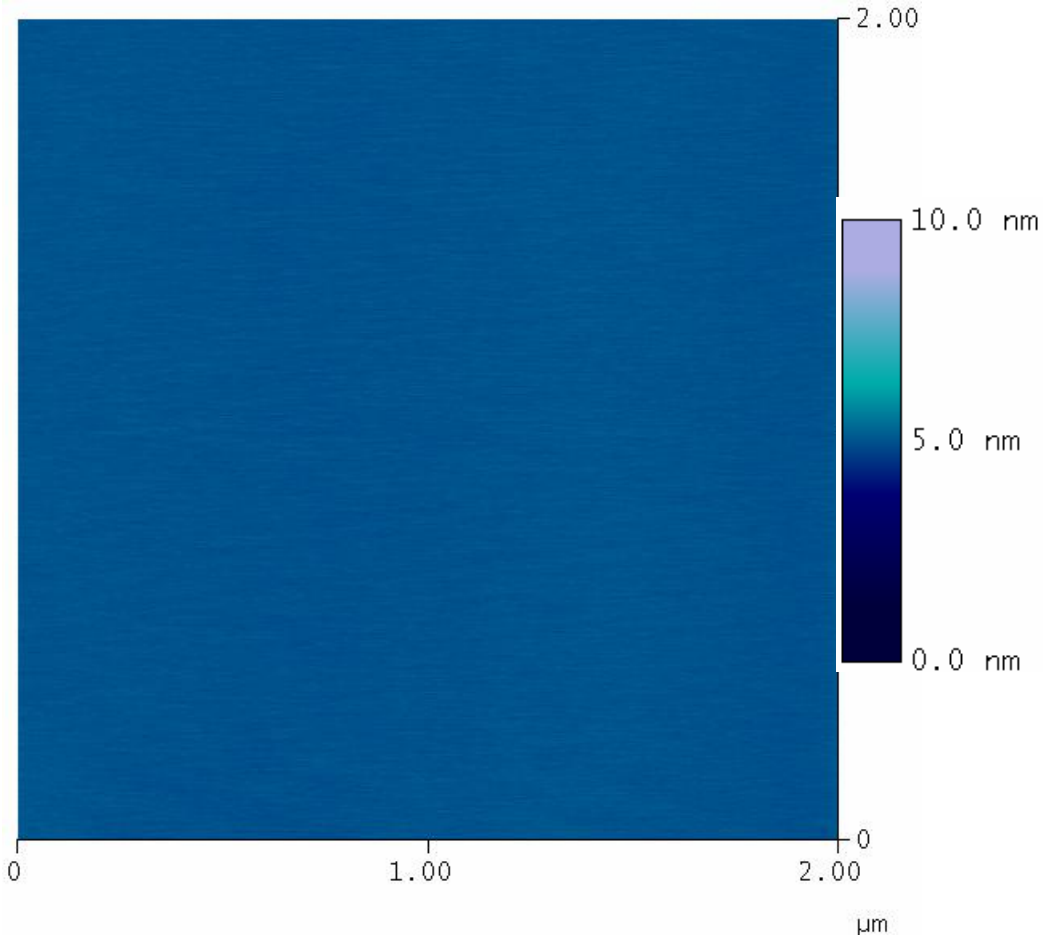

Figure 4.7: AFM height image of atomically flat mucosiva mica, 2.00 µm x 2.00 µm scan area with a 10.0 nm height scale.

After a clean mica surface was confirmed by imaging, the protein was adsorbed to the surface as discussed previously. Spots showed up due to protein adsorbed to surface. A 325 nanometer by 325 nanometer image of ATPase adsorbed to mica was analyzed (Figure 4.8). Protein molecules adsorbed on the surface are higher than the surface and thus are the brighter spots on the image. Zooming in on individual molecules and obtaining cross sections through proteins within this image showed a somewhat surprising result. Not just one, but three main orientations of F_1-ATPase were observed as indicated in Figure 4.8. One type cross section observed of the protein had a dip or depression in the center of the protein (darker color), indicative of either the gamma subunit missing or the protein adsorbed to the mica upside down. Another observed type of cross section of a protein was just rounded, thought to be of the protein molecule adsorbed on its side. (Another alternative would be that the resolution was too low to distinguish the central gamma subunit – however since some molecules were observed within the same image this theory was dismissed). And finally, one type of protein cross section observed had a protrusion from the center of the protein (brighter color), indicative of the protein adsorbed in the correct orientation with the gamma subunit pointed upright. Analysis of cross-sectionals through multiple protein molecules and corresponding three-dimensional AFM height images resulted in observation of repeated molecules for each type of orientation. Three example cross-section cuts (one for each type) highlight the various orientations (Figure 4.8). The first example was of a molecule with a protrusion (higher point) in the middle of the peak due to the gamma subunit pointed

upright (denoted Type I). The second cross-section molecule was either upside down or missing its gamma subunit. The corresponding cross-section showed a distinct depression in the center of the molecule (denoted Type II). And finally, the third cross-section was representative of a rounded molecule with a single peak for the molecule (denoted Type III).

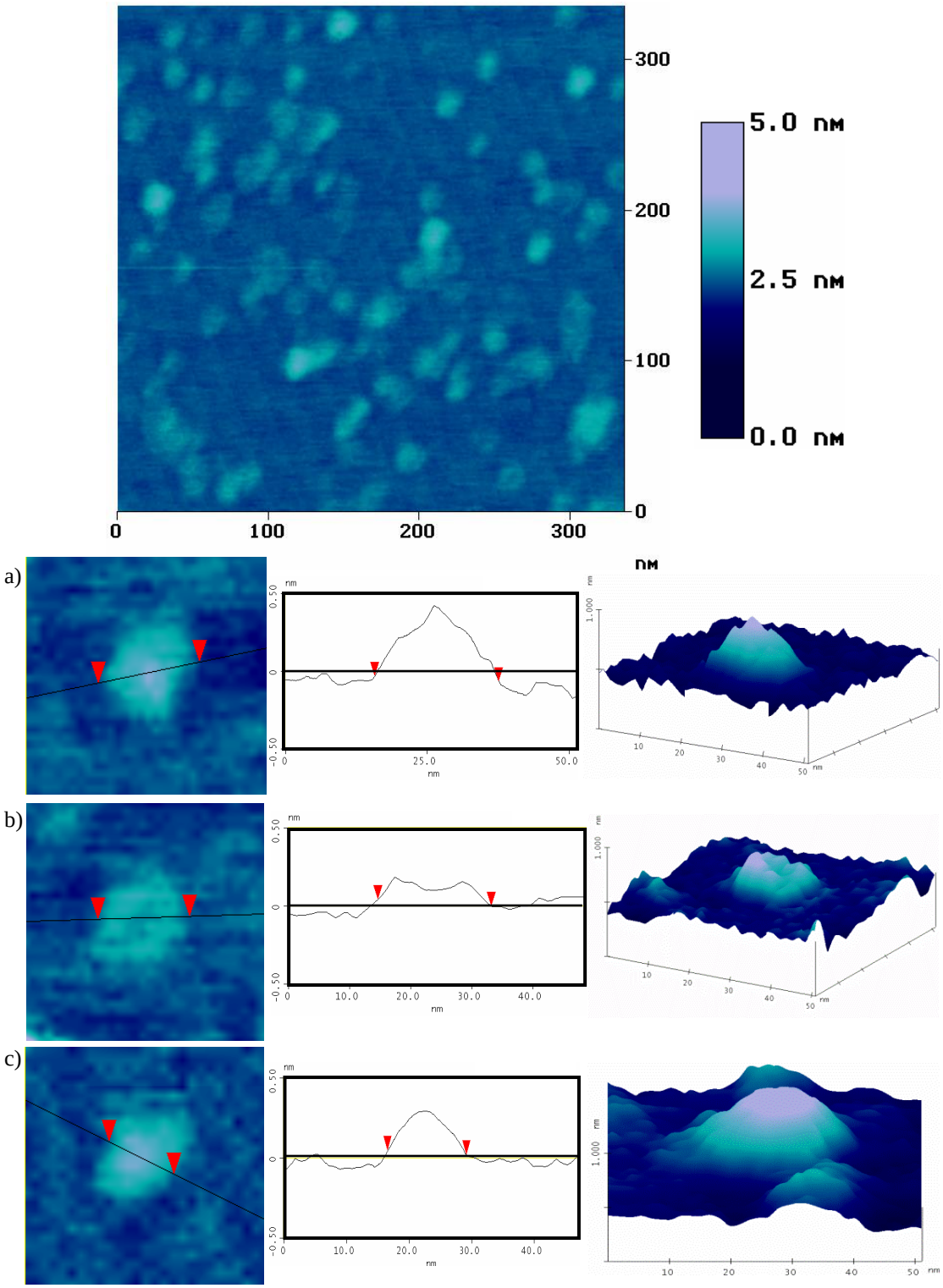

Figure 4.8: AFM height image of 2 µg/mL ATPase in Tris-HCl, pH 8 adsorbed to mucosiva mica 325 nm x 325 nm scan area with a 5.0 nm height scale with respective cross-sections through individual protein molecules with corresponding 3D images of a) Type I, b) Type II, and c) Type III.

It is likely that only the first of these orientations will lead to a functional protein on the surface, as with the other orientations the gamma subunit is missing or not free to rotate in the plane parallel to the surface. Therefore, control over the orientation of the protein is essential in enhancing the number of functional proteins within hybrid nanobiodevices. Another observation gleaned from these nonspecific adsorption studies was that the protein adsorbed all over the surface. Thus, control over placement will also be an essential component in hybrid nanobiodevice construction. This type of resolution on the F_1-ATPase motor with the rotor has not been observed before and is critical for determination of the orientation of the protein bound to the surface.

Although resolution is usually sufficient when imaging dry, one must consider how the design of the experiment might affect the results obtained for protein orientation and size. ATPase is typically in a fluid environment. When imaging dry, the protein has been exposed to the air-liquid interface. This may alter both the apparent size and the structure of the protein. The protein is no longer hydrated and may denature (spread out) upon drying. Alternatively, the protein may decrease in size upon drying due to dehydration effects.[28] Therefore, careful assessment must be made in determining the results of such studies and how they might relate to the native protein state.

4.3.1.1.2. Fluid

Fluid adsorption was performed using the AFM and fluid cell. The mica surface was initially imaged in buffer to confirm that nothing from the buffer solution would adsorb to the surface. The AFM height image of a mica surface in buffer was consistent with images of freshly cleaved mica. Then same method as in dry adsorption was followed except the protein concentration was higher (~mg/mL), imaging was performed in Tris-HCl buffer pH 8, and no rinsing with water or drying steps were performed. Liquid can be exchanged in the fluid cell without introducing exposure to air-water interface.

This maintains the environment around the protein to be pseudo-physiological. Figure 4.9 shows the results of these studies. Fluid cell studies resulted in the same variation of protein orientations (protrusion, depression, or rounded) as dry immobilization. Cross-sections, as with dry measurements, were provided for each type of orientation. For further visual clarification, a 3D AFM image was provided for each representative molecule. Additionally, Figure 4.10 provides general schematics for the various types of protein orientations observed upon nonspecific adsorption of this protein to mica.

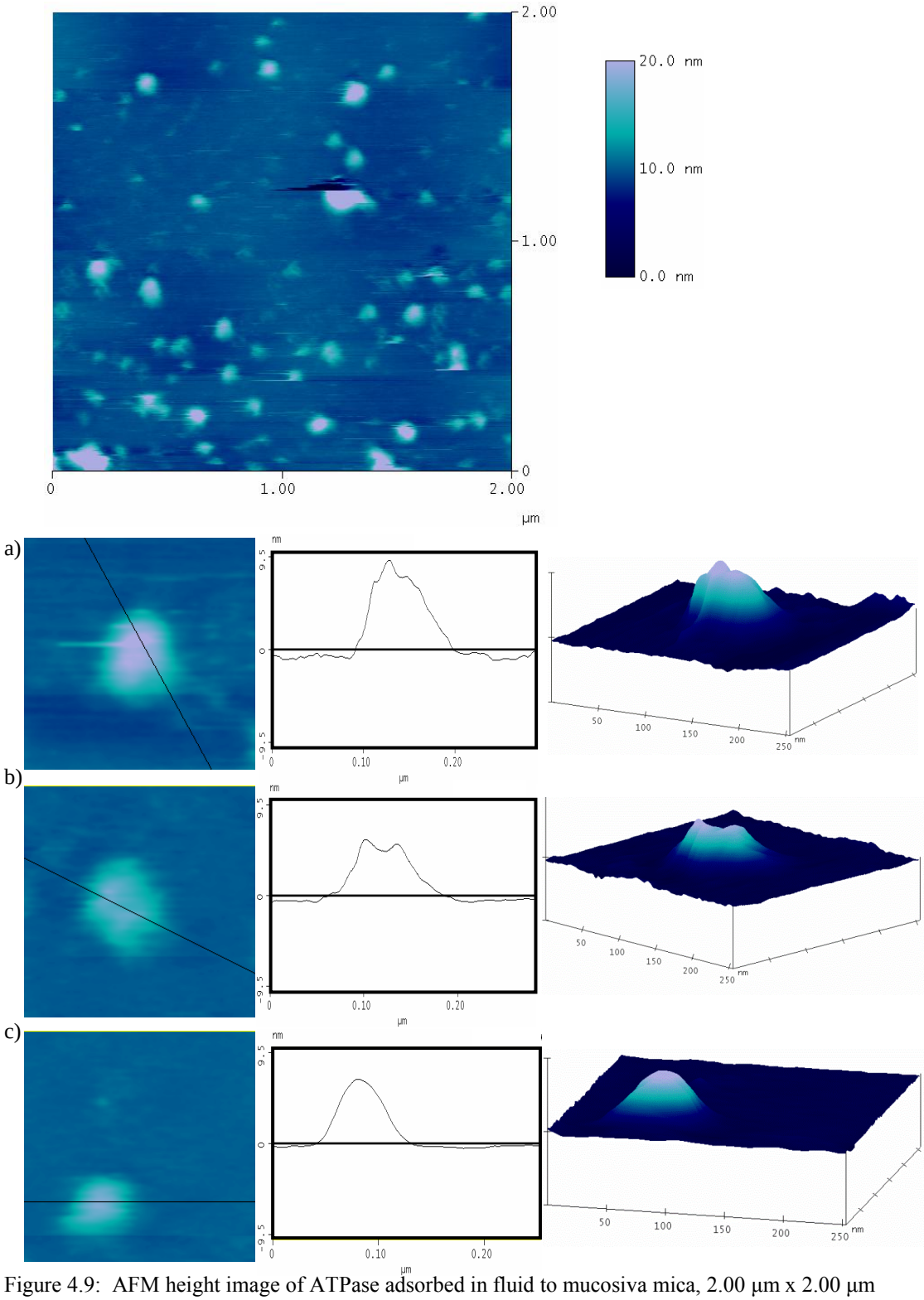

Figure 4.9: AFM height image of ATPase adsorbed in fluid to mucosiva mica, 2.00 µm x 2.00 µm scan area with 20.0 nm height scale with respective cross-sections through individual protein molecules with corresponding 3D images of a) Type I, b) Type II, and c) Type III.

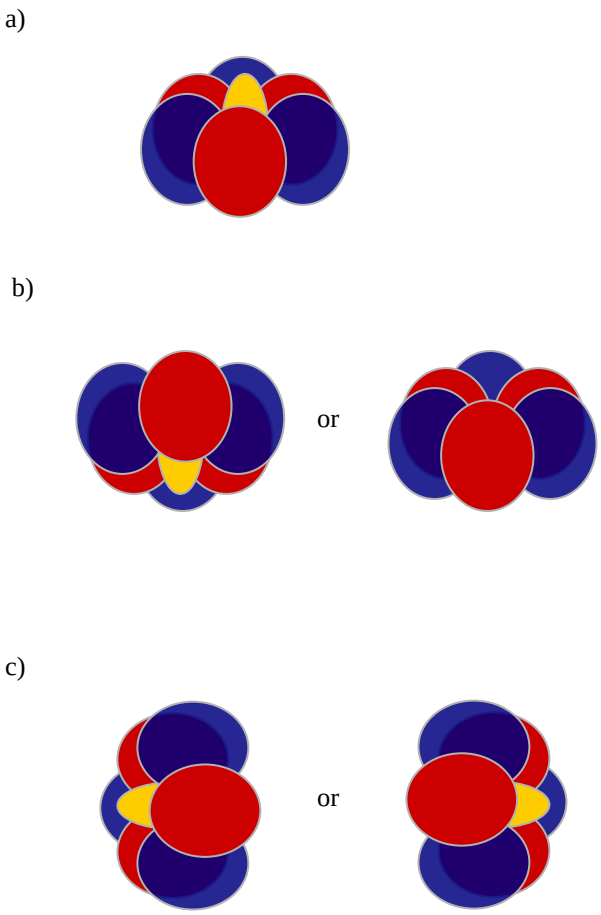

Figure 4.10: Schematics of three typical orientations of F1-ATPase adsorbed nonspecifically to mica. a) Type 1 (Protrusion), b) Type II (Depression), and c) Type III (Rounded).

However, the size and resolution of the protein molecules were different between dry and fluid experiments. The protein molecules immobilized in fluid were larger and more sporadic while proteins immobilization followed by drying were smaller and covered more surface area by comparison (Table 4.1). The differences in the size of the protein may be due to different conditions, different tip-sample interactions, and the protein may be deformed differently under dry conditions in contrast to fluid conditions. Figure 4.11 provides a schematic of the protein dimensions measured. The height of the ATPase for the hexameric alpha-beta barrel, the width of ATPase at half height, and the feature height (or depression), as represented by the white arrow were measured.

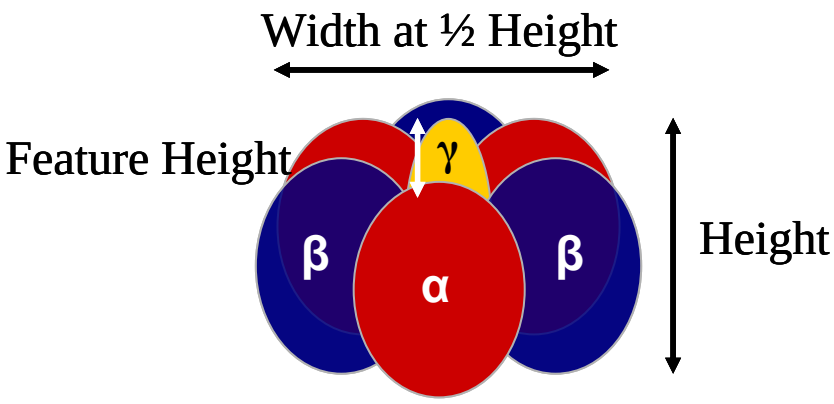

Figure 4.11: Schematic of F_1-ATPase and measured components of protein height, width at half height and feature height (or depression).

Table 4.1: F_1-ATPase dimensions determined from tapping mode AFM images from dry and fluid imaging on mica substrate.

Imaging Conditions	*Type*	*Protein Height (nm)*	*Width at ½ Height (nm)*	*Feature Height (nm)*
Dry	I (Protrusion) n = 7	0.7 ± 0.1	12 ± 2	0.13 ± 0.05
	II (Depression) n = 7	0.27 ± 0.02	16 ± 2	- 0.08 ± 0.02
	III (Rounded) n = 7	0.7 ± 0.1	14.7 ± 0.8	n/a
Fluid	I (Protrusion) n=7	10 ± 4	69 ± 13	1.9 ± 0.7
	II (Depression) n = 7	8.5 ± 0.3	70 ± 11	- 1.0 ± 0.2
	III (Rounded) n = 7	7 ± 2	55 ± 7	n/a

The height, width at half height, and feature height values measured for proteins adsorbed and dried were lower than those adsorbed and imaged in fluid for all three types of orientations. This phenomenon of smaller features in dry imaging versus fluid imaging has been observed previously.[28] For example, the values for height measurements of the protrusion orientation proteins were smaller when imaged dry (at 0.7 nanometers) versus when imaged in fluid (at 10.1 nanometers). The fluid values for height of about 10 nanometers were close to the expected value of about 8 nanometers from crystal structure data; dry measurements were low comparatively.[6] The width at half height of the hexameric barrel measured in fluid was much larger at 50-70 nanometers compared to the expected value of 10 nanometers from crystal structure data; dry measurements were slightly above expected values.[6] This can be explained by the tip broadening effect. If the cone angle of the tip is large relative to the size of the protein molecule, then in addition to the apex interactions with the

sample there are cone-sample interactions, causing the protein to appear wider than the true width. The feature height for the protrusion or gamma subunit over the hexameric barrel was about two nanometers in fluid was about double the expected value of 1 nanometer obtained from crystal structure data; dry measurements of about 0.1 nanometers were less than expected values (probably due an increased amount of force from the tip to the sample when imaging dry).[6]

Nonspecific adsorption results in a variety of orientation, only one of which is desired (protrusion of gamma subunit). Also, protein was observed all over the surface. Therefore, both a landing pad and control over immobilization are critical for incorporation of this protein motor within a hybrid nanobiodevice. Thus, in order to have better odds of a functional device, it is necessary to control the orientation of the molecule at the surface.

4.3.2. Specific Adsorption Studies of ATPase-His

Since nonspecific adsorption studies of ATPase to surfaces yielded various orientations, only one of which was desired, control over ATPase adsorption was necessary to enhance this probability. To achieve this, a specific adsorption scheme is utilized. For further discussion of specific adsorption methods, see Chapter 1 section 3. Briefly, specific adsorption involves utilizing a characteristic (anchoring) group within the molecule to adsorb it onto a surface via specific chemistry and perhaps even at a precise location. Examples of specific adsorption methods include amine coupling, streptavidin-biotin coupling, and others as discussed in chapter one.

Another form of specific attachment chemistry involves histidine tags. This idea stems from immobilized metal affinity chromatography, a typical method of protein purification. Basically, a series of histidines (in this case, a sequence of six separate histidines) are incorporated into the sequence of the protein to form a His-tag. This histidine tag can then coordinate with a nickel ion (cobalt, zinc, copper ions have also been used). This nickel ion is also coordinated to the carboxylic acids in a nitrilotriacetic acid (NTA) group. By having a column functionalized with this chemistry, those proteins with a histidine tag should bind strongly to the nickel ion and the other proteins should flow through the column, thus purifying the protein of interest. One of the great assets of this technique is that then mild elution conditions (imidazole) can be utilized to elute the protein of interest. By incorporating these histidine tags (His_6 tags) into the N-terminus of the three noncatalytic alpha helices of the alpha-beta barrel, the ATPase can be specifically attached to the surface via this functionality without adversely affecting proteins. There are three alpha subunits; therefore each ATPase molecule will have three sets of hexahistidine tags. Additionally, placement of these his-tags on the cytoplasmic side of the barrel resulted in the gamma unit protruding from the opposite end as in the desired orientation and configuration.

To incorporate this scheme into a nanobiodevice, a surface nanoengineering scheme has been developed. First gold surfaces were formed. Then a resist monolayer was formed. This monolayer was either a methyl terminated SAM or a PEG SAM. The purpose of the resist was to have a surface where little to no protein

adsorbs nonspecifically. A methyl-terminated SAM was shown to be a decent resist (See section 4.3.3.1.1, Selective Adsorption on Hydrophilic Nanopatterns) as the hydrophobic methyl surface has little nonspecific adsorption under the conditions utilized. As discussed in chapter 1, for initial *in vitro* studies, PEG may also be used a protein resist matrix.

This general schematic for the surface patterning is outlined as follows (Figure 4.12). Grafting conditions were confirmed by grafting in a longer chain thiol in this case, an octadecanethiol pattern. Dithiols (1,6-hexanedithiol and/or 1,11-undecanedithiol) were then grafted into the resist matrix. Maleimide-NTA solution was added to the system to allow the maleimide functional group to covalently bind to the exposed thiol functional group. This reaction is highly chemoselective and forms a covalent thioether bond between the thiol and maleimide group upon selective addition into the double bond.[29] A nickel-chloride solution was added to the system. This allowed the nickel ions to coordinate to the carboxylic acids in the NTA portion of the surface. Finally, histidine tagged F_1-ATPase was added to the system and allowed to bind. His-tags coordinated to the nickel ions, aligning the ATPase both spatially and in the correct orientation. The protein orientation was imaged. The gamma subunit should then be exposed at the surface and should be functional. Functionality tests will be performed by our collaborators.

Before embarking upon the specific attachment studies via AFM, confirmation that this specific attachment worked as expected was demonstrated via SPR. These SPR experiments allowed the kinetics of binding to be evaluated.

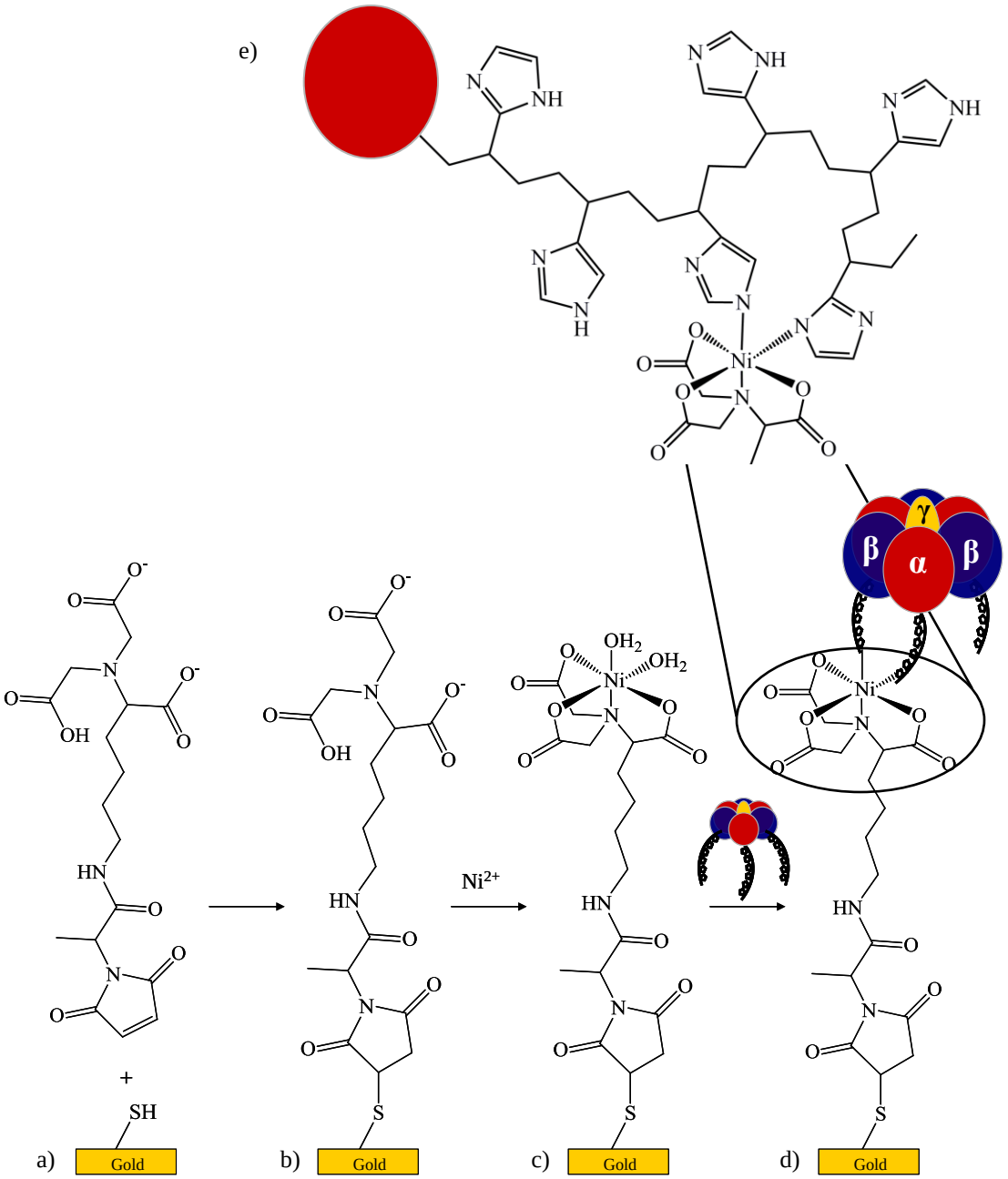

Figure 4.12: Schematic of specific chemistry utilized to adsorb ATPase-His to surfaces. a) Step one is to form a 1,6-hexanedithiol or 1,11-undecanedithiol SAM (full surface coverage or patterned area) on gold. b) Addition of maleimide-NTA and coordination to the terminal thiol. c) Addition of nickel ions which coordinate to the NTA groups. d) Finally, histidine-tagged ATPase is added and the histidine tags coordinate to the nickel ions, selectively immobilizing ATPase-His. e) Insert of zoomed view of histidines coordinating to nickel ions and NTA showing only one histidine tag on an alpha subunit for clarity.

4.3.2.1. Surface Plasmon Resonance

Goals for SPR studies included verification that the last two steps (nickel ion and histidine-tag coordination) of the specific chemistry schematic (Figure 4.12) work and determination of the robustness of the F_1-ATPase-histidine-nickel ion-NTA coordination. Additionally, these studies allowed for investigation of the kinetics of binding and the adsorption and desorption rates. Ideally, a small K_D was desired such that large k_{on} and a small k_{off} were obtained. This would mean that a lot of the protein adsorbs to the surface and only a small amount of adsorbed protein is easily removed. SPR can be used to indirectly check the orientation of the protein in future studies. Additionally, this technique allows for the determination of interaction specificity with hopefully only a little nonspecific adsorption occurring, another key goal of these studies. Also, new information was determined about kinetics of binding (multiple rate constants required).

4.3.2.1.1. Substrates (BiaCore NTA chip)

SPR was used to check the chemistry of the coordination of nickel ions to the carboxylic acid groups of NTA, and then coordination of histidines in F_1-ATPase-Histidine tag to those immobilized nickel ions. A modification of the protocol for NTA chips from GE Healthcare was utilized for this experimental portion.[30] First, a BiaCore NTA chip was docked into the SPR. This gold chip has a carboxymethylated dextran matrix with some NTA groups incorporated on the surface. Using a HEPES running buffer, nickel chloride was injected over the surface. An initial change in the response indicates a difference in refractive indices

between the nickel chloride solution and the buffer. If after the injection a positive response unit was observed compared to initial baseline response, then nickel ions have coordinated to the NTA groups on the surface (Figure 4.13). After this step, the histidine-tagged ATPase was injected. As the protein was injected, the SPR response increased, again partially due to a change in refractive index to the surface. As more protein was introduced to the surface, the initial curve increases as protein adsorbed and desorbed from solution. After switching back to buffer, some of the protein desorbed, as indicated by the decreasing response. A comparison between the baseline before protein injection and after returning to buffer and allowing stabilization provides an idea of how much protein remains bound to the surface. The magnitude of this response is indicative of the amount of protein bound to the surface; the higher the response, the more protein that was bound to the surface. The shape of the curve indicated the kinetics of the reaction; injections of varying protein concentrations allowed a fit to a kinetic model. Additionally, a reference cell was run in parallel and used to determine nonspecific binding and to eliminate the difference in refractive index between the buffer and the sample. The surface was completely regenerated by a series of washes (all the F_1-ATPase-his was removed, unlike fibrinogen), as can be seen by the return of the response to the initial baseline level. For an example sensorgram of this immobilization and regeneration process (Figure 4.14).

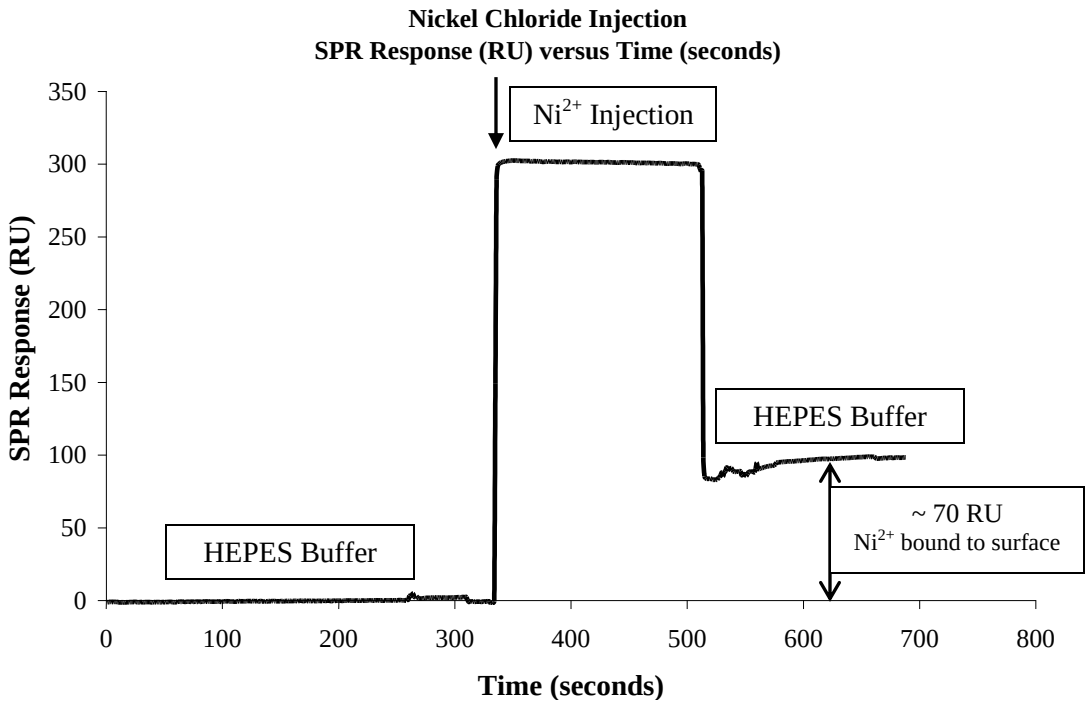

Figure 4.13: SPR sensorgram Response (RU) versus Time (s) of NTA chip with nickel chloride injection, showing nickel ions immobilized on NTA groups.

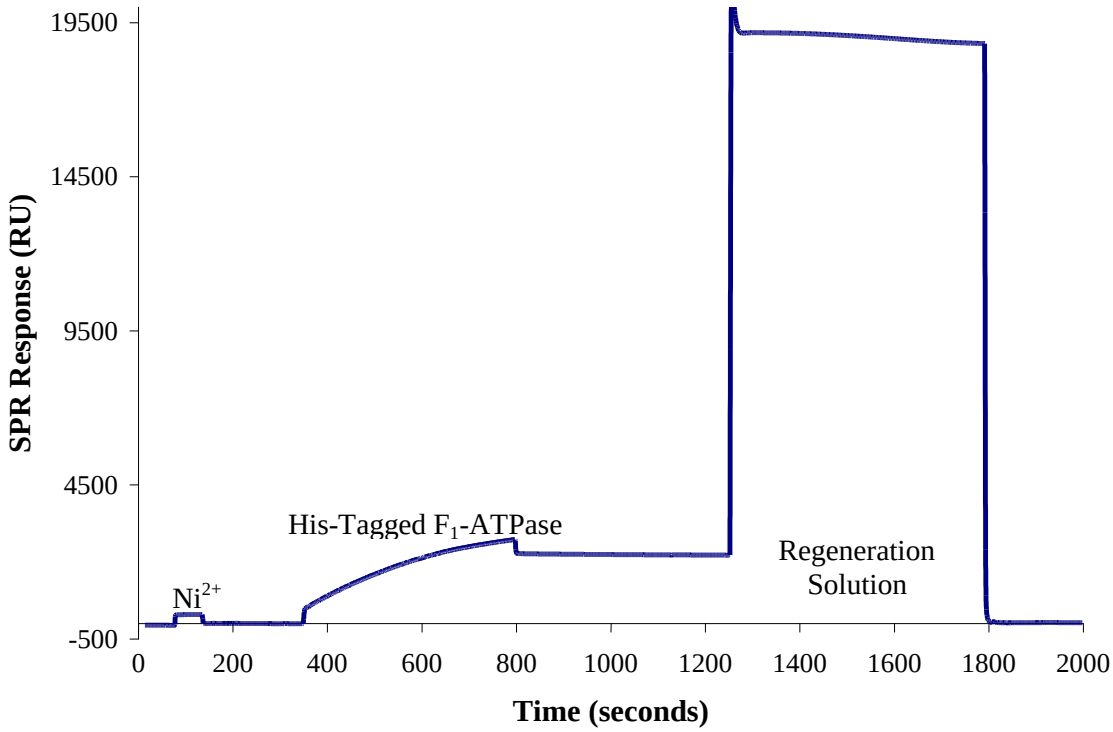

Figure 4.14: SPR sensorgram Response (RU) versus Time (s) of NTA chip with injections of nickel chloride, 125 nM F_1-ATPase-His, and regeneration solution.

A BiaCore NTA chip consists of a dextran matrix with some nitrilotriacetic acid (NTA) groups exposed. Nickel ions were tetracoordinated to carboxylic acids and nitrogen of the NTA groups, leaving two free coordination sites for fulfillment of nickel octet (Figure 4.12c). Rinsing, buffer transfer, and needle washing were crucial to remove residual nickel ions from the needle and needle surface in order to obtain an adequate reference curve. Histidine tags on the ATPase coordinated specifically to the nickel-NTA groups (Figure 4.12d-e). This interaction was concentration dependent as expected. The higher the concentration, the more protein adsorbed to the surface (Figure 4.15). A slight amount of nonspecific adsorption occurred as indicated by the reference cell. The protein remained immobilized on the surface even after changing back to buffer during dissociation and after the injection, indicative of a strong binding of the protein to the nickel-NTA surface, thus protein should remain bound to the hybrid nanobiodevice after successful immobilization. However, the chip can be regenerated through a series of washes, meaning that immobilization can be specifically interrupted when desired. Thus, after incorporation within a hybrid nanobiodevice if the protein motor(s) becomes inactive (stop rotating), protein(s) can easily be removed from the surface and replaced with fresh protein motor(s), essentially regenerating the device. This regeneration step also allows another concentration of protein to be tested as needed for kinetic studies.

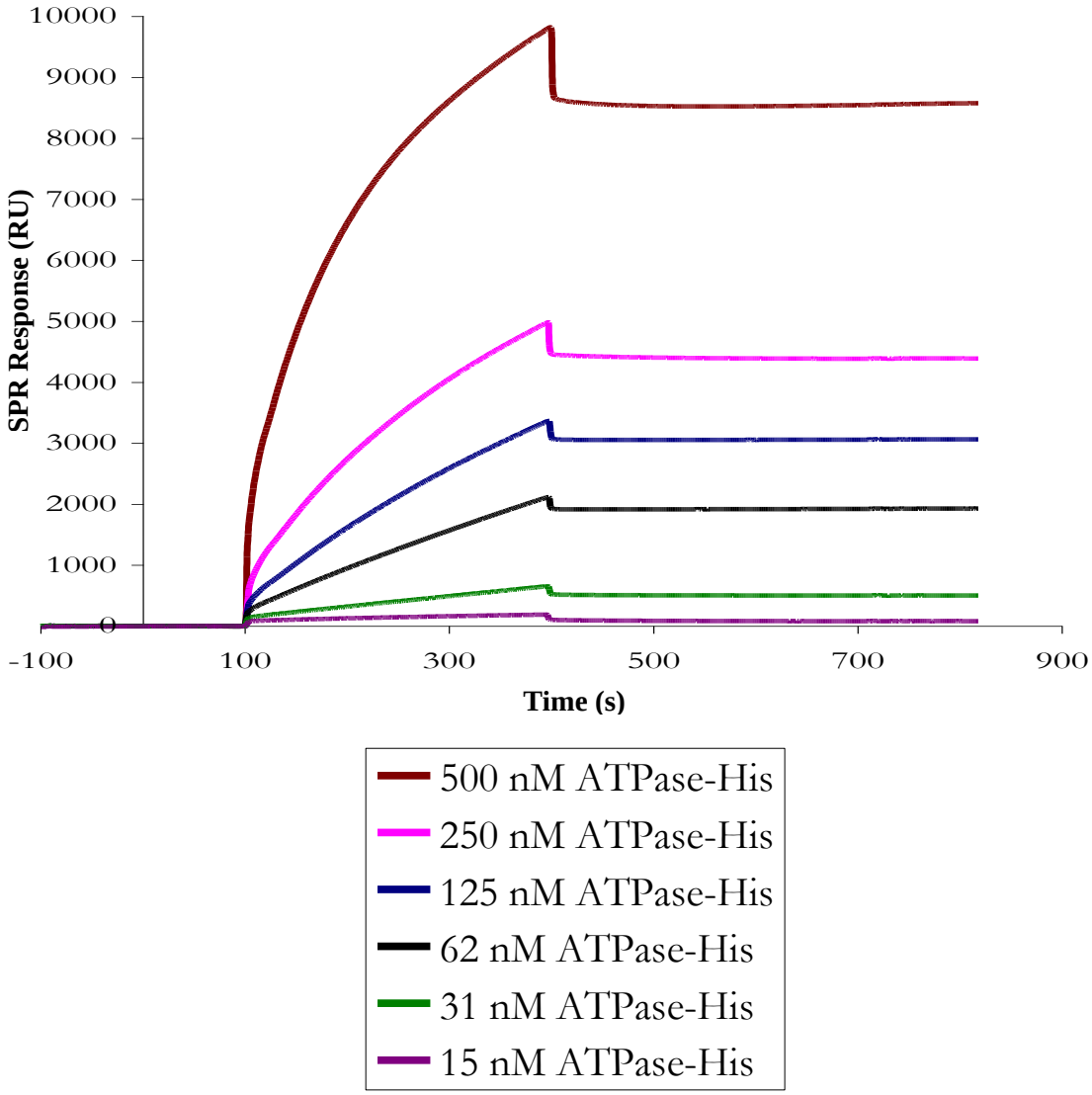

Figure 4.15: SPR sensorgram Response (RU) versus Time (s) of NTA chip with injections increasing concentrations of F_1-ATPase-His.

Before successful analysis of immobilized F_1-ATPase-His was achieved, some difficulties were overcome. The first attempt was unsuccessful because the protein sample solution was from a previously diluted sample for AFM experiments and contained additional EDTA (about one millimolar). This was enough to chelate the nickel ions on the surface, removing bound nickel ions from the surface, and disrupting histidine-protein binding to the surface by eliminating specific binding chemistry. This was overcome by using fresh undiluted protein solutions and diluting with only running buffer.

Additionally, the reference cell was exhibiting greater binding than expected (Figure 4.16). Ideally, reference cell response should increase immediately upon injection, have a constant value over the course of the injection, and return to baseline at the end of injection. Reference cells account for the change in refractive index between the sample solution and the running buffer. They can also account for nonspecific protein binding to the surface. This nonspecific binding is expected to slightly increase the response on the reference cell; instead of a flat line during the injection, a slight positive slope would be observed. Additionally, if some of this nonspecific binding is not removed upon switching back to buffer at the end of the injection, a slight increase over initial baseline would be observed. The reference cell provides more specific analysis as it allows subtraction of both the change in refractive index between buffer and sample solution as well as nonspecific protein adsorption from the sample curve. Since initial experiments did not achieve this, additional steps were performed to correct this issue. It was thought that there was

some nickel transfer onto the reference cell upon sample injection because the curve started out relatively flat as expected but then angled sharply up (unexpected) and during the dissociation phase the baseline did not drop back down to the initial starting point (which it should have done had the response been due to only a refractive index difference between the buffer and sample solution) (Figure 4.16). The curve is indicative of protein binding and little protein desorbed (similar to sample cell after initial flatness), rather than little to no protein binding, as one would expect if there were no nickel on the reference cell. This was thought to be due to contamination of the reference cell with nickel ions (from nickel ion carryover) and then subsequent protein adsorption to the activated surface; the reference cell appears similar to the sample cell. This reference cell issue was overcome by following the nickel chloride injection with a needle wash, transfer of buffer from the needle, and injection of buffer solution to eliminate nickel ion carryover (Figure 4.17). Comparison of the initial reference cell to that after additional washing steps shows that a drastic improvement had been made. Some nonspecific adsorption was still observed, but specific adsorption from nickel ion carryover was eliminated. Comparison of the sample cell response to the protein injection both without and with additional washing steps showed that less ATPase adsorption was observed on the initial sample cell response (without extra cleaning steps) than the sample cell response with extra cleaning steps (Figure 4.18). This is thought to be due to a combination of slightly more nickel ions on the sample cell with cleaning (65 RU) versus without cleaning (57 RU) and in the case of the sample cell without cleaning,

potential needle contamination with the nickel ions (leading to the protein binding nickel ions before exposure to the surface which changes the binding affinity, possibly reducing overall protein response). Comparison of the reference subtracted sample data showed a drastic improvement after the washing steps were employed (Figure 4.19). The initial reference cell subtracted sample data was not useful in determining kinetic information while the corrected reference cell subtracted sample data was. Finally, this improved method produced adequate data for reference cell and sample cell data analysis (Figure 4.20), a vast improvement over initial method data (Figure 4.16).

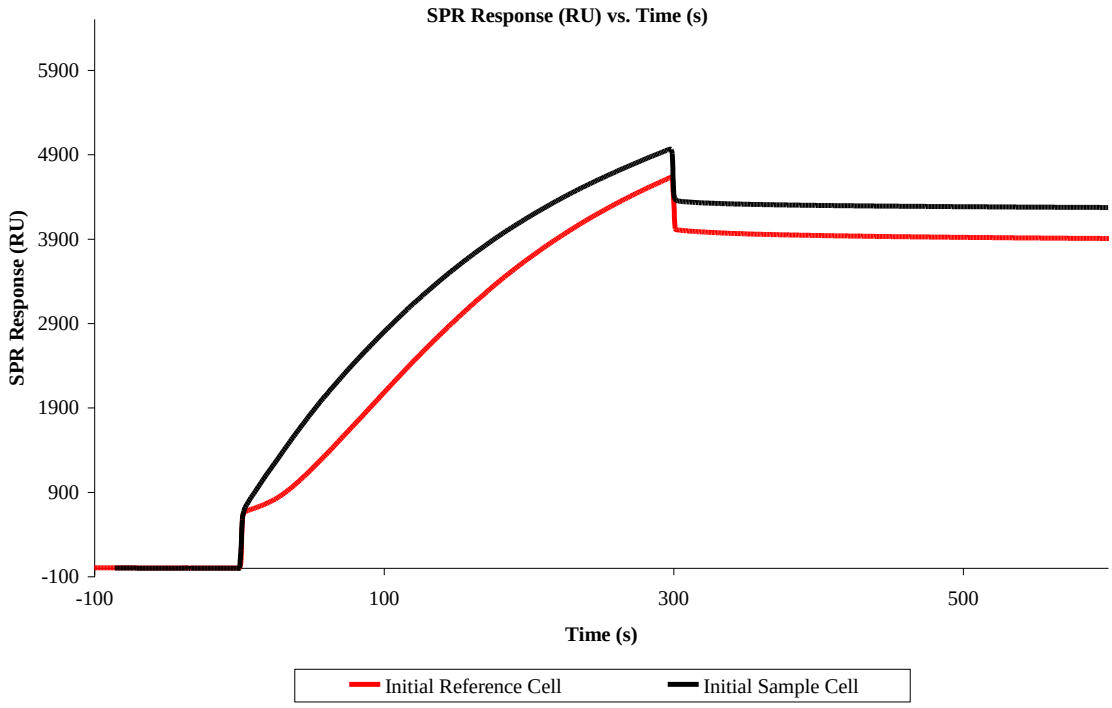

Figure 4.16: SPR sensorgrams of initial reference cell and sample cell F_1-ATPase-His injection.

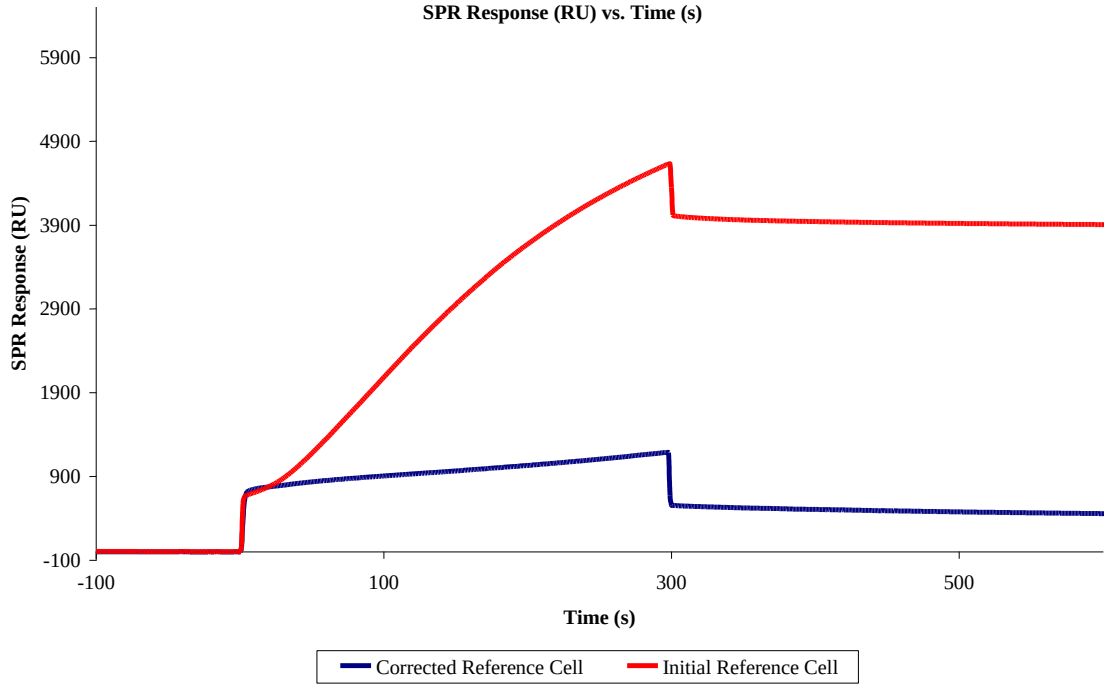

Figure 4.17: SPR sensorgrams of F_1-ATPase-His injections reference cell responses with (Corrected) and without (Initial) extra cleaning steps.

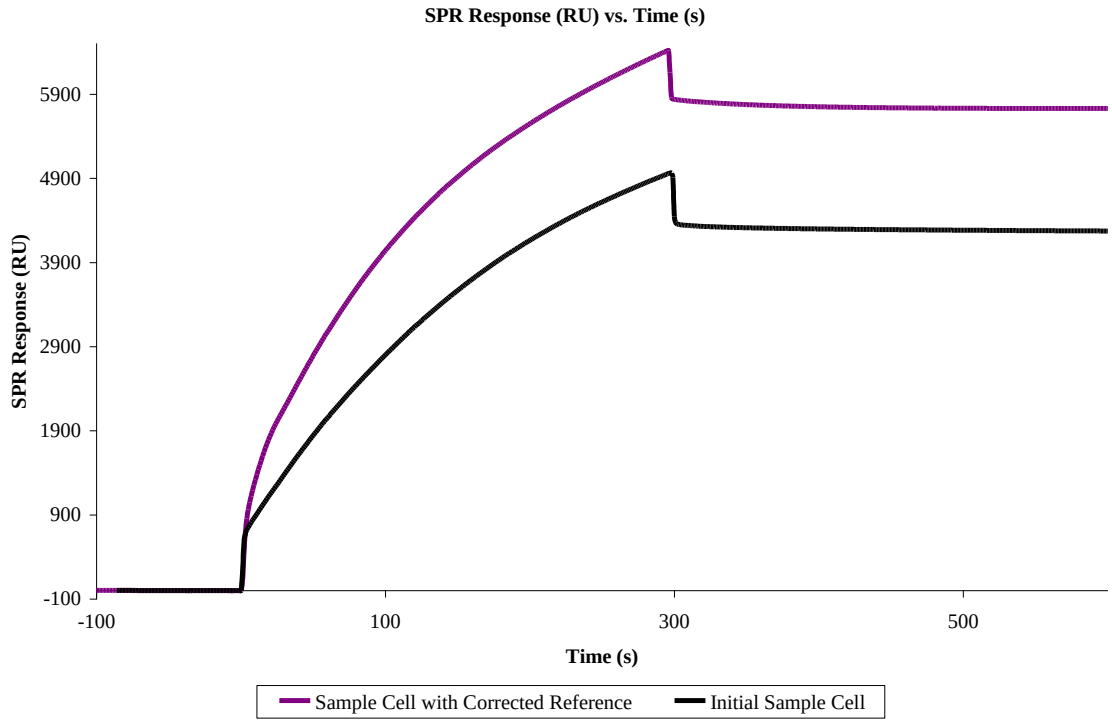

Figure 4.18: SPR sensorgrams of F_1-ATPase-His injections with sample cell response with (Corrected) and without (Initial) extra cleaning steps.

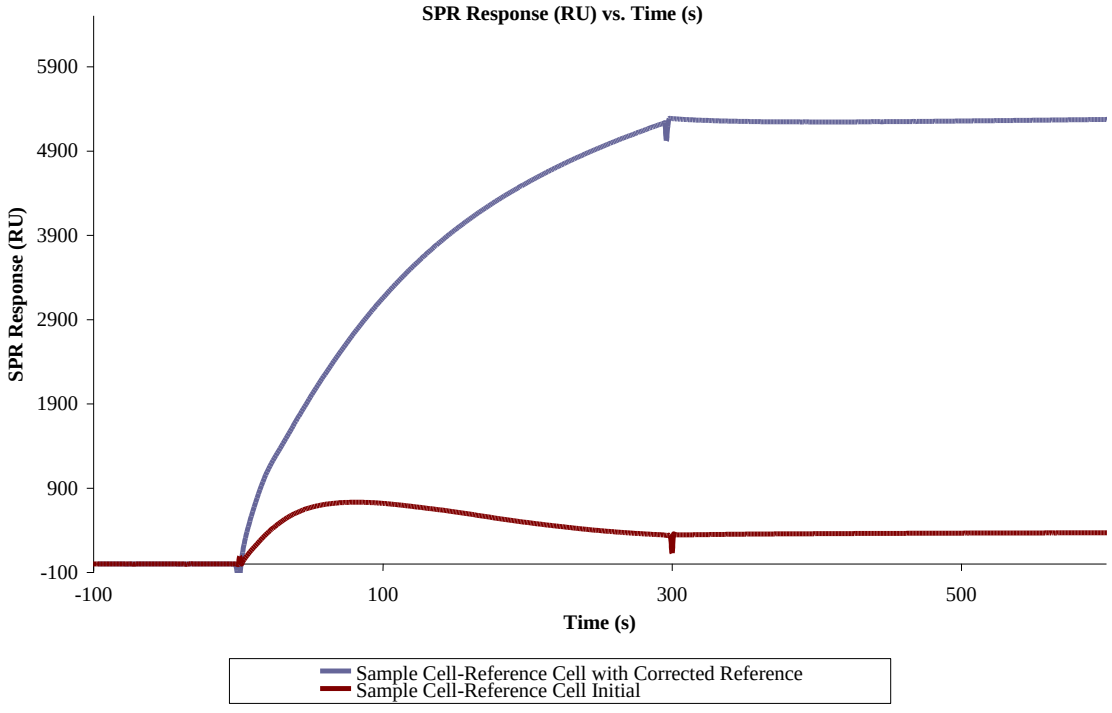

Figure 4.19: SPR sensorgrams of F_1-ATPase-His injections with difference between sample cell responses and reference cell responses with (Corrected) and without (Initial) extra cleaning steps.

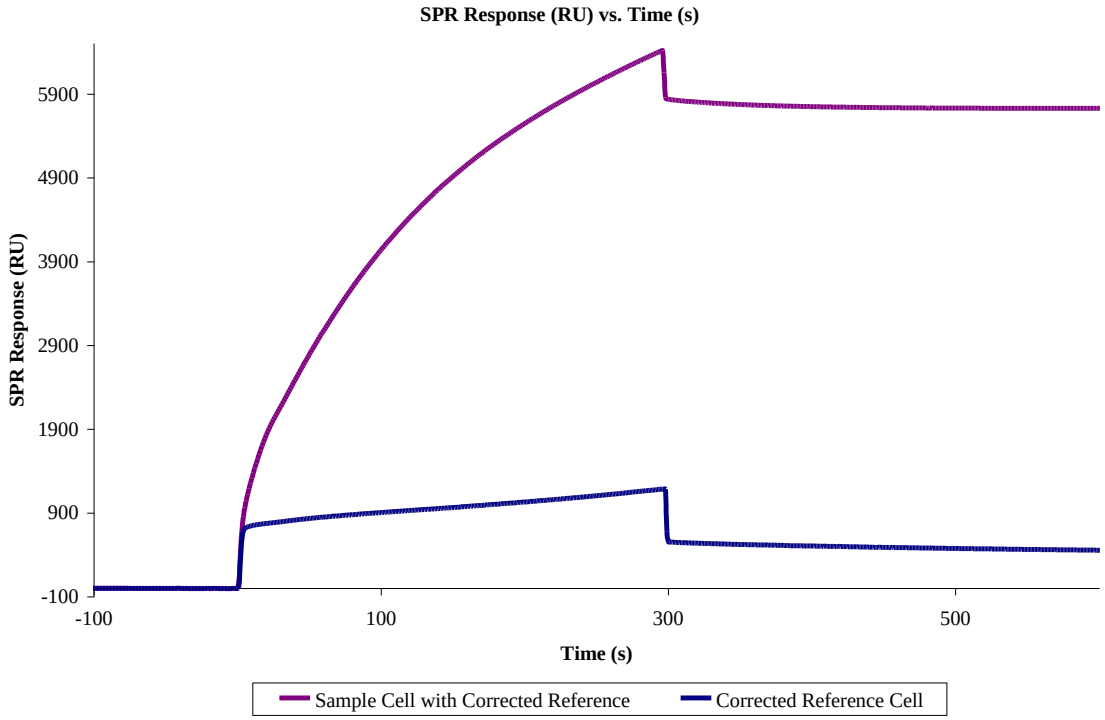

Figure 4.20: SPR sensorgrams of sample and reference cell responses of F_1-ATPase-His injection after correcting reference cell with extra cleaning steps.

Various divalent cations were tested to determine the specificity of histidine tags to those ions. Magnesium, cobalt, and copper ions were all tested in addition to nickel ions. Magnesium ions were tested as a control study. Some protein solutions utilized for initial studies contained 1.6 mM magnesium sulfate in solution. Therefore, a control test was performed to determine if magnesium cations would bind to the NTA chip and if histidine-tags would subsequently bind to the magnesium ions. Magnesium cations only bound minimally to the surface and histidine-tagged protein did not specifically adsorbed to this surface. The other divalent cations are of interest for different reasons. Specifically, cobalt provides an enhanced specific activity to histidine tags and copper provides an increased binding strength to the histidine tags, improving binding capacity but with decreased specificity.[31] Nickel ions are less expensive and provide sufficient binding.

SPR immobilization (Figure 4.14) with a NTA chip with HEPES buffer demonstrated that the immobilization scheme as detailed previously works. Addition of nickel ions produced a slight increase in response and injection of F_1-ATPase-His produces a response dependent upon the concentration injected. The NTA chip was successfully regenerated with either just a regeneration solution (section 2.7.3) injection or sequential injections of imidazole, regeneration solution, and 0.5% sodium dodecyl sulfate. These regeneration steps were made possible based on the relative affinities for each pair. According to Nieba, the K_D for nickel ions to a hexahistidine protein is approximately 1×10^{-6} M.[32] This histidine-nickel ion interaction can be disrupted by a high concentration of imidazole which has a K_D of

approximately 9.8 x 10^{-4} M, allowing for mild elution of the protein.[33] Nickel ion coordination to NTA has a K_D of approximately 1.8 x 10^{-11} M.[33] This nickel ion coordination to NTA can be disrupted by EDTA which has a K_D of approximately 4.0 x 10^{-19} M.[33] Thus, it is possible to successfully and efficiently elute the histidine tag protein with imidazole and remove the remaining nickel ions from the NTA support with a higher concentration of EDTA. The SDS removes any other denatured proteins that may be on the surface. This series of regeneration steps allowed additional trials of varying concentrations to be injected over the same surface, eliminating chip to chip variability. This enabled achievement of kinetic studies for this protein-surface attachment.

4.3.2.1.2. Kinetics

To perform kinetic studies, a series of protein injections at different concentrations must be made. SPR sensorgrams provide information about the adsorption (binding) and desorption (removal) of molecules to and from the surface. The shapes of these curves are indicative of the binding properties. As concentration increases, the total response increases. The initial rise and subsequent increase of the curve (during protein injection) corresponds to the kinetics of both adsorption (k_{on}) and desorption (k_{off}) components. The downward slope of the curve (after switching back to buffer) corresponds only to the k_{off} component. Basically the k_{on} tells about the affinity and binding of the protein to the surface while the k_{off} is indicative of how easily the protein is removed from the surface (desorbs on its own – an indication relative binding strength). Kinetic measurements produced the following results.

The rate of association of F_1-ATPase-His to a BiaCore NTA chip was determined to be 3.84 x 10^4 $M^{-1}s^{-1}$ and the rate of dissociation 9.04 x 10^{-5} s^{-1} via the Langmuir 1:1 binding model as shown in the plot below (Figure 4.21 and Table 4.2). However, the fits to the data were not as precise as desired, as seen in comparison fits 4.21 and 4.22.

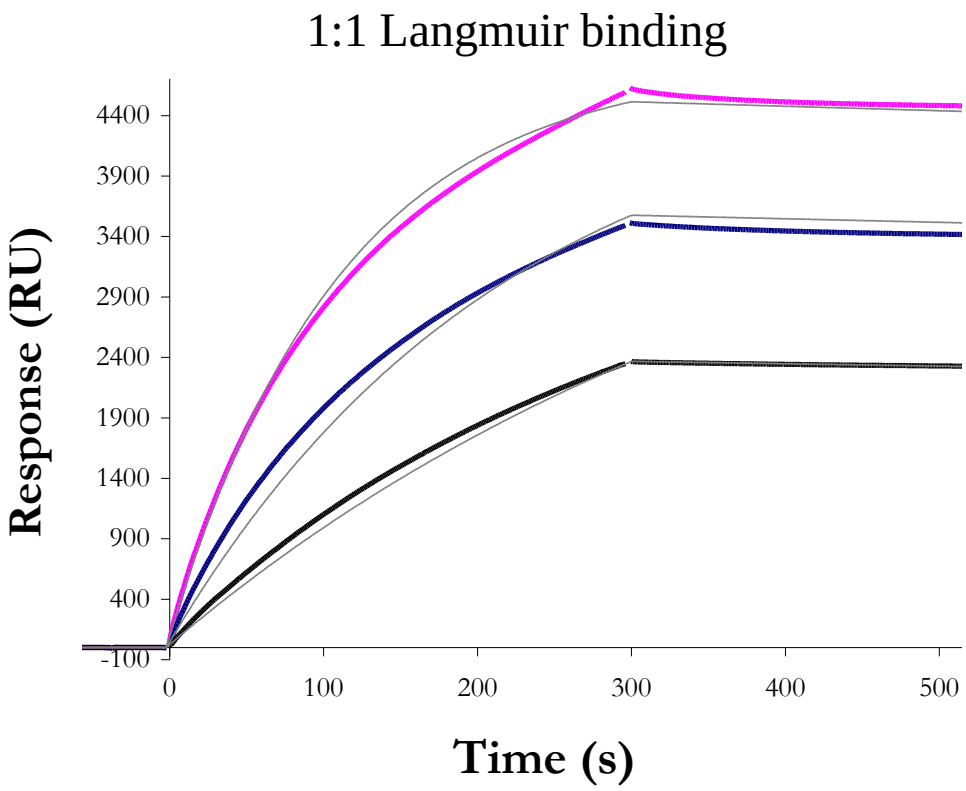

Figure 4.21: SPR sensorgram of 1:1 Langmuir fits (gray lines) to reference subtracted data (colored lines), where the pink line was for 250 nM, blue was 125 nM and black 62 nM F_1-ATPase-His.

4.3.2.1.2.1. Multivalency in His-Binding

When another model, heterogeneous binding with parallel reactions, was employed, the fits matched much better with the data. This heterogeneous binding model allows for more than one type of interaction with the surface, where the analyte can bind to two sites on the surface. The rates of association and dissociation of F_1-ATPase-His to a BiaCore NTA chip were determined to be 2.52 x 10^4 $M^{-1}s^{-1}$ and 1.02 x 10^{-4} s^{-1} for the first set of rate constants and 1.54 x 10^5 $M^{-1}s^{-1}$ and 1.32 x 10^{-5} s^{-1} for the second set of rate constants via the Langmuir heterogeneous binding model as shown in the plot below (Figure 4.22 and Table 4.2). Or, a K_D of 4.0 x 10^{-9} and 8.6 x 10^{-11}, respectively (Table 4.2), both an enhancement of binding stability over the literature value for hexahistidine K_D of 1 x 10^{-6}.[32] The first constants in the heterogeneous model are really not much different than the 1:1 Langmuir model, but the fits are much better. Reasonable fits could not be achieved with the 1:1 Langmuir binding model, but were achievable with the heterogeneous binding model. This lead us to believe that there is more than one binding mode involved in F_1-ATPase immobilization to nickel ions with different strengths of adsorption and desorption characteristics. The second fit has a lower association constant but also a lower dissociation constant. Meaning the protein takes longer to adsorb, but once it does, a stronger binding was observed. This is consistent with the idea of more than one histidine coordinating to either the same or different nickel ions. More binding sites should make the binding harder to disrupt as more coordination sites must be broken.

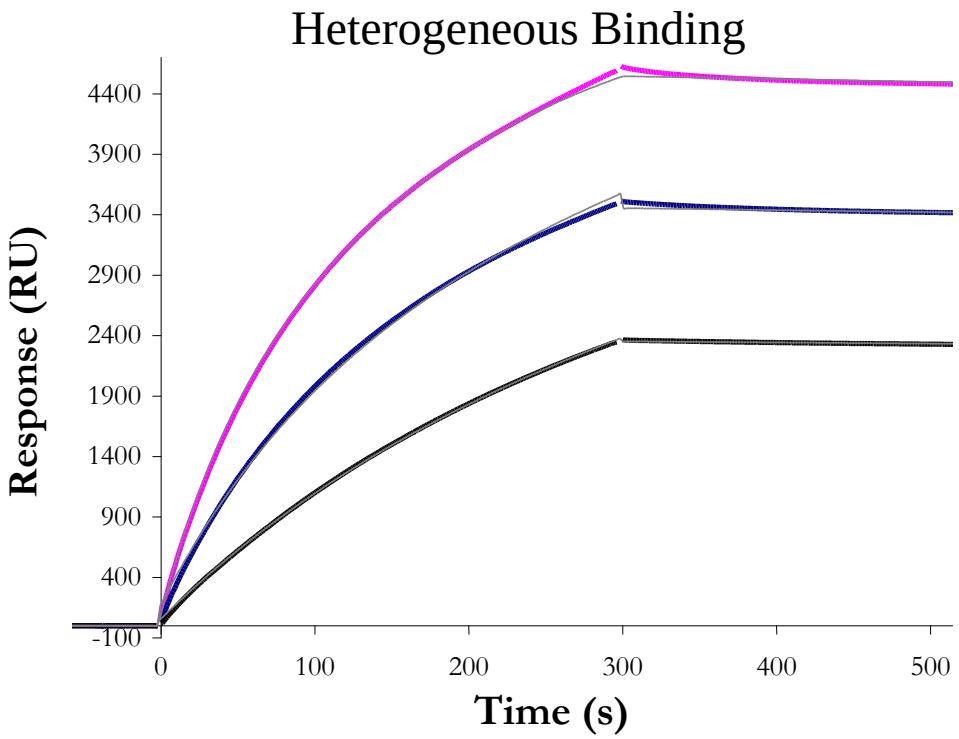

Figure 4.22: SPR sensorgram of heterogeneous binding model fits (gray lines) to reference subtracted data (colored lines) where the pink line was for 250 nM, blue was 125 nM and black 62 nM F_1-ATPase-His.

Table 4.2: Kinetics data table for wild type F_1-ATPase-his from SPR data.

Binding Model	k_{a1} ($M^{-1}s^{-1}$)	k_{d1} (s^{-1})	K_{D1}	k_{a2} ($M^{-1}s^{-1}$)	k_{d2} (s^{-1})	K_{D2}
Langmuir 1:1	3.84×10^{4}	9.04×10^{-5}	2.35×10^{-9}	n/a	n/a	n/a
Heterogeneous	2.52×10^{4}	1.02×10^{-4}	4.05×10^{-9}	1.54×10^{5}	1.32×10^{-5}	8.57×10^{-11}

4.3.2.1.2.2. Implications of Multivalency

A closer look at the curves and fits in the 1:1 Langmuir binding model versus the heterogeneous binding model indicated that the heterogeneous model fits were better. The lines of the fits matched much better to the data via the heterogeneous model as compared to the 1:1 Langmuir binding model. This led to an investigation into the possible properties and potential binding modes of ATPase-His. Unlike some histidine-tagged proteins, the ATPase-His studied here has three sets of histidine tags. All three tag sets are potentially capable of coordinating with the nickel ions. This means that one, two, or three of the histidine-tags will bind to the nickel ions. If multiple tags bind to the surface, this helps to stabilize the protein coordination to the surface. That the fit of the heterogeneous model was better than the simple 1:1 model suggests that at least one, two, or maybe even all three histidine tags bind to the surface, and do so at different rates.

4.3.2.1.2.3. Improvements to Model

Unfortunately, the heterogeneous model only accounts for two possible binding modes. Additionally, multiple histidines within one tag may bind to the surface coordinated nickel groups. Each tag contains six histidines, this gives numerous different options for binding, of which only some are probable based upon / depending on the number and proximity of nickel ions, the flexibility of the histidine tags, and steric hindrance. Since three sets of hexahistidine tags are present in the F_1-ATPase, a model that considers multiple possible binding modes at minimum is required in order to successfully model the adsorption of the ATPase. This multiple

attachment scheme should be good for stabilization of orientation of molecule in the pattern if more than one group is bound. This also ensures that the protein is in the right orientation as attachment through two or three histidine-tags will allow less flexibility of the protein from side to side.

4.3.2.1.3. ATPase modification

In addition to the wild type $\alpha_3\beta_3\gamma$-His protein, a modified protein was tested $\alpha_3\beta_3\gamma$-His-Rop protein. This form of the F_1-ATPase had a Rop protein (arm) incorporated into the gamma subunit. SPR studies were performed with the NTA chip and with this modified protein. Results of binding were similar to that for the wild type ATPase indicating no significant adverse effects of adding the Rop protein to the gamma subunit in terms of the histidine tags binding to the nickel ion NTA surfaces. An increase in SPR response was observed upon binding the same concentrations of ATPase for the Rop versus the native protein. This is consistent with the fact that the Rop adds about 10,000 Da to the molecular weight of the protein. Higher molecular weight means a greater change in refractive index for the same concentration of protein. Comparative and parallel analysis of the Rop protein can be seen below (Figure 4.23). Numerical values for protein adsorbed to surface were 6220 RU for wild type versus about 8548 RU for wild type with Rop (at a specific concentration of 250 nM). This corresponds to approximate mass per area of 6.220 ng/mm^2 versus 8.548 ng/mm^2, respectively given that 1000 RU is equivalent to a change in surface concentration of about 1 ng/mm^2.[34,35] Taking the corresponding molecule weights into account to determine moles/mm^2, the calculated values were

1.728×10^{-14} moles/mm^2 and 2.310×10^{-14} moles/mm^2 for wild type and Rop mutant, respectively. Thus, the amount of protein on the surface was roughly equivalent at about 2×10^{-14} moles/mm^2 for the two different protein forms.

An additional study comparing the two forms of this motor includes activity studies via a phosphate assay. These resulted in a slightly reduced activity for the Rop mutant as compared to the wild type protein.

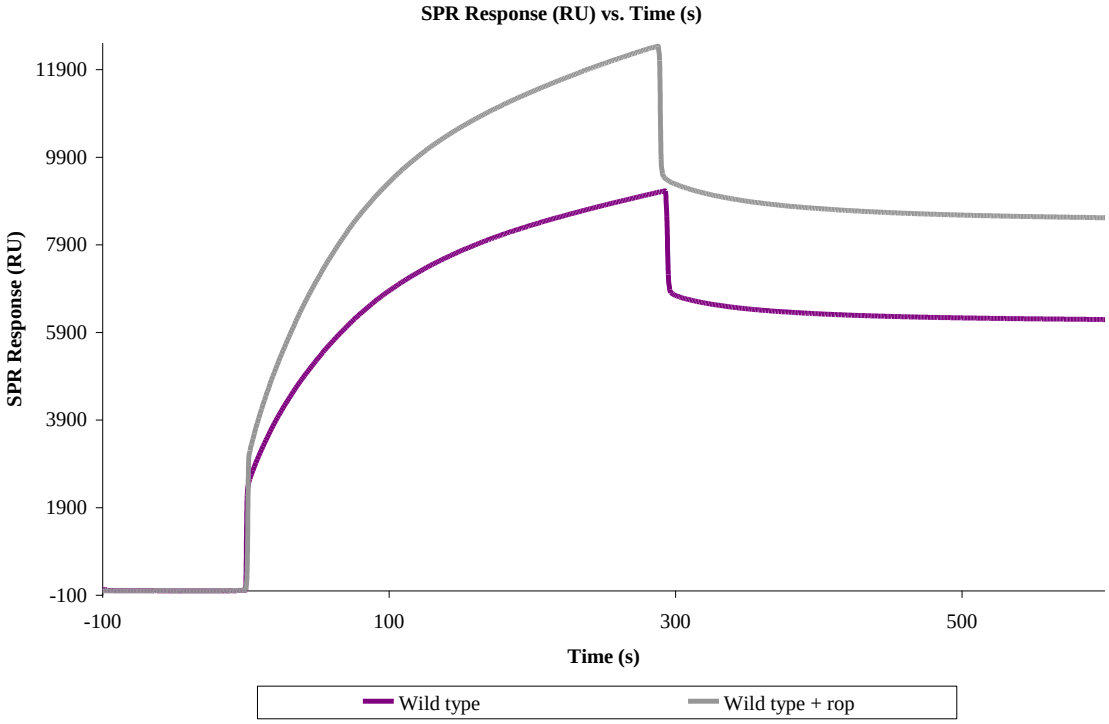

Figure 4.23: SPR sensorgram Response (RU) versus Time (s) of NTA chip with 250 nM injections of F_1-ATPase-his and F_1-ATPase-His-Rop.

4.3.3. Adsorption Studies of ATPase on Nanopatterned Substrates

After evidence that the binding model works, we wanted to perform this chemistry within a resist matrix. Figure 4.12 details the steps for this process. A matrix SAM which was protein resistant was made. Then, a dithiol SAM was grafted into the surface. Note, once dithiols have bound to the surface, the terminal thiol may oxidize and form disulfide bonds with solution thiols, or neighboring thiols (Figure 4.24). Thus, it is imperative to add a reagent to break these potential bonds before attempting maleimide binding. TCEP was used to perform this reduction (Figure 4.25).

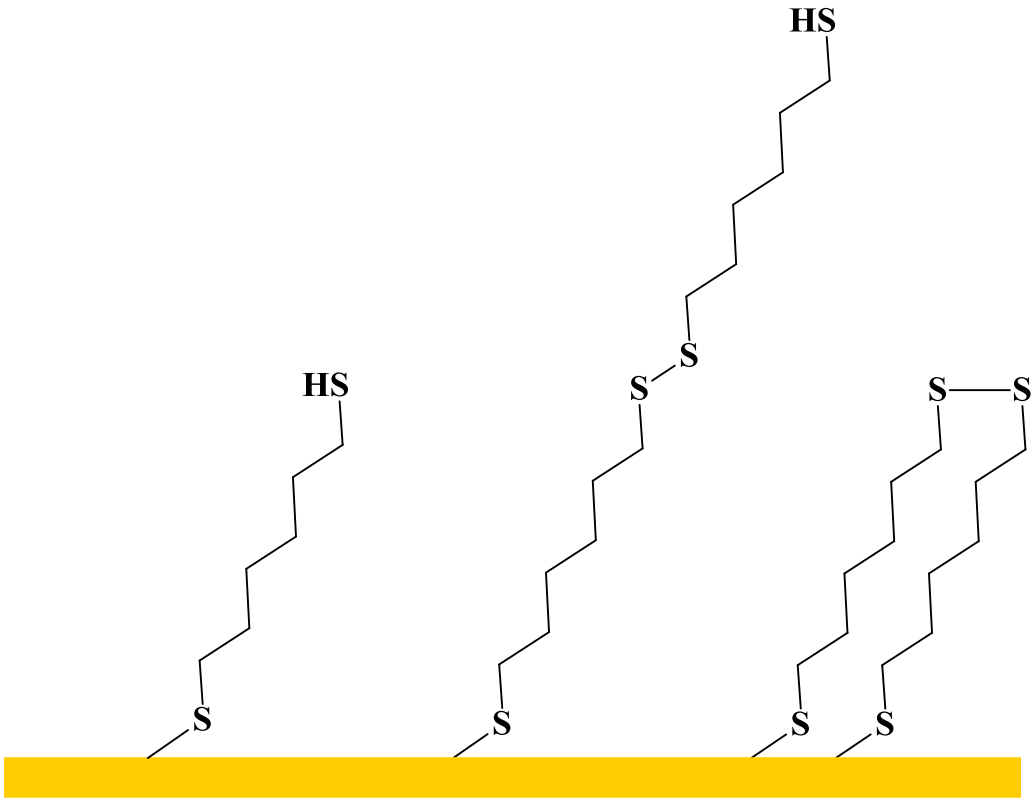

Figure 4.24: Schematic of potential 1,6-hexanedithol adsorption to gold during SAM formation. a) Ideal adsorption of 1,6-hexanedithiol SAM formation of single monolayer, b) 1,6-hexanedithiol bound to the surface with disulfide bond between terminal thiol and a free dithiol in solution, and c) two 1,6-hexanedithiol molecules bound to the surface with a disulfide bound between the terminal thiols.

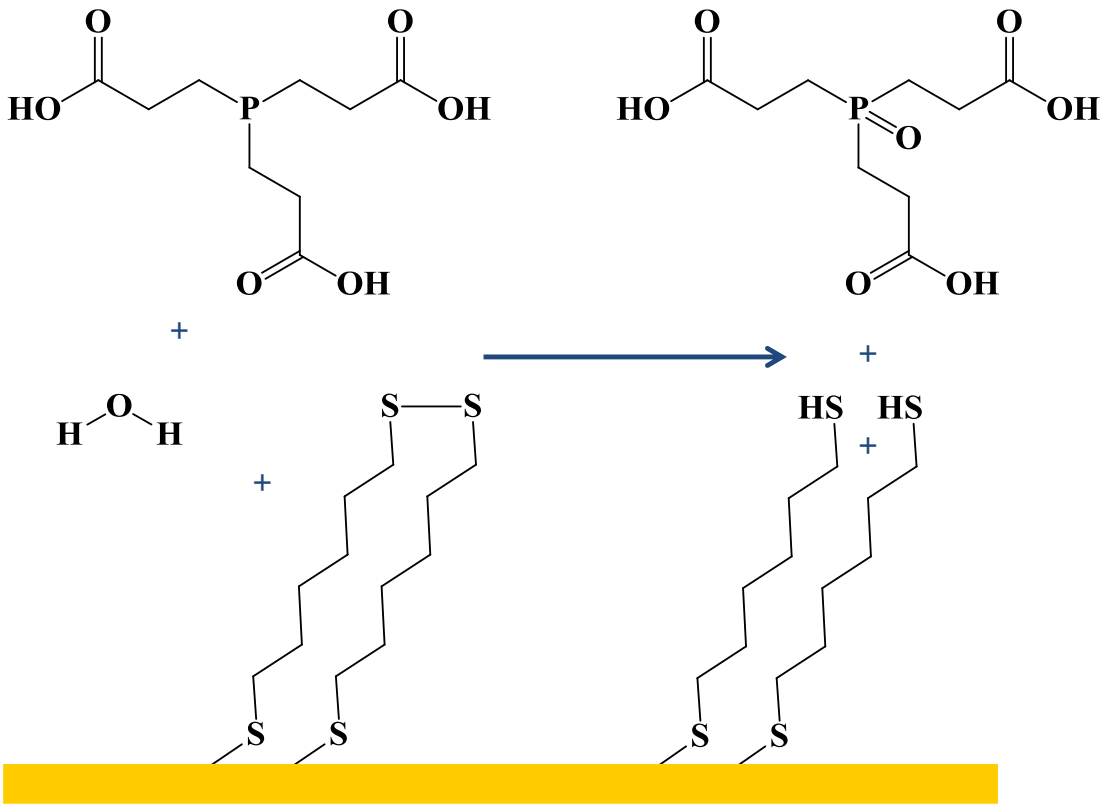

Figure 4.25: Schematic of disulfide bonds disrupted by TCEP. a) TCEP, water, and two 1,6-hexanedithiol molecules bound to the surface with a disulfide bound between the terminal thiols, and b) After reaction TCEP is oxidized and the disulfide bond between the two 1,6-hexanedithiol molecules on the surface has been reduced yielding free terminal thiols.

Maleimide-NTA solution was added to the system and covalently bound to the exposed thiol. A nickel-chloride solution was added to the system. This allowed the nickel ions to coordinate to the carboxylic acid groups in the NTA portion of the surface. Finally, histidine tagged F_1-ATPase was added to the system. The histidine-tags coordinated to the nickel ions, aligning the ATPase both spatially and in the correct orientation. The gamma subunit should then be exposed at the surface. Both nonspecific and specific adsorption of ATPase to nanopatterns was performed to gain information about the adsorption properties of ATPase.

4.3.3.1. Nonspecific Adsorption of ATPase to Patterns

To determine if F_1-ATPase had any binding preference to hydrophobic versus hydrophilic surfaces, a pattern was made which contained distinct regions of both. Nonspecific adsorption was studied on a methyl terminated SAM (1-dodecene on hydrogen-terminated silicon) with etched patterns via AFM. Again highlighting the ability of this technique to both modify the surface and then probe the resulting changes. Conditions for creating patterns as outlined in section 2.4.3 include high force and greater scanning rates. Removal of a portion of the hydrophobic SAM film from the surface exposed the silicon surface which then oxidized to create a hydrophilic region within the etched box. For example, patterns four 400 nm by 400 nm boxes were etched into 1-dodecene and were about 3-4 nanometers deep (darker in color on height scale) as indicated by the cross-sectional image. The monolayer (~2 nm) was successfully removed and the etch also went into the silicon substrate beneath (Figures 4.26-27). F_1-ATPase adsorption steps were performed as per

section 4.3.1.1.2. Tapping mode AFM was utilized to observe adsorption properties on this patterned surface. Preferential adsorption of F_1-ATPase for the hydrophilic portion over the hydrophobic area was observed (Figure 4.28). Again, as in the nonspecific adsorption to mica, the protein orientation on this patterned surface varied. Thus, while this provided a sufficient landing pad for the protein, it would not enable a large amount of fully functional proteins as the gamma subunit would not be able to freely rotate in all orientations observed.

Etching and grafting have the advantage that theoretically any shape and size (nanometer-micrometer) of feature can be constructed.

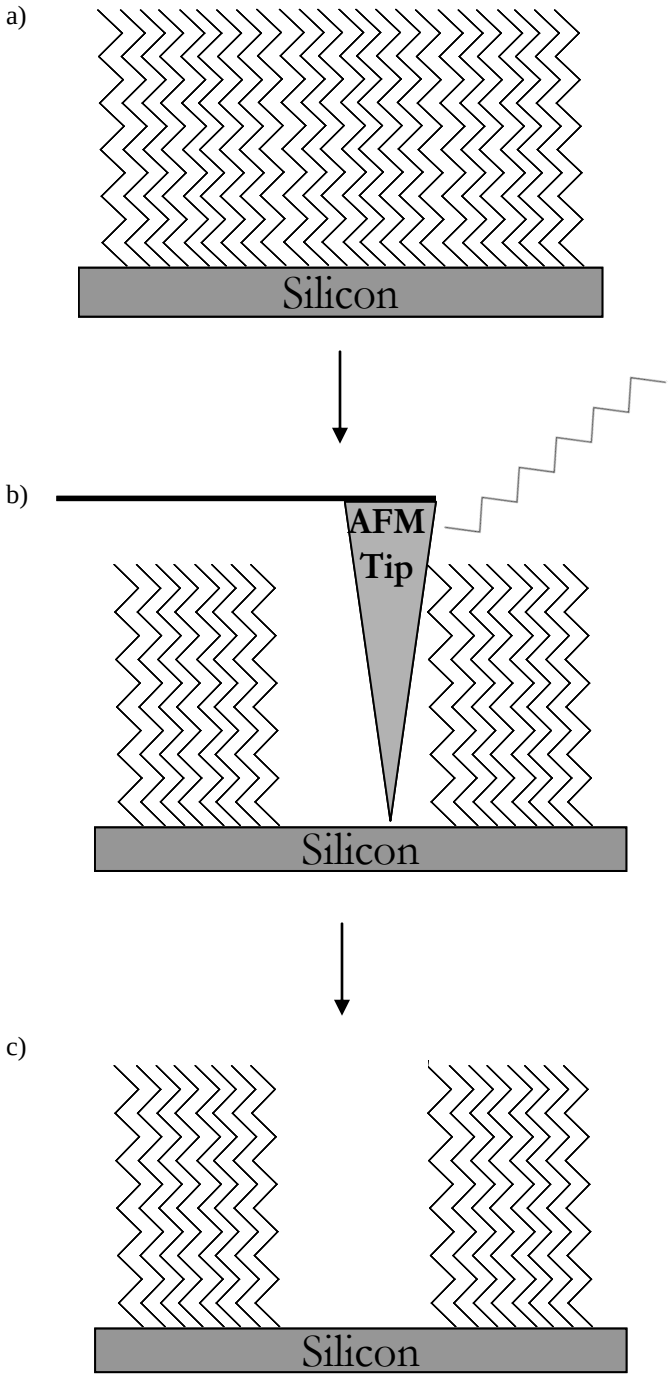

Figure 4.26: Etching schematic. a) Schematic of 1-dodecene SAM on Silicon. b) Schematic showing that by applying more force at a faster scan rate with the AFM tip, the monolayer of scanned area is selectively removed. c) Schematic of resultant etch produced by backing off the force (decreasing) and scan rates. The monolayer with etched area may then be imaged (Figure 4.27).

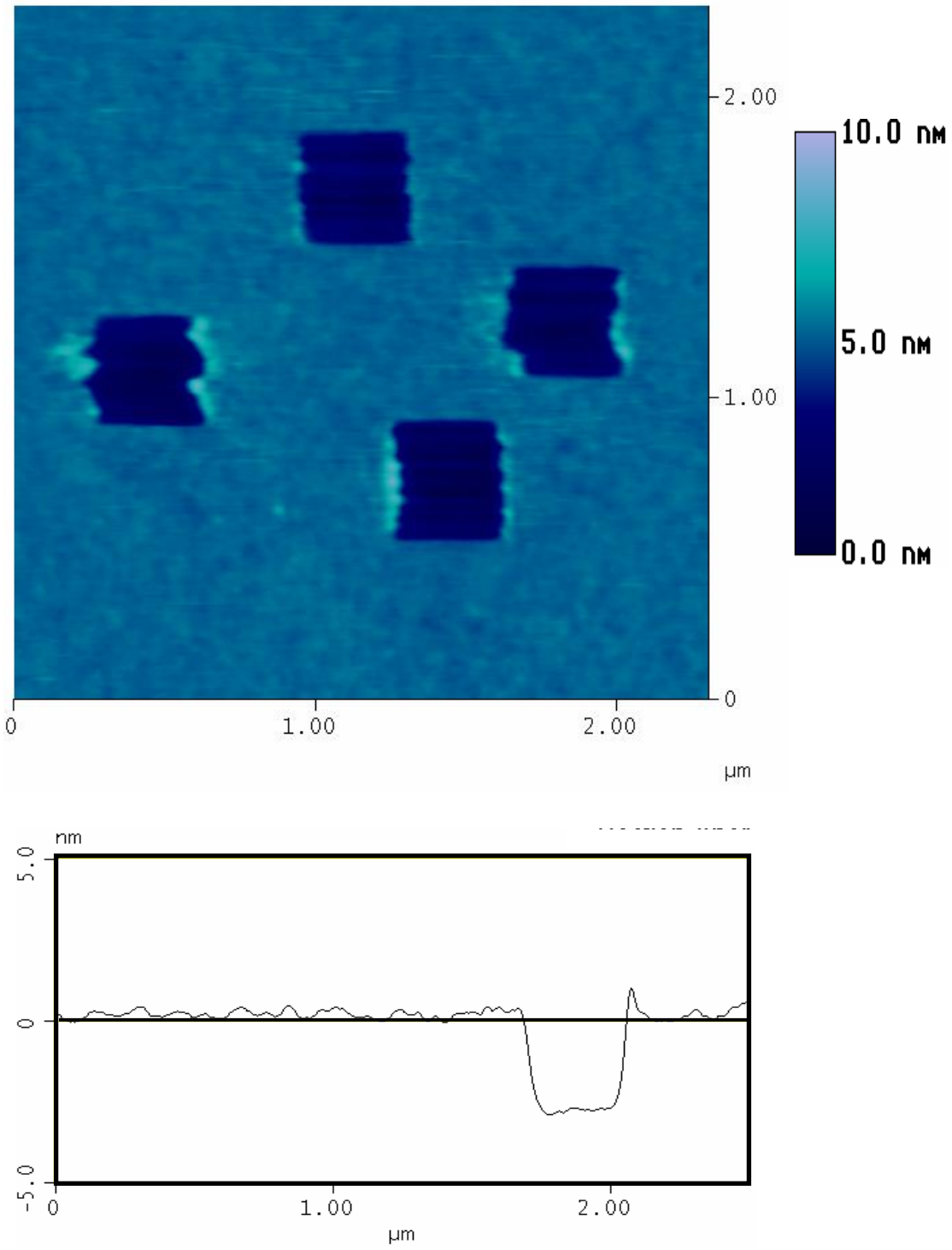

Figure 4.27: Contact mode AFM height image of 1-dodecene SAM on silicon with four nanoetched boxes of ~400 nm^2 dimensions. Scan area of 2.25 µm x 2.25 µm and height scale 10.0 nm. Corresponding cross-section through one of the etched areas is below the AFM image.

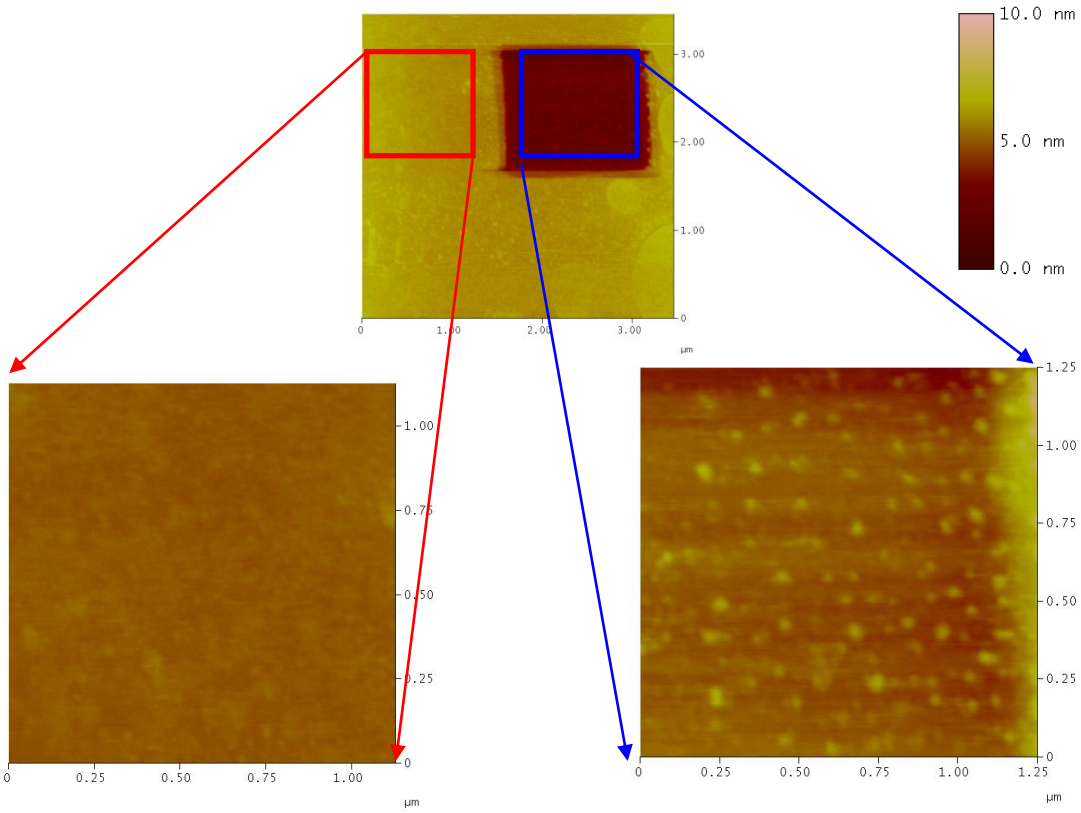

Figure 4.28: Tapping mode ~3.50 µm x ~3.50 µm AFM height images of 1-dodecene SAM on silicon with nanoetched box of ~1.50 µm x ~1.50 µm dimensions after ATPase adsorption with a height scale of 10.0 nm. To the bottom left is a zoomed in area outside etched area and to the right is a zoomed in area inside the etched box area. ATPase preferentially adsorbed to the hydrophilic etch surface over the hydrophobic SAM surface. (Image courtesy of Jill E. Koehler).

4.3.3.2. Specific Adsorption of ATPase to Patterns

The following subsections discuss the control and patterning studies of specific adsorption of ATPase-His to patterns using AFM and fluorescence microscopy. Patterns were created using a nanografting technique (Figure 4.29) as discussed in section 2.4.3, which can selectively replace sections or patterns of the monolayer with another thiol with desired terminal chemistry. Evidence that the technique was successful was observed upon nanografting a 500 nm pattern of octadecanethiol into a matrix monolayer of dodecanethiol. See Figure 4.30 for an AFM example image of this nanografting and a cross section through the patterned box indicated a height increase of about 0.9 nm over the matrix monolayer (pattern was a brighter shade of blue than the matrix), which was close to the expected theoretical difference between the length of the two molecules of 0.76 nanometers for 12 to 18 alkanethiol (or 0.8-0.9 nanometers per ellipsometric measurements of comparable SAMs in Allara 1987 paper).[36]

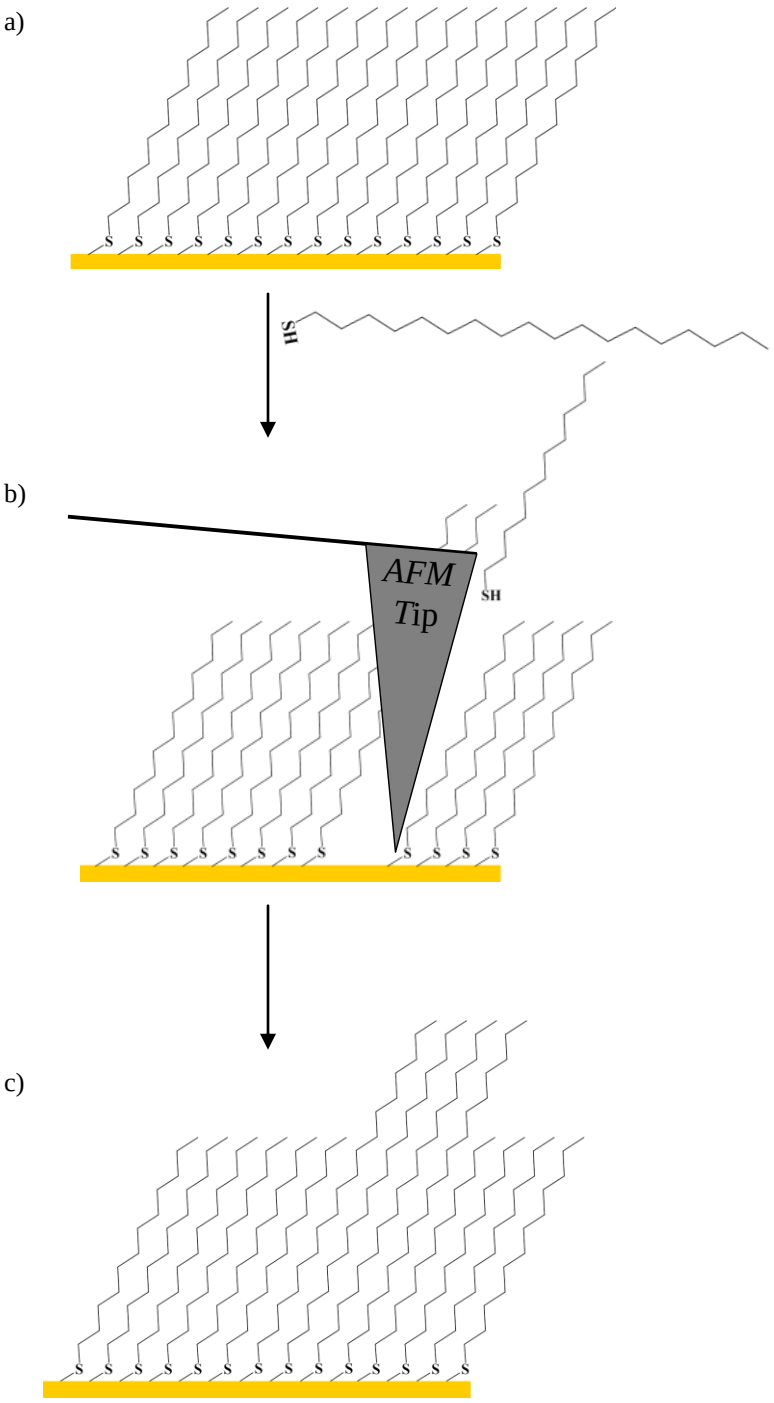

Figure 4.29: Grafting Schematic. a) 1-dodecanethiol SAM on gold. b) Schematic shows that by applying more force at a faster scan rate with the AFM tip, the monolayer of scanned area is selectively removed and by performing this in a solution of another thiol (1-octadecanethiol in this case), that new thiol is grafted into the patterned area. c) Schematic of resultant pattern of 1-octadecanethiol within the 1-dodecanethiol matrix SAM. By decreasing the force and scan rates, the monolayer with this grafted area may be imaged (Figure 4.30).

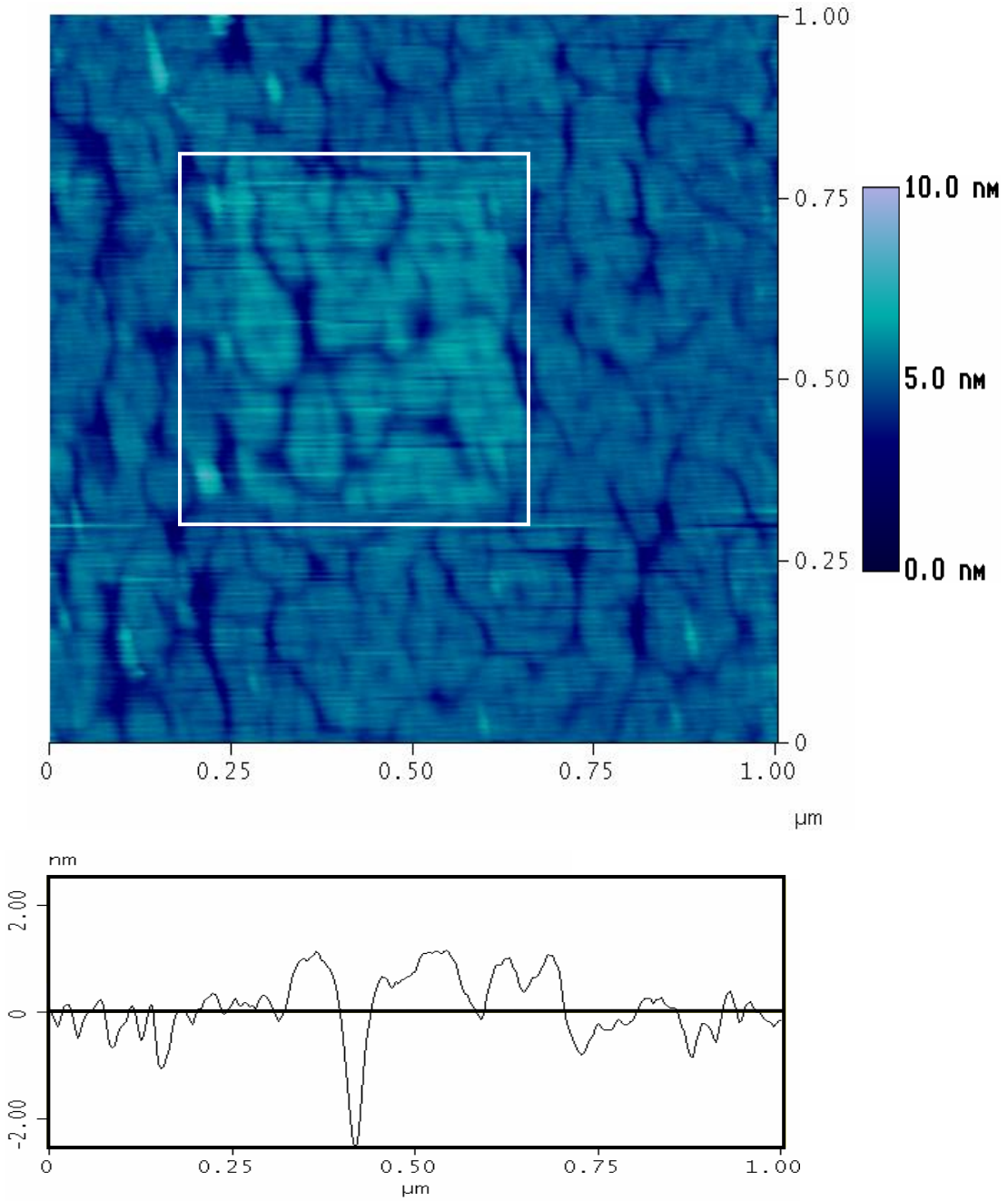

Figure 4.30: Thiol grafting. 1.00 µm x 1.00 µm AFM height image of 1-dodecanethiol matrix with grafted 500 nm x 500 nm 1-octadecanethiol box on template-stripped gold, outlined with a white box for clarity, with a 10.0 nm height scale. A cross-section through the patterned box shows an approximately 0.9 nm height increase of the pattern above the matrix thiol, as expected.

4.3.3.2.1. Surface Engineering

Since it had been established through the nonspecific adsorption experiments that the protein orientation had to be controlled to ensure proper orientation (gamma subunit perpendicular to the surface), and that the final steps in the chemistry schematic should work, we needed to create a specific landing pad for the protein with the correct chemistry. To achieve this, a surface engineering scheme was employed. This was outlined earlier, but consists of creating a region of exposed thiols in which maleimide-NTA can be attached, followed by nickel ion and histidine-tagged protein coordination. Once maleimide-thiol coupling was confirmed, this step was performed with maleimide-NTA followed by nickel ion addition and F_1-ATPase-His adsorption.

The first step in this process was to pattern a dithiol into a resist SAM matrix. Patterning a dithiol of shorter length (1,11-undecanedithiol) than the resist octadecanethiol SAM resulted in a decrease in height between the pattern and the matrix SAM (slight deeper blue hue within the pattern), and resulted in a change in the friction trace and retrace within the rectangular pattern (darker and lighter shades of blue within pattern) (Figure 4.32). Patterning a box of shorter dithiol (1,6-hexanedithiol) than the resist dodecanethiol SAM also resulted in both a decrease in height seen by a darker hue (expected depth value of 0.61 nm) and a change in the friction trace and retrace (darker and brighter hue) within the patterned area (Figure 4.33). Control over which dithiol (1,6-hexanedithiol versus 1,11-undecanedithiol) was utilized within a 1-dodecanethiol matrix meant that it was possible to vary the

vertical position of the motor over the resist matrix as desired (Figure 4.31). Using a shorter dithiol would make the M-NTA height less over the matrix SAM which would make the protein position closer to the matrix SAM. Using a longer dithiol would extend the height of the protein over the resist matrix. Depending on the height of the nanoelectrodes over which the protein armature and attached bead must rotate without colliding, the appropriate length dithiol can be chosen to engineer the height appropriately. Or, one could promote the coupling of dithiols into longer chains via disulfide bonds between dithiols although this might have an issue with non-uniformity.

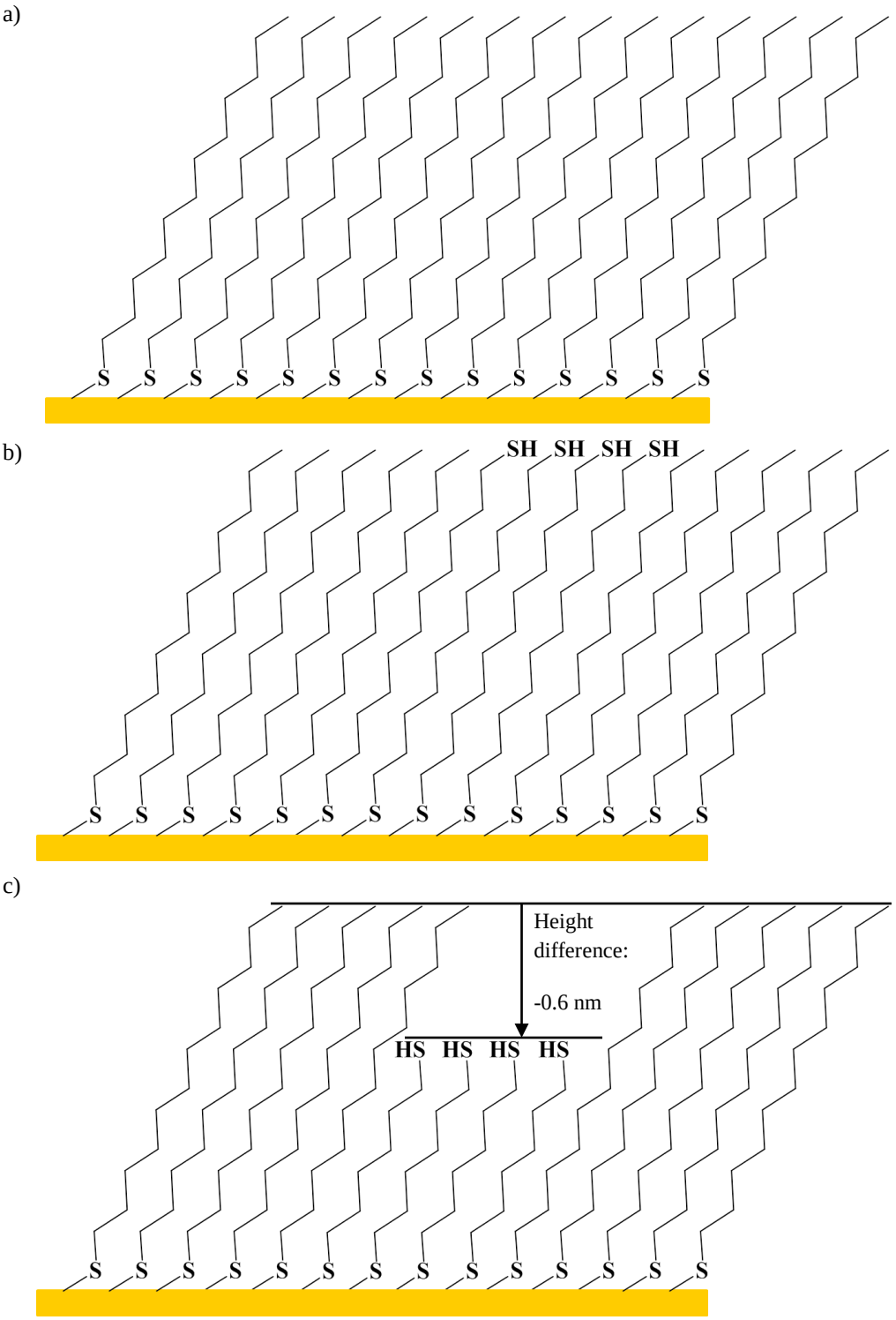

Figure 4.31: Schematics of 1-dodecanethiol SAM on gold and grafting. a) 1-dodecanethiol SAM, b) 1,11-undecanedithiol grafted into 1-dodecanethiol matrix SAM on gold, and c) 1,6-hexanedithiol grafted into 1-dodecanethiol matrix SAM on gold.

a)

b)

c)

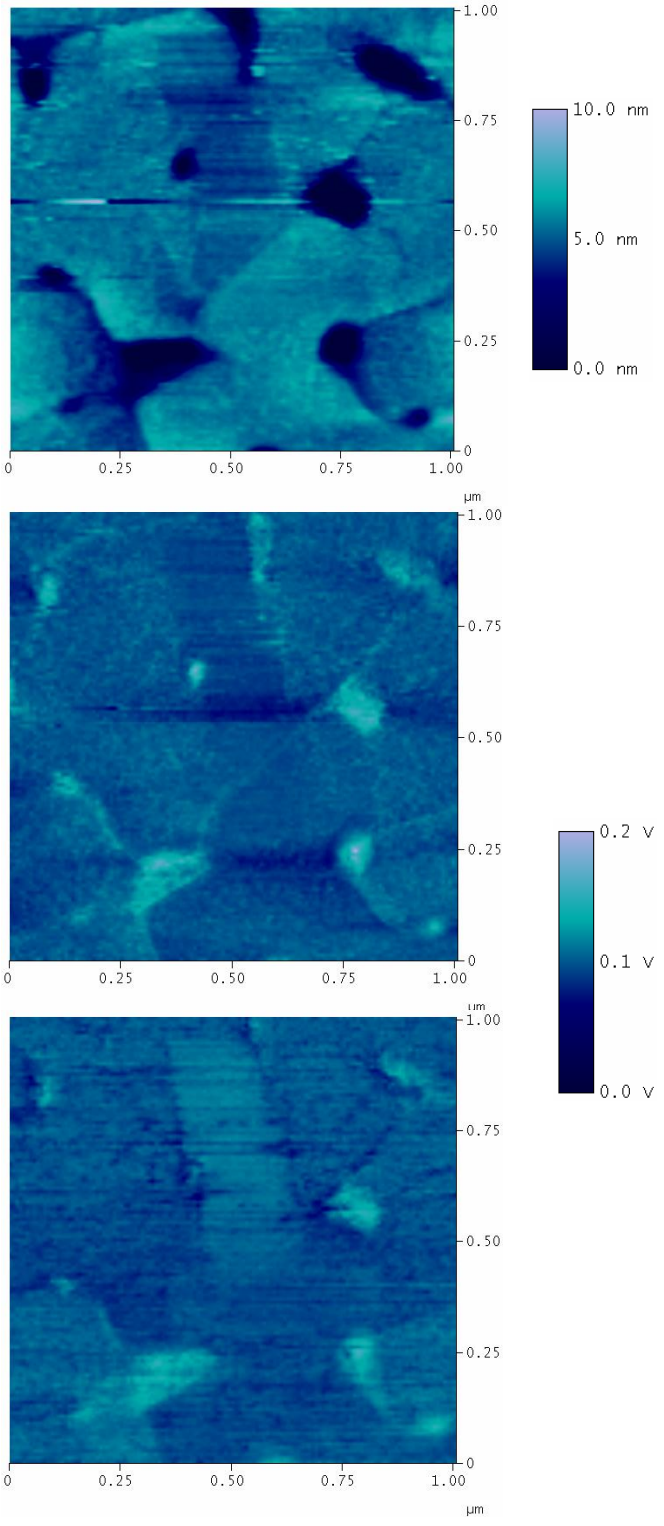

Figure 4.32: Dithiol grafting, 1.00 µm x 1.00 µm AFM height images of 1,11-undecanedithiol rectangle patterned into 1-octadecanethiol resist matrix on gold. a) Height image with 10.0 nm height scale, b) friction trace image, and c) friction retrace image with 0.2 V scales.

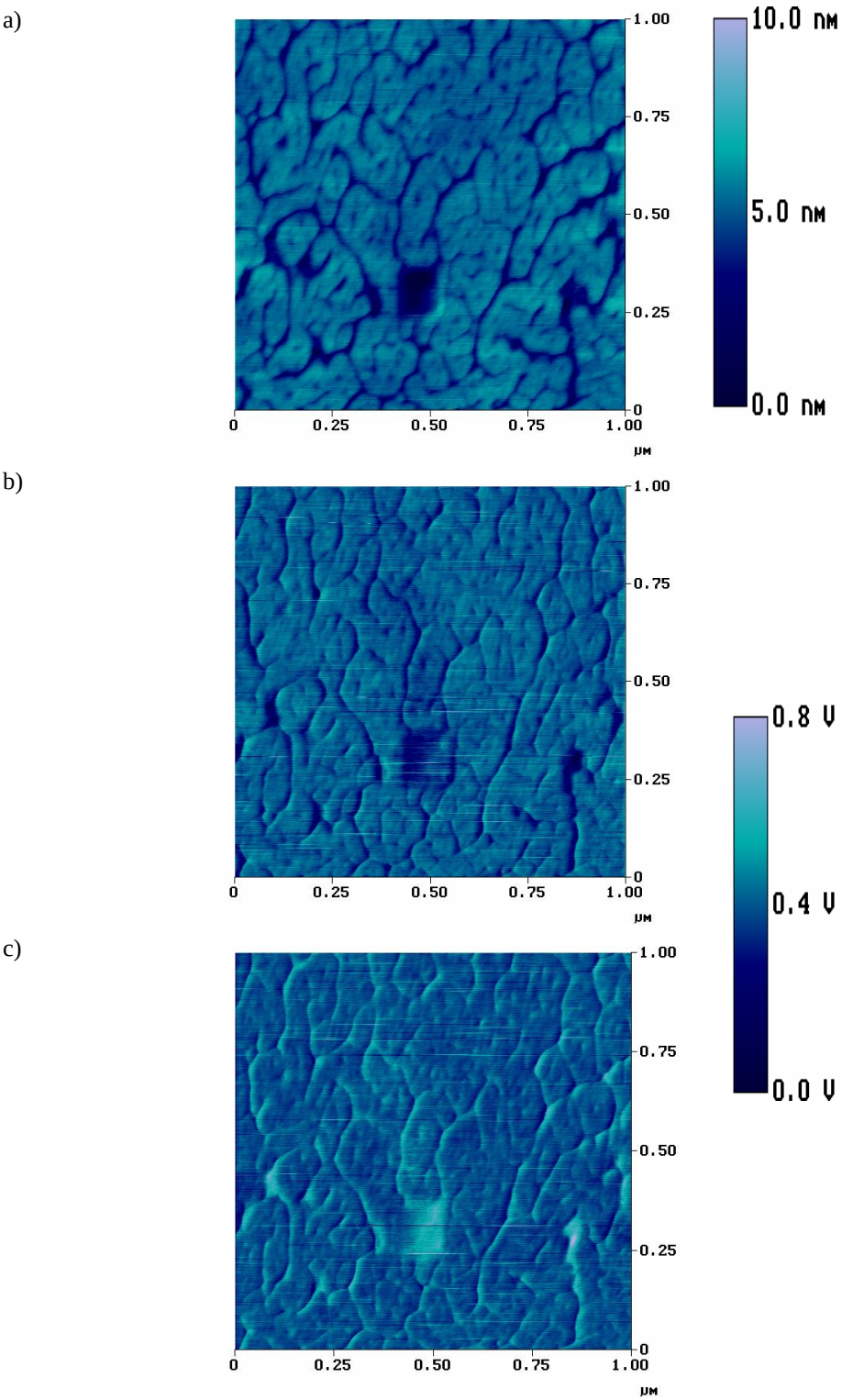

Figure 4.33: Dithiol grafting. 1.00 µm x 1.00 µm AFM images of a 1,6-hexanedithiol 250 nm x 250 nm square patterned into 1-dodecanethiol resist matrix on template stripped gold. a) Height image with a 10.0 nm height scale, b) friction trace image, and c) friction retrace image with 0.8 V scales.

A concern with grafting any thiol or dithiol into a pattern is that the patterning process must expose the whole surface to this molecule. The thiol can bind to any open site on the surface, and thus will adsorb not only to the patterned region, but also into defect sites within the monolayer.[37, 38] An additional concern with dithiols is that one or both thiol ends can bind to the gold surface. By spatially confining the reaction area, this can lead to a greater number of exposed thiol terminal groups.[39, 40] If a thiol is not exposed, then additional binding steps and chemistry would not be successful.

After successful dithiol grafting, the exposed thiol can then be reacted with the maleimide group of the maleimide-NTA molecule. Addition of maleimide-NTA to either nanoscale patterns of dithiol within the resist monolayer resulted in a height increase within the 150 nanometer by 150 nanometer square pattern of about 1.4 to 4.5 nanometers, as indicated by a brighter shade of blue, and was in line with or above expected height increase of about 1.5-2.0 nanometers (Figure 4.34). The higher end of the height range may be due to the NTA groups of the bound molecule hydrogen bonding with an NTA group of a solution molecule to create a double-layer. This could be tested by attempting to disrupt the hydrogen bonding (as with carboxyl-terminated SAMs) and measuring the height thereafter (a decrease in height to the expected length of the M-NTA would confirm this possibility). These results show that the dithiol can be successfully patterned into the resist matrix and that M-NTA can be introduced selectively into the pattern to create a landing site for the protein and should control the orientation as well.

a)

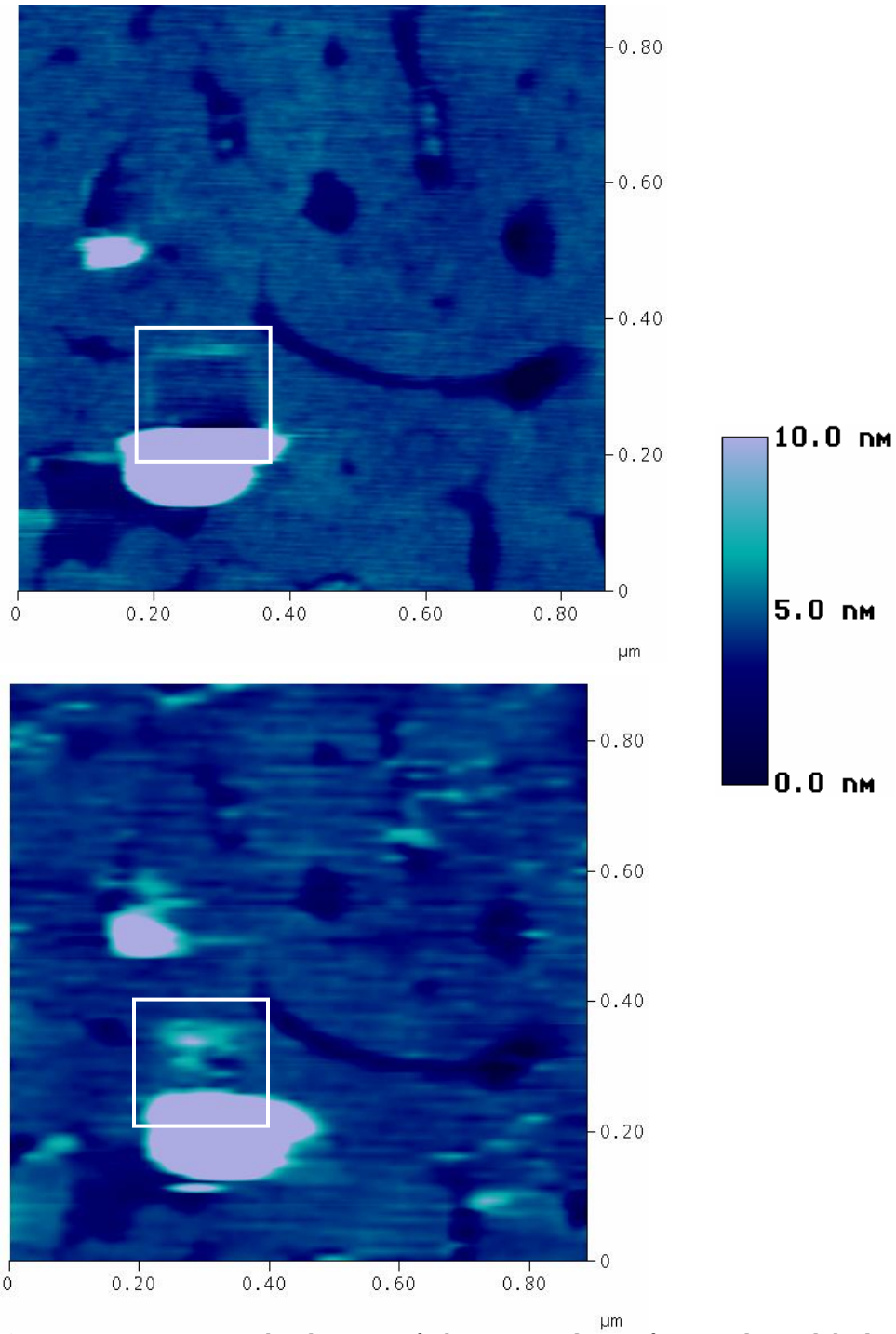

b)

Figure 4.34: a) 900 nm x 900 nm AFM height image of a box patterned area of 1,11-undecanedithiol patterned into 1-dodecanethiol resist matrix on template stripped gold with 10.0 nm height scale. b) 900 nm x 900 nm AFM height image of 1,11-undecanedithiol patterned into 1-dodecanethiol resist matrix on template stripped gold after addition of maleimide-NTA with 10.0 nm height scale. Height increase of about 1.4 to 4.5 nm was observed upon M-NTA addition.

4.3.4. Fluorescence Microscopy

Fluorescence microscopy was utilized for control experiments to verify that the chemistry proposed in the surface nanoengineering schematic was occurring as expected under the reaction conditions used. Specifically, the maleimide thiol chemistry and nickel ion – histidine tag coordination were verified via fluorescence microscopy.

a)

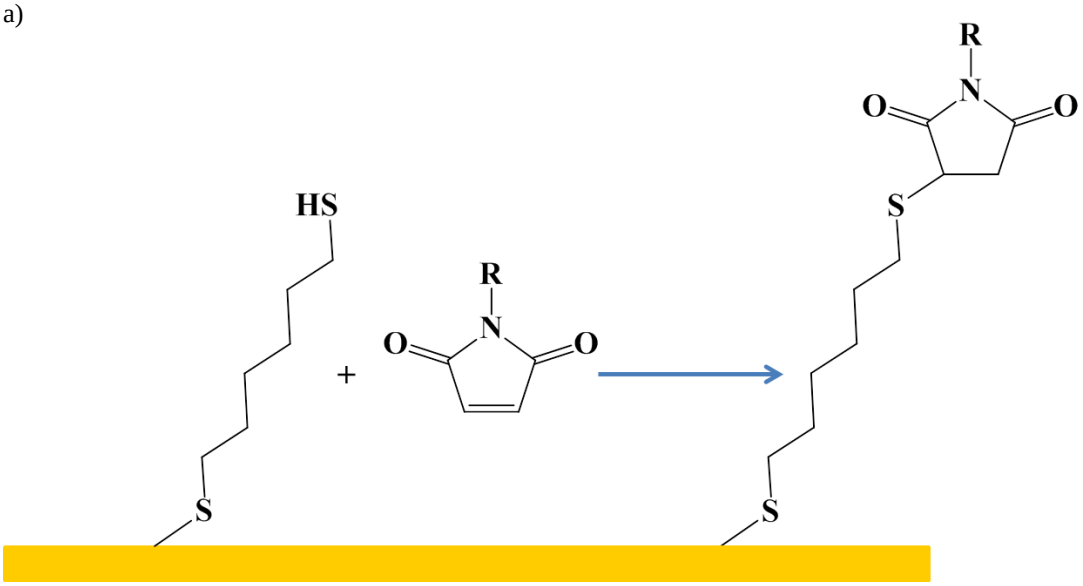

b)

Figure 4.35: a) 1,6-hexanedithiol bound to the surface and b) 1,11-undecanedithiol bound to surface. Either terminal thiol can react with a maleimide group on a fluorescent dye (R) to form a covalent thioester bond.

4.3.4.1. Fluorescent Dye Controls

Since AFM surface engineering studies provided only height increase upon maleimide-NTA attachment, one way to confirm that a thiol is exposed within the patterned region was to attempt to attach a fluorescent maleimide dye. Figure 4.35 schematically depicts a 1,6-hexanedithiol or a 1,11-undecanedithiol before and after interaction with a maleimide group of the dye where R represents the conjugated dye ring. Successful attachment confirms that the chemistry (terminal thiol) was available for attachment. Advantages of this method include easy observation of fluorescence and conclusive evidence of dye attachment.

Texas Red C_2-maleimide dye was utilized in these experiments. First, two control surfaces were prepared. A methyl-terminated SAM film (prepared from 0.1 millimolar 1-dodecanethiol in ethanol for approximately 24 hours) was formed on Platypus gold as a negative control. A positive control was made from a dithiol SAM film on Platypus gold (prepared from 25 millimolar 1,6-hexanedithol in ethanol for approximately one hour). The higher concentration of dithiol is to help molecules to stand straight up on the surface and not have both thiols attached to the surface. Another way to achieve this upright alignment is by limiting the available binding surface area as in the patterns made in the surface engineering section.[39,40] A shorter dithiol such as the 1,6-hexanedithiol has less flexibility to fold over and have both thiols attaching to the surface as the 1,11-undecanedithiol, and was therefore chosen for full coverage SAM film. After characterizing the SAMs, both SAM films were incubated in buffer with TCEP for about five minutes to disrupt any disulfide bonds.

Following this, the SAMs were exposed to the fluorescent dye in buffer and TCEP for approximately one hour. Then the surfaces were removed from the dye solution, rinsed with buffer and water and dried with nitrogen gas. Then an epifluorescence microscope equipped with a CCD camera was used to obtain fluorescent images by exciting at 540-550 nm and monitoring the emission at 590 nm. The excitation light was green and the fluorescent emission was brilliant red. Fluorescence study results included little to no fluorescence observed on the methyl terminated SAM (Figure 4.36). However, the surface was covered with fluorescence on the dithiol SAM (Figure 4.37). Fluorescence studies confirm the 1-dodecanethiol was a decent resist to maleimide binding as little to no fluorescence was observed upon the addition of a maleimide dye to the SAM. Confirmation that the maleimide dye binds to the dithiol was also observed above as the surface fluoresced red.

To further establish the specificity of this maleimide-thiol reaction, the same controls were performed with another dye, Oregon Green® 488 Maleimide. In this case, excitation was performed at 492 nm and emission monitored at 515 nm. Therefore the excitation light was blue and the observed fluorescent emission was brilliant green. Results of this study indicated specific binding of the fluorescent dye to the thiol terminal group and minimal nonspecific binding of the fluorescent dye to the methyl terminal group as there was minimal green fluorescence on the alkane SAM (Figure 4.38) and extensive green fluorescence on the dithiol SAM (Figure 4.39). This study confirmed the previous fluorescence study in that maleimide

binding was specific for the terminal thiol and the methyl terminated thiol served as a decent resist matrix.

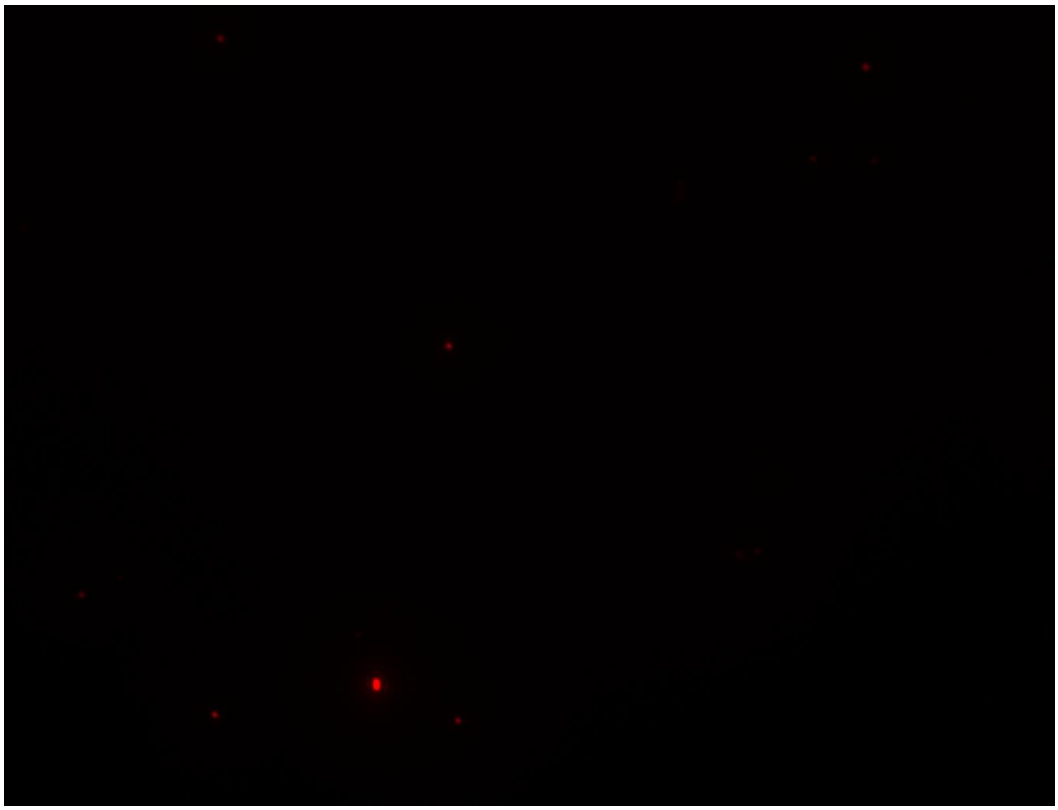

Figure 4.36: 1-dodecanethiol SAM on Platypus gold with maleimide fluorescent dye (Texas Red). Minimum nonspecific adsorption of dye was observed.

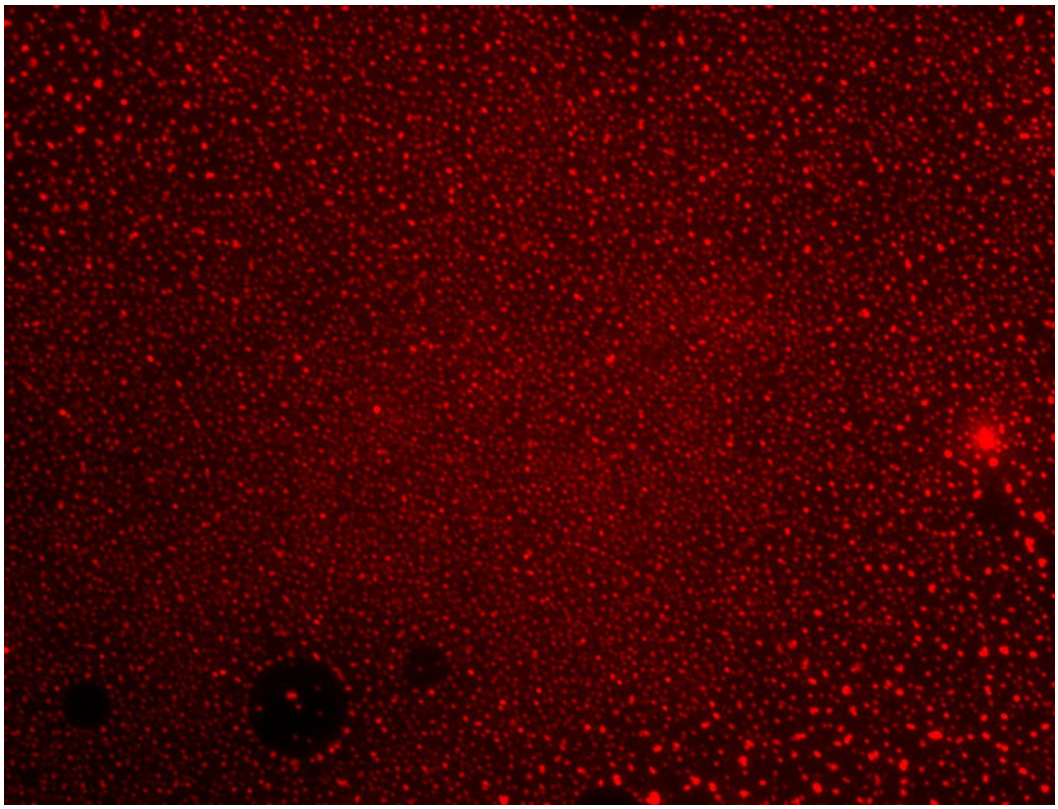

Figure 4.37: 1,6-hexanedithiol SAM on Platypus gold with maleimide fluorescent dye. Dye was observed everywhere indicating specific binding of maleimide to dithiol.

Figure 4.38: 1-dodecanethiol SAM on Platypus gold with maleimide fluorescent dye (Oregon Green). Minimum nonspecific adsorption of dye was observed.

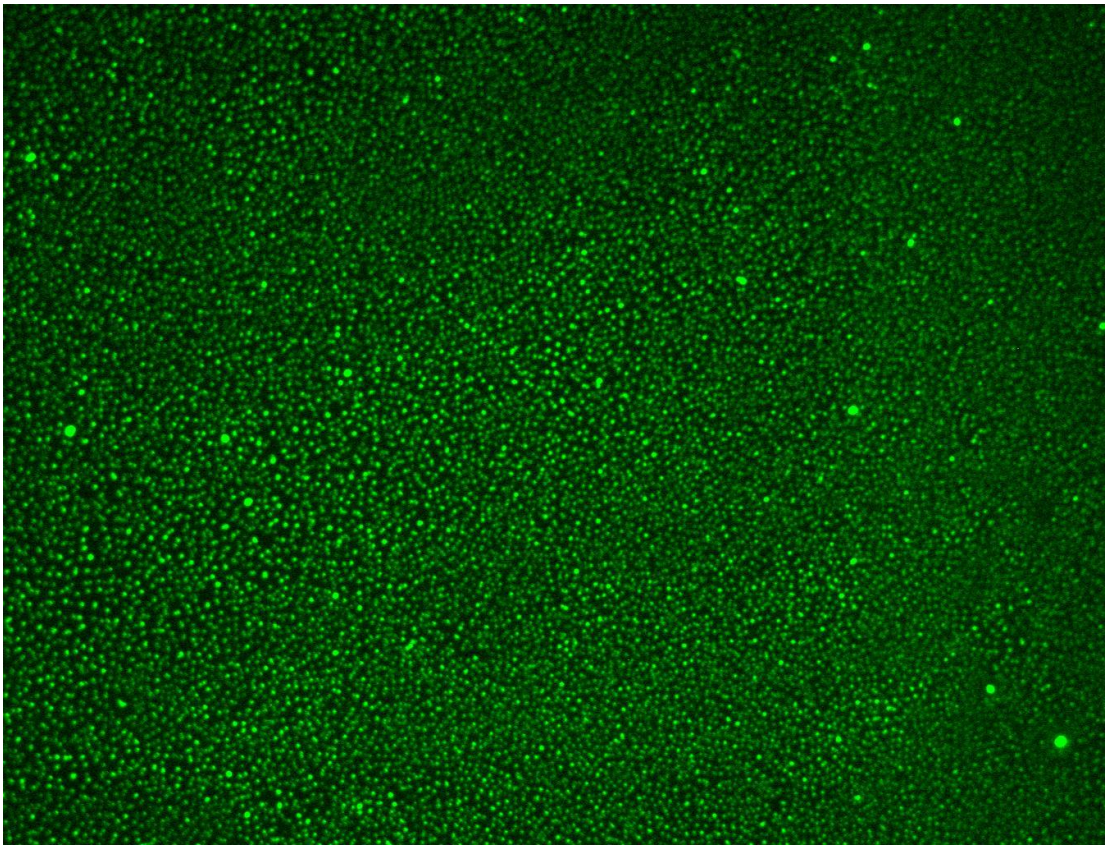

Figure 4.39: 1,6-hexanedithiol SAM on Platypus gold with maleimide fluorescent dye (Oregon Green). Dye was observed everywhere indicating specific binding of maleimide to dithiol.

A modification of the specific attachment experiment was also performed with a fluorescently tagged ATPase-His-Rop protein. ATPase-His-Rop was fluorescently labeled via a free cysteine at the end of the Rop armature with 20 micromolar fluorescein-5-maleimide for ten minutes. This labeling reaction was stopped with one millimolar dithiothreitol (DTT) which bound to all remaining free dye. This solution was filtered via a size-exclusion column to remove free dye from the fluorescently labeled ATPase-His-Rop sample. This control study involved adsorption of the fluorescent protein to SAMs that were initially either methyl or thiol terminated (negative and positive controls, respectively) on Platypus gold. Prior to the protein adsorption step, M-NTA and then nickel ions were allowed to interact with the surfaces. M-NTA should bind only to the thiol terminal groups and not the methyl terminal groups (as demonstrated in previous control experiments). Thus, only the dithiol SAM surface should be functionalized with the appropriate M-NTA chemistry to coordinate to nickel ions and thus F_1-ATPase-His-rop-fluorescent tag. Following protein adsorption, the sample was rinsed thoroughly with buffer and water and dried with nitrogen gas. Then an epifluorescence microscope was used to obtain a fluorescent image by exciting at 450-490 nm and monitoring the emission at 515-555 nm. The excitation light was blue and the fluorescent emission was brilliant green. Results show that on the methyl terminated SAM, little to no adsorption occurred as expected (Figure 4.40). While on the thiol terminated SAM with M-NTA and nickel ions, an abundance of fluorescence was observed (Figures 4.41). This was further

confirmation that the methyl terminated SAM was a suitable resist for these studies and also confirmed that the designed chemistry schematic should work as expected.

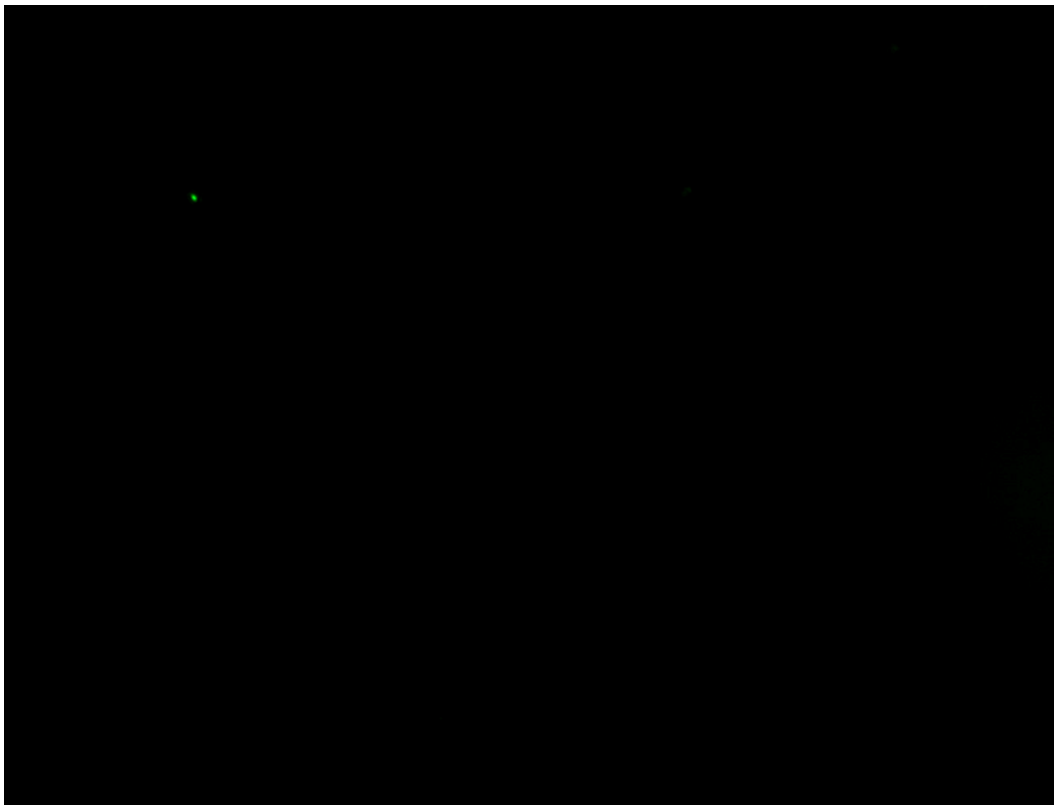

Figure 4.40: 1-dodecanethiol SAM on Platypus gold after incubation in maleimide-NTA, nickel ions, and ATPase-His-Rop* fluorescent dye. Green fluorescence was sparse indicating minimal nonspecific binding of ATPase-His-Rop* to the methyl terminated surface.

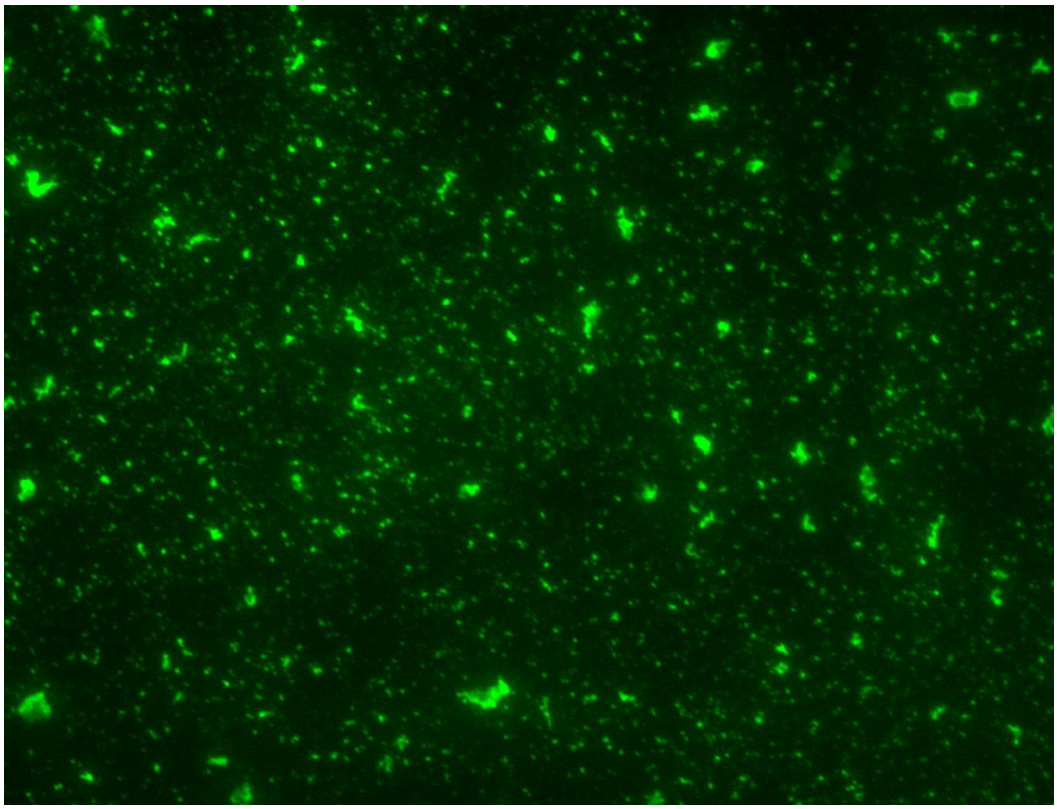

Figure 4.41: 1,6-hexanedithiol SAM on Platypus gold after incubation in maleimide-NTA, nickel ions, and ATPase-His-Rop* fluorescent dye. Green fluorescence was observed everywhere indicating specific binding of ATPase-His-Rop* to nickel ions coordinated to NTA on dithiol SAM surface.

4.3.4.2. Fluorescent Dye Patterning

Next, a modified surface engineered sample was tested. The surface was prepared as per the initial steps in the surface engineering section, with dithiol grafting except with a J scanner which allowed for larger imaging and patterns. However, instead of M-NTA, a maleimide dye was added. This served as a control study to confirm that the thiol maleimide reaction worked not only on the whole surface but also within a patterned area of dithiols. Additionally, identification markers locating the spot were incorporated via a scribe and AFM to facilitate locating the patterned area later. To achieve this patterning, micropatterns of dithiol (1,11-undecanedithiol and 1,6-hexanedithiol) were grafted into a resist matrix of 11-undecanethiol via contact mode AFM at 90º to enable frictional contrast to be observed as well. Analysis of the height image resulted in no significant difference in the height of the matrix background versus the 1,11-undecanedithiol t pattern. Analysis of the friction trace and retrace images resulted in a significant difference within versus outside the pattern, confirming that a change was made within this pattern.

This spatial confinement of dithiol patterning increased the number of upright molecules and therefore the number of available terminal thiols for additional reaction.[40] A comparison of patterned dithiol height versus resist matrix verified this with our patterns. The ellipsometric thickness of the dodecanethiol SAM was about as expected. Patterning of a dithiol (1,11-undecanedithiol) about the same length as the resist SAM (1-dodecanethiol) resulted in minimal height change as expected (0.02

nm). Evidence of pattern was achieved with trace and retrace frictional images which show distinct patterns due to the differences in the terminal chemistry inside and outside the patterned region (Figures 4.42 and 4.43). To further confirm that this change was due to insertion of dithiol within the pattern (as evidenced by the height similarity and friction difference), maleimide dye was added. To confirm that this height difference was due to binding of maleimide dye, fluorescence microscopy was utilized. The patterned area location was first located via markers with a light which illuminated the surface. Then, an epifluorescence microscope was utilized to excite the fluorescent dye. After excitation, emission images of the sample were taken. These resulted in fluorescence within the t pattern with minimal fluorescence outside the pattern. In summary, upon maleimide dye addition, preliminary evidence suggests that a feature in fluorescence was observed in a shape corresponding to the shape of the feature from grafting, suggesting successful attachment of maleimide to thiol terminal groups.

This surface engineered sample showed little nonspecific fluorescence, some fluorescence in the scribed x, and fluorescence in shape of pattern (t) was observed (Figure 4.43).

a)

b)

c)

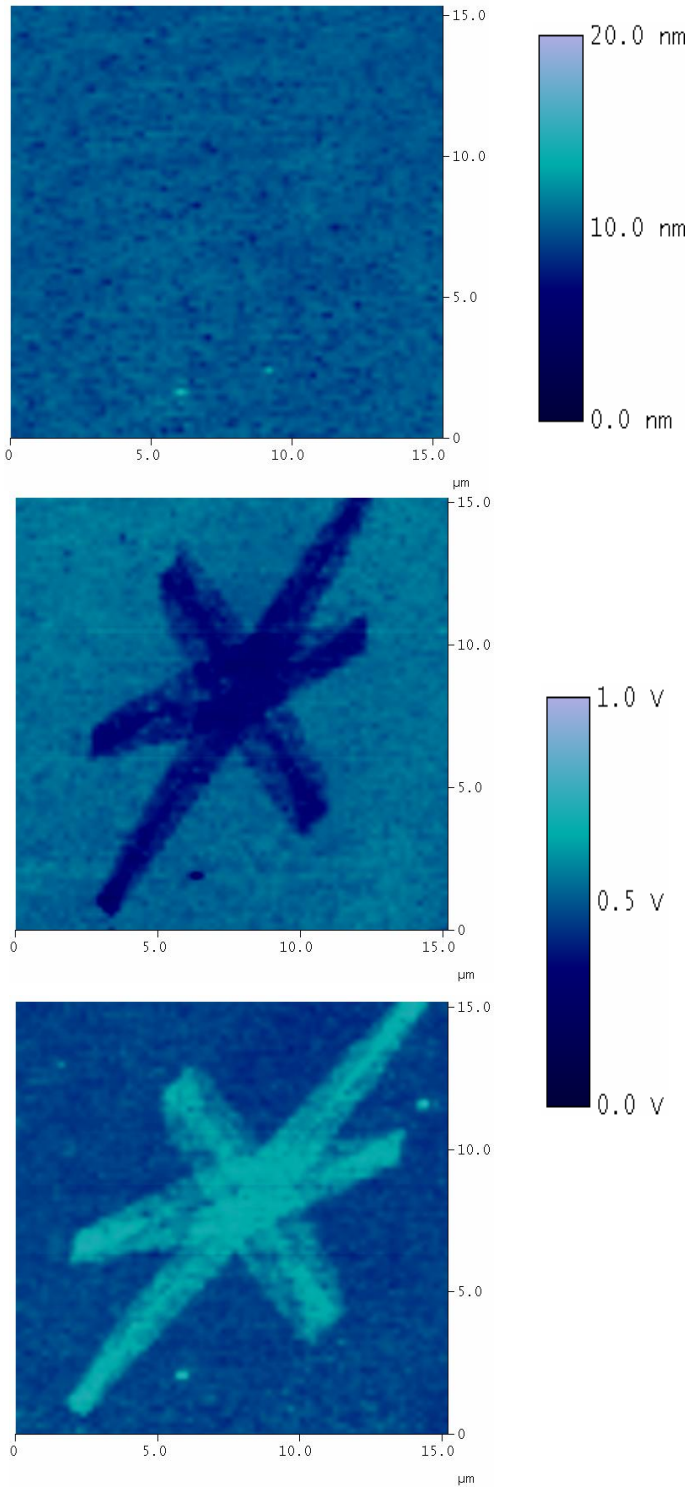

Figure 4.42: Dithiol grafting. 15.0 µm x 15.0 µm AFM images of 1,11-undecanedithiol star patterned into 1-dodecanethiol resist matrix on gold. a) Height image with 20.0 nm height scale, b) friction trace image and c) friction retrace image with 1.0 V scales.

a)

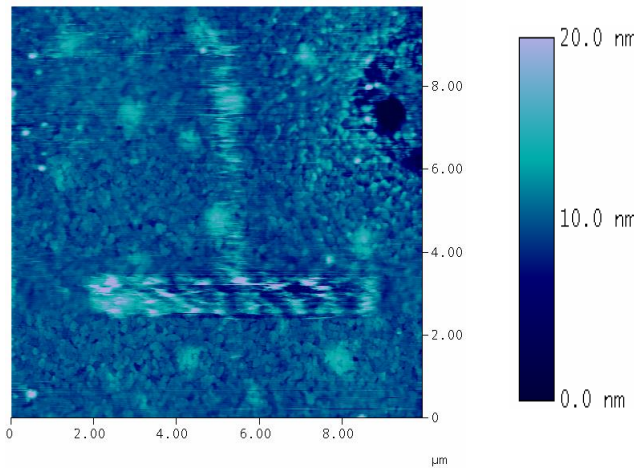

b)

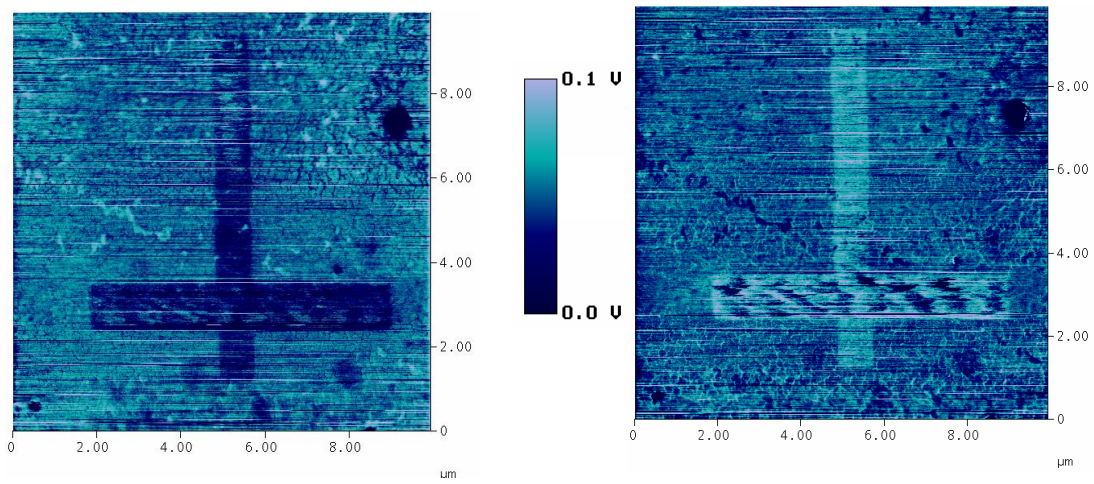

c)

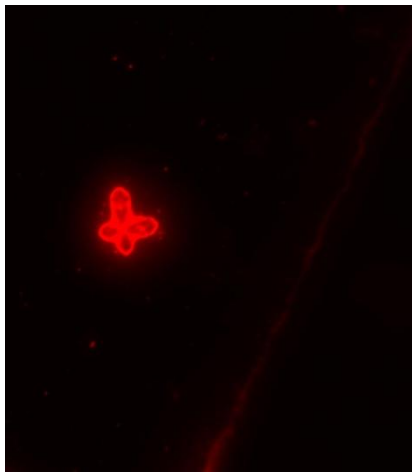

Figure 4.43: 10.0 µm x 10.0 µm AFM a) height with 20.0 nm height scale and b) friction trace and retrace images with 0.1 V scales, of 1,11-undecanedithiol SAM patterned into a dodecanethiol matrix. c) Fluorescent image of 1,11-undecanedithiol patterned t into 1,11-undecanethiol resist matrix after maleimide dye addition.

A modification of the specific attachment surface engineering patterning experiment was also performed with a fluorescently tagged F_1-ATPase-His-rop protein. The patterning study involved adsorption of the fluorescent protein to patterned dithiol areas within a resist methyl matrix SAM. Prior to the protein adsorption step, M-NTA and then nickel ions were allowed to interact with the surfaces. M-NTA should bind only to the thiol terminal groups and not the methyl terminal groups and had expected increase of height within the patterns of the star l and t of 2.5-2.8 nanometers as indicated by a brighter shade of blue and was in line with expected height increase of about 1.5-2.0 nanometers (Figure 4.44). The next step, currently in progress is to introduce the fluorescently tagged F_1-ATPase-His-Rop into the system and allowing binding. A height increase of about 10 nanometers is expected and will be monitored with tapping mode AFM. Then, a fluorescent image will be obtained via epifluorescence microscope with a CCD camera. Results should show that within the resist methyl terminated SAM portion, little to no adsorption occurred while on the patterned thiol terminated SAM, an abundance of fluorescence should be observed. This will provide evidence to minimal protein adsorption to the resist matrix and the specific attachment of protein to the patterned landing pads.

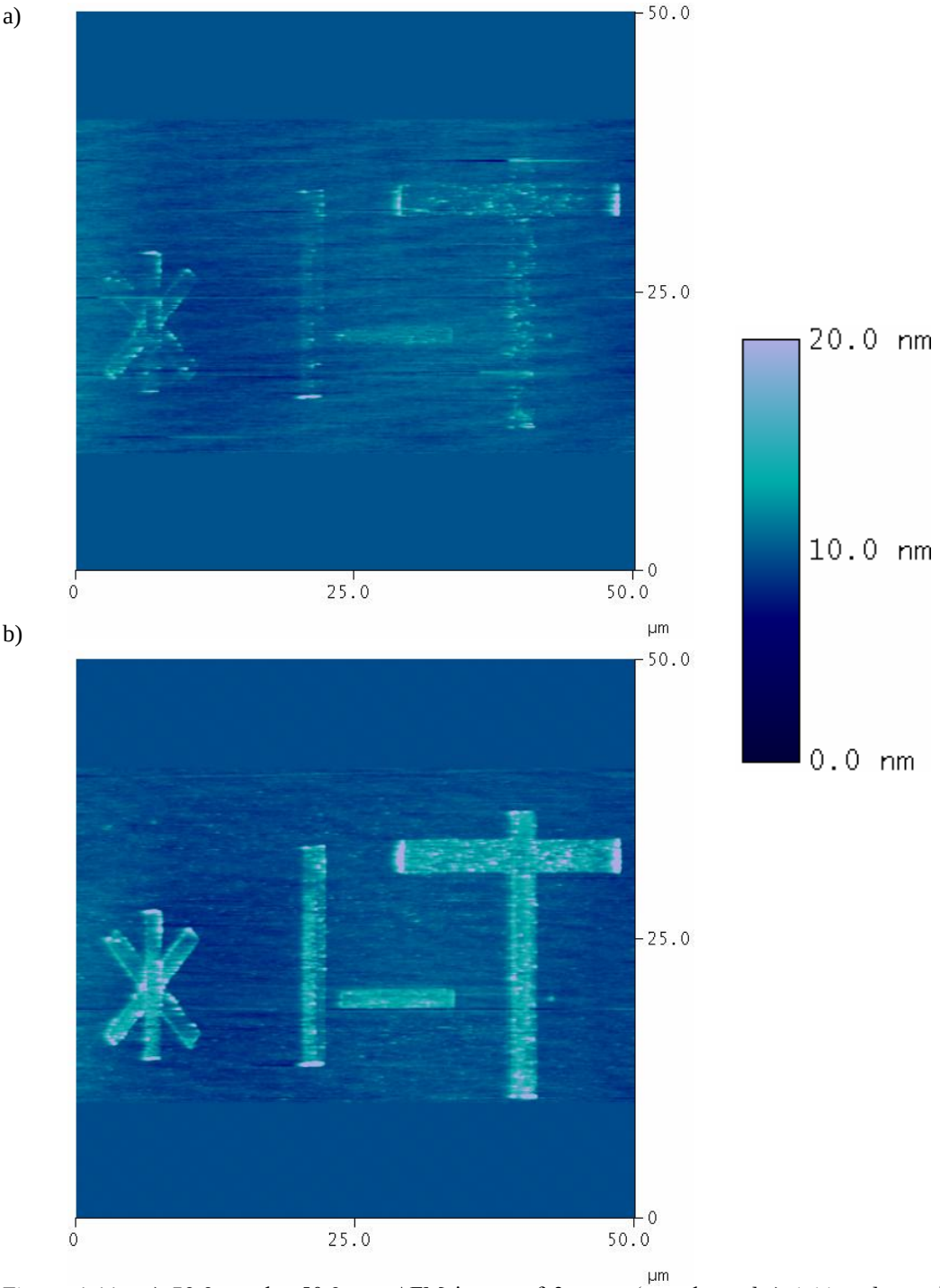

Figure 4.44: a) 50.0 µm by 50.0 µm AFM image of 3 areas (star, l-, and t) 1,11-undecanedithiol patterned into 1-dodecanethiol resist matrix on Platypus gold with 20.0 nm height scale. b) 50.0 µm by 50.0 µm AFM image of 1,11-undecanedithiol patterned into 1-dodecanethiol resist matrix on Platypus gold after addition of maleimide-NTA with 20.0 nm height scale. Height increase of about 2.5-2.8 nm was observed upon M-NTA addition, compared to the expected increase of 1.5-2 nm with upright M-NTA.

4.3.4.3. Challenges with Fluorescence Microscopy

Fluorescence microscopy offered additional verification of chemical modification responsible for specific maleimide and protein binding. However, nonspecific adsorption of dye to the surface was possible. If the dye adsorbed nonspecifically, it would not be an adequate control surface chemistry test. The dye itself could quench prior to excitation. If quenching occurred, even if the dye was adhered to the surface, it would not be observed. When imaging fluorescence patterns, finding the pattern and correlating the location between the two techniques (AFM and fluorescence) were difficult. This was partially overcome by placing optical markers on the surface. Additionally, large patterns were required to be able to observe fluorescence. It is possible that the density of NTA groups may differ when we move to smaller patterns (eventually nanometers) and we will need to confirm that the immobilization scheme still works and confirm that reducing the size of the pattern does not adversely impact this chemistry. A way to overcome this would be to create a series of patterns of decreasing size and confirm the height increase via AFM and see how small a pattern could be observable in fluorescence imaging. However, with control over these parameters by using a stable dye and creating identifying markers fluorescence was a valuable tool for control studies.

4.4. Summary

Nonspecific adsorption of F_1-ATPase to mica either dry or in fluid, resulted in at least three main orientations of ATPase, protrusion, depression, and rounded, as observed by tapping AFM. The desired orientation is with the gamma unit

perpendicular to the surface as seen in the protrusion cross-section. In order to use the motor, the rotating portion must be available for additional attachments and free to rotate without hitting the surface. This work clearly demonstrates that the nonspecific adsorption of the F_1-ATPase results in a very heterogeneous distribution of orientations, all which will not be appropriate for device fabrication. Thus, in order to have better odds of a functional device, it is necessary to control the orientation of the molecule at the surface. Additionally, protein was evenly distributed over the surface. This necessitated a specific or controlled landing area.

The patterning and nonspecific binding experiment revealed three key aspects to ATPase interactions with surfaces. One, it was possible to control the placement of ATPase. Secondly, F_1-ATPase prefers hydrophilic surfaces. And thirdly, hydrophobic SAM should make a decent resist monolayer. However, this nonspecific adsorption failed to meet the criteria of appropriate orientation (gamma subunit perpendicular to the surface).

Therefore, specific attachment through the histidine tags incorporated into the end of the alpha subunits opposite of the protrusion of the gamma subunit (Figure 4.12) should improve functionality. Control studies via SPR and fluorescence microscopy demonstrated controlled attachment through NTA-nickel ion-histidine tag binding strategy. Kinetic studies via SPR suggested that multivalent attachment was important in ATPase binding to the surface. SPR also indicated that a good fraction of ATPase-his remained bound to the surface, even after buffer exchange. This immobilization was specific and reversible with regeneration steps and additional

ligand and analyte capture steps. These adsorption qualities are promising for incorporation of the protein motor within a device in that the protein should stay stably bound to the surface through multiple sites and can be removed and regenerated if need be.

Controlled patterns of these proteins on the surface were also successfully constructed. By controlling the length of the dithiol utilized (1,6-hexanedithiol versus 1,11-undecanedithiol) was possible to vary the vertical position of the motor over the resist matrix as desired. Fluorescence studies with a maleimide dye confirmed specific attachment of maleimide to the dithiol terminal group since little fluorescence was observed on methyl terminated SAMs while a lot of fluorescence was observed on dithiol SAMs. Patterning with fluorescence had little nonspecific fluorescence to the background matrix and specific adsorption within pattern as fluorescence was observed within shape of pattern. Thus, nanoengineering the surface for both specific placement and orientation of F_1-ATPase should be feasible.

The incorporation of the protein motors in practical devices will rely on future (and currently in progress) steps in collaboration with other group members and the physics department as outlined below. The arm extending from the gamma subunit and a magnetic bead will be added unless it is already incorporated into the gamma subunit. Nanoelectrodes and microelectrodes will be inserted into the surface matrix. Current will be monitored upon ATP addition due to the bead rotating across the nanoelectrodes. As the bead crosses electrodes placed within the surface, a current registered its movement. These studies will confirm the functionality of the

immobilized proteins. This design involves a slow serial process which may not be the most practical method for device fabrication. This process could be scaled up via utilizing an AFM probe containing multiple cantilevers on the same substrate to create parallel patterns. Alternatively, to reduce the time and cost for device fabrication, other faster techniques could be utilized to incorporate the design aspects and immobilization schemes laid out here, although some control over shapes and sizes of the patterns will be sacrificed. Fundamentals of this research along with nanoelectrode and microelectrode collaborations could lead to successful production of hybrid nanobiodevices.

4.5. References

1. Fillingame, R. H., Getting to the bottom of the F1-ATPase. *Nat Struct Mol Biol* **2000,** *7* (11), 1002-1004.
2. Wang, H.; Oster, G., Energy transduction in the F1 motor of ATP synthase. *Nature* **1998,** *396* (6708), 279-282.
3. Seelert, H.; Poetsch, A.; Dencher, N. A.; Engel, A.; Stahlberg, H.; Muller, D. J., Structural biology: Proton-powered turbine of a plant motor. *Nature* **2000,** *405* (6785), 418-419.
4. Stahlberg, H.; Muller, D. J.; Suda, K.; Fotiadis, D.; Engel, A.; Meier, T.; Matthey, U.; Dimroth, P., Bacterial Na+-ATP synthase has an undecameric rotor. *EMBO Reports* **2001,** *2* (3), 229-233.
5. Stock, D.; Leslie, A. G. W.; Walker, J. E., Molecular Architecture of the Rotary Motor in ATP Synthase. *Science* **1999,** *286* (5445), 1700-1705.
6. Abrahams, J. P.; Leslie, A. G. W.; Lutter, R.; Walker, J. E., Structure at 2.8 A resolution of F_1-ATPase from bovine heart mitochondria. *Nature* **1994,** *370* (6491), 621-628.
7. Okuno, D.; Iino, R.; Noji, H., Rotation and structure of FoF1-ATP synthase. *Journal of Biochemistry* **2011,** *149* (6), 655-664.
8. Boyer, P. D., Molecular motors: What makes ATP synthase spin? *Nature* **1999,** *402* (6759), 247-249.
9. Neff, D.; Tripathi, S.; Middendorf, K.; Stahlberg, H.; Butt, H.-J.; Bamberg, E.; Dencher, N. A., Chloroplast F_0F_1ATP Synthase Imaged by Atomic Force Microscopy. *Journal of Structural Biology* **1997,** *119* (2), 139-148.
10. Takeyasu, K.; Omote, H.; Nettikadan, S.; Tokumasu, F.; Iwamoto-Kihara, A.; Futai, M., Molecular imaging of Escherichia coli F_0F_1-ATPase in reconstituted membranes using atomic force microscopy. *FEBS Letters* **1996,** *392* (2), 110-113.
11. Böttcher, B.; Bertsche, I.; Reuter, R.; Gräber, P., Direct visualisation of conformational changes in EF0F1 by electron microscopy. *Journal of Molecular Biology* **2000,** *296* (2), 449-457.
12. Uchihashi, T.; Iino, R.; Ando, T.; Noji, H., High-Speed Atomic Force Microscopy Reveals Rotary Catalysis of Rotorless F1-ATPase. *Science* **2011,** *333* (6043), 755-758.
13. Junge, W.; Müller, D. J., Seeing a Molecular Motor at Work. *Science* **2011,** *333* (6043), 704-705.
14. Noji, H.; Yasuda, R.; Yoshida, M.; Kinosita, K., Direct observation of the rotation of F_1-ATPase. *Nature* **1997,** *386* (6622), 299-302.
15. Masaike, T.; Koyama-Horibe, F.; Oiwa, K.; Yoshida, M.; Nishizaka, T., Cooperative three-step motions in catalytic subunits of F1-ATPase correlate with 80[deg] and 40[deg] substep rotations. *Nat Struct Mol Biol* **2008,** *15* (12), 1326-1333.
16. Yasuda, R.; Noji, H.; Yoshida, M.; Kinosita, K.; Itoh, H., Resolution of distinct rotational substeps by submillisecond kinetic analysis of F1-ATPase. *Nature* **2001,** *410* (6831), 898-904.

17. Soong, R. K.; Bachand, G. D.; Neves, H. P.; Olkhovets, A. G.; Craighead, H. G.; Montemagno, C. D., Powering an Inorganic Nanodevice with a Biomolecular Motor. *Science* **2000,** *290* (5496), 1555-1558.
18. Samra, H. S.; Gao, F.; He, F.; Hoang, E.; Chen, Z.; Gegenheimer, P. A.; Berrie, C. L.; Richter, M. L., Structural Analysis of the Regulatory Dithiol-containing Domain of the Chloroplast ATP Synthase γ Subunit. *Journal of Biological Chemistry* **2006,** *281* (41), 31041-31049.
19. Liu, H.; Schmidt, J. J.; Bachand, G. D.; Rizk, S. S.; Looger, L. L.; Hellinga, H. W.; Montemagno, C. D., Control of a biomolecular motor-powered nanodevice with an engineered chemical switch. *Nat Mater* **2002,** *1* (3), 173-177.
20. Carlo, M.; George, B., Constructing nanomechanical devices powered by biomolecular motors. *Nanotechnology* **1999,** *10* (3), 225.
21. Agarwal, G.; Sowards, L. A.; Naik, R. R.; Stone, M. O., Dip-Pen Nanolithography in Tapping Mode. *Journal of the American Chemical Society* **2003,** *125* (2), 580-583.
22. Agarwal, G.; Naik, R. R.; Stone, M. O., Immobilization of Histidine-Tagged Proteins on Nickel by Electrochemical Dip Pen Nanolithography. *Journal of the American Chemical Society* **2003,** *125* (24), 7408-7412.
23. Yang, Z. Z., Y.-P., Multi-Scale Simulation of an Immobilizting F_1-ATPase Molecular Motor. *Journal of the Korean Physical Society* **2008,** *52* (4), 1211-1216.
24. Verma, V.; Hancock, W. O.; Catchmark, J. M., Micro- and nanofabrication processes for hybrid synthetic and biological system fabrication. *Advanced Packaging, IEEE Transactions on* **2005,** *28* (4), 584-593.
25. Wasylycia, J. R.; Sapelnikova, S.; Jeong, H.; Dragoljic, J.; Marcus, S. L.; Harrison, D. J., Nano-biopower supplies for biomolecular motors: the use of metabolic pathway-based fuel generating systems in microfluidic devices. *Lab on a Chip* **2008,** *8* (6), 979-982.
26. Henry, H.; George, D. B.; Viola, V., Powering Nanodevices with Biomolecular Motors. *Chemistry - A European Journal* **2004,** *10* (9), 2110-2116.
27. Luo, T.-J. M.; Soong, R.; Lan, E.; Dunn, B.; Montemagno, C., Photo-induced proton gradients and ATP biosynthesis produced by vesicles encapsulated in a silica matrix. *Nat Mater* **2005,** *4* (3), 220-224.
28. Apell, H.-J.; Colchero, J.; Linder, A.; Marti, O.; Mlynek, J., Na, K-ATPase in crystalline form investigated by scanning force microscopy. *Ultramicroscopy* **1992,** *42–44, Part 2* (0), 1133-1140.
29. Camarero, J. A., New developments for the site-specific attachment of protein to surfaces. *Biophysical Reviews and Letters* **2006,** *1* (1), 1-28.
30. Laboratory Guideline 29-0057-17 AB: Biacore protein analysis: Capture of histidine-tagged molecules to Sensor Chip NTA. In *General Electric Company*, Sciences, G. H. L., Ed. 2011.
31. Protein Methods Library: His-tagged Proteins. http://www.piercenet.com/browse.cfm?fldID=1470D72F-469A-424B-90F7-2EDBCFBD33FC (Dec 2010).

32. Nieba, L.; Nieba-Axmann, S. E.; Persson, A.; Hämäläinen, M.; Edebratt, F.; Hansson, A.; Lidholm, J.; Magnusson, K.; Karlsson, Å. F.; Plückthun, A., BIACORE Analysis of Histidine-Tagged Proteins Using a Chelating NTA Sensor Chip. *Analytical Biochemistry* **1997,** *252* (2), 217-228.
33. Martell, A. E. S., R.M.; Motekaitis, R.J., NIST Standard Reference Database 46: Critically Selected Stability Constants of Metal Complexes. Texas A&M University, College Station, TX, 2001.
34. Davis, T. M.; Wilson, W. D., Determination of the Refractive Index Increments of Small Molecules for Correction of Surface Plasmon Resonance Data. *Analytical Biochemistry* **2000,** *284* (2), 348-353.
35. Buckle, M.; Williams, R. M.; Negroni, M.; Buc, H., Real time measurements of elongation by a reverse transcriptase using surface plasmon resonance. *Proceedings of the National Academy of Sciences* **1996,** *93* (2), 889-894.
36. Porter, M. D.; Bright, T. B.; Allara, D. L.; Chidsey, C. E. D., Spontaneously organized molecular assemblies. 4. Structural characterization of n-alkyl thiol monolayers on gold by optical ellipsometry, infrared spectroscopy, and electrochemistry. *Journal of the American Chemical Society* **1987,** *109* (12), 3559-3568.
37. Fuchs, D., J.; Weiss, P. S., Insertion of 1,10-decanedithiol in decanethiolate self-assembled monolayers on Au{111}. *Nanotechnology* **2007,** *18* (4), 1-7.
38. Dunbar, T. D.; Cygan, M. T.; Bumm, L. A.; McCarty, G. S.; Burgin, T. P.; Reinerth, W. A.; Jones, L.; Jackiw, J. J.; Tour, J. M.; Weiss, P. S.; Allara, D. L., Combined Scanning Tunneling Microscopy and Infrared Spectroscopic Characterization of Mixed Surface Assemblies of Linear Conjugated Guest Molecules in Host Alkanethiolate Monolayers on Gold. *The Journal of Physical Chemistry B* **2000,** *104* (20), 4880-4893.
39. Xu, S.; Laibinis, P. E.; Liu, G.-y., Accelerating the Kinetics of Thiol Self-Assembly on GoldA Spatial Confinement Effect. *Journal of the American Chemical Society* **1998,** *120* (36), 9356-9361.
40. Yu, J.-J.; Ngunjiri, J. N.; Kelley, A. T.; Garno, J. C., Nanografting versus Solution Self-Assembly of α,ω-Alkanedithiols on Au(111) Investigated by AFM. *Langmuir* **2008,** *24* (20), 11661-11668.

CHAPTER FIVE:

Conclusions and Future Directions

5. Conclusions and Future Directions

A greater understanding of protein surface interactions and the underlying mechanisms should enable the advancement of a wide variety of biotechnological and materials developments. Potential applications relevant to this dissertation include development of more biocompatible surfaces and improved functionality of proteins immobilized on surfaces by controlling orientation within nanobiomolecular hybrid devices. Atomic force microscopy and surface plasmon resonance are powerful techniques in determining the structure and dynamics of protein adsorption to surfaces. By controlling the surface chemistry, solution conditions, and surface topography, one can more effectively manipulate the adsorption of proteins.

Specifically, fibrinogen adsorption can be minimized or adsorbed in a non-reactive state to improve biocompatible surfaces. Surface chemistry influenced both the shape and the dynamics of fibrinogen adsorption to the surface as studied via AFM and SPR. AFM studies revealed that on hydrophilic surfaces such as mica, gold, and an amine-terminated SAM, fibrinogen assumed a rounded or globular structure and was evenly distributed across the surfaces, while on hydrophobic surfaces such as graphite and a methyl-terminated SAM the conformation was trinodular in a linear or bent fashion and had more aggregation, especially at the step-edges of graphite. SPR studies demonstrated that surface chemistry influences both the adsorption properties and desorption properties of fibrinogen. Fibrinogen adsorbed to an amine-terminated SAM and a methyl-terminated SAM at saturation exhibit different responses to a washing solution. Fibrinogen adsorbed to the methyl-

terminated SAM desorbed upon surfactant addition while the fibrinogen adsorbed to the amine-terminated surface was only partially desorbed. This is indicative of different binding mechanisms of fibrinogen to the two surfaces. In terms of the sequential kinetic titrations with a variety of SAMs, the initial rate of adsorption was essentially the same for all surfaces, as expected. Fibrinogen adsorbed to all surfaces, as expected. The desorption curves of fibrinogen varied amongst the surfaces, with the carboxyl-terminated and hydroxyl-terminated SAMs with the largest observed desorption rates. Chemistry beyond just hydrophobic/hydrophilic nature must play a role in the dynamics of fibrinogen interactions with surfaces, such as electrostatic interactions.

F_1-ATPase studies revealed that the molecular motor adsorbs to mica in at least three distinct conformations. Since only one of these provided an orientation which would allow functional, active protein, control over orientation is imperative in improving the immobilization for device applications. Patterning studies of a hydrophilic surface within a hydrophobic resist determined that the protein adsorbs preferentially to the hydrophilic surface. Thus, a methyl-terminated surface can be used as a resist and it is feasible to create a landing pad for spatial discrimination of the protein. These studies also revealed that improving the functionality of adsorbed proteins by controlling orientation such as through histidine-tags and a nickel ion-nitrilotriacetic acid tether via maleimide-thiol bond to the surface are imperative steps in the device fabrication schematic. SPR and fluorescence studies verified the feasibility of this process. SPR studies also demonstrated that ATPase-his adsorption

most likely involves more than one histidine tag, which should help to further control and stabilize orientation. AFM-based nanopatterning approaches enabled localized adsorption of the protein in the correct orientation. This should improve the feasibility of using ATPase will be a strong contender for powering nanobiomolecular hybrid devices.

Future studies with ATPase may include fabrication on silicon surfaces (instead of gold). This could be achieved through the same maleimide-NTA chemistry with nickel (or cobalt) ions and the histidine-tag as well, but with incorporation of a thiol into silane monolayer. If a thiol silane is not available, one could start with a silane with a double bond (or make double bond via oxidative lithography to graft in) and expose this to H_2S and light.[1, 2] Patterning with dithiols can lead to insertion of dithiols within the resist matrix at defect sites and may lead to adsorption through both thiol groups which would be detrimental to future reactions. Thus, a similar experiment on gold with the oxidative lithography could be performed to achieve better packing with alkane chain and molecules upright on surface. To provide additional evidence of the availability of the reactive thiol groups at the surface, an addition of Au nanoparticles to the surface and observation of height increase via AFM could be performed.

Future studies include utilizing a PEG SAM as a protein resist monolayer with an etched pattern to create a region without PEG and studied via nonspecific adsorption technique as well as with the nanografting per surface engineering schematic.

To check the orientation of the protein, a modified protein could be utilized. This ATPase-His tag would also have a biotin group incorporated onto the end of the gamma subunit. After repeating the nickel ion and protein injections as in the previous SPR NTA experiments, streptavidin would be injected. This should bind to the biotin on the protein if the protein is oriented such that the gamma unit is pointed up (via specific attachment of the histidine tags to the nickel ions). If binding is observed, this would provide evidence that the gamma subunit is accessible, presumably in the upright orientation.

To further check the chemistry and stability with conditions similar to AFM experiments of the system, a chip similar to the NTA chip could be produced using the chemistry of the surface engineering experiment. Confirmation of these steps could be performed via ellipsometry, goniometry, and FTIR. The previous experiments with the NTA chip would be repeated to compare F_1-ATPase-His immobilization onto the two different chip formations. The basic chemistry should still work on this chip as with the commercial NTA chip. A difference in the density of NTA groups on the chemically modified gold surface as compared to the NTA chip is likely. This would help to verify the binding kinetics and determine if the NTA density influences the binding.

If the protein was determined to wobble on the surface, it is possible to stabilize the thiol chains with cross-linking. Alternatively, the charge density of the thiol/NTA groups on the surface could be controlled to control the number of his-tags bound per molecule. These should help to stabilize the protein such that the currents

measured were due to rotation and not just flexibility in the movement of the molecule.

Activity studies could be performed after binding ATPase to the entire surface. We have verified that the chemistry works, and that the attachment should occur with the proper orientation, but this does not ensure functional protein. The activity of the surface bound proteins needs to be checked (perhaps by rotating bead experiments). An additional activity test could be with the phosphate assay. These studies would confirm that the protein was still functional after immobilization.

For fibrinogen studies, continued investigation of different SAM surfaces to build up the library of AFM and SPR data could be obtained. The studies could be repeated with various pH and salt concentration conditions to help tease out which interactions are important in fibrinogen adsorption to various surfaces. Regeneration solutions could be tested with AFM and then transferred to SPR experiments this would provide further insight into the interactions of fibrinogen with the surface and would potentially improve the kinetic experiments by enabling multiple protein concentrations to be injected on the same chip. Patterning of surfaces via etching and/or grafting could be performed to further investigate fibrinogen adsorption properties to nanostructured materials. This would help to relate the adsorption properties to more realistic materials which most likely have some degree of surface roughness.

While a great amount of additional experiments can be envisioned, this dissertation discussed steps towards understanding fundamental properties of protein-

surface interactions. Studies of nonspecific fibrinogen adsorption could be translated into improved biocompatible material design. The M-NTA, nickel ion, histidine tag immobilization scheme (Figure 4.12) is a versatile method that could be used for patterning any protein with a histidine tag. Since a number of proteins are purified via histidine tags, this could prove to be a very universal technique to create a wide variety of protein patterns with control over the shape and size of the patterns. Hopefully continued progress will be made towards the ultimate goal of improving materials design in both biocompatibility and hybrid nanobiodevices applications.

5.1. References

1. Maoz, R.; Frydman, E.; Cohen, S. R.; Sagiv, J., "Constructive Nanolithography": Inert Monolayers as Patternable Templates for In-Situ Nanofabrication of Metal–Semiconductor–Organic Surface Structures—A Generic Approach. *Advanced Materials* **2000,** *12* (10), 725-731.

2. Maoz, R.; Frydman, E.; Cohen, S. R.; Sagiv, J., Constructive Nanolithography: Site-Defined Silver Self-Assembly on Nanoelectrochemically Patterned Monolayer Templates. *Advanced Materials* **2000,** *12* (6), 424-429.